WEB STRENGTH OF ROLLED STEEL BEAMS

FROSSO GERMANOU B.SC.

A THESIS SUBMITTED FOR THE DEGREE

OF

DOCTOR OF PHILOSOPHY

DEPARTMENT OF CIVIL ENGINEERING

THE UNIVERSITY OF ASTON IN BIRMINGHAM

APRIL 1979

TO MY PARENTS

WEB STRENGTH OF ROLLED STEEL BEAMS

BY

FROSSO GERMANOU

THESIS SUBMITTED FOR THE DEGREE OF

DOCTOR OF PHILOSOPHY 1979

SUMMARY

This thesis examines the behaviour of universal beams, when subjected to concentrated loads applied on the top flange, and simply supported on small lengths of bearing at the end of the beam. The stresses produced from this type of loading cause a localised failure either at the centre under the applied load, or at the end at the point of support.

A total number of ninety tests have been carried out on different universal beam serial sizes for various loading and supporting conditions. These beams appeared to fail in an manner characterised by yielding at the flange and elastoplastic buckling or crushing of the web. Two modes of failure were observed: a) Mode 1 - This failure mode was found to occur to beams loaded or supported with relatively small or zero lengths of bearing and it is characterised by the transverse bending of the flanges. b) Mode 2 - This failure mode was found to occur when the beams were loaded or supported with large lengths of bearing. The flanges were slightly distorted without any significant transverse bending.

The test results are compared with various design codes such as BS 449, American Specification, the recently published Draft Code and empirical relationships. The comparisons show that these codes, although conservative in some cases, are very unsatisfactory in others.

Two theoretical approaches are developed, an Elastic Buckling analysis, examining the stability of the web plate and a Crushing theory which considers the stress system attainable at the web root combined with the ultimate moment of resistance due to bending of the web and the flange. An expression for the minimum thickness of the loading plate is also formulated.

The derived theories are compared with the experimental results and the Crushing theory is further simplified to a suitable form for design purposes.

Beam, Bearing, Buckling, Web, Yielding.

ACKNOWLEDGEMENTS

The author wishes to express her sincere appreciation to Mr A W Astill for his invaluable supervision and encouraging guidance throughout the period of this study.

The author would also like to express her gratitude to Professor M Holmes, Head of the Department of Civil Engineering at the University of Aston, for the opportunity to carry out this work and to Dr L H Martin for acting as advisor.

Thanks are due to Mr W Parsons and all the technical staff who helped during the experimental work.

Finally, the author would like to thank the University of Aston in Birmingham for providing the scholarship.

NOTATION

A	Half wave length, or half length of plate.
A'	Area.
A_o, A_1, A_2, A_3	Coefficients, as defined in chapter 6.
a	Half wave length, as defined in chapter 5.
a'	Robertson constant.
B	Beam flange width, or half depth of plate.
B_o, B_1, B_2, B_3, B_4	Coefficients, as defined in chapter 6.
b	Effective strut length.
b_1, b_2	Length of stiff bearing (Draft Code).
C_o	Euler Buckling load (BS 449).
C_o, C_1, C_2, C_3	Coefficients, as defined in chapter 6.
D	Overall depth of beam, or as defined in chapter 5 ($D = A/B$).
D_o, D_1, D_2, D_3, D_4	Coefficients, as defined in chapter 6.
D_1	Plate Flexural Rigidity.
d	Web depth between root fillets.
E	Young's Modulus.
E_s	Secant Modulus.
E_t	Tangent Modulus.
e	Initial eccentricity of the web.
F	As defined in chapter 5 ($F = \frac{a}{B}$).
F_c	Axial compression in member.
F_w	Applied force.
f_b	Permissible ultimate stress (Perry formula).
f_{bc}	Bending stress.
f_{br}	Buckling stress.
f_y	Yield stress.

f_{yf}	Flange yield stress.
f_{yp}	Yield stress for spreader.
f_{yr}	Root yield stress.
f_{yw}	Web yield stress.
G	As defined in chapter 5 (G = 12I/Bldt).
h	Clear distance between the flanges.
I	Moment of Inertia.
K, K_1	Elastic buckling coefficient
k	Distance from the outer face of flange to web toe or fillet.
k_1	Factor of safety (BS 449).
L	Span of the beam.
L'	Overall length of the plate.
L_1	Length, as defined in chapter 6.
l	As defined in chapter 2 for Series V.
l_a	Length of the applied load.
l_a'	Length of support, as defined in chapter 6.
l_e	Length, as defined in chapter 2 for series I.
l_k	Length, as defined in chapter 2 for Series III.
l_m	Length, as defined in chapter 2, for Series II.
l_p	Length, as defined in chapter 2 for Series VI.
l_s	Length, as defined in chapter 2 for Series IV.
M	As defined in chapter 6.
M'	Applied moment in the member.
M_p	Moment capacity of the member.

M_{PF}	Plastic moment of resistance for the flange.
M_{PT}	Plastic moment of resistance for the flange at the end of the failed zone.
M_{pp}	Plastic moment of resistance for the plate.
M_w	Plastic moment of resistance for the web.
N	Length of bearing (American Specification).
N_{bx}	Sum of longitudinal loadings N_x and N_b.
N_{cr}	Critical force per unit length.
N_p	Length of bearing for internal load.
N_r	Length of bearing for end reaction.
N_x	Longitudinal compressive force per unit length.
N_y	Vertical compressive force per unit length.
N_{xy}	Shear force per unit length.
N_o	Maximum compressive value of N_b.
n	Perry factor.
n_1	Length obtained by dispersion at 45^o through half the depth of the section.
n_2	Length obtained by dispersion at a slope of 1 to 2.5.
P	Load.
P_B	Ultimate load due to web buckling (BS 449).
P_b	Ultimate load due to web bearing (Draft Code).
P_c	Ultimate load due to web bearing (BS 449).
P_{cr}	Critical load.
P_{exp}	Experimental load.
P_n	nth critical load.
P_{th}	Theoretical load.
P_w	Ultimate load due to web buckling (Draft Code).

P_1, P_2, P_3, P_4	Crushing load as defined in chapter 6.
p_c	Compressive strength (Draft Code).
P_E	Euler strength.
P_y	Design strength, ($p_y = 0.93\ f_y$).
R	Concentrated load or reaction (American Specification).
r	Root radius.
r_s	Slenderness ratio.
T	Beam flange thickness.
t	Beam web thickness.
t_p	Thickness of bearing plate.
W_a	Axial load.
W_1, W_2, W_3, W_4	Work done, as defined in chapter 6.
w	Resistance provided by the web per unit length.
x,y,z	Cartezian co-ordinates.
x_o	Overhang of beam.
$Z_1, Z_2 \ldots . Z_6$	Factors, as defined in chapter 7.
α	Factor, as defined in chapter 6.
α_o	Numerical factor, as defined in chapter 5.
$\alpha_1, \alpha_2, \alpha_3$	Arbitrary angles.
γ	Factors, as defined in chapter 5.
Δ	Vertical movement.
Δ_H	Horizontal movement
$\delta_1, \delta_2, \delta_3$ etc	Deflections (experimental recordings).
$\varepsilon, \varepsilon_a, \varepsilon_b$	Strains.
η	Reduction factor (Inelastic buckling).
θ, θ_1	Arbitrary angles.
λ	Numerical factor, as defined in chapter 5.

λ'	Slenderness ratio (Draft Code).
λ_o	Limiting slenderness (Draft Code).
λ_1	Load length to plate length ratio ($\lambda_1 = c/b$).
ν	Poisson's ratio.
ξ	Coefficient of restraint.
ρ	Panel aspect ratio ($\rho = b/d$).
σ_{cr}	Critical stress.
σ_{max}	Maximum value of applied stress.
$\sigma_1, \sigma_2, \sigma_3$	Stress.
ϕ	Arbitrary angle.
ψ	Arbitrary angle.
ω	Amplitude of buckled wave.
ω_o	Initial plate deflection.
$\omega_1, \omega_2, \omega_3, \omega_4$	Deflections, as defined in chapter 6.

Note: Some notations not included in the above list, will be specifically defined when they are first introduced.

CONTENTS

LIST OF TABLES

LIST OF FIGURES

LIST OF PLATES

CHAPTER 1

INTRODUCTION AND HISTORICAL REVIEW

1.1 INTRODUCTION

In current design practice, when considering rolled steel beams, it is very common to place a bearing stiffener at the location of a concentrated load or support to prevent web crushing or web buckling. There are some situations, however, when the exact location of an expected concentrated load is not known or cannot be determined. Such a situation occurs in rolled steel beams or plate girders which support crane rails or railroad tracks directly on top of the compression flange. Massonnet (1) in 1968, while presenting the review of present state of knowledge of thin wall deep girders at the annual conference of International Association of Bridge and Structural Engineering, emphasized that this type of loading requires attention.

Due to failure of load bearing falsework involving the use of I-beam grillages, notably Vancouver Narrows Bridge in 1958 and Loddon Viaduct in 1972, it was indicated that more research was needed for revision of the design rules and investigation of factors not fully appreciated in the then design codes, particularly those concerned with the web capacities of rolled steel I-beams.

In 1961 Hrennikoff (2), when investigating the collapse of the Vancouver 2nd Narrows Bridge, published a paper which is concerned with the grillage of the falsework supporting the bridge during erection. This grillage proved to be the cause of the collapse. Hrennikoff believed that the lessons to be learned from the catastrophe are:

1) the inapplicability of the usual column formulae for the design of the webs of the grillage beams in buckling,

2) the weakening effect of the plywood pads interposed in the grillage,

3) the inapplicability of the column formulae given by the Canadian Specifications CSA 1952.

More recently, in the report of the collapse of falsework for the river Loddon Viaduct (3) the circumstances which lead up to the collapse and the appearance of the falsework after failure had occurred are described. The buckled and twisted shape of the beams after collapse suggests the possibility of the collapse, being initially due to buckling of the webs of the rolled steel beams. The major criticism of a general design matter referred to was: "There were no stiffeners fitted to the thin webs of the 10 x 10 x 49 lb universal columns and 12 x 6½ x 31 lb universal beams of the mild steel grillage assemblies supporting the Hannebeck trusses. These were subject in our opinion to considerable buckling and twisting loads".

In 1964 Holmes (4) showed that universal beam sections have relatively little resistance to cross sectional deformation and that the stresses associated with such deformation are quite high. Comparing Universal Beam Sections and British Standard Beams of either equal moment of inertia or section modulus, the stresses associated with cross-sectional deformation are between two and four times greater in universal beams than in the equivalent rolled steel joist.

A similar failure occurred at Koblenz in 1972 for a deep I-beam without stiffeners, as reported in the 'New Civil Engineer' December 20, 1973.

1.2 BRITISH STANDARDS

The most widely used design standards for Steelwork in Great Britain is BS 449 (1969) "The Use of Structural Steel in Buildings"

(5) and BS 153 (1972) "Specification for Steel Girder Bridges" (6). The former was first introduced in 1932 and since then it has been revised many times. Before the publication of BS 449 in 1932, Glanville (7) conducted ten tests on rolled steel beams to determine the advisability of providing web stiffeners for steel I beams. These tests were performed at the request of the British Steelwork Association. In the final report it is stated, "It is impossible from the results of these few tests to draw conclusions of such an exact nature as to constitute a basis for purposes of design, certain general conclusions may, however, be stated". These conclusions could be summarised as

1) Beams where restraints are not imposed fail in torsion; such form of failure must be prevented by the provision of proper top cleats connecting beams and stanchions.
2) When torsion failure is prevented and the points of support are at the ends of the beam the failure in every case occurred by vertical buckling of the web over the supports.
3) In beams which were allowed to overhang the supports the additional stiffness of the ends given by the overhanging portion was sufficient to increase the failing load.

The current edition of BS 449 and the original publication have different clauses dealing with rolled steel beams when subjected to concentrated loads. Both editions, however, require consideration of two criteria, the overall buckling of the web and the local crushing in the vicinity of the applied load or support. The clause which deals with rolled steel beams which are subjected to concentrated loads, in BS 449 (1969) is 28 (a) (i) in chapter 4. This is based on the assumption that a length of the web acts as a strut in which the ends are restrained both in position and direction, thus

the effective length is d/2 where d is the depth of the beam between root fillets. The effective length of the strut is obtained by using a 45^{o} angle of dispersion from the ends of the stiff bearing to the neutral axis. The web crushing clause is 27(e) in chapter 4. An effective length of the web along which crushing will occur is determined by assuming a 30^{o} angle of dispersion to the plane of the web and the root radius, or edge of the beam whichever is the shortest. These clauses are discussed in more detail in chapter 4.

1.2.1 Draft Standard Specification for the Structural Use of Steelwork in Buildings

During the period of completing the present work the "Draft Standard Specification for the Structural Use of Steelwork in Buildings" (8) was published. Some alterations have been made concerning web buckling and web bearing. The clauses dealing with web buckling and web bearing are 7.3 and 7.4 respectively in chapter 8. For web buckling the slenderness of the web is changed to 2.5 d/t and the compressive strength p_c is calculated based on a different Robertson constant a' and design strength p_y, which is taken as 0.93 times the yield stress of the material. This section is discussed in more detail in chapter 4.

1.3 ELASTIC PLATE BUCKLING THEORY

Thin plates, which are stressed in their own plane are often present in steel structures as webs of rolled steel beams and plate girders. However, where designs involve concentrated and partial edge loads, such as the web-plate of a crane girder under the action of heavy wheel loads applied to the flanges, the stress distributions change, thus causing tremendous mathematical difficulties in obtaining solutions.

When a plate is stressed in its plane under the action of external applied forces and a critical loading is reached, the plane state becomes unstable. For larger loads after any disturbance a change in equilibrium results, the plate deflects laterally and it becomes buckled. For a plate this does not necessarily imply failure, because the buckles are restrained in the transverse direction and the plate is usually capable of carrying loads beyond the first buckling load.

1.3.1 Uniform Edge Loading on Two Opposite Edges of a Rectangular Plate

The web of a rolled steel I-beam can be considered as a rectangular plate loaded by a uniformly distributed load on two opposite edges, subjected to different boundary conditions. Many authors have investigated this problem from the early days such as Bryan (9) in 1891 for simply supported boundary conditions.

For more complex boundary conditions other authors, such as Stowell (10), have published work dealing with this problem. Stowell considered the case of a plate with either simply supported or clamped edges and free unloaded edges. The case of a rectangular plate with loaded edges free and unloaded edges simply supported has been analysed by Woinowsky - Kreiger (11). Many other boundary conditions have been examined by several authors such as Timoshenko (12), Bleich (13), as shown in figures (1.1) and (1.2) and Stowell(14).

Gerard and Becker (15) collected the work of other authors and gave a very comprehensive summary. They also considered the case of buckling of a simply supported rectangular plate under combined bending and compression and for other boundary conditions as well. They provided values of the plate buckling coefficient in each case,

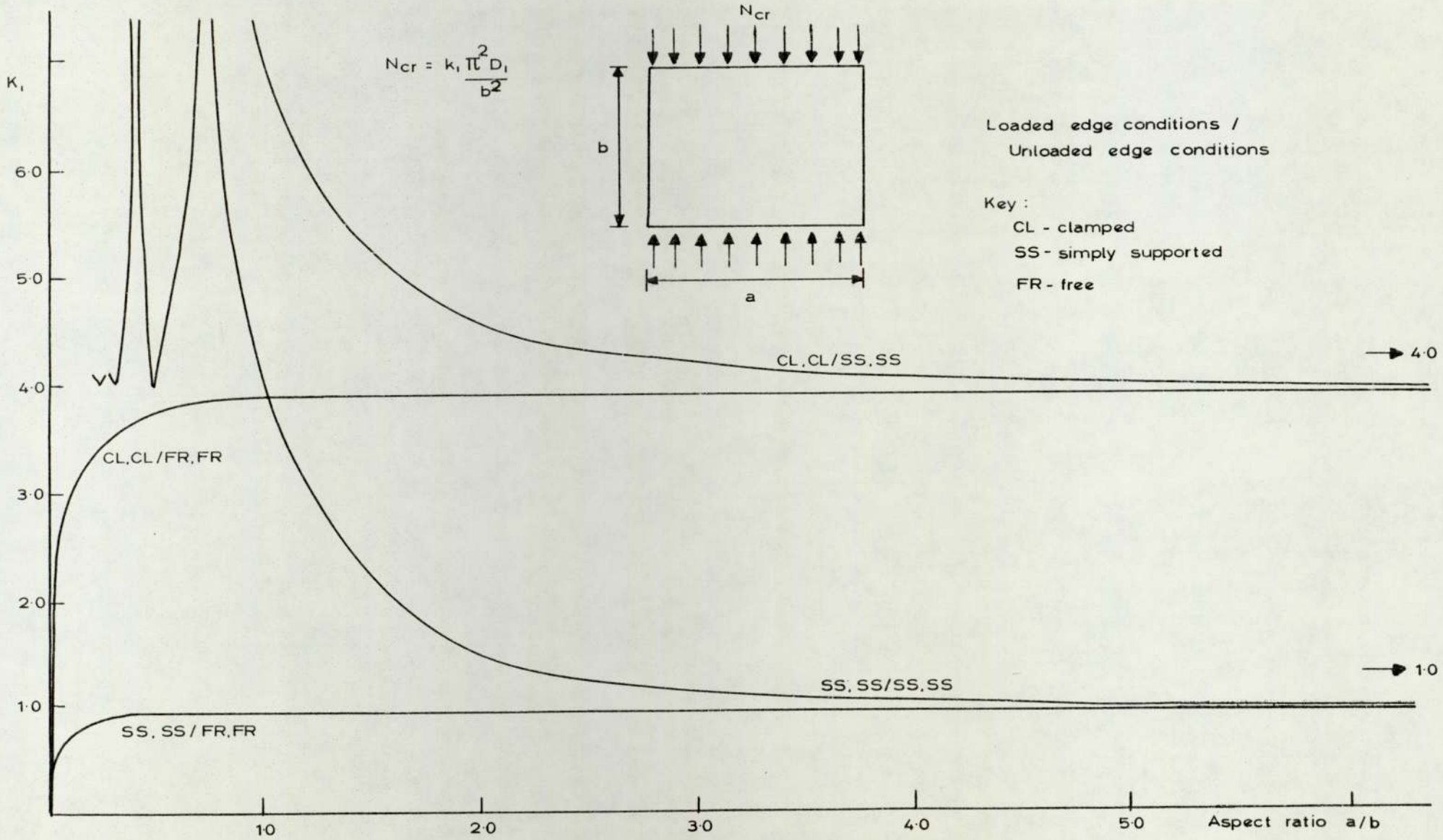

FIGURE 1·1 ELASTIC BUCKLING COEFFICIENT K_1 FOR VARIOUS BOUNDARY CONDITIONS

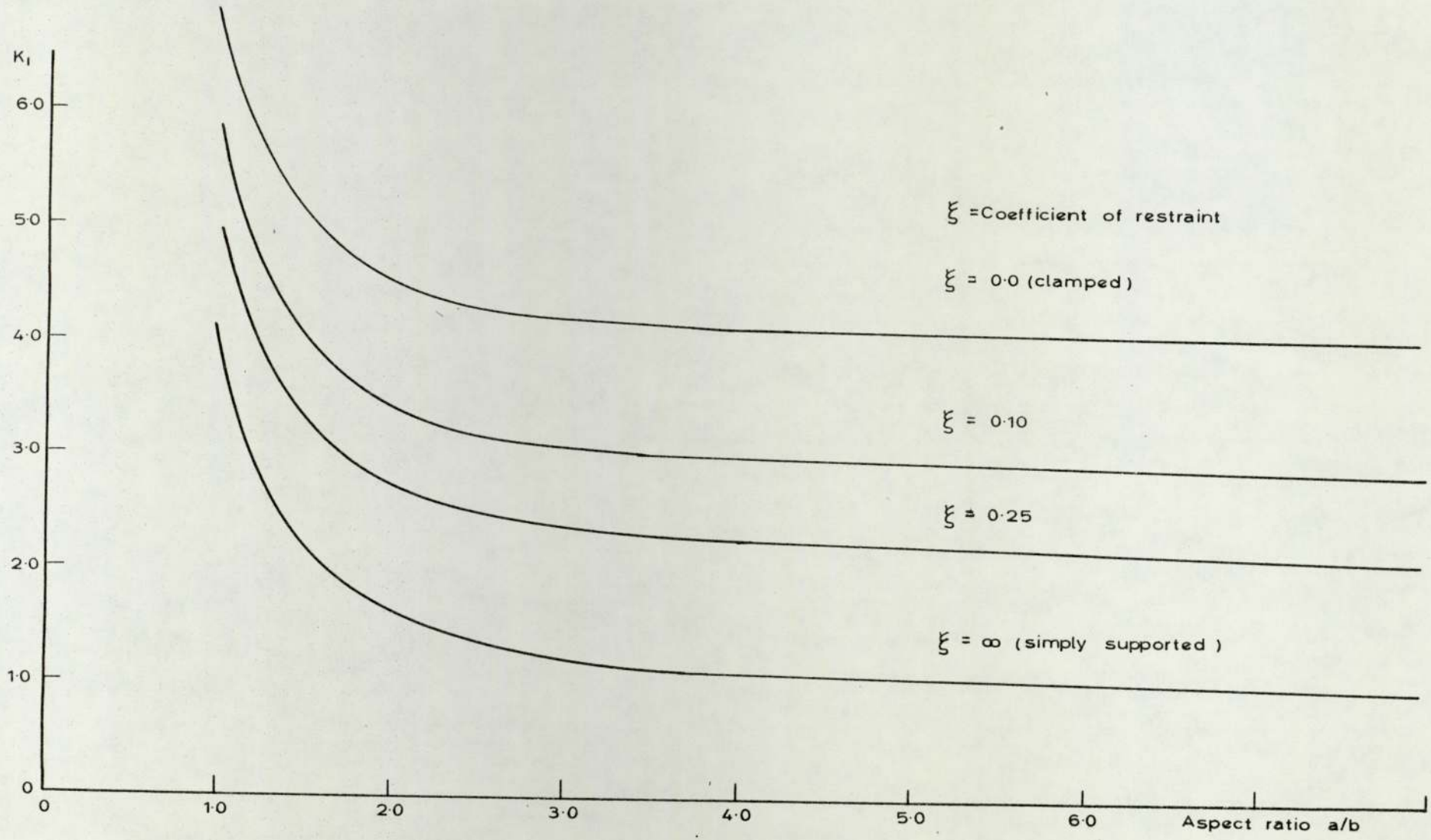

FIGURE 1·2 ELASTIC BUCKLING COEFFICIENT K_1 FOR RESTRAINED LOADED EDGES GIVEN BY BLEICH

for various aspects ratios.

Shulesko (16) (17) considered the elastic stability of rectangular plates compressed in two perpendicular directions by forces uniformly distributed along the edges. In his paper he dealt with the case of a plate with one edge free and the opposite edge elastically restrained.

More recently Johnson (18) considered the problem of buckling of a plate under the combined action of longitudinal compression, transverse compression and shear.

An important problem, especially for the design of box beam webs, is the stability of a rectangular plate under longitudinal bending and transverse compression, this type of loading is shown in figure (1.3a). Timoshenko who investigated this problem, states that the critical stress is reduced, due to the compression, compared with the case when the plate is under the action of bending only. This reduction depends on the ratio of the applied forces and the aspect ratio of the plate.

Grossman (19) later investigated the same problem and presented interaction curves, that is curves which determine the value of one stress required to produce buckling when a given value of another stress is also acting.

Some years later Wittrick (20) investigated the buckling of an infinite strip, simply supported on its edges and subjected to the combined action of longitudinal and transverse compression, bending and shear, using Galerkin's method; he presented charts covering all possible combinations of the basic stress system.

A theoretical investigation of the buckling of a simply supported flat rectangular plate, under critical combinations of longitudinal bending, longitudinal compression and transverse

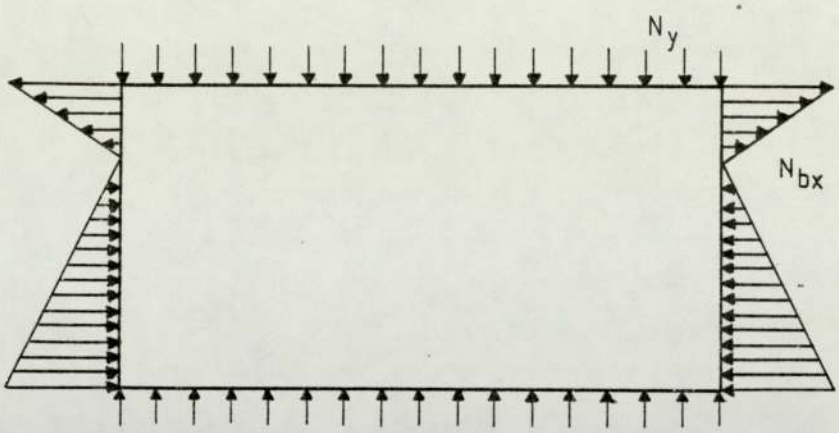

a. Type of loading solved by Timoshenko

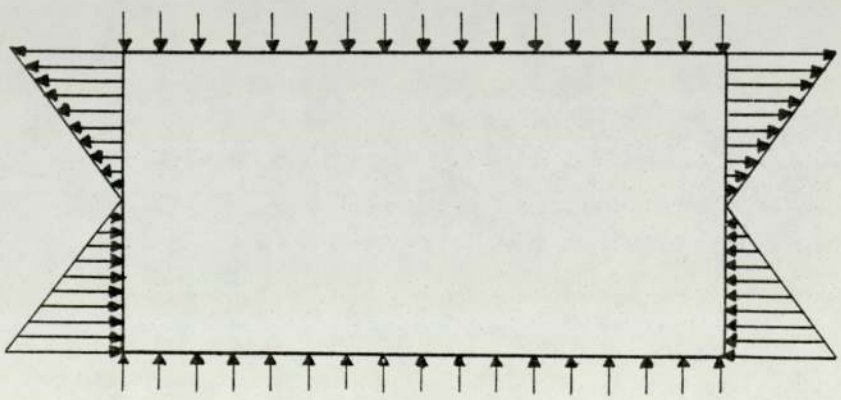

b. Type of loading solved by Noel

FIGURE 1.3 PLATE UNDER COMBINED LOADING

compression, was made by Noel (21). He presented interaction curves for these loading types for various plate aspect ratios. He also included curves of critical buckling coefficients for simply supported flat rectangular plate under combined unsymmetrical bending and lateral compression, as shown in figure (1.3b). This type of loading occurs in beams having unsymmetrical cross-section. These results indicate that the reduction in the allowable bending stress due to the addition of lateral compression is greatly magnified by the further addition of only a small longitudinal compressive load.

Theodor Von Karman (22) in 1932, produced an equation for the effective width of a buckled plate under uniform compressive loading. This was investigated by Sechler and was found to be accurate for very thin wide plates.

Winter (23) in 1946, published an empirical equation for the effective width of a compressive flange based on tests, carried out on U and I section beams, under pure moment loading. The equation was based on that of Von Karman but modified to increase its validity over an extended range of plate width to thickness ratios.

1.3.2 Concentrated Edge Loading

When a rectangular plate is subjected to a concentrated load the analysis becomes more difficult. Some of the analyses require the use of an approximate energy method if the deflected shape is not known; this happens when the boundary conditions are complicated.

The problem of a simply supported plate, which is compressed by two equal and opposite forces applied to the plate, as shown in figure (1.4a), has been investigated by Sommerfeld (24) in 1906 and a few years later in 1910, by Timoshenko (12). They came to the

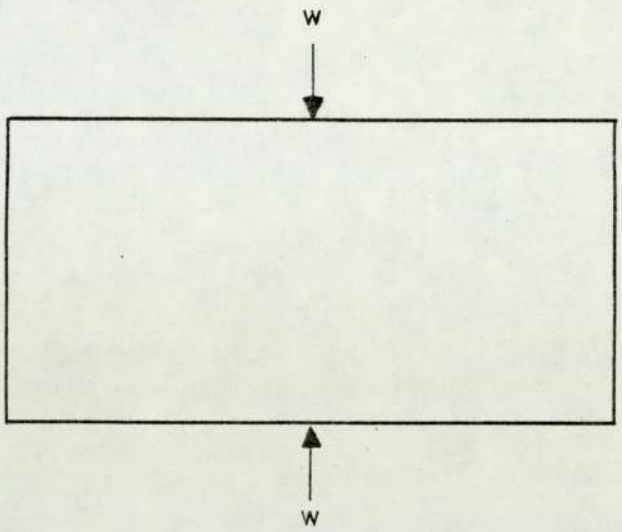

a. Plate examined by references (12), (25), (26) etc

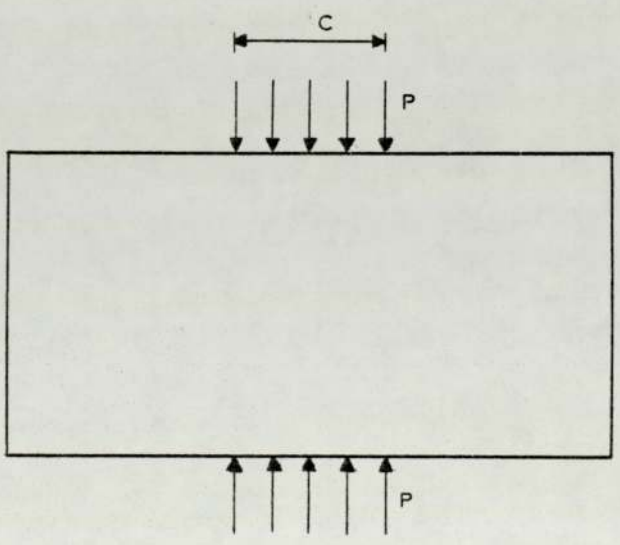

b. Plate examined by Yamaki

FIGURE 1.4 PLATE SUBJECTED TO CONCENTRATED LOADS.

conclusion that the plate will buckle when the applied load W has the value of $\frac{4\pi D_1}{b}$, where b is the distance between the loaded edges and D_1 is the plate rigidity.

The case of a plate subjected to a single load was first investigated by Girkman (25) in 1936 but his results were in a form unusable by engineers and applied to plates with an aspect ratio greater than 0.9.

In 1937 Leggett (26) investigated the same problem, that Timoshenko examined, when all the edges of the plate were simply supported. Leggett found that the critical load for an infinite plate is 12.5% larger than that estimated by Timoshenko.

In 1949 Hopkins (27) considered the case of a simply supported rectangular strip, subjected to loads distributed over small lengths of the longitudinal edges. His results were underestimated compared to Timoshenko's results by about 10%. This under-estimation is due to neglecting the extensional deformation of the middle surface during buckling in the manner of Timoshenko.

In 1952 Yamaki (28) investigated the buckling of a rectangular plate, under loads distributed uniformly along a certain range of two opposite edges as shown in figure (1.4b), using the integration method. For the boundary conditions of the plate, three different cases were considered; the loaded edges are always simply supported and the other two edges are simply supported, clamped or free. Unfortunately his results were not in agreement with the results obtained by Timoshenko. The results obtained by Timoshenko, Leggett, Hopkins and Yamaki are summarised in figure (1.5).

Zetlin (29) in 1952 using a Rayleigh-Ritz method of solution, studied the same problem as Girkman and presented his data in the form of graphs, which can easily be used by designers. He

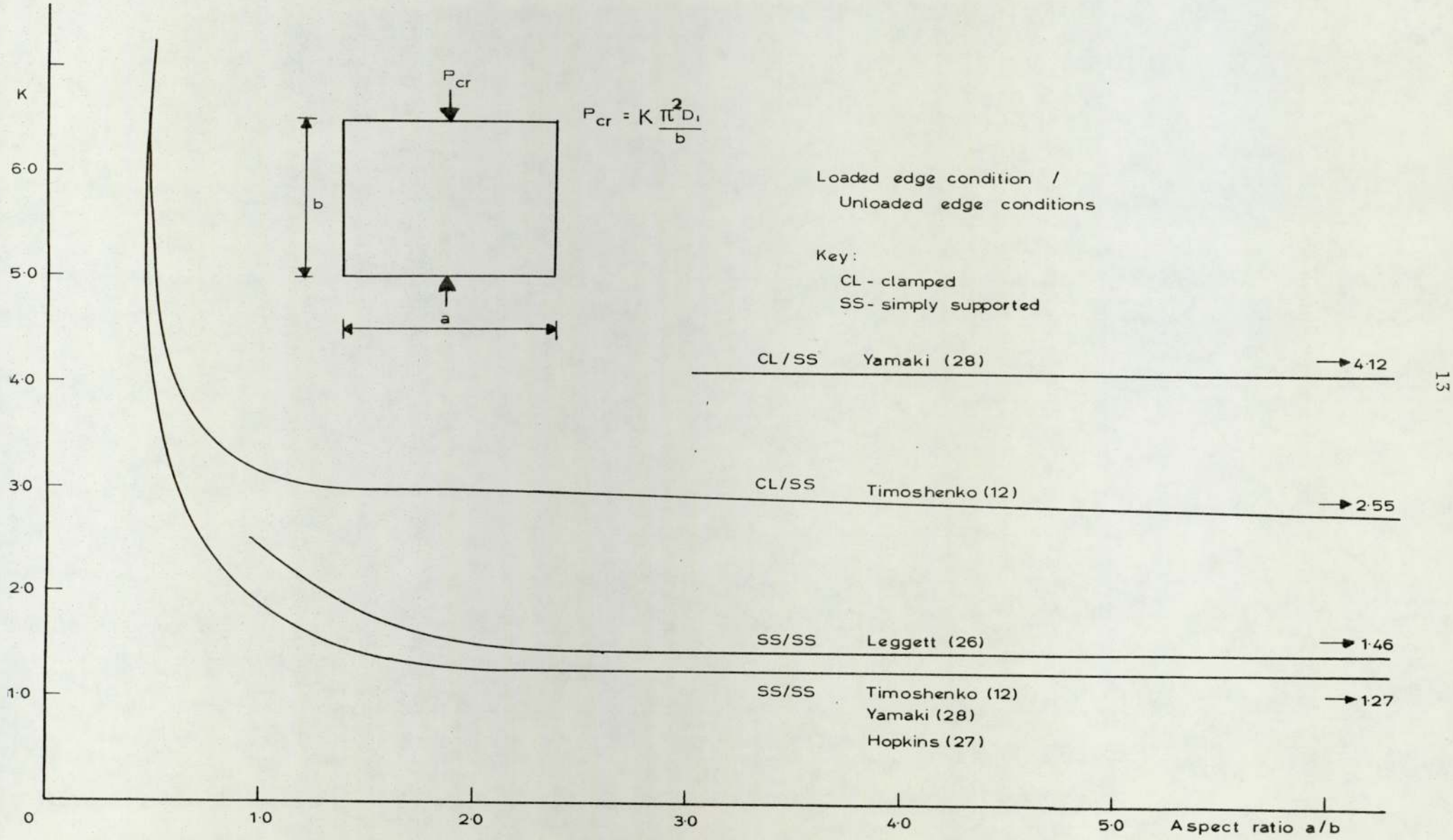

FIGURE 1·5 ELASTIC BUCKLING COEFFICIENT K FOR VARIOUS BOUNDARY CONDITIONS

considered a rectangular plate simply supported along all edges with the load W applied at mid-span along the top longitudinal edges over a length c. This load was balanced by shear stresses in a parabolic distribution along the vertical edges, as shown in figure (1.6). Zetlin showed that the buckling load W_{cr} of the plate under consideration can be obtained from the equation below.

$$\frac{W_{cr}}{ct} = K \frac{\pi^2 D_1}{b^2 t} \qquad 1.1$$

where

t is the thickness of the plate

b is the length of the loaded edge

K is the plate buckling coefficient

He provided values of K for different panel aspect ratio ρ and load length to plate length ratio λ_1. Equation (1.1) can be written as

$$W_{cr} = K \frac{\pi^2 D_1}{d} \frac{\lambda_1}{\rho} \qquad 1.2$$

where $\rho = \frac{b}{d}$ and $\lambda_1 = \frac{c}{b}$

and, therefore, the critical load W_{cr} can directly be calculated using equation (1.2). The values for K given by Zetlin are shown in table (1.1).

1.4 FURTHER PLATE BUCLKING THEORY

As has been stated earlier, the difficulty in the analysis of plate subjected to concentrated loads is to determine the deflected shape and the initial state of stress.

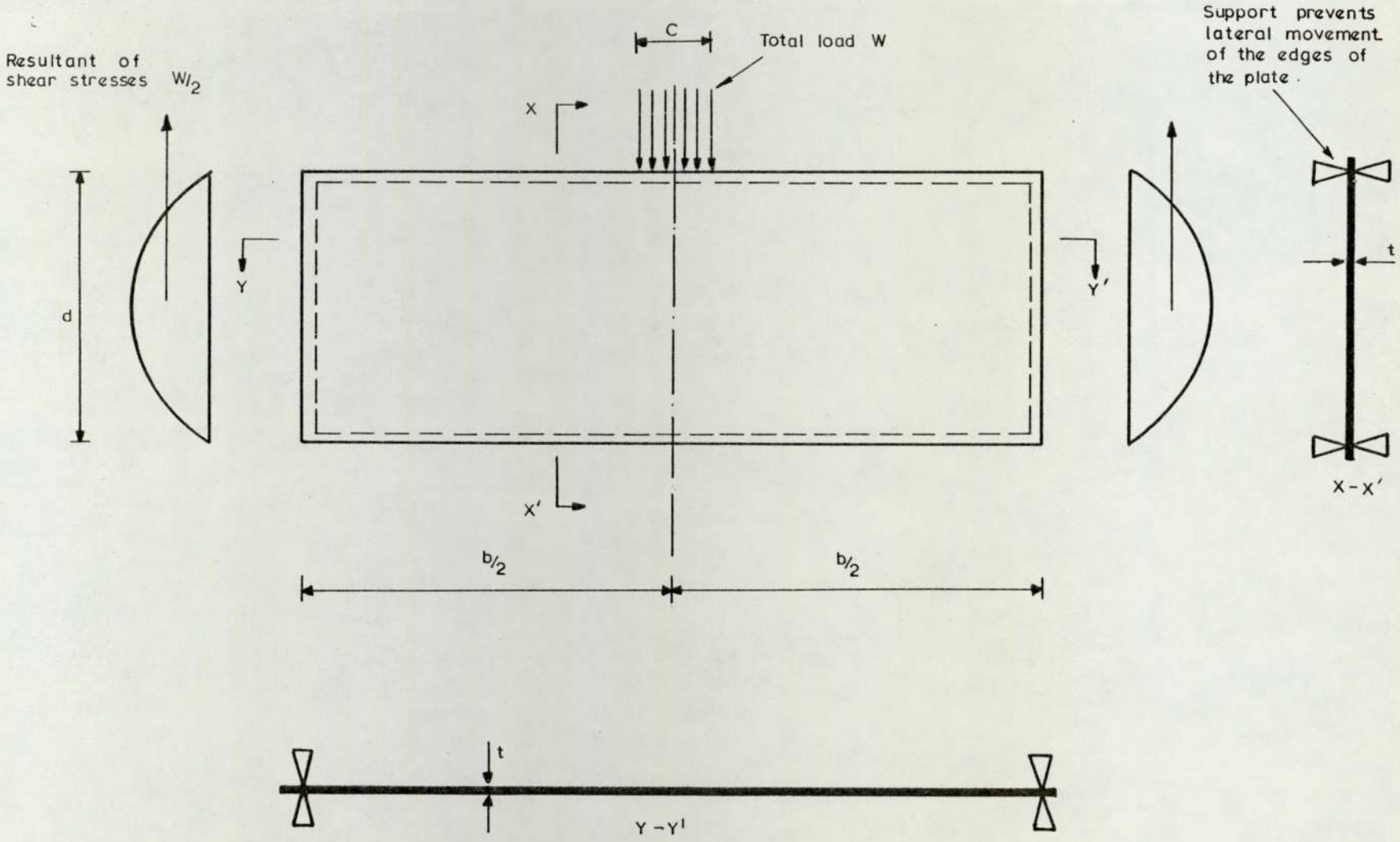

FIGURE 1.6 DETAILS OF STRUCTURAL SYSTEM SOLVED BY ZETLIN

Case No	p = b/d	λ_1 = c/b	K
1	2	1/65	378.00
2	2	1/20	116.30
3	2	1	10.67
4	1	1/65	216.00
5	1	1/20	67.30
6	1	1	6.20
7	1/4	1/65	559.00
8	1/4	1/20	169.20
9	1/4	1	26.60

TABLE 1.1 VALUES FOR THE BUCKLING COEFFICIENT K OBTAINED BY ZETLIN

In 1962 White and Cottingham (30), using the finite difference method considered the case of a plate simply supported on its bottom edge and loaded over a part of the top edge. The same loading condition has been examined by Zetlin, as shown in figure (1.7a). White and Cottingham presented their results in a graphical form, for plates of different support and geometric conditions. These results are reproduced in figure (1.8). Both investigators, Zetlin and White and Cottingham, agreed that the buckling coefficient K decreases as the length of the loading increases.

Several investigators such as Gallagher and Padlog (31), Kapur and Hartz (32) used the finite element techniques in determining the critical load of plates.

In 1969 Rockey and Bagchi (33), using the finite element method, solved the same problem investigated by Zetlin and White and Cottingham; the loading condition is shown in figure (1.7b). They considered cases of plates with the length to depth ratio values up to 2. By this method they dealt with the interaction of the flange and web plate, a factor which has not been considered in previous solutions. They showed how the flange members influence both the stress distribution of the web-plate and the combined structure. Their results are presented in a graphical form providing relationships between the critical load, the ratio of the load length to the length of the plate (c/b), the panel aspect ratio (b/d') and the ratio of the flange to web thickness (t_f/t). These results are reproduced in figure (1.9) and figure (1.10).

However in 1967 Alfutov and Balabukh (34), (35) introduced a simplified theoretical method, using the energy method, in which only a statically determinate stress distribution and a deflected shape were needed to be formulated.

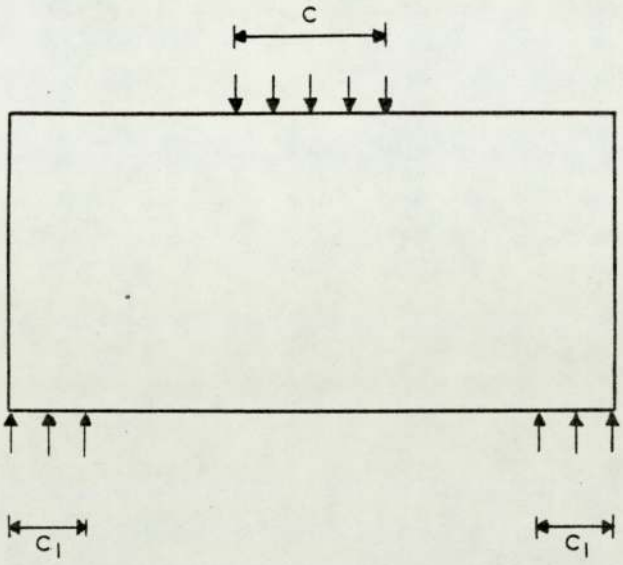

a. Plate examined by White and Cottingham

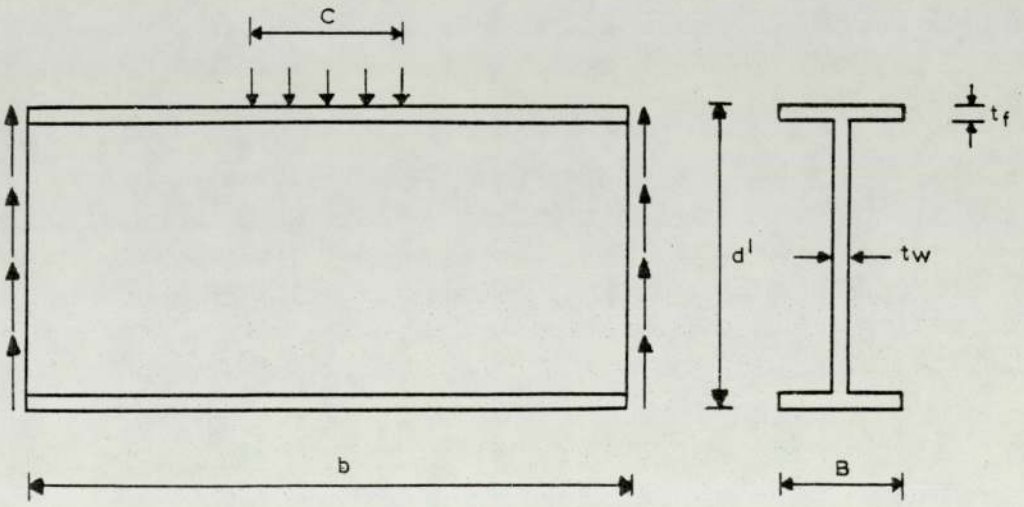

b. Plate examined by Rockey and Bagchi

FIGURE 1.7 PLATE SUBJECTED TO CONCENTRATED LOADS ON ONE SIDE.

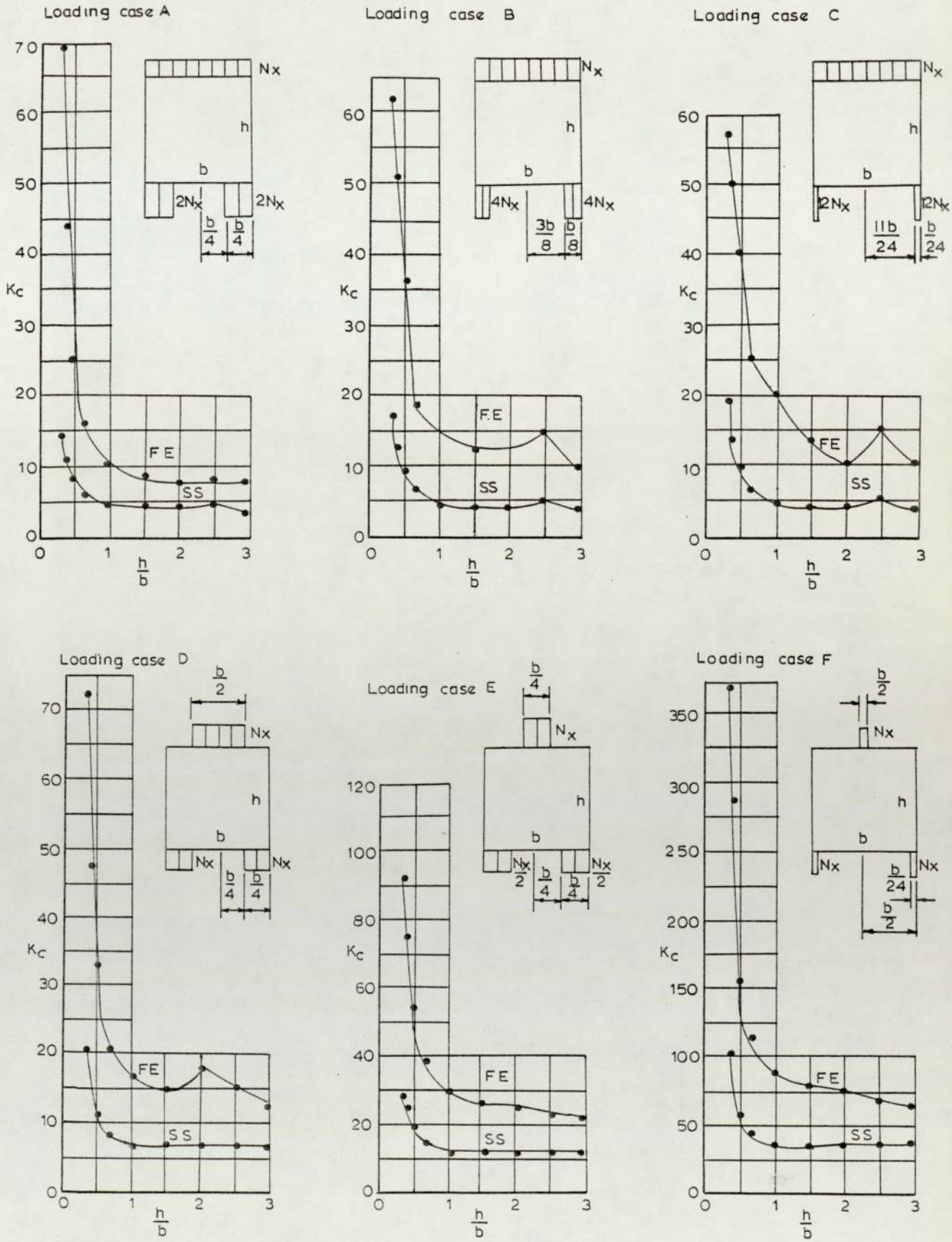

$$N_{x\,cr} = K_c \left(\pi^2 \, D_1 / b^2\right)$$

FIGURE 1.8 RESULTS OBTAINED BY WHITE AND COTTINGHAM

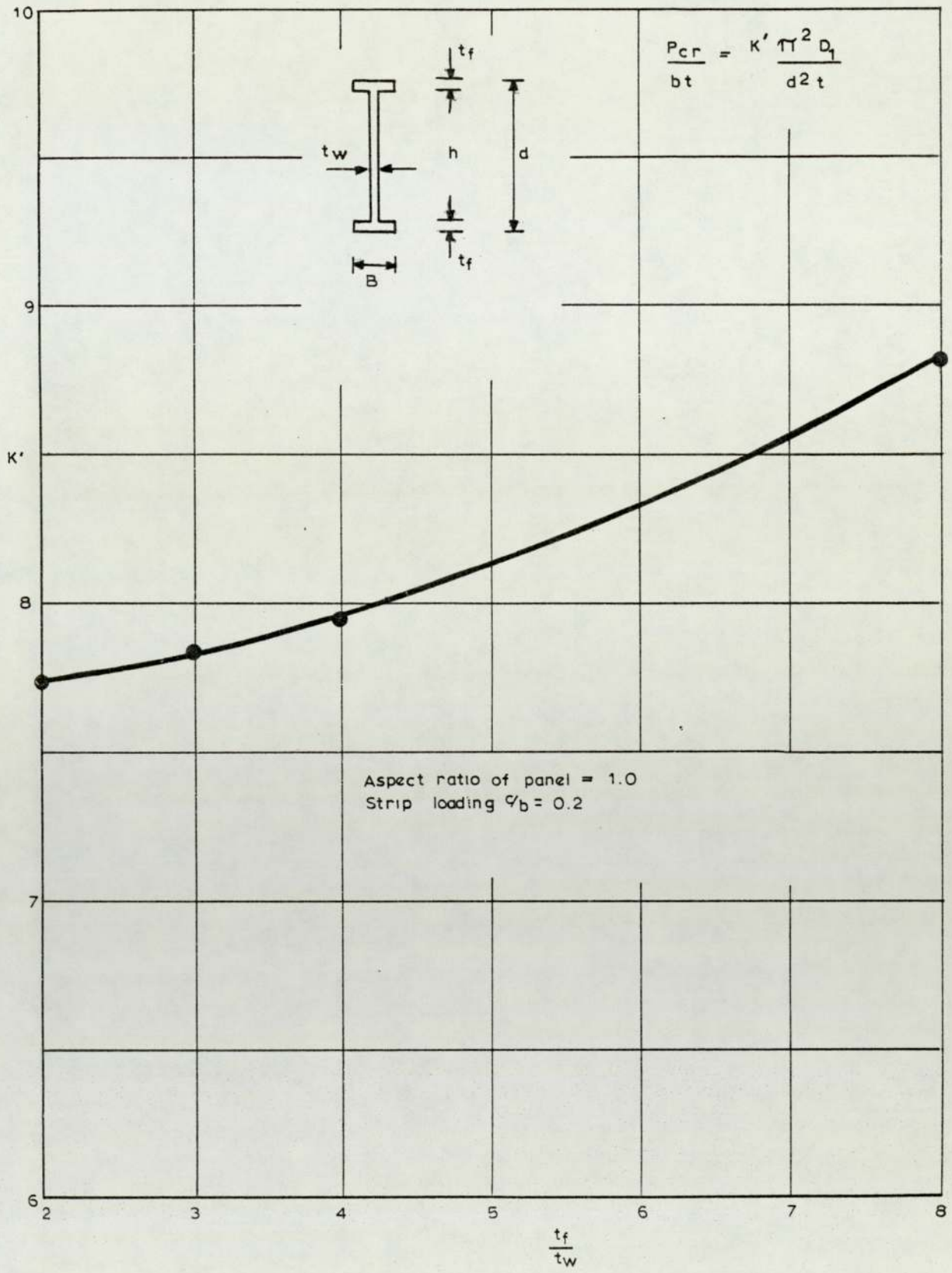

FIGURE 1.9 RESULTS OBTAINED BY ROCKEY AND BAGCHI

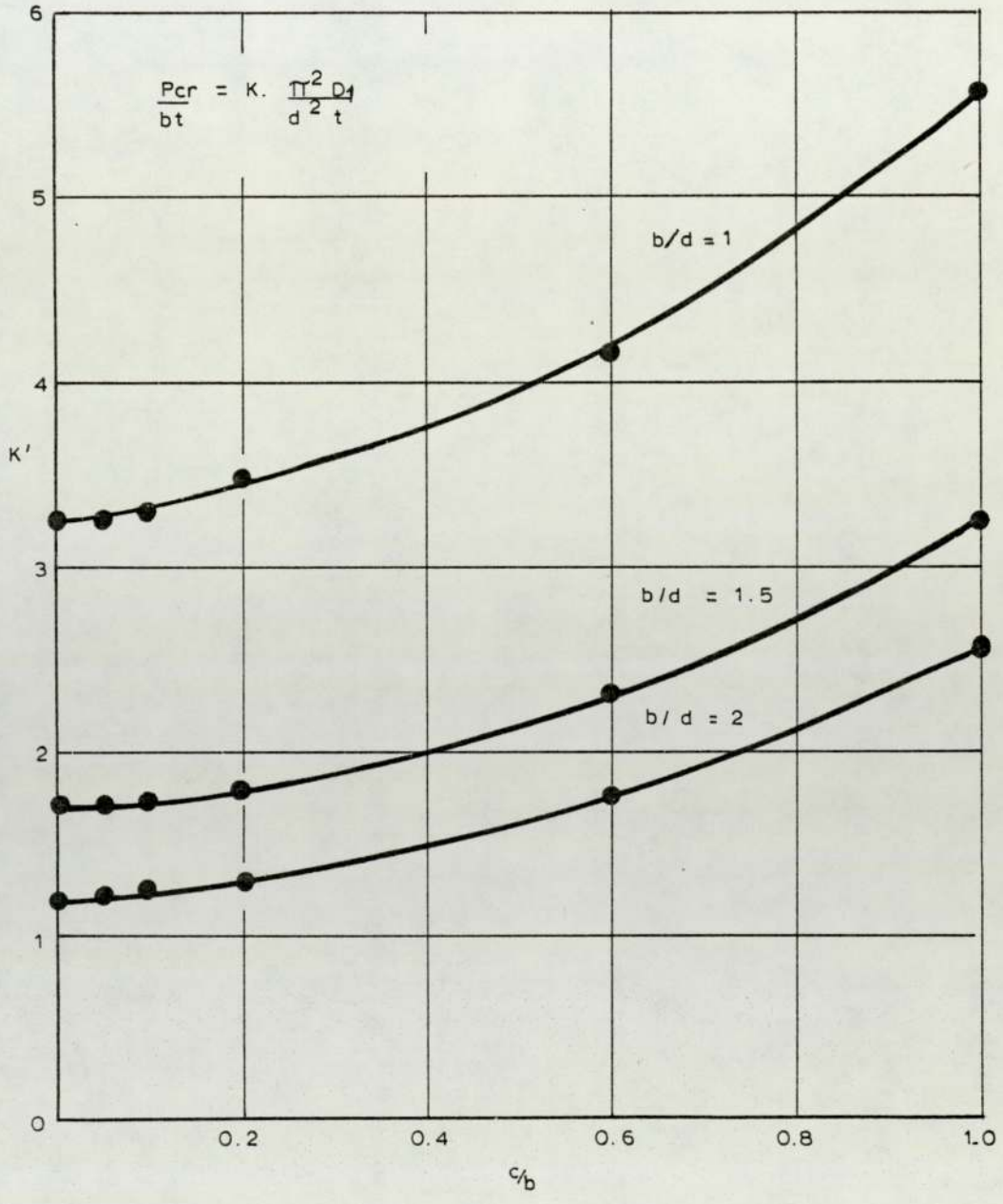

FIGURE 1.10 RESULTS OBTAINED BY ROCKEY AND BAGCHI

Khan and Walker (36) in 1972 adopted the above method and obtained buckling loads which agree to within 5 per cent with those calculated using the more laborious finite element method. The critical load can be obtained using equation (1.3).

$$P_{cr} = K \frac{\pi^2 D_1}{b^2} \qquad 1.3$$

This expression has a similar form to the formula for the critical load of a plate, uniformly loaded on two opposite edges. Some of the results obtained by these investigators are shown in figure (1.11) and table (1.2).

Typical results, obtained by the mentioned investigators, for various boundary conditions are shown in table (1.3). Rockey and Bagchis' results are in good agreement with those by Khan and Walker and Zetlin for a point load. For the case, though, when the plate is loaded over the whole length Zetlin overestimates the critical load specifically for an aspect ratio of 4.0 and c/B = 1.0; this overestimation is about 16%.

1.5 INELASTIC PLATE BUCKLING

It is known that after a perfectly flat plate buckles at the elastic critical stress σ_{cr}, it is possible to carry additional loads as the lateral deflections grow sufficiently large to harness the extra resistance due to stretching of the middle plane. Finally due to plasticity, the plate fails and a maximum value of applied stress σ_{max} is reached. It is, therefore, true to state that $\sigma_{max} > \sigma_{cr}$ for postbuckled rectangular plates. However, it is possible for break down of the material to occur when the plate is still flat and before σ_{cr} is reached. When this happens, the plate buckles and collapses at a lower value of applied stress than σ_{cr}, so that

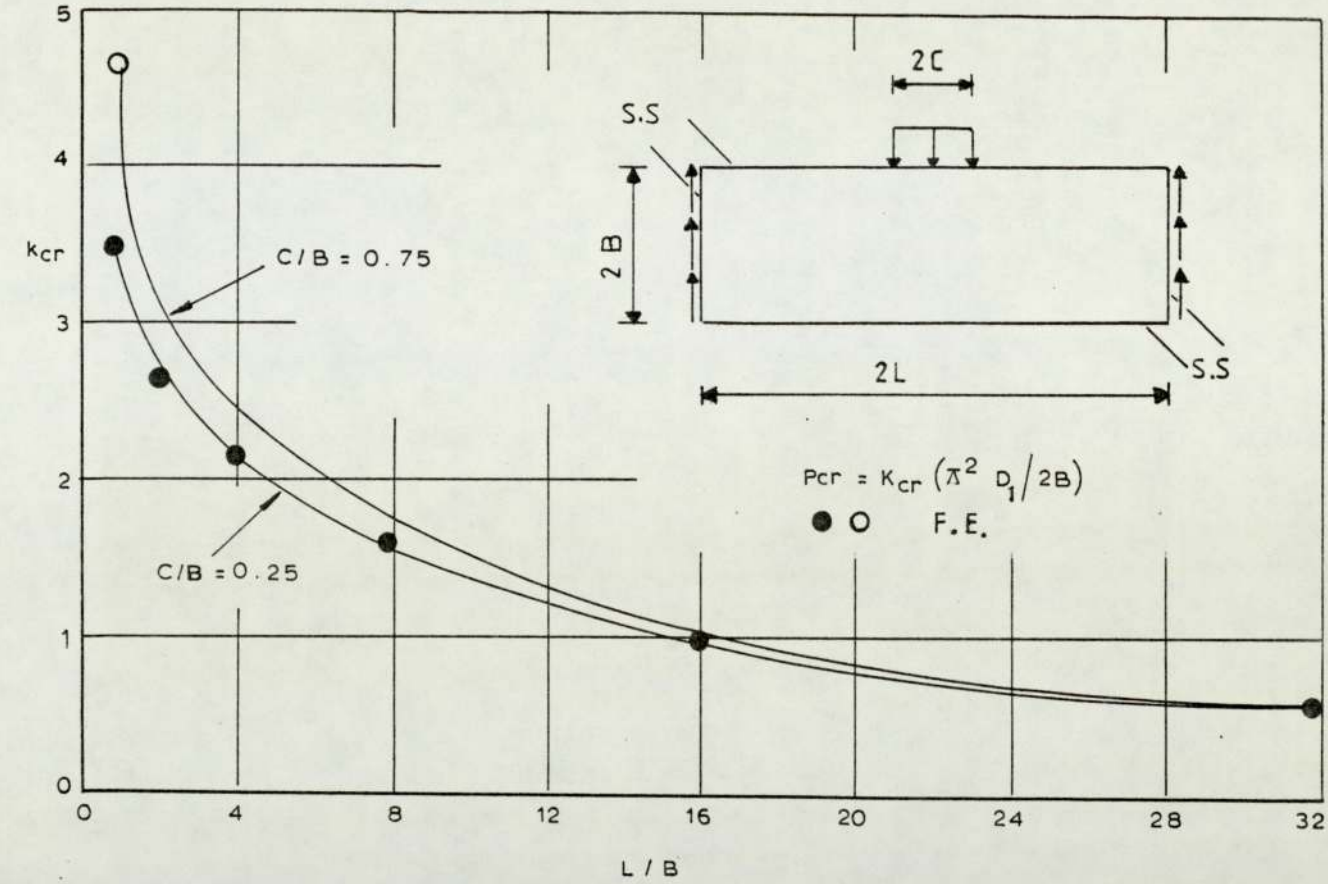

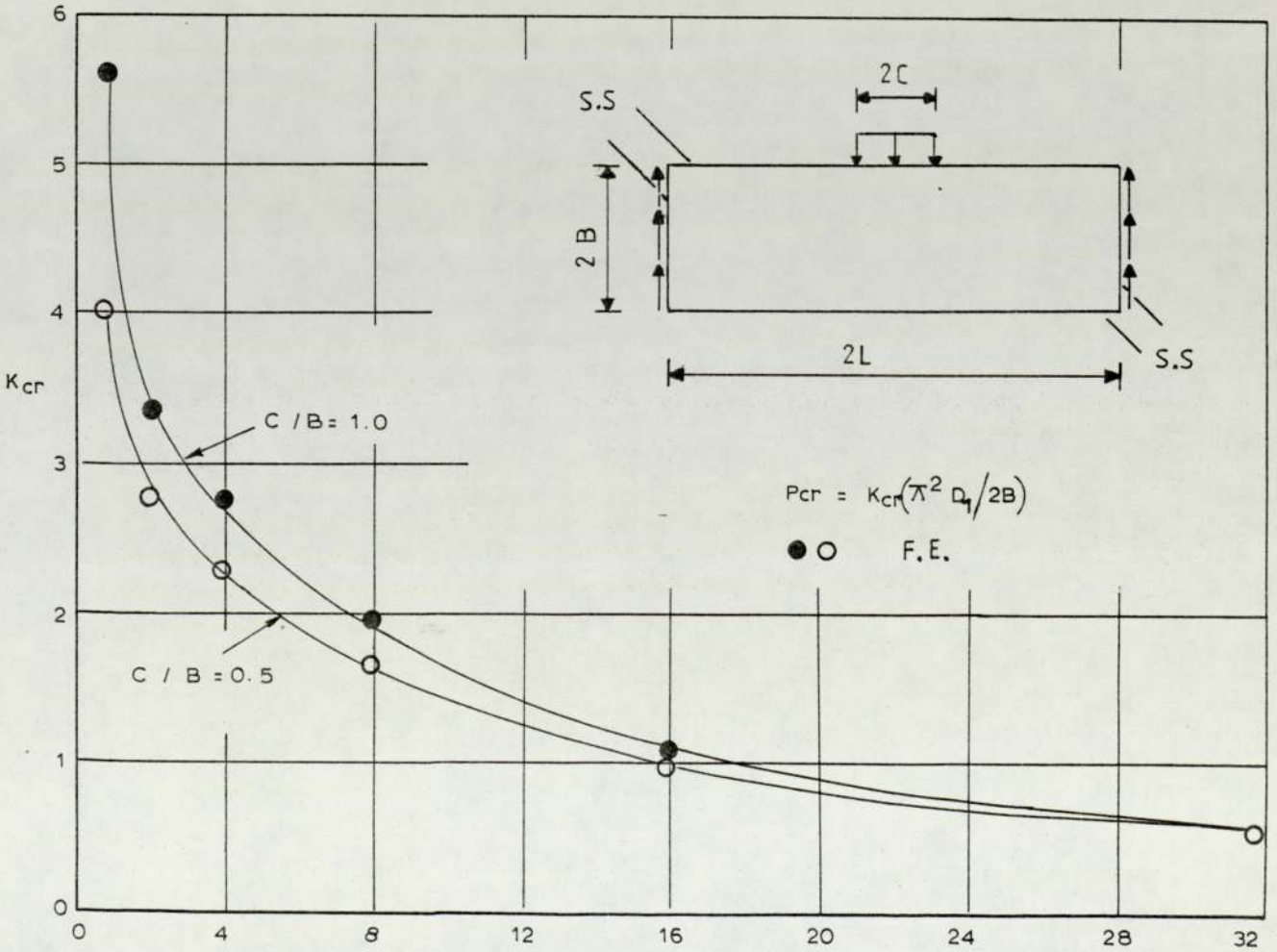

FIGURE 1.11 RESULTS OBTAINED BY KHAN AND WALKER

A/B	$c_1/2B$	c/B	K_{cr}
1.0	0	0.25	2.84
1.0	0	0.50	3.42
1.0	0	1.00	4.39
1.0	0.25	0.50	3.47
2.0	0	0.50	2.67
3.0	0	0.50	2.46
2.0	0	0.25	2.50
4.0	0	0.25	2.12
8.0	0	0.25	1.60
16.0	0	0.25	0.98
32.0	0	0.25	0.53
2.0	0	1.0	3.21
4.0	0	1.0	2.74
8.0	0	1.0	1.95
16.0	0	1.0	1.05
32.0	0	1.0	0.53
4.0	0	0.5	2.27
8.0	0	0.5	1.69
16.0	0	0.5	0.99
4.0	0.25	1.0	2.88
4.0	0.25	0.5	2.40
4.0	0.25	0.25	2.26
4.0	0.50	1.0	3.01
4.0	0.50	0.5	2.52
4.0	0.50	0.25	2.37
4.0	0.375	0.75	2.69
6.0	0.125	0.50	1.96
6.0	end shears	0.50	2.05

$$P_{cr} = K_{cr} \ (\pi^2 D/2B)$$

TABLE 1.2 CRITICAL COEFFICIENT USING FINITE ELEMENTS

Investigator	Boundary Conditions	K_{cr}
Timoshenko Hopkins Yamaki	SS/SS†	1.27
Leggett	SS/SS	1.46
Khan and Walker	SS/SS	1.48 1.62*
Timoshenko	FE/SS††	2.55
Yamaki	FE/SS	4.12
Khan and Walker	FE/SS	4.22*

† Simply supported

†† Fixed/Simply supported

* Obtained by an Approximate Method

TABLE 1.3 VALUES OF CRITICAL COEFFICIENT K_{cr}

$\sigma_{max} < \sigma_{cr}$. This is known as inelastic or plastic buckling.

The inelastic buckling theory for plates parallels to a great extent the inelastic buckling of struts. Shanley (37) has shown that the effective value of the Reduced modulus $\overline{E}$ for a strut, introduced by Engesser, Considère and Von Karman was the Tangent modulus E_t.

Many attempts have been made to introduce the laws of plastic theory into plate buckling analysis. In 1940, Bijlaard (38) and in 1947 Ilyushin (39) used the total strain theory to define stress/strain relationships.

In 1946 Gerard (40) solved the problem of a simply supported plate subjected to a uniform edge loading, using a secant modulus method. He verified his results with small scale tests, on alluminium alloy specimens which showed good agreement with the theory.

Stowell (41) in 1948 modified the plate buckling theory of Ilyushin, using the total strain theory. This theory states that the relationship between stress and strain takes the form $\sigma = E_s \varepsilon$, where E_s is the Secant modulus, for material which is being loaded. He presented a table of plastic reduction factors η, the ratio of the minimum buckling stress to the minimum elastic stress, in terms of the Secant modulus of elasticity E_s, the Tangent modulus of elasticity E_t and the Young's modulus of elasticity E.

Gerard and Becker (15) have summarised the work of many other authors providing plasticity reduction factors for a number of different cases.

1.6 PUBLISHED TEST RESULTS AND EMPIRICAL METHOD OF ANALYSIS

A large number of tests, performed on steel rolled beams and plate girders subjected to concentrated loads, have been published.

Usually these test results are accompanied by theoretical, semi-empirical or purely empirical formulas and suggestions for design. These recommendations, mainly concern beams with thin webs, with stiffeners at the supports and at the load points, and not with universal beam sections which have relatively thick webs.

In 1913 Moore (42) reported some 40 tests on steel I-beams with various loading and end restraining conditions. He also made some observations on the variation of steel strength with its location in the beam cross section. In the report the difficulty of distinguishing between the final failure pattern and the initial cause of failure of the tested beams is pointed out.

Moore and Wilson (43) in 1916 published results of tests on six I-beams and two built up girders. These tests were made to study the web strains in I-beams and girders, so designed that the primary failure would be a web failure. Two types of failure were observed; diagonal shear buckling of the web and torsional buckling of the beam rotating in plan about a vertical axis at mid-span.

As previously mentioned Glanville in 1931 reported ten tests on rolled steel beams, carried out for the British Steelwork Association.

In 1932 Ketchum and Draffin (44) reported tests made on rolled steel I-beams with various loading and restraining conditions. These tests were performed on beams with upper flanges restrained from sideways buckling, with upper flanges free to buckle sideways and compression of the web over a bearing block. For the latter case the investigators stated that it is the distance from the inner edge of the bearing block to the end of the beam and not the length of the block itself which determines the ultimate bearing strength of the beams.

Lyse and Godfrey (45) in 1934 published some tests on rolled steel beams and on sections made from plates by welding for a large range of depth to thickness ratio of the web. The investigators came to the conclusion that no possibility of web-buckling existed for beams with a depth to thickness ratio up to 70. It is clearly stated that buckling may be expected to occur at a depth to thickness ratio of the web of 80 or more. However, the authors were mostly concerned with the incidence of shear buckling.

Winter and Pian (46) in 1946 performed some 136 tests on cold formed steel sections. They concluded that the failure loads were irrespective of the depth of the section; they also provided two empirical expressions for the ultimate load of the beam, depending on the location of failure.

In 1947 Wastlund and Bergman (47) published results of tests performed on welded steel I-girders, subjected to shearing stresses, normal stresses (bending moments) and combined shearing and normal stresses. They discussed appropriate factors of safety against buckling of webs and also provided a general design procedure. In their report it is stated that the theoretical critical load of plane web-plates bears no direct relation to the ultimate load and the ratio of the ultimate loads to the theoretical load increases with the slenderness ratio of the web.

A considerable amount of theoretical and experimental work has been done on plate girders. The design and analysis of plate girders involve problems such as buckling of the web plate and yielding of the compression flange. Massonnet (48) (1) discusses the behaviour of plate girders in great detail. In the former reference some tests on plate girders conducted by Thurlimann and Basler are reported.

Many problems connected with plate girders having stiffened web-plates have been examined by Rockey (49) (50) (51) who evolved a simple criterion for the minimum rigidity of flanges from experiments. Similar work has been done by Skaloud (52), (53).

All the above mentioned researchers concur to demonstrate that buckling of the web of a plate girder is a progressive phenomenon which does not involve a sudden collapse of the girder as the buckling of a column, due to progressive growth of membrane stresses.

In 1974 Delesques (54) published some work, based on some 60 tests performed by other researchers. He provided formulae for practical applications and curves which simplify the use of these formulae.

Recently, in 1977 a research programme was completed in the Department of Civil Engineering, University of Aston, supported by the Construction Industries Research and Information Association. In the final report RP.219 (55) some 50 tests are described carried out on universal beam sections. The test programme included various degrees of top flange restraint and load eccentricities. Two distinct types of failure were observed. The first was an elastic torsional buckling failure in which the top flange rotated relative to the bottom flange about a vertical axis through mid-span. The second type of failure was characterised by yielding of the top flange and elastoplastic buckling or crushing of the web area adjacent to the applied load.

Guy (56) in 1977 published some tests on several universal beam section sizes having various types of loading conditions. The majority of the beams were tested by loading with two opposite loads, thus eliminating the effects of bending and shear.

Most of the mentioned authors presented excellent theoretical

work but they failed to produce any experimental results which would indicate the validity of their theories. Unfortunately, such theories without any experimental evidence cannot be considered in design.

1.7 CONCLUSIONS FROM PREVIOUS WORK AND SCOPE OF PRESENT INVESTIGATION

When rolled steel beams are subjected to concentrated loads, applied on their flanges they behave in a complex manner and many variables are involved. Such variables are the geometrical and physical properties of the beams as well as the various stresses induced due to the loading type and supporting conditions. The known published works have considered many of the variables, unfortunately they often failed to examine the influence of a particular variable on the ultimate strength of the beam so firm conclusions could not be drawn. Only Winter and Pian examined certain variables and their results are used for design of cold formed sections in America.

In view of these gaps in the behaviour of rolled steel beams, when acted upon by concentrated loads, it was felt that more systematic tests on universal beam sections, examining only a particular variable at any one time, should be undertaken. Obviously, the range of each variable will be limited for the present work and these limitations will be stated in the relevant chapters. The results to be obtained from these tests, would be compared with the various design practices and theories associated with the strength of universal beam sections and examine the factor of safety of these practices. Further theories or semiempirical theories might be needed to be developed, where more consideration will be given

to the investigated variables.

The proposed tests will be performed on universal beam sections, simply supported, loaded on one flange and supported at the ends. These tests will be so designed that failure will be expected either at the centre of the beam, under the applied load, or at the end at the support.

CHAPTER 2

EXPERIMENTATION AND INSTRUMENTATION

2.1 INTRODUCTION

This chapter refers to the experimental details and procedures employed for the tested beams. Due to the large number of tests conducted for this work, a total number of ninety, it is impractical to refer individually to each test. Therefore, a rather general description of the experimentation and instrumentation will be outlined here.

The tests were performed on grade 43 mild steel rolled universal beam sections, supplied by a steel stockholder. Imperfections like dents, bends and flame cut ends were removed by cold sawing.

All the beams were simply supported and according to the location of failure they were broadly divided into two groups. In the first group are those tested for end failure and in the other, those tested for central failure.

2.1.1 Sections of Tested Beams

The universal beam sections used for testing were chosen to give a range of web depth to thickness (d/t) ratio. For the present study this ratio varies from 56.7 to 24.1. The majority of the tests were performed on the 254 x 102 x 22 kg and 406 x 140 x 39 kg universal beam sections. Some of the tested beams had certain of their dimensions altered by reducing the flange thicknesses or widths.

Table (2.1) shows all the universal beam sections used for the present study with the corresponding depth to thickness ratio of the web.

Metric U.B. Size D(mm) x B(mm) x kg/m	Depth to thickness Ratio d/t
457 x 191 x 98	35.5
406 x 140 x 39	56.7
254 x 102 x 28	35.1
254 x 102 x 28†	35.1
254 x 102 x 25	36.8
254 x 102 x 22	38.7
254 x 102 x 22†	38.7
254 x 102 x 22*	38.7
152 x 89 x 17.09	24.1

* Indicates Flange Width Reduced

† Indicates Flange Thickness Reduced

TABLE 2.1 BEAM SERIAL SIZES USED IN THE TESTS

2.1.2 Referencing of Tested Beams

According to the type of loading, type of support, point of application of load and the variables investigated the tests are classified into eight series, defined by I to VIII.

The beams are identified by numerals and in some cases where beams were tested for end failure at both ends, by suffices a and b and are considered as separate tests. There is a certain amount of cross referencing and any coincident results will be shown with different series where necessary.

2.1.3 Description of Series of Tested Beams

All the beams were tested simply supported on various lengths of span; this length was determined by the distance between the centres of the supports. Beams tested for central failure had an overhang of 75 mm at each end and beams tested for end failure had a total of 150 mm overhang.

The beams included in series I to V were tested for end failure and the beams of series VI to VIII for central failure. For the beams tested for end failure the load was vertically applied to the top flange through a stiff bearing plate, 100 mm long and 65 mm thick. These tests, as stated above, were arranged so that failure would occur at the end. To enable this to happen a stiffening clamp was fixed to the web of the beams of series I to VI to prevent failure under the applied load. This device will be discussed in a following section. At the end where failure was expected to occur, the support was different for each series and will be described below. The support at the other end was kept the same for all the above mentioned series. It consisted of a bearing plate, 100 mm long, situated across the full width of the flange. All the series of the tested

beams are shown diagrammatically in figure (2.1) and are described in detail below.

Series I - All the beams in this series, except beam No 3, were supported by a 12.7 mm long stiff bearing across the full width of the flange of the beam. Between the stiff bearing and the beam a packing plate was placed as shown in figure (2.1). The length of the plate l_e was varied for each test but the support was always at the end of the plate and the beam. Beam No 3 was supported in a similar manner, the difference being that the plate and 12.7 mm long stiff bearing plate were continuous and the plate was bolted to the beam.

Series II - Beams in this series were supported in a similar manner to series I, the difference being that the centre line of the 12.7 mm long stiff bearing was always in line with the centre line of the top plate. The thickness of the plate for test Nos 1, 2a and 2b in this series was varying.

Series III - Beams in this series were supported on a 12.7 mm long stiff bearing without a packing plate. The distance of the centre line of the stiff bearing to the end of the beam, denoted by l_k, was varied for each test. Certain beams in this series had their dimensions altered and were tested for a constant value of l_k.

Series VI - Beams in this series were supported on a fixed bearing plate, as shown in figure (2.1). The length of this plate l_s was varied for each test.

Series V - Beams in this series were supported on a 12.7 mm long stiff bearing situated at the end of the beam, as shown in figure (2.1). The point of application of the applied load was varied along the beam. The distance of the centre line of the 100 mm long

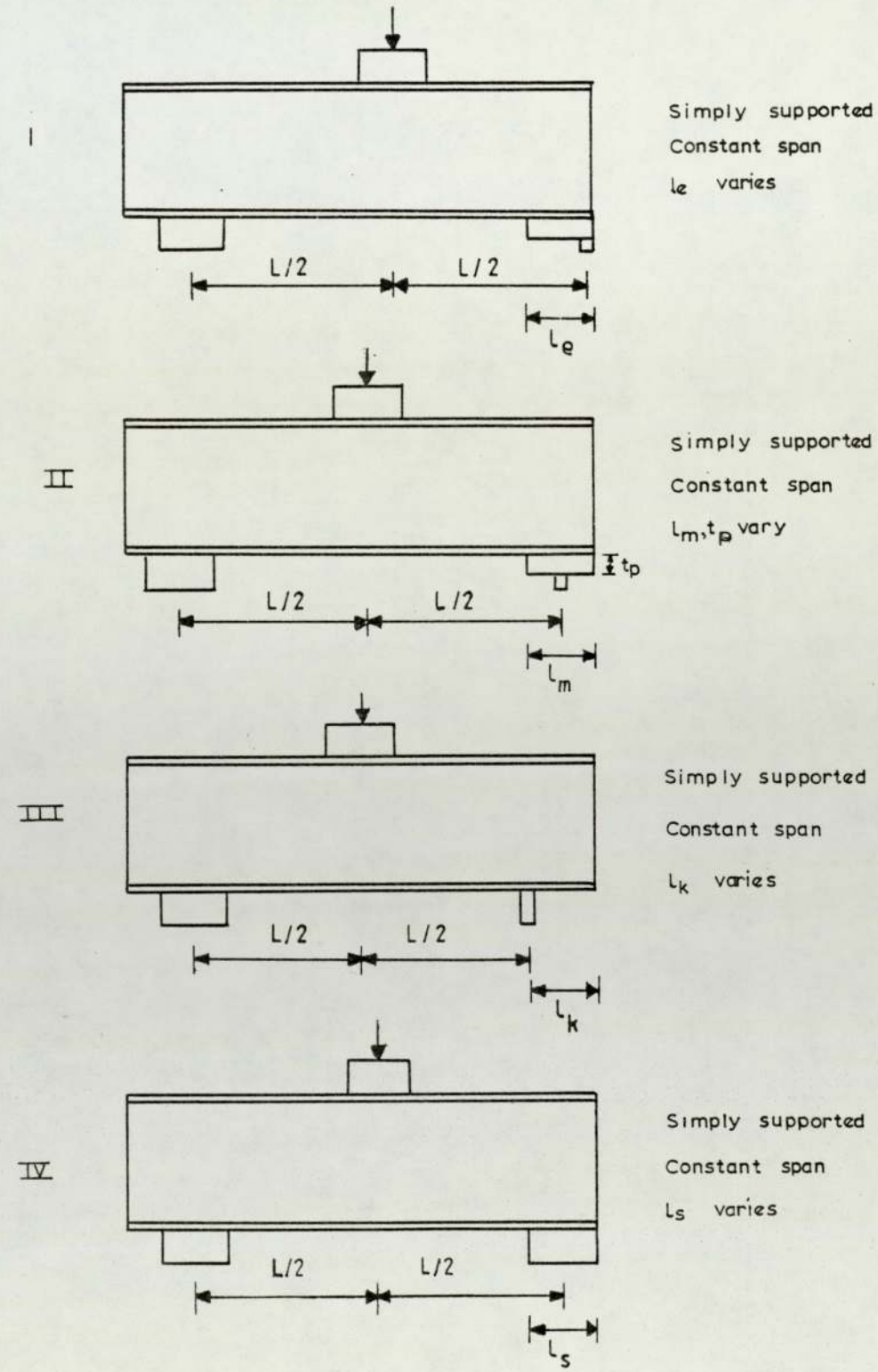

FIGURE 2.1. SUMMARY OF TEST SERIES I TO VIII

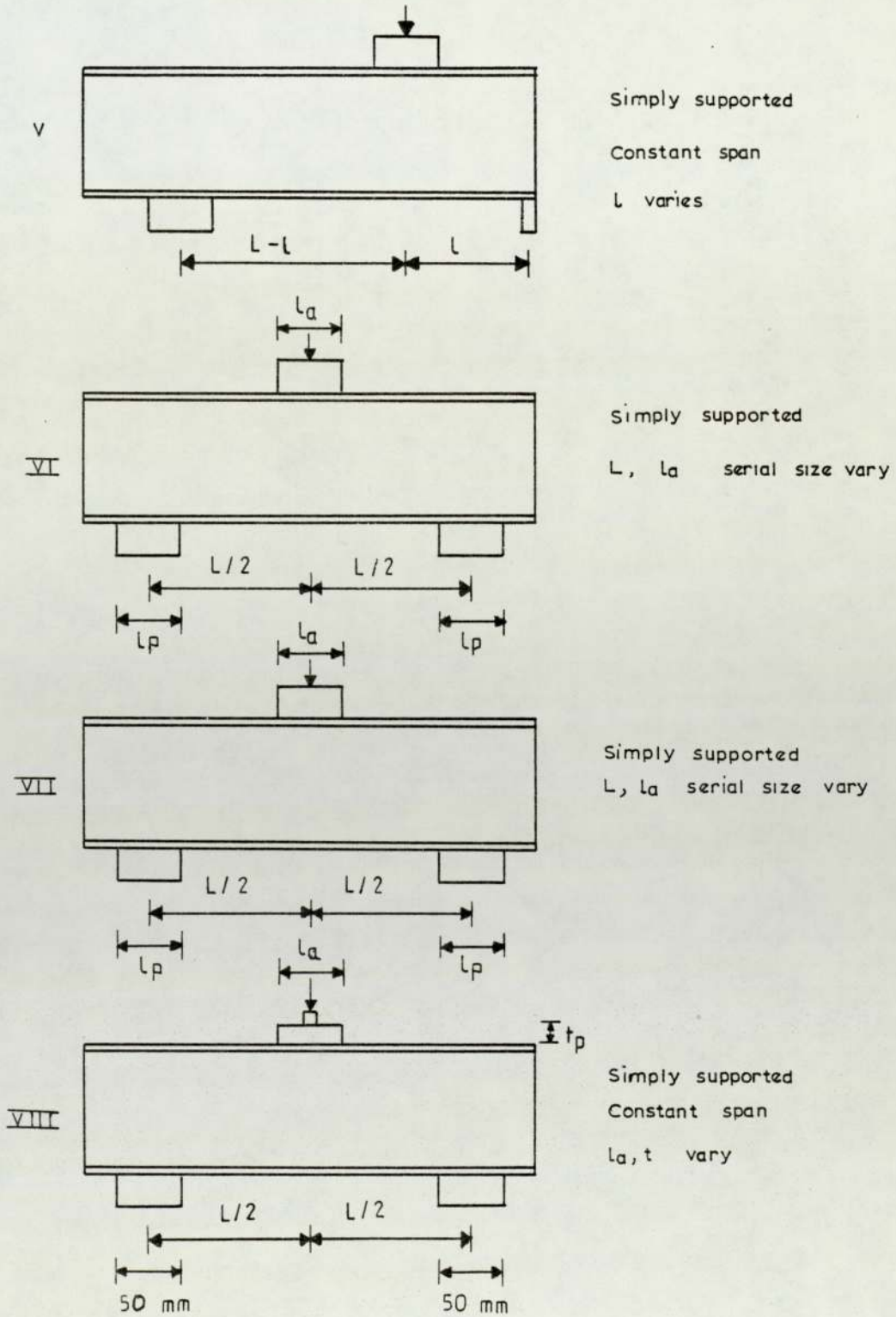

FIGURE 2.1. CONTINUED

plate, on the top flange, to the centre line of the 12.7 mm stiff bearing is denoted by 1. For this series, as has previously been mentioned, the stiffening clamp was not used.

Series VI - Beams in this series were rested on stiff bearings of lengths l_p, as shown in figure (2.1). The load was applied through another stiff plate on the top flange at mid-span. The length of this stiff plate l_a was varied for beams of a constant span. The same procedure was repeated for different lengths of span and different beam sections.

Series VII - Beams in this series were supported by stiff bearings of length l_p at both ends and loaded through another stiff plate, placed on the top flange of the beam at mid-span, of constant length l_a for various lengths of span. The same procedure was repeated for different beam sections and different lengths of l_p and l_a.

Series VIII - Beams in this series were supported in the same way as the beams in series VI. The load was applied at mid-span through a stiff bearing of 12.7 mm long placed in the middle of another plate of length l_a. The parameter under investigation for the beams of this series was the thickness of the above mentioned plate.

2.2 DETERMINATION OF PROPERTIES OF BEAM MATERIAL

In order to determine the properties of the material in the beams, tensile tests were performed on specimens. These specimens were obtained from a sample length, cold sawn from each 12 m length of universal beam section supplied. Some tensile tests were also performed on specimens cut from the material of the spreader plates.

2.2.1 Tensile Tests

Two types of tensile tests were performed, one using large tensile specimens and another using small tensile specimens. For all the lengths large specimens were prepared except for small beam section sizes, where this was impossible, and where only a small length of beam was available. In these cases small specimens were taken. In a few cases both types of specimens were taken for the purpose of cross-checking of the results.

Each tensile test is referred to by numerals such as T1, T2, T3 etc and so beams will refer to the particular material test to which it relates. A complete list of the beams tested in the present work is given in table (2.2), which shows the tests carried out in each test series, the test number, the serial size of the beam section and the reference number of the 12m length from which each beam was cut.

The tensile tests for the spreader plates are identified by TP1, TP2, TP3, etc and large tensile test specimens were used for this purpose.

2.2.1.1 Large Tensile Test Specimens

Specimens were cold-sawn from each sample length to 275-300 mm long. The location of these specimens in relation to the beam cross-section is shown in figure (2.2a) and in an isometric view in figure (2.2b). It was impossible to have these specimens taken from beams with overall depth D of less than 250 mm, as these would have been too short to ensure adequate grip in the jaws of the testing machine.

The cold sawn specimens were then machined to a uniform rectangular cross-section and their cross-sectional dimensions were

Test Series	Test No	Serial Size D(mm) x B(mm) x kg/m	Material Test Reference
I	11a	254 x 102 x 22	T3
	7a	254 x 102 x 22	T2
	7b	254 x 102 x 22	T2
	6b	254 x 102 x 22	T2
	8a	254 x 102 x 22	T2
	8b	254 x 102 x 22	T2
	3	254 x 102 x 22	T17
II	11a	254 x 102 x 22	T3
	5a	254 x 102 x 22	T2
	5b	254 x 102 x 22	T2
	6a	254 x 102 x 22	T2
	10a	254 x 102 x 22	T3
	12	254 x 102 x 22	T3
	1	254 x 102 x 22	T17
	2a	254 x 102 x 22	T17
	2b	254 x 102 x 22	T17
III	4b	254 x 102 x 22	T1
	11b	254 x 102 x 22	T3
	13a	254 x 102 x 22	T3
	13b	254 x 102 x 22	T3
	14	254 x 102 x 22	T3

TABLE 2.2 BEAM SERIES AND SERIAL SIZES

Test Series	Test No	Serial Size D(mm) x B(mm) x kg/m	Material Test Reference
III	15	254 x 102 x 22	T4
	16	254 x 102 x 22	T4
	18	254 x 102 x 22	T4
	20	254 x 102 x 22	T5
	22	254 x 102 x 22	T5
	36*	254 x 102 x 22	T10
	37*	254 x 102 x 22	T10
	38*	254 x 102 x 22	T10
	39†	254 x 102 x 28	T9
	40†	254 x 102 x 28	T9
	41†	254 x 102 x 28	T9
	42†	254 x 102 x 28	T9
	43†	254 x 102 x 28	T9
IV	4b	254 x 102 x 22	T1
	26a	254 x 102 x 22	T6
	25a	254 x 102 x 22	T6
	25b	254 x 102 x 22	T6
	26b	254 x 102 x 22	T6
	24b	254 x 102 x 22	T6
	27	254 x 102 x 22	T6
	28	254 x 102 x 22	T6

* Flange Width Varied

† Flange Thickness Varied

TABLE 2.2 (CONTINUED)

Test Series	Test No	Serial Size D(mm) x B(mm) x kg/m	Material Test Reference
IV	R1b	254 x 102 x 25	T7
	R1a	254 x 102 x 25	T7
	R2	254 x 102 x 25	T7
V	4b	254 x 102 x 22	T1
	23b	254 x 102 x 22	T5
	23a	254 x 102 x 22	T5
	29a	254 x 102 x 22	T8
	29b	254 x 102 x 22	T8
VI	31	254 x 102 x 22	T8
	30	254 x 102 x 22	T8
	32	254 x 102 x 22	T8
	33	254 x 102 x 22	T8
	34	254 x 102 x 22	T8
	50	254 x 102 x 22	T10
	51	254 x 102 x 22	T10
	52	254 x 102 x 22	T10
	53	254 x 102 x 22	T10
	62	406 x 140 x 39	T15
	63	406 x 140 x 39	T15
	60	457 x 191 x 98	T14
	61	457 x 191 x 98	T14

TABLE 2.2 (CONTINUED)

Test Series	Test No	Serial Size D(mm) x b(mm) x kg/m	Material Test Reference
VI	64	406 x 140 x 39	T15
	65	406 x 140 x 39	T15
	66	406 x 140 x 39	T15
	67	406 x 140 x 39	T15
	68*	254 x 102 x 22	T16
	69*	254 x 102 x 22	T16
	70*	254 x 102 x 22	T16
	71*	254 x 102 x 22	T16
	72*	254 x 102 x 22	T16
	73*	254 x 102 x 22	T16
	74*	254 x 102 x 22	T16
	75*	254 x 102 x 22	T16
VII	44	254 x 102 x 22	T10
	35	254 x 102 x 22	T10
	45	254 x 102 x 22	T10
	46	254 x 102 x 22	T10
	48	254 x 102 x 28	T9
	47	254 x 102 x 28	T9
	49	254 x 102 x 28	T8
	58	406 x 140 x 39	T11
	59	152 x 89 x 17.09	T13

TABLE 2.2 (CONTINUED)

Test Series	Test No	Serial Size D(mm) x B(mm) x kg/m	Material Test Reference
VII	54	406 x 140 x 39	T11
	55	406 x 140 x 39	T11
	56	406 x 140 x 39	T11
	57	406 x 140 x 39	T12
VIII	77	254 x 102 x 22	T17
	76	254 x 102 x 22	T17
	78	254 x 102 x 22	T17
	79	254 x 102 x 22	T17
	80	254 x 102 x 22	T17

TABLE 2.2 (CONTINUED)

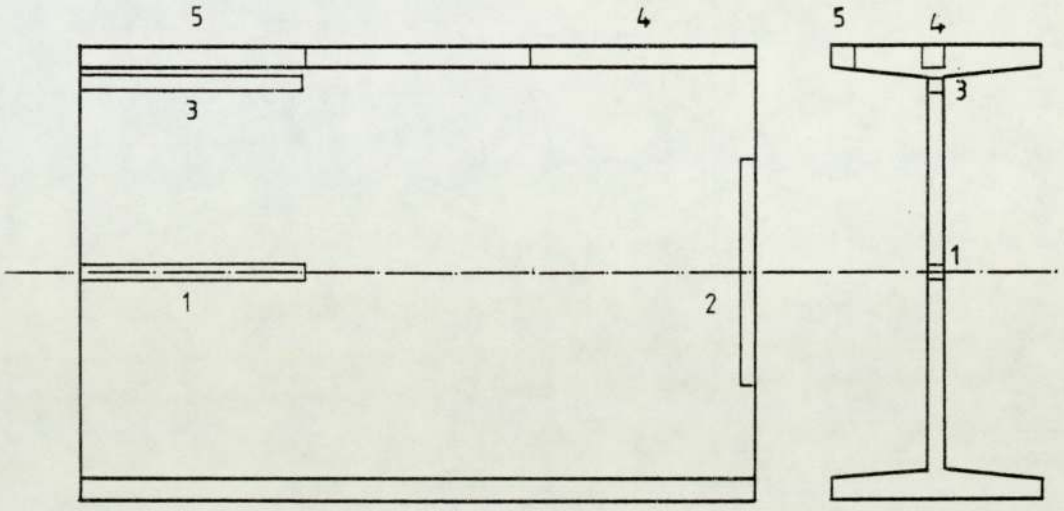

a. Large Tensile Test Specimens Location

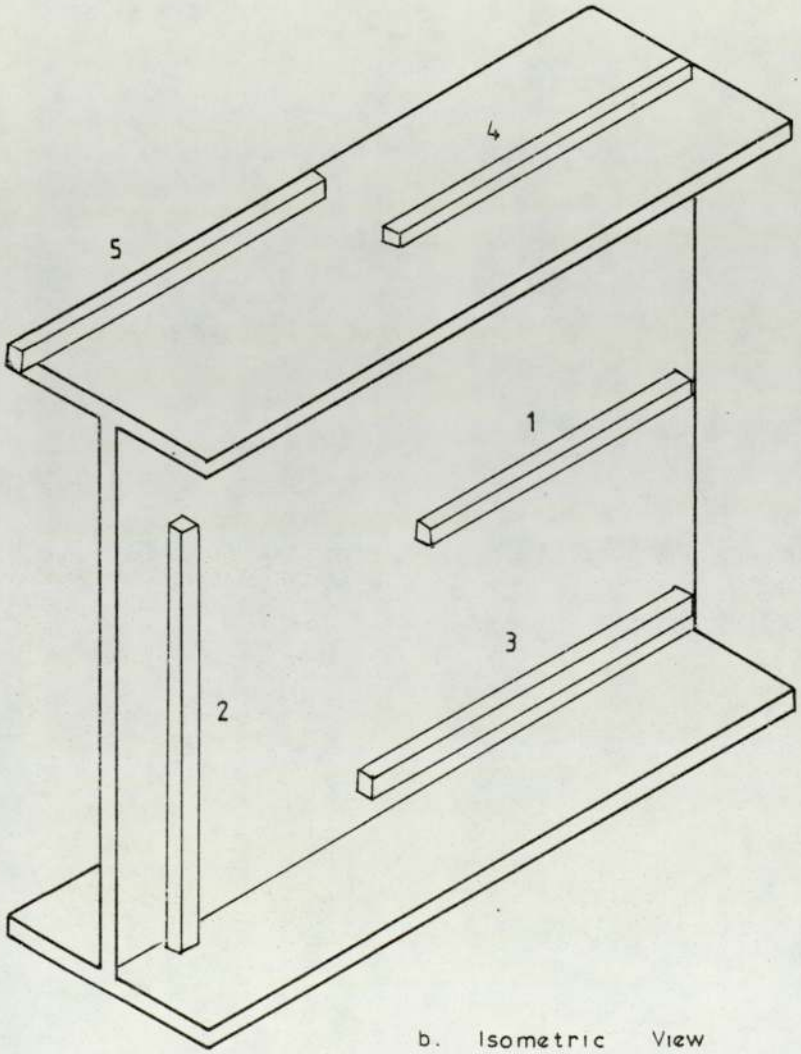

b. Isometric View

FIGURE 2.2 LARGE TENSILE TEST SPECIMENS

accurately measured. These specimens were tested in a Denison hydraulic compression-tension testing machine, which incorporates a 50 mm gauge length strain recorder and automatic plotter.

2.2.1.2 Small Tensile Test Specimens

These specimens were cold sawn from localised areas at the locations of the beam cross-section shown in figure (2.3a). They were machined to the shape and dimensions of a Hounsfield specimen No 12, as shown in figure (2.3b). After recording the dimensions of these specimens they were tested in a Hounsfield tensometer.

The small specimens were taken as a check on the results obtained by the previous method and also to investigate any variation in the material strength with location in the beam cross-section.

2.2.2 Tensile Test Results

The material characteristics obtained from the tensile tests were the yield stress f_y, the ultimate stress f_{ult} and the modulus of elasticity E at various locations in the cross section for each 12 m length. The resulting values of these material properties, of each individual specimen of all the tensile tests, are shown in table (2.3). In the same table are also shown the average yield and ultimate stresses for the web and flange and the yield stress, the ultimate stress and modulus of elasticity for the section as a whole.

The results for the tensile tests performed for determination of the properties of the material are shown in table (2.4).

2.2.3 Observation from the Tensile Test Results

As can be seen from the tensile test results, shown in table (2.3), the beam material at the junction of the web and the flange of the beam has in many cases a yield stress value somewhat lower

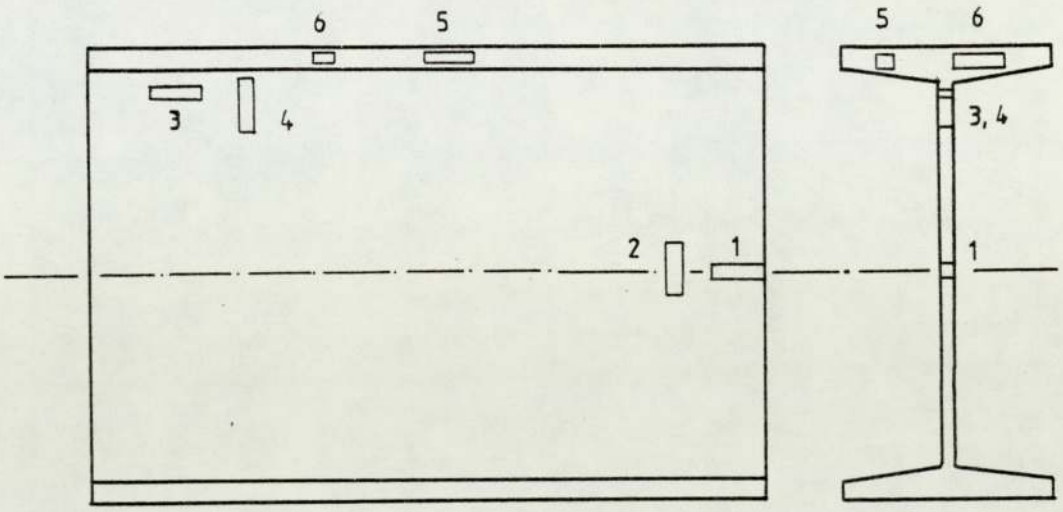

a. Small Tensile Test Specimens Location

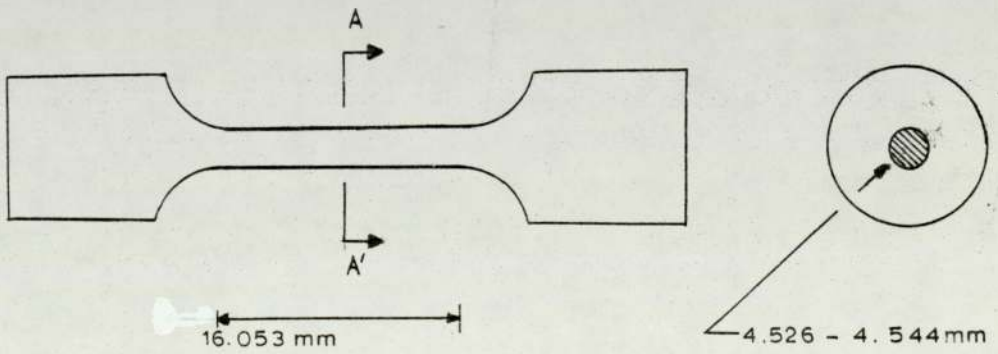

b. Hounsfield Tensile Specimen No 12

FIGURE 2.3 SMALL TENSILE TEST SPECIMENS

Tensile Test	Specimen Type	Properties	Specimen 1	Specimen 2	Specimen 3	Specimen 4	Specimen 5	Specimen 6	Web	Flange	Overall
T1	Large	f_y N/mm^2	298.99	322.15	290.26	299.56	290.77		300.42	295.17	297.78
		f_{ult} N/mm^2	479.95	482.96	481.37	477.24	477.15		481.41	477.20	479.30
		E kN/mm^2	207.05	209.53	205.97	219.46	198.26				208.06
T2	Large	f_y N/mm^2	309.29	323.98	294.27	293.36	303.18		305.45	298.27	301.86
		f_{ult} N/mm^2	471.26	437.65	478.57	469.38	472.40		466.51	470.89	468.70
		E KN/mm^2	186.48	188.68	191.13	188.91	183.93				187.83
T3	Large	f_y N/mm^2	323.76	342.99	316.11	314.37	302.57		324.74	308.47	316.61
		f_{ult} N/mm^2	469.39	476.82	458.60	464.82	464.40		465.85	464.61	465.23
		E kN/mm^2	181.09	202.42	188.08	203.50	198.67				194.75

TABLE 2.3 TENSILE TEST RESULTS

Tensile Test	Specimen Type	Properties	Specimen 1	Specimen 2	Specimen 3	Specimen 4	Specimen 5	Specimen 6	Web	Flange	Overall
T4	Large	f_y N/mm^2	324.62	336.41	305.74	304.12	286.76		318.13	295.44	306.76
		f_{ult} N/mm^2	477.61	468.38	459.02	474.82	460.37		466.01	467.60	466.80
		E kN/mm^2	191.27	215.65	194.12	221.17	191.59				202.76
T5	Large	f_y N/mm^2	317.43	345.51	345.99	327.34	330.06		338.73	328.70	333.72
		f_{ult} N/mm^2	459.31	468.24	465.29	469.65	451.02		464.53	460.34	462.43
		E kN/mm^2	194.34	210.40	190.89	203.11	210.93				201.94
T6	Large	f_y N/mm^2	299.39	323.66	316.71	322.59	298.79		314.12	310.69	312.41
		f_{ult} N/mm^2	448.50	458.70	467.58	476.10	449.44		460.59	462.77	461.68
		E kN/mm^2	185.99	213.07	189.69	194.67	197.73				196.23

TABLE 2.3 (CONTINUED)

Tensile Test	Specimen Type	Properties	Specimen 1	Specimen 2	Specimen 3	Specimen 4	Specimen 5	Specimen 6	Web	Flange	Overall
T7	Large	f_y N/mm^2	329.12	340.46	299.23	327.93	311.20		317.01	319.57	318.29
		f_{ult} N/mm^2	464.55	482.32	461.40	497.43	486.34		467.42	491.89	479.65
		E kN/mm^2	206.34	189.46	200.48	193.44	195.09				196.90
T8	Large	f_y N/mm^2	336.78	352.67	316.52	314.11	316.02		320.56	315.07	322.84
		f_{ult} N/mm^2	489.86	493.18	486.01	48(.21	487.71		500.85	483.96	486.37
		E kN/mm^2	204.11	201.18	194.48	182.53	198.10				196.08
T9	Large	f_y N/mm^2	344.92	355.95	290.69	297.25	279.28		320.56	288.27	304.41
		f_{ult} N/mm^2	509.17	500.39	496.92	490.29	483.16		500.85	486.73	493.79
		E kN/mm^2	207.47	217.81	205.68	198.78	202.48				206.44

TABLE 2.3 (CONTINUED)

Tensile Test	Specimen Type	Properties	Specimen 1	Specimen 2	Specimen 3	Specimen 4	Specimen 5	Specimen 6	Web	Flange	Overall
T10	Small	f_y N/mm^2	302.25	287.05	309.85	322.24	331.01	309.85	305.35	320.43	312.89
		f_{ult} N/mm^2	501.96	501.96	495.77	501.96	505.76	477.17	498.87	491.47	495.17
		E kN/mm^2	-	-	-	-	-	-			-
T11	Large	f_y N/mm^2	378.82	378.18	340.28	311.83	365.88		359.39	338.86	349.12
		f_{ult} N/mm^2	495.93	506.06	496.82	481.47	506.61		498.91	494.04	496.48
		E kN/mm^2	196.80	199.65	202.51	198.60	208.09				201.13
T11	Small	f_y N/mm^2	333.88	325.29	376.16	312.28	358.36	378.69	336.91	368.53	352.72
		f_{ult} N/mm^2	506.29	519.42	507.74	504.28	510.36	522.83	509.45	516.60	513.02
		E kN/mm^2	-	-	-	-	-	-			-

TABLE 2.3 (CONTINUED)

Tensile Test	Specimen Type	Properties	Specimen 1	Specimen 2	Specimen 3	Specimen 4	Specimen 5	Specimen 6	Web	Flange	Overall
T12	Large	f_y N/mm 2	384.90	382.05	375.45	342.63	377.38		379.46	360.01	369.73
		f_{ult} N/mm 2	494.16	511.38	469.48	503.12	497.14		486.13	500.13	493.14
		E kN/mm 2	198.44	196.04	203.65	200.40	195.48				198.80
T13	Small	f_y N/mm 2	337.98	327.27	374.24	315.20	348.36	388.69	338.66	368.53	353.60
		f_{ult} N/mm 2	516.19	509.79	504.14	494.44	520.96	532.00	506.14	526.48	516.31
		E kN/mm 2	-	-	-	-	-	-			-
T14	Large	f_y N/mm 2	279.17	264.08	265.43	249.93	257.19		268.53	253.56	261.05
		f_{ult} N/mm2	436.06	439.15	463.29	448.74	435.06		450.45	441.90	446.18
		E kN/mm2	197.06	215.80	180.97	204.49	191.94				198.05

TABLE 2.3 (CONTINUED)

Tensile Test	Specimen Type	Properties	Specimen 1	Specimen 2	Specimen 3	Specimen 4	Specimen 5	Specimen 6	Web	Flange	Overall
T15	Large	f_y N/mm^2	385.64	338.65	297.76	322.42	353.82		329.95	338.12	334.04
		f_{ult} N/mm^2	507.76	547.11	465.59	494.63	499.37		496.51	497.00	496.76
		E kN/mm^2	194.77	194.78	173.24	196.35	229.76				197.78
T16	Large	f_y N/mm^2	342.22	355.24	320.78	330.60	305.98		334.76	318.29	326.53
		f_{ult} N/mm^2	488.32	490.05	475.92	485.51	475.96		482.55	480.74	481.64
		E kN/mm^2	200.07	175.17	194.41	202.41	194.27				193.27
T17	Large	f_y N/mm^2	346.93	353.26	324.91	320.86	327.77		337.50	324.32	330.91
		f_{ult} N/mm^2	493.70	496.58	494.16	483.75	529.04		494.65	506.40	500.52
		E kN/mm^2	216.83	204.92	201.49	197.45	207.02				205.54

TABLE 2.3 (CONTINUED)

Tensile Test	Plate Thickness t_p/mm	Beam No	f_y N/mm^2	f_{ult} N/mm^2	E kN/mm^2
TP1	10.0	77, 80, 1	271.74	424.10	200.16
TP2	15.0	76, 78, 2a	268.42	409.69	192.13
TP3	20.0	78, 2b	320.44	462.61	208.59
TP4	25.0	3	256.29	422.61	200.12
TP5	39.0	79	303.05	475.10	205.65

TABLE 2.4 TENSILE TEST RESULTS FOR SPREADERS

than the material in the web and the flange. This is probably due to the hot rolling process during manufacture, because of the rate of heat dispersion from the section when cooling. It is also clear from these results that the material at the junction of the web and the flange was well rolled since the specimens cut from this part of the beam had an ultimate strength as high as the specimens cut from the web or the flanges.

The yield stress was found to vary with the thickness of the section and the thinner the section the higher the yield stress. This could be explained for the same reason given above. The ultimate stress was reasonably constant as well as the modulus of elasticity at a mean value of 199.04 kN/mm^2. Both types of tensile tests were performed on specimens from beam with physical properties T11, so the results can be compared. The small specimens give values for the overall yield stress of 1.03% higher than those of large specimens, while the overall ultimate stress of the section was 3.33% higher than the values obtained from the large specimens. However this variation is small and can be neglected.

The guaranteed tensile yield stress for a grade 43 rolled steel beam, given by the manufacturer(57) is 250 N/mm^2. The average yield stress obtained from the tensile test results is well above this value, at a mean of 322.56 N/mm^2.

For the purpose of comparing the test results with current design practices and theoretical predictions the actual values, obtained from the tensile tests, will be used.

2.3 PREPARATION OF BEAMS

A brief description of the preparation of the beams is outlined in this section. From lengths of the standard sections

provided by the supplier, usually 12 m long, required lengths were cold sawn to an accuracy of ±0.5 mm. Some of the beams had their dimensions altered. In series III beam Nos 36, 37 and 38 and in series VI beam Nos 68, 69, 70, 71, 72, 73, 74 and 75 of the serial size 254 x 102 x 22 kg, had the width of both flanges reduced to obtain a range of flange width to thickness ratio (B/T). Also in series III beam Nos 39, 40, 41, 42 and 43 of the serial size 254 x 102 x 28 kg had the thickness of both flanges reduced, to obtain a range of flange to web thickness ratio (T/t).

All the beams were cleaned with a wire brush and afterwards painted with white-wash which has been found useful in showing stress lines. It was hoped that these lines would help to indicate the critical load and give a general stress distribution in the beam.

2.3.1 Test Beams Dimensions

Due to manufacturing imperfections there was a variation in the cross-sectional dimensions of the tested beams. Therefore, the dimensions of each individual beam were measured before testing by means of a vernier caliper and a micrometer, both calibrated to an accuracy of 0.01 mm. This was so that the actual dimensions of the beams be included in any relevant theory when considered and also a comparison could be made between the manufacturers specified dimensions and the actual dimensions of the beams.

The dimensions measured were the overall depth of the section D, the width of the flanges B, the thickness of the web t and the thickness of the flanges T. The depth between the root fillets d was not included in the measured dimensions since this measurement will not be accurate due to the root radius. The overall

depth D was measured in the plane of the web at both ends of the beam and the width of both flanges was measured along the beam at about 150 mm intervals. These measurements were done by means of a vernier caliper. The thickness of the web was measured at five points across the depth of the web, at every quarter depth and adjacent to the root radius. From these measurements it was noticed that the lesser value was that corresponding to the mid-depth of the section. The web is thicker adjacent to each flange, usually over a depth of approximately 50 mm, than at the centre by 2-5%. The thickness of the flanges was measured mid-way between the web and the flange edges.

The average values of the measured dimensions of all the beams are shown in table (2.5). Also in the same table is recorded the initial eccentricity of the web. To determine this reading the beam was set with its flange edges on the bed of a planing machine, as shown in figure (2.4). Measurements were taken to the centre of the web at its junction with each flange and the centre of the web at mid-depth, marked A_1, B_1 and C_1 respectively. The distances y_1, y_2 and y_3 from the machine bed to the web face at the above points were measured with a vernier caliper. A stiff steel straight edge was placed on the other flange edges and the distances y'_1, y'_2 and y'_3 were also measured. From the known thickness of the web the required eccentricity of the web could be determined. It was generally noticed that the more slender the web the greater the initial curvature. The maximum eccentricity of the web recorded was 1.18 mm for the beam No 13.

2.3.2 Instrumentation

Instrumentation was needed to measure strains at a number of points on the web surface, lateral deflections of the web and vertical

Beam No	Overall Depth D	Flange Width B	Web Thickness t	Flange Thickness T	Overall Length L'	Web Eccentricity e
1	256.22	102.63	5.99	6.70	1150	0.22
2	256.40	102.41	6.02	6.72	1150	0.17
3	256.41	102.31	5.89	6.66	1150	0.08
4	256.46	102.54	6.35	6.78	1150	0.07
5	256.77	101.62	6.29	6.99	1150	0.14
6	256.62	101.70	6.26	6.73	1150	0.06
7	256.67	101.64	6.29	6.70	1150	0.12
8	256.30	101.79	6.23	6.80	1150	0.31
10	256.56	101.67	6.26	6.79	1150	0.11
11	256.48	101.65	6.22	6.86	1150	0.07
12	256.43	101.65	6.23	6.80	1150	0.24
13	256.25	101.75	6.20	6.87	1150	1.18
14	256.26	101.51	6.35	6.95	1150	0.06
15	256.42	102.47	6.47	6.93	1150	0.13
16	256.54	102.33	6.38	7.28	1150	0.17
18	256.40	102.08	6.38	7.16	1150	0.18
20	256.13	101.69	6.31	6.85	1150	0.04
22	256.33	101.61	6.25	6.81	1150	0.51
23	256.09	101.53	6.04	6.82	1150	0.41
24	256.08	101.32	6.03	6.84	1150	0.10
25	256.19	101.38	5.98	6.88	1150	0.13

All dimensions in mm

TABLE 2.5 DIMENSIONS OF TESTED BEAMS

Beam No	Overall Depth D	Flange Width B	Web Thickness t	Flange Thickness T	Overall Length L'	Web Eccentricity e
26	256.23	101.33	6.08	6.96	1150	0.17
27	256.45	101.53	6.37	6.90	1150	0.22
28	256.38	101.78	6.43	7.07	1150	0.30
R1	258.40	102.70	6.62	8.69	1150	0.27
R2	258.77	102.48	6.70	8.75	1150	0.14
29	255.61	101.02	5.96	6.86	1150	0.04
30	255.64	101.24	6.13	6.88	1150	0.09
31	255.76	101.41	5.95	6.82	1150	0.05
32	255.87	101.43	6.27	7.11	1150	0.11
33	255.88	101.47	6.25	7.18	1150	0.17
34	255.99	101.65	6.00	6.82	1150	0.06
35	255.95	101.48	6.51	6.94	1150	0.96
36	255.63	87.26	6.18	6.96	1150	0.15
37	255.69	73.28	5.98	6.86	1150	0.19
38	255.65	59.81	6.03	6.97	1150	0.22
39	262.69	101.05	6.65	9.78	1150	0.37
40	261.48	101.10	6.62	9.08	1150	0.18
41	260.08	101.25	6.54	8.29	1150	0.01
42	259.98	101.06	6.58	7.85	1150	0.29
43	258.10	101.14	6.46	6.90	1150	0.14
44	255.95	101.54	6.05	6.88	650	0.39

TABLE 2.5 (CONTINUED)

Beam No	Overall Depth D	Flange Width B	Web Thickness t	Flange Thickness T	Overall Length L'	Web Eccentricity e
45	255.91	101.24	5.95	6.89	2150	0.47
46	255.74	101.35	5.96	6.79	3150	0.50
47	263.60	100.06	6.51	9.77	1150	0.09
48	263.15	100.27	6.53	9.79	650	0.04
49	263.27	100.25	6.55	9.79	3150	0.05
50	255.96	101.45	5.98	6.89	1150	0.21
51	255.97	101.37	6.02	6.93	1550	0.17
52	256.00	101.45	5.90	6.72	1550	0.03
53	256.03	101.62	5.86	6.72	1550	0.09
54	400.75	141.53	6.77	8.98	650	0.64
55	400.82	141.63	6.80	8.88	1150	0.78
56	401.08	141.69	6.88	8.98	2150	0.53
57	401.25	141.56	6.82	8.81	3150	0.94
58	401.19	142.25	6.64	8.95	3650	0.34
59	153.21	87.94	4.90	7.87	900	0.25
60	466.28	192.87	11.65	19.87	1400	0.16
61	466.34	192.88	11.60	19.77	1400	0.08
62	400.90	140.74	6.56	8.65	650	0.43
63	400.62	141.69	6.67	8.68	650	0.28
64	400.79	141.34	6.80	8.89	2150	0.52
65	400.88	141.30	6.69	8.88	2150	0.39

TABLE 2.5 (CONTINUED)

Beam No	Overall Depth D	Flange Width B	Web Thickness t	Flange Thickness T	Overall Length L'	Web Eccentricity e
66	400.96	141.44	6.62	8.75	2150	0.32
67	400.56	141.59	6.76	8.83	2150	0.47
68	256.71	72.64	6.03	6.76	1150	0.12
69	256.50	58.23	6.05	6.79	1150	0.04
70	256.53	73.89	6.06	6.83	1150	0.13
71	256.40	58.77	6.03	6.77	1150	0.09
72	256.68	72.40	6.03	6.80	1550	0.10
73	256.63	58.32	6.03	6.76	1550	0.02
74	256.56	73.29	6.05	6.77	1550	0.11
75	256.69	58.42	6.06	6.76	1550	0.07
76	256.45	102.75	6.04	6.78	1150	0.17
77	256.25	102.38	5.95	6.64	1150	0.12
78	256.23	102.15	5.98	6.70	1150	0.09
79	256.51	102.34	5.94	6.65	1150	0.06
80	256.31	102.54	5.94	6.65	1150	0.04

TABLE 2.5 (CONTINUED)

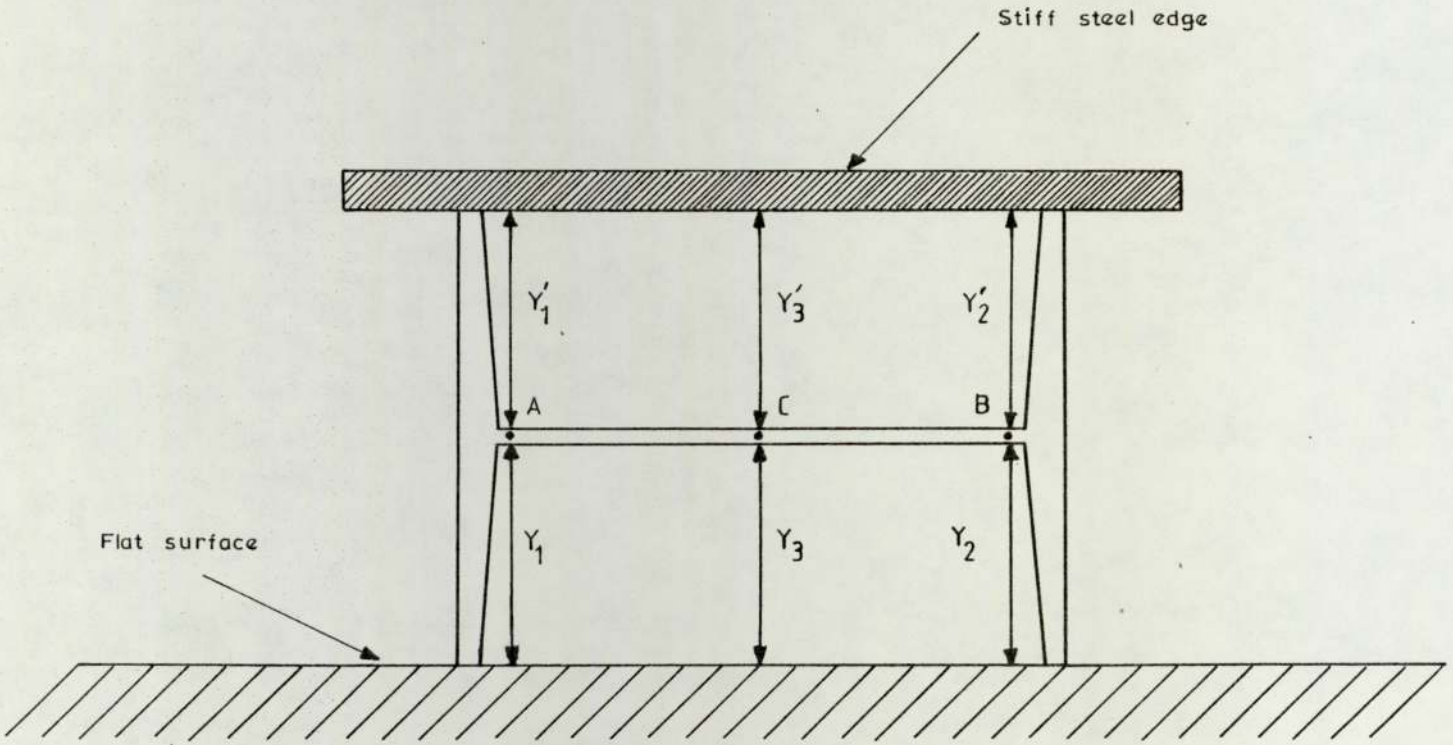

FIGURE 2.4. DETERMINATION OF THE WEB ECCENTRICITY

deflections of the entire beam. Correspondingly, the instrumentation consisted of strain gauges and a deflection gauges frame.

Electric resistance strain gauges were used which had a gauge length of 5 mm and a gauge resistance of 120 ohms. The accuracy of the strain gauge readings was one microstrain. The deflection gauges had the finest division of one hundredth of a millimetre. A set of strain and deflection measurements was taken after each increment of load. As mentioned earlier all the beams were white-washed for detecting and recording the plastified regions.

2.3.2.1 Strain Indicators

The determination of stress distribution through an elastic medium when it is subjected to concentrated loads is very complex and a very large number of strain gauges and strain rosettes would be needed to obtain a complete picture. The reader is referred to Hendry (58), Coker (59), Frocht (60) et al, where such a stress distribution is examined using photoelastic analysis. Since such a determination is beyond the scope of the present work and it is money and time consuming, to avoid any complications only a limited number of strain gauges were used.

Electrical resistance strain gauges were attached to all the tested beams but in varying positions and numbers. The beams tested for end failure, that is the beams in series I to V, had only one pair of strain gauges attached, to record any sudden change in stress in the beam web due to yielding or buckling. These gauges, shown in figure (2.5a) were positioned at the mid-depth of the web, along the centre line of the support at each face of the web. Larger numbers of strain gauges along the mid-depth of the web could not be attached due to the clamping device. Where only two strain

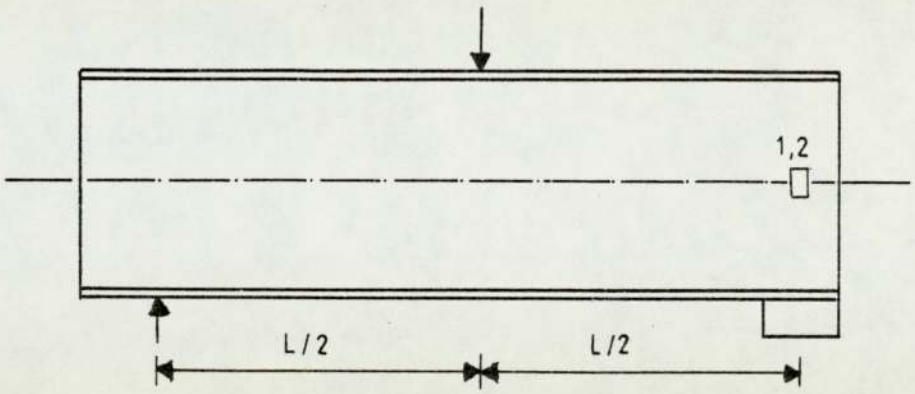

a. End Failure

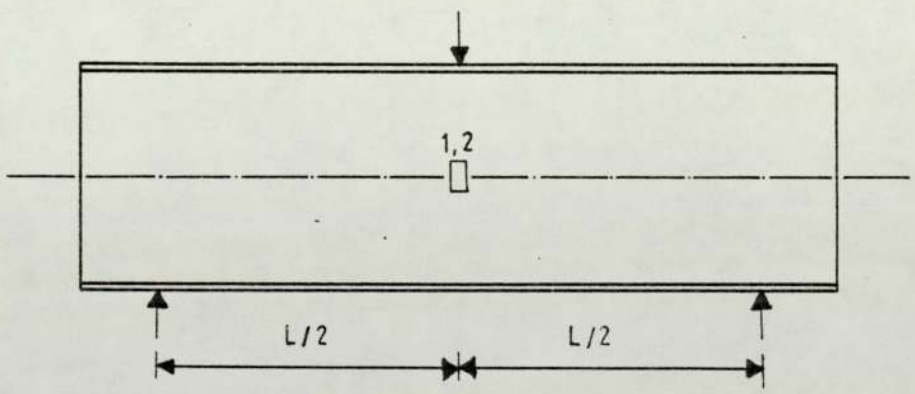

b. Central Failure

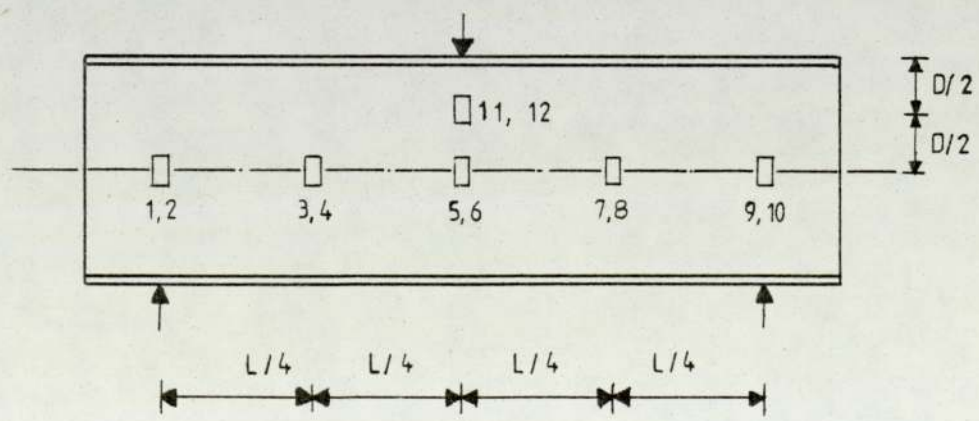

c. Central Failure

FIGURE 2.5. TYPICAL STRAIN GAUGE LOCATION AND REFERENCING

gauges were used for beams tested for central failure, these were positioned at the mid-depth of the web along the line of action of the centre of the applied load on each face of the web, as shown in figure (2.5b), for the purpose of recording any sudden change in stress. For other cases, where a larger number of strain gauges were used, the position and referencing of these gauges is shown in figure (2.5c). Two objectives were achieved by positioning the strain gauges at these locations. Firstly, the decrease of strain at the mid-depth of the web away from the load application point would be indicated and secondly, the progression of the area of the web which has yielded from the load application point would also be indicated.

The positions of the strain gauges were marked and cleaned with a hand-grinder. These areas were further cleaned with 'genclene' and finally neutralised with ammonia solution. The strain gauges were then glued to the steel and left to dry. The connectors were then soldered to suitable cables with care to avoid any damage to the gauges. The strain gauge readings, where only two gauges were used, were taken manually using a Peckel strain recorder. For beams with larger number of gauges the readings were recorded automatically using a Compulog Data Logger.

As has been mentioned in a previous section the beams were white-washed to obtain a general stress distribution throughout the section, in addition to the strain gauges attachment. This white-washing technique was used by Moore and Wilson (43), Lyse and Godfrey (45), Massonnet (61) etc and found to be quite effective. Although no actual strain values have been recorded in this way, definite crack lines have been obtained in the white-wash at high strains.

2.3.2.2 Deflection Indicators

The deflected shape of the web of a universal beam when it is subjected to concentrated loads is also complex as the strain distribution. For the purpose of the present study it was decided to measure lateral deflections of the top flange and web at different points, vertical deflection of the beam and any other deflection considered to be important. The deflections were measured by means of mechanical deflection gauges and could be read to an accuracy of 0.01 mm. The position of the gauges varied throughout the tests and typical locations and referencing are shown in figure (2.6a to c). The referencing of these gauges is that given in the test readings in appendix 1.

The location of the deflection gauges used for the beams tested for end failure is shown in figure (2.6a). Dial gauge No 1 was always in line with the centre line of the support at the end where failure was expected, and indicated the vertical movement of the web above this point. Dial gauge No 2 was always in line with the applied load, indicating the vertical movement of the beam at mid-span. Dial gauges No 3 and No 4 were indicating the lateral deflection of the top flange and web at mid-depth above the support respectively. For the beams tested for central failure the number and position of the dial gauges was varied for different tests. The location and referencing of these gauges according to the number used is shown in figure (2.6b to e).

In some tests it was noticed that the top flange of the beam, at mid-span, moved horizontally. This movement, possibly caused by eccentricity of the vertical applied load in relation to the line of the web, was usually relatively sudden. In general regions of high strains, indicated by flaking of the white-wash, were

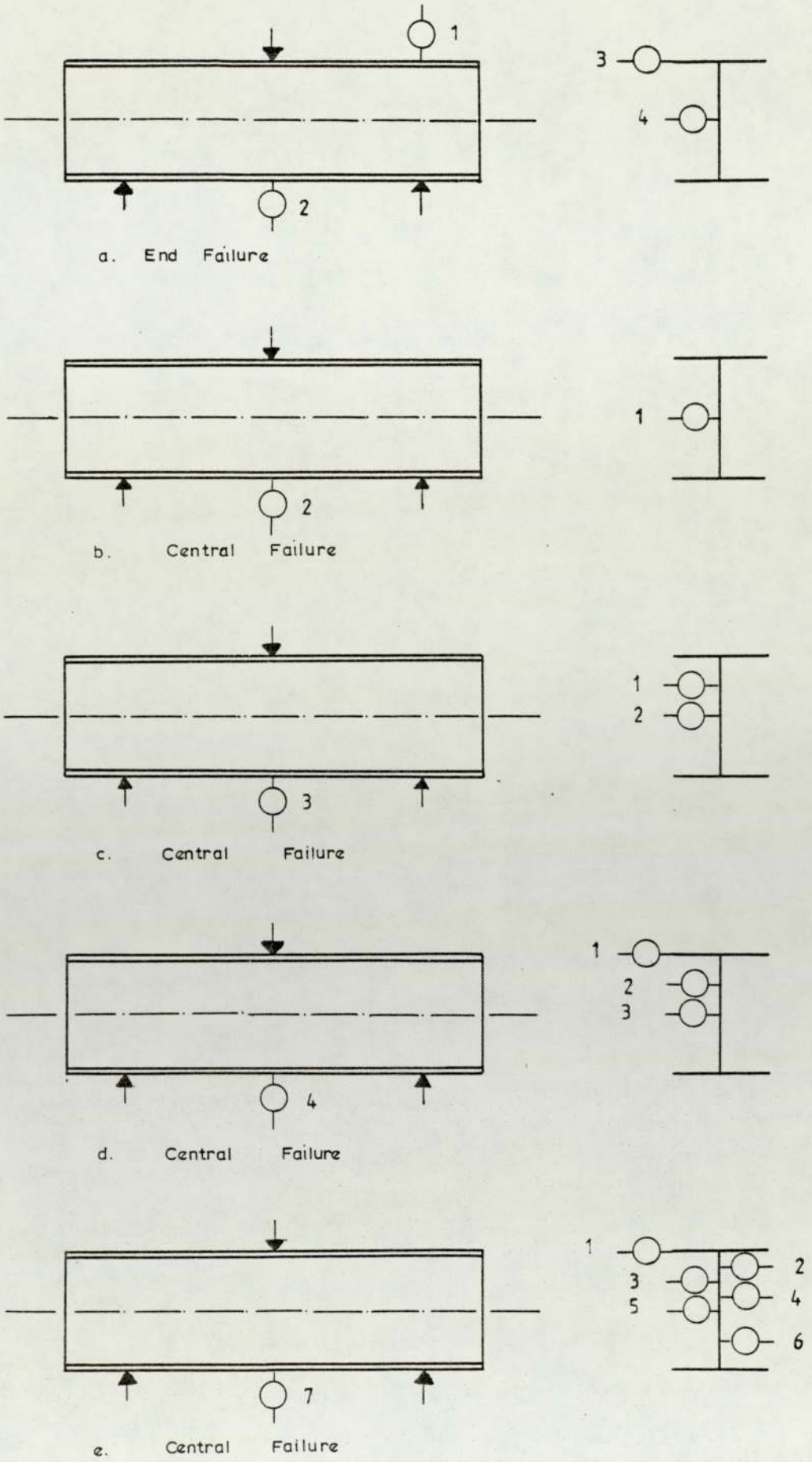

FIGURE 2.6. DEFLECTION GAUGES LOCATION AND REFERENCING

accompanied by large out of plane web deflections.

2.4 LOADING DEVICES

The majority of the beams were tested in a large testing rig shown in plate (2.1a). The load was applied to the top flange of the beam by means of a motorised hydraulic ram of 1000 kN capacity. This load was measured by a load cell attached to the bottom of the ram and connected to an automatic recording machine. The rest of the tested beams namely beam Nos 60 and 61 were tested on an Avery 2500 kN capacity machine shown in plate (2.1b)., the selection depending on the expected failure load.

2.4.1 Test Beam Set-Ups

Due to inaccuracies in manufacture of rolled steel beams the webs of the beams were not at right angles to the flanges, that is to say the beams had a degree of 'out of squareness'. To compensate for these imperfections small packing pieces were inserted under the bearing plates at the supports, so that the web was always vertical under the applied load. To set up the web of the test beam vertical along the whole span was not possible, because there was a variation in the shape along the length and also because the web is not perfectly flat.

All the beams were set with the bottom flange horizontal with respect to the length and the centre of the applied load plumb. For each failure all the beams were tested under a load applied at mid-span with a stiffening clamp, designed to prevent failure under the applied load, except beam Nos 23a, 23b, 29a and 29b. The stiffening device is shown in plate (2.2) and figure (2.7). To control any appreciable sideways movement of the top flange an angle-iron frame was introduced at each end of all the

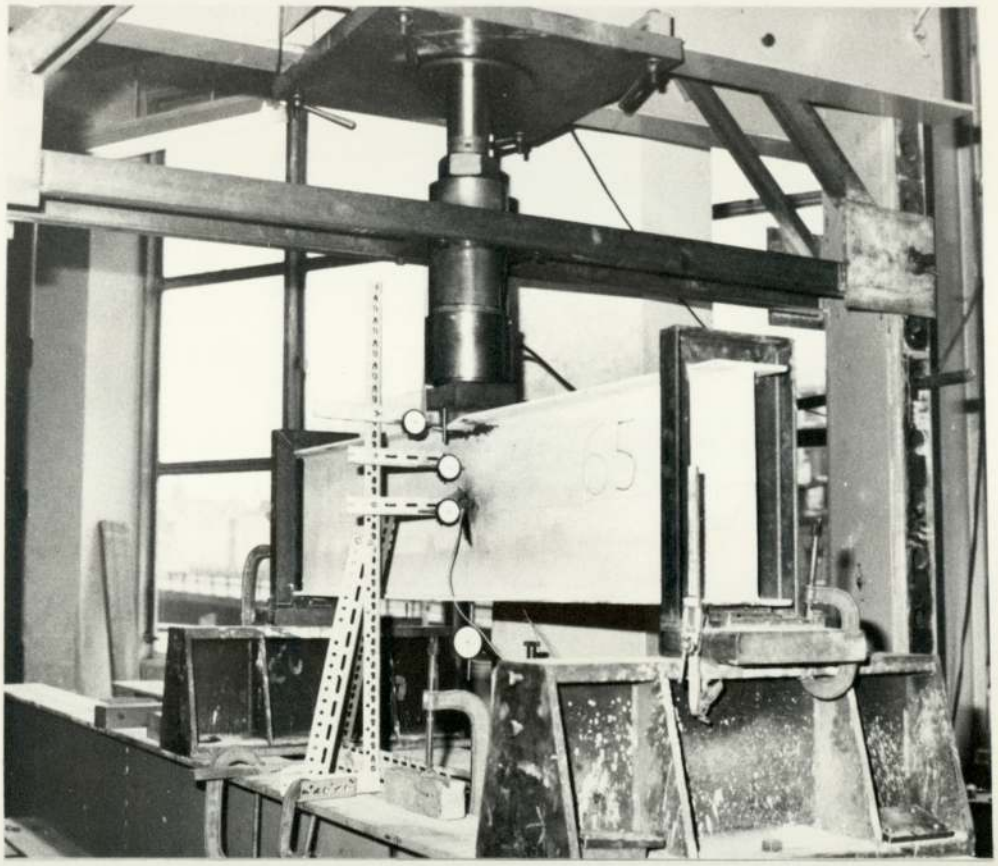

(a) Testing Rig - 1000 kN Capacity

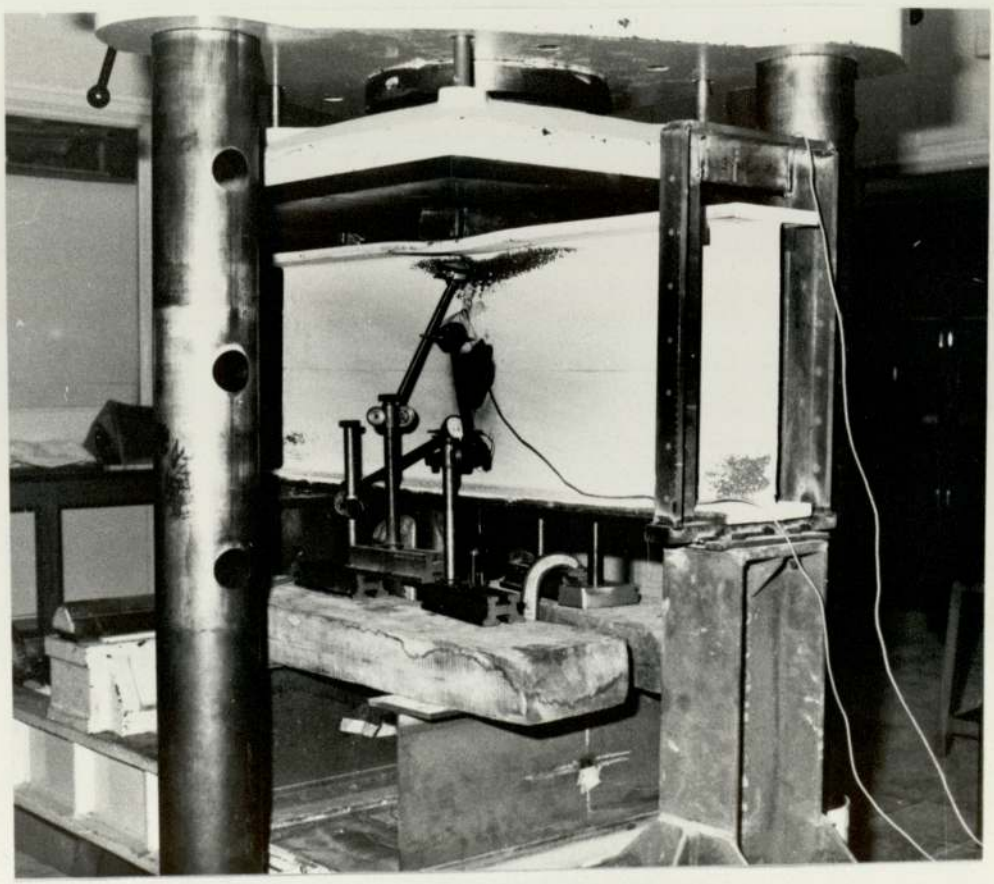

(b) Avery - 2500 kN Capacity

PLATE 2.1 LOADING DEVICES

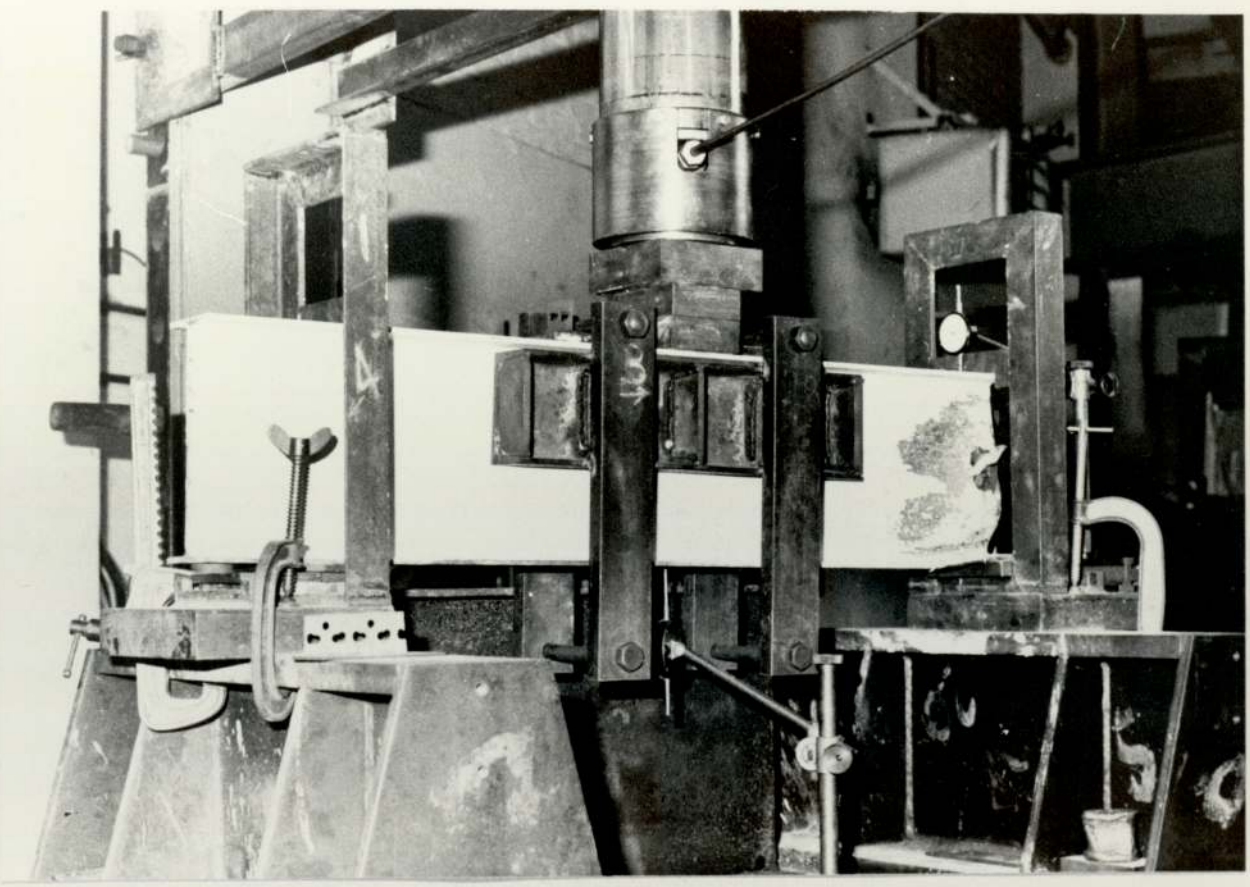

PLATE 2.2 STIFFENING CLAMP USED FOR SERIES I to IV

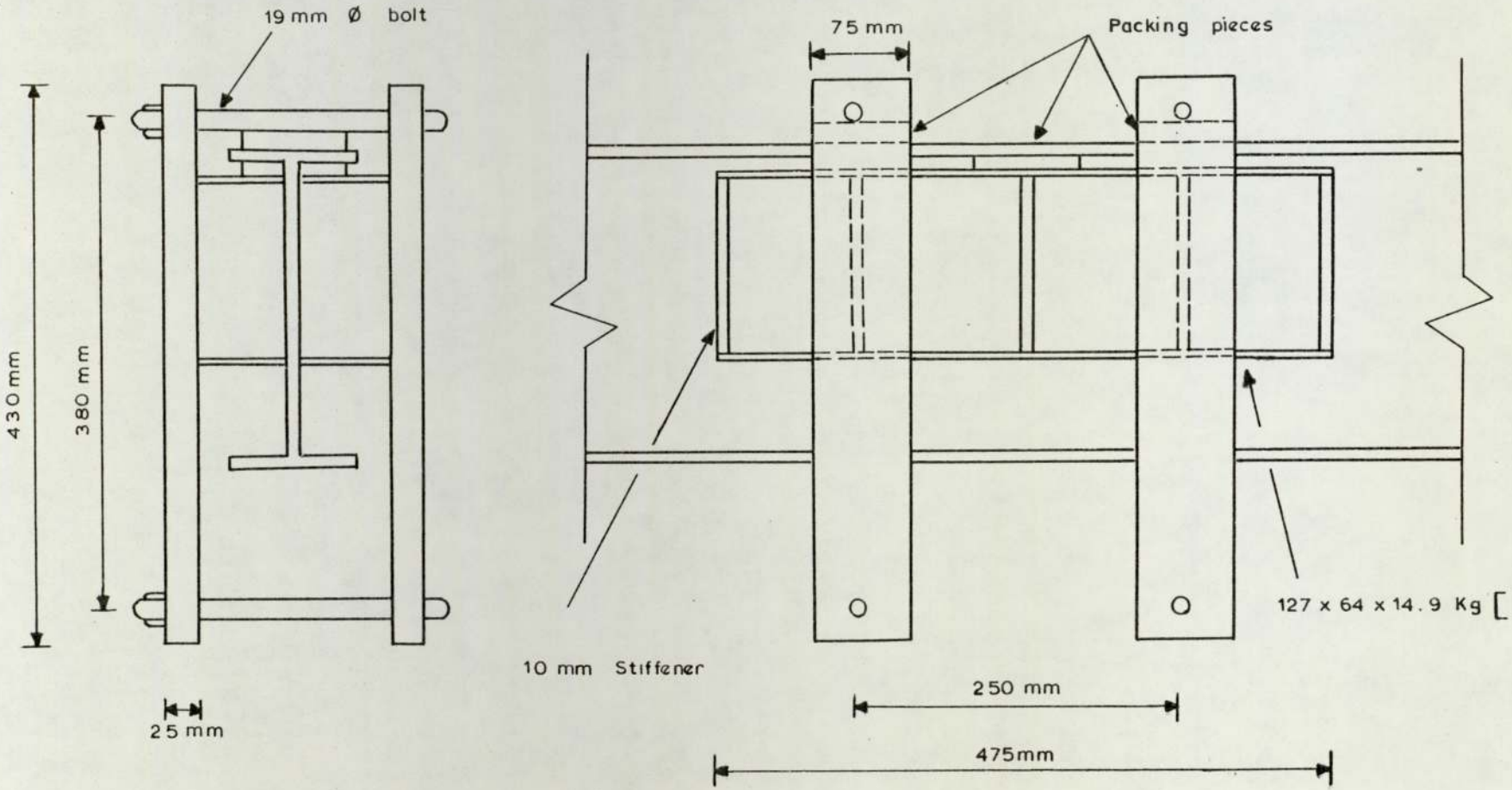

FIGURE 2.7. STIFFENING CLAMP

tested beams, shown in plate (2.1a, b) at the ends of the beam.

2.4.2 Load Application

The load applied to the upper flange of the beam was one of the following types:

1 Knife Edge Load - These knife edges were used throughout the tests. They were made from mild steel and were manufactured with a radiused bearing edge of very small diameter and finally hardened before using. The area of contact with the flange of the beam was very small and assumed to be zero. These knife edges were welded to a stiff plate so they were more stable when they were in contact with the head of the ram, but they were not attached to the tested beam in any way; the friction on the contact area provided the only restraint. They were found to be very good and although applied to high loads did not flatten or distort.

2 Uniform Distributed Load - In these cases the load was applied to the top flange by means of stiff steel plates, usually 50 mm thick and of the required length. For this type of loading as for the previous one, the flanges could have lifted off if such a failure mode was possible. Some tests namely test No 3 in Series I, tests Nos 1, 2a and 2b in Series II and all the tests included in series VIII had the thickness of these plates reduced as this variable was under investigation.

2.4.3 Testing Procedure

Basically, the testing procedure for all the tests was the same. First zero readings were taken for all the strain and deflection gauges. An approximate failure load was predicted for the beam to be tested and increments of loadings were applied slowly

at a constant rate. At each increment the load was held constant and all deformations were allowed to stop before a set of readings was taken. This procedure was continued until failure. Usually, when inelastic behaviour was detected in the web or in the beam as a whole, the load increment was cut to a half. The load then was held constant and the reading deferred until the needle on the dial gauges stopped moving. Usually, the dial needle would move a few divisions during the reading, but at this point the lateral deflections of the web were large so that this change was negligible. Failure was defined by large increase in deflections and a band of yielding. After the formation of the yield band the beam could not sustain any higher load. At this point the load was removed quickly to avoid any further deformations. It was not possible to record any strain or deflection readings at failure due to their large rate of increase.

A large number of beams were reloaded one or two times and repeating loading cycles carried out to a few beams only. For the reloading of these beams only the final load was recorded. Some other observations during testing were noted such as flange movements, bending and the appearance of crack lines in the white-wash were recorded.

CHAPTER 3

PRESENTATION OF THE TEST RESULTS

3.1 INTRODUCTION

In this chapter the test results of all the tested beams are presented. As has been mentioned in chapter 2 the recordings made during testing were:

1) The failure load
2) Strain recordings
3) Deflection recordings.

In the following sections, therefore, the different variations of the failure load with the variables investigated for each series of tests as well as strain versus load and deflection versus load relationships will be examined and discussed. It is impossible, due to the large number of tests conducted, to refer to the behaviour of each beam, under test, individually. Representative tests are selected from each series and discussed.

3.2 TEST FAILURE LOADS

The most important information gained from the experimental recordings of the beams is the variation of the ultimate load with respect to the variable investigated. The failure loads obtained for each test as well as any retest loads and the mode of failure are shown in table (3.1a to h).

The failure loads for each test series vary with the corresponding variable. In cases where in a particular test series different beam serial sizes have been used, or the actual dimensions of the beams altered, the general variation of the ultimate load with the variable investigated is of the same form. The failure

Series	Beam	l_e /mm	Failure Load /kN	Retest 1 /kN	Retest 2 /kN	Failure Mode
I	11a	12.7	255.0	-	-	1
	7a	20.0	260.0	-	-	1
	7b	30.0	270.0	-	-	1
	6b	50.0	257.5	-	-	1
	8a	70.0	260.0	-	-	1
	8b	90.0	285.0	-	-	1
	3	90.0	280.0	-	-	1

(a) SERIES I

TABLE 3.1 FAILURE LOAD OF TESTED BEAMS

Series	Beam	l_c /mm	t /mm	Failure Load /kN	Retest 1 /kN	Retest 2 /kN	Failure Mode
	11a	12.7	25.0	255.0	-	-	1
	5a	20.0	25.0	310.0	-	-	1
	5b	30.0	25.0	320.0	-	-	1
	6a	50.0	25.0	339.0	-	-	1
II	10a	70.0	25.0	410.0	-	-	1
	12a	90.0	25.0	450.0	-	-	1
	1	50.0	10.0	315.0	222.5	-	1
	2a	50.0	15.0	325.0	240.0	-	1
	2b	50.0	20.0	340.0	215.0	-	1

(b) SERIES II

Series	Beam	l_k /mm	Failure Load /kN	Retest 1 /kN	Retest 2 /kN	Failure Mode
III	4b	6.35	245.0	-	-	1
	11b	15.0	265.0	-	-	1
	13a	25.0	297.5	-	-	1
	13b	35.0	340.0	-	-	1
	14	40.0	390.0	-	-	1
	15	60.0	400.0	-	-	1
	16	90.0	420.0	-	-	2
	18	100.0	440.0	-	-	2
	20	120.0	450.0	-	-	2
	22	130.0	455.0	310.0	-	2
	36	35.0	330.0	210.0	-	1
	37	35.0	310.0	212.5	-	1
	38	35.0	290.0	-	-	1
	39	35.0	407.5	260.0	-	1
	40	35.0	400.0	272.5	-	1
	41	35.0	397.5	255.0	-	1
	42	35.0	390.0	-	-	1
	43	35.0	385.0	270.0	-	1

(c) SERIES III

Series	Beam	l_s /mm	Failure Load /kN	Retest 1 /kN	Retest 2 /kN	Failure Mode
IV	4b	12.7	245.0	-	-	1
	26a	20.0	258.0	-	-	1
	25a	30.0	270.0	-	-	1
	25b	40.0	320.0	-	-	1
	26b	50.0	340.0	-	-	1
	24b	60.0	350.0	-	-	2
	27	70.0	390.0	-	-	2
	28	80.0	420.0	-	-	2
	R1b	20.0	295.0	-	-	1
	R1a	50.0	420.0	-	-	1
	R2	70.0	460.0	-	-	2

(d) SERIES IV

Series	Beam	l /mm	Failure Load /kN	Retest 1 /kN	Retest 2 /kN	Failure Mode
V	4b	500.0	245.0	-	-	1
	23a	400.0	198.0	-	-	1
	23a	300.0	180.0	-	-	1
	29a	200.0	140.0	-	-	1
	29b	150.0	140.0	-	-	1

(e) SERIES V

Series	Beam	Span /m	l_a /mm	Failure Load /kN	Retest 1 /kN	Retest 2 /kN	Failure Mode
	31	1.0	0	208.0	185.0	-	1
	30	1.0	50.0	270.0	190.0	-	1
	32	1.0	100.0	310.0	270.0	248.0	2
	33	1.0	150.0	350.0	320.0	-	2
	34	1.0	250.0	395.0	350.0	-	2
	50	1.4	0	185.0	175.0	-	1
	51	1.4	50.0	217.5	195.0	-	1
	52	1.4	150.0	240.0	217.5	-	2
	53	1.4	250.0	265.0	230.0	-	2
	62	0.5	0	322.5	280.0	260.0	1
	63	0.5	150.0	495.0	195.0	-	2
	60	1.25	12.7	860.0	710.0	-	1
VI	61	1.25	100.0	1060.0	720.0	-	2
	64	2.0	0	285.0	280.0	260.0	1
	65	2.0	50.0	350.0	290.0	-	1
	66	2.0	150.0	460.0	285.0	-	2
	67	2.0	300.0	530.0	165.0	-	2
	68	1.0	0	190.0	165.0	117.5	1
	69	1.0	0	180.0	147.5	137.5	1
	70	1.0	150.0	297.5	145.0	122.5	2
	71	1.0	150.0	260.0	107.5	90.0	2
	72	1.4	0	140.0	92.5	67.5	1
	73	1.4	0	127.5	72.5	62.5	1
	74	1.4	150.0	190.0	157.5	125.0	2
	75	1.4	150.0	172.5	85.0	75.0	2

(f) SERIES VI

Series	Beam	Span /m	l_a /mm	l_o /mm	Failure Load /kN	Retest 1 /kN	Retest 2 /kN	Failure Mode
	44	0.50	12.7	12.7	237.5	210.0	205.0	1
	35	1.00	12.7	12.7	215.0	205.0	185.0	1
	45	2.00	12.7	12.7	145.0	125.0	-	1
	46	3.00	12.7	12.7	100.0	85.0	-	1
	48	0.50	12.7	2.17	300.0	275.0	-	1
	47	1.00	12.7	12.7	272.5	255.5	-	1
VII	49	3.00	12.7	12.7	135.0	120.0	-	1
	58	3.50	12.7	12.7	250.0	-	-	1
	59	0.75	12.7	12.7	168.75	-	-	1
	54	0.50	100.0	50.0	470.0	450.0	-	2
	55	1.00	100.0	50.0	430.0	430.0	385.0	2
	56	2.00	100.0	50.0	350.0	325.0	315.0	2
	57	3.00	100.0	50.0	280.0	175.0	-	2

(g) SERIES VII

Series	Beam	l_a /mm	t /mm	Failure Load /kN	Retest 1 /kN	Retest 2 /kN	Failure Mode
VIII	77	50.0	10.0	240.0	212.5	200.0	1
	76	50.0	15.0	260.0	217.5	-	1
	78	250.0	15.0	300.0	245.0	240.0	2
	79	250.0	39.0	390.0	-	-	2
	80	50.0	10.0	250.0	210.0	-	1

(h) SERIES VIII

loads are also represented in a series of graphs shown in figure (3.1a to k). Where convenient, two or more beam sections are shown on the same graph. On these graphs appropriate test results of reference (55) are included.

Figure (3.1a), representing the failure loads of series I, shows that the length of the bearing plate l_e, placed on top of the 12.7 mm long stiff bearing has no very significant effect on the failure load.

When the position of the stiff bearing is changed as for series II then the length of the bearing plate has an influence on the failure load of the beams. This variation is shown in figure (3.1b) and can be best represented by a straight line. On the same graph are included the tests with the plates of differing thicknesses.

When the bearing plate is removed and the stiff bearing is placed towards the centre of beam as in series III, the failure loads increase with the length l_k, as shown in figure (3.1c). Figure (3.1d) shows the variation of the failure load with the flange width B and the flange thickness T. The basic section sizes, before alteration, were 254 x 102 x 22 kg and 254 x 102 x 28 kg respectively. These variations could be represented by straight lines.

Figure (3.1e) shows the variation of the failure loads of beams in series IV with the length of bearing l_s.

Figure (3.1f), for beams in series V, indicates that the failure load decreases with the distance 1 and for small values of 1 the load seems to become constant.

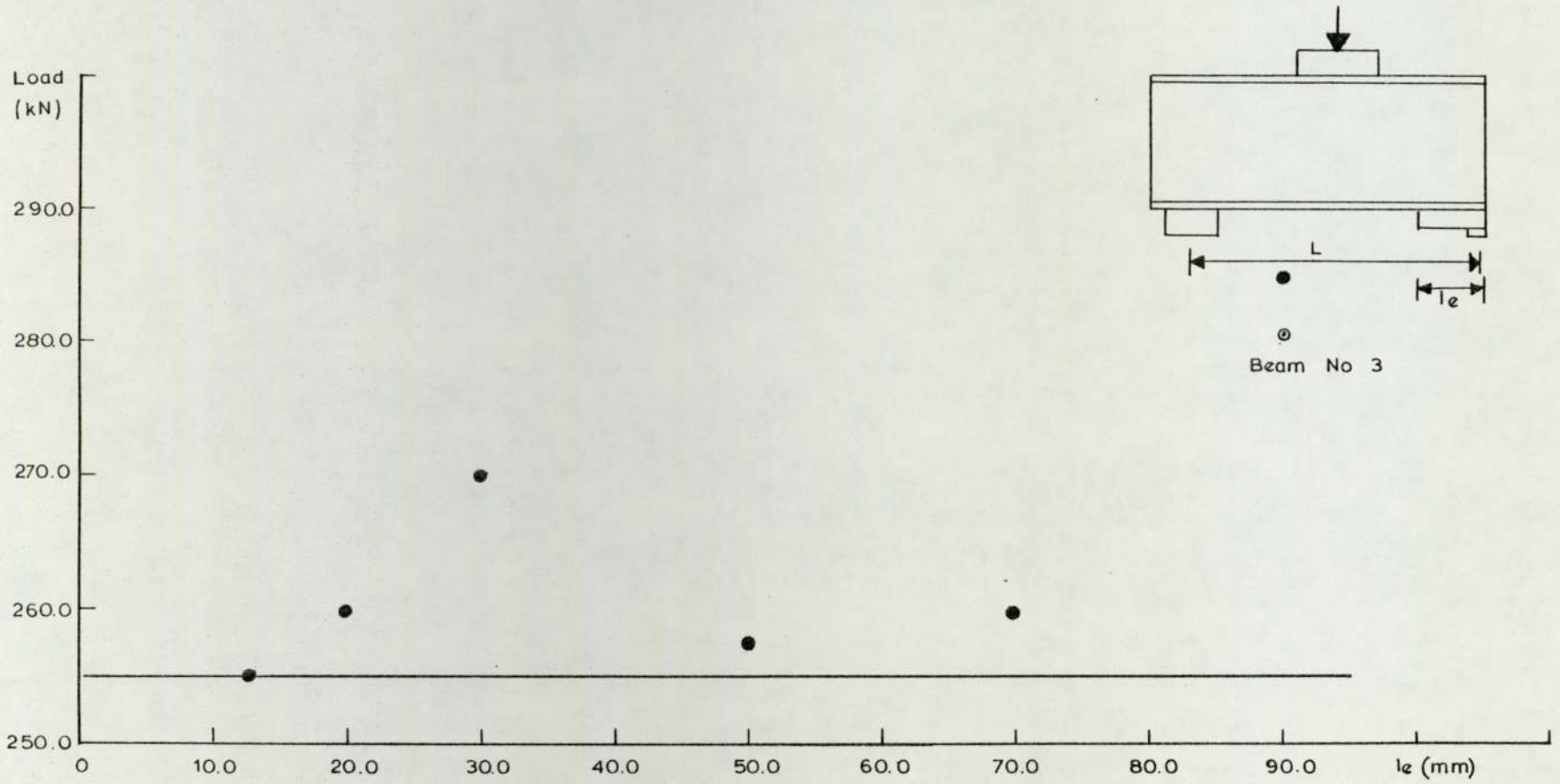

a. Series I

FIGURE 3.1 EXPERIMENTAL RESULTS OF TESTED BEAMS

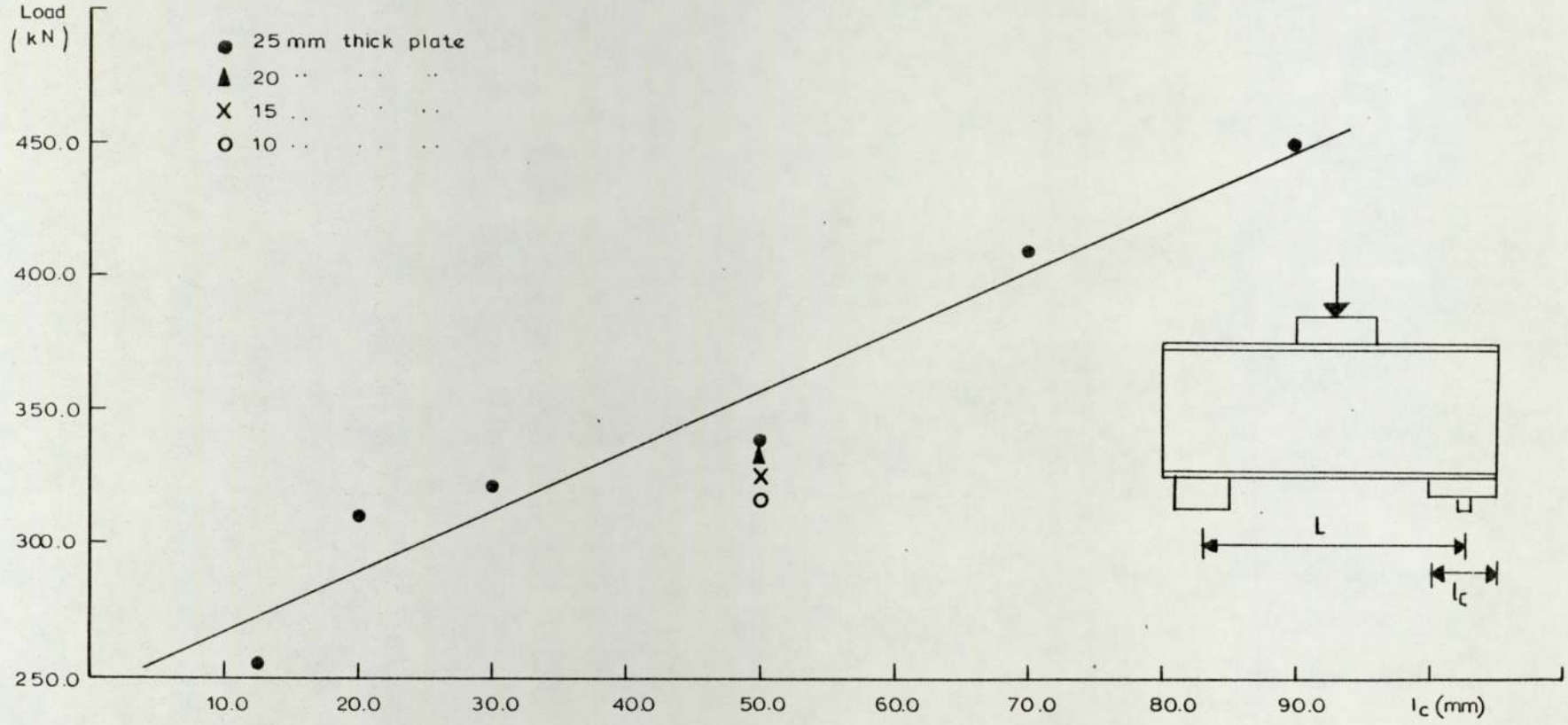

b. Series II

FIGURE 3.1 CONTINUED

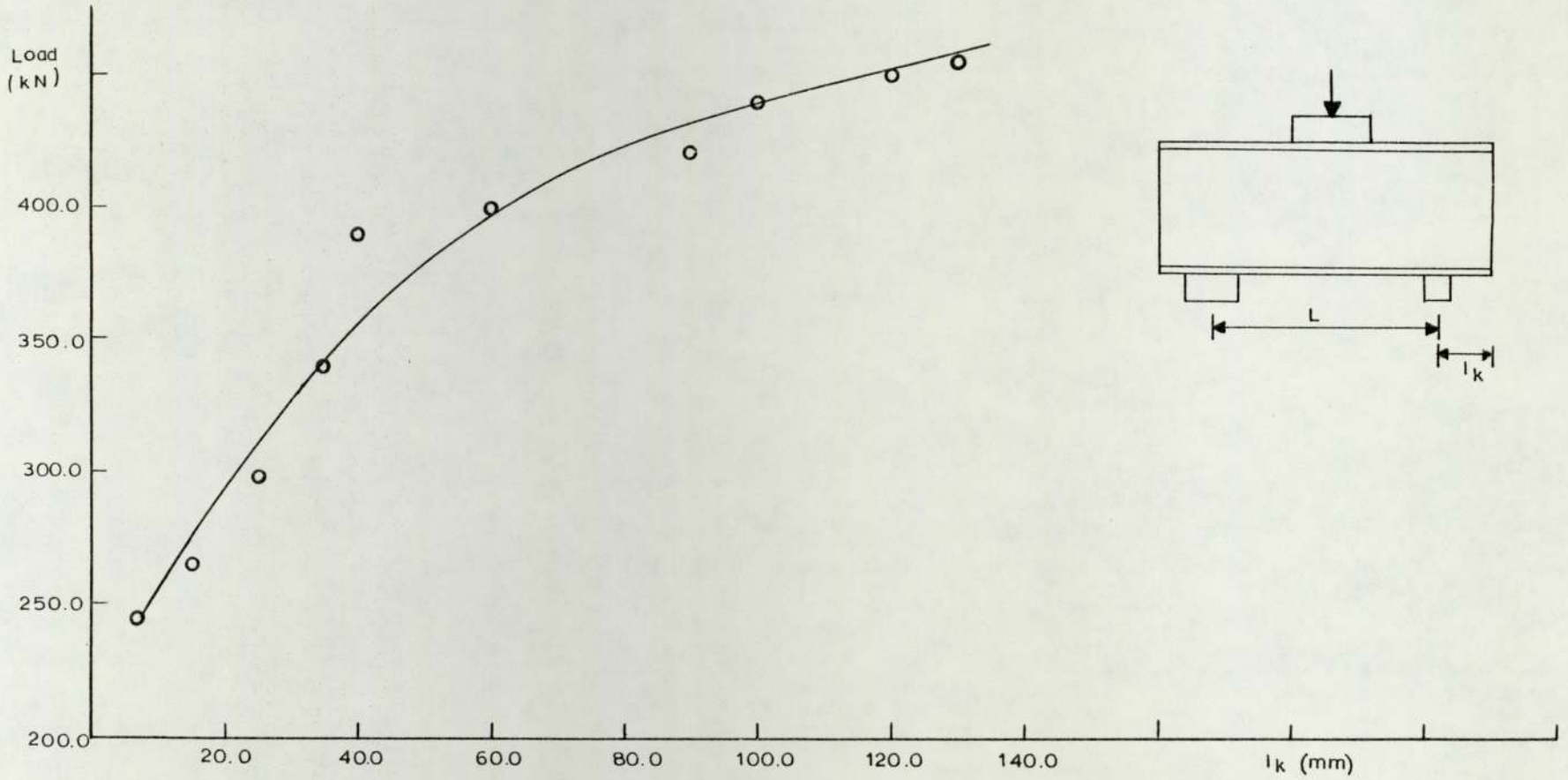

c. Series III

FIGURE 3.1 CONTINUED

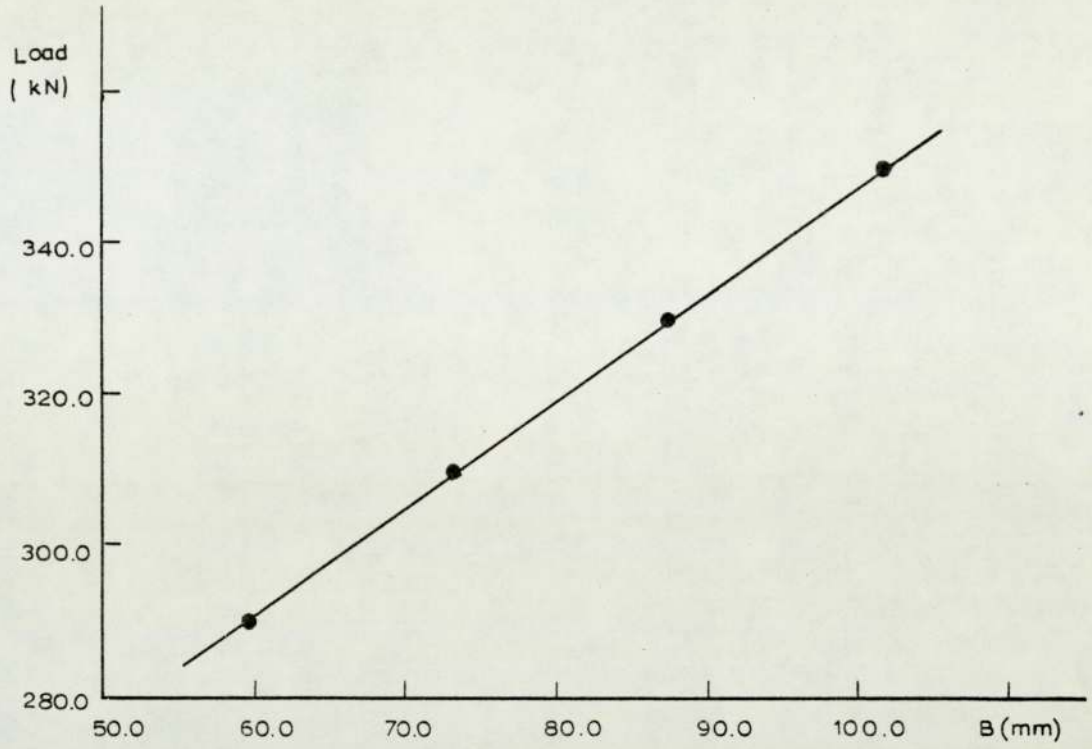

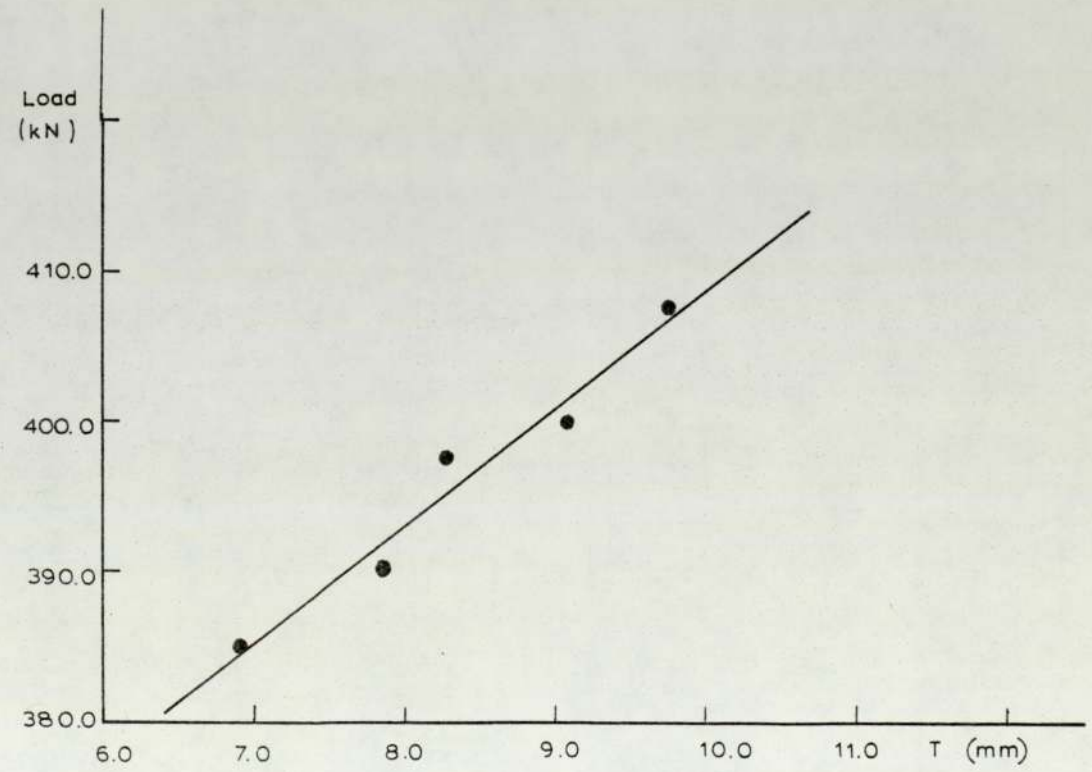

d. Series III

FIGURE 3.1 CONTINUED

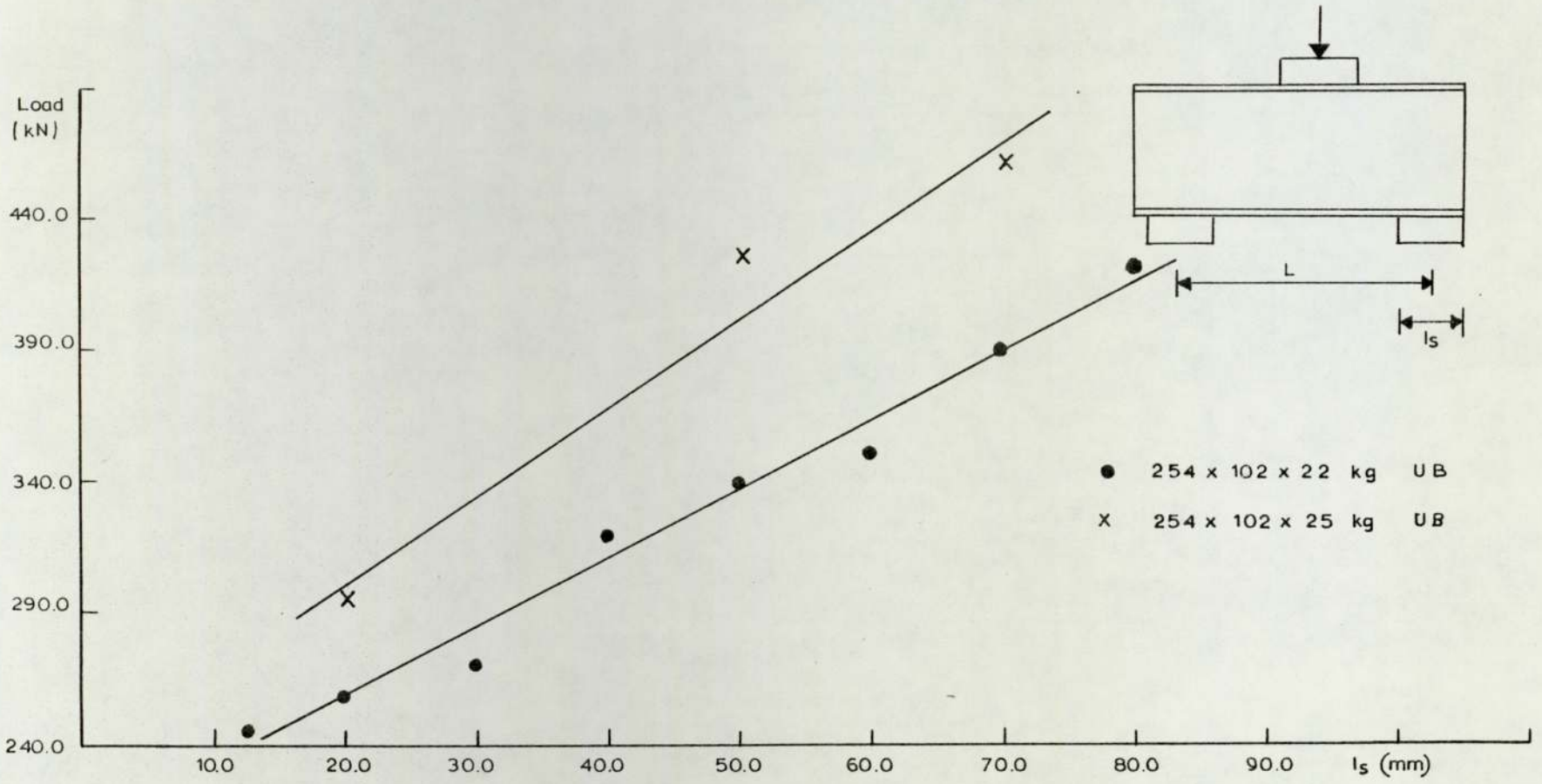

e. Series IV

FIGURE 3.1 CONTINUED

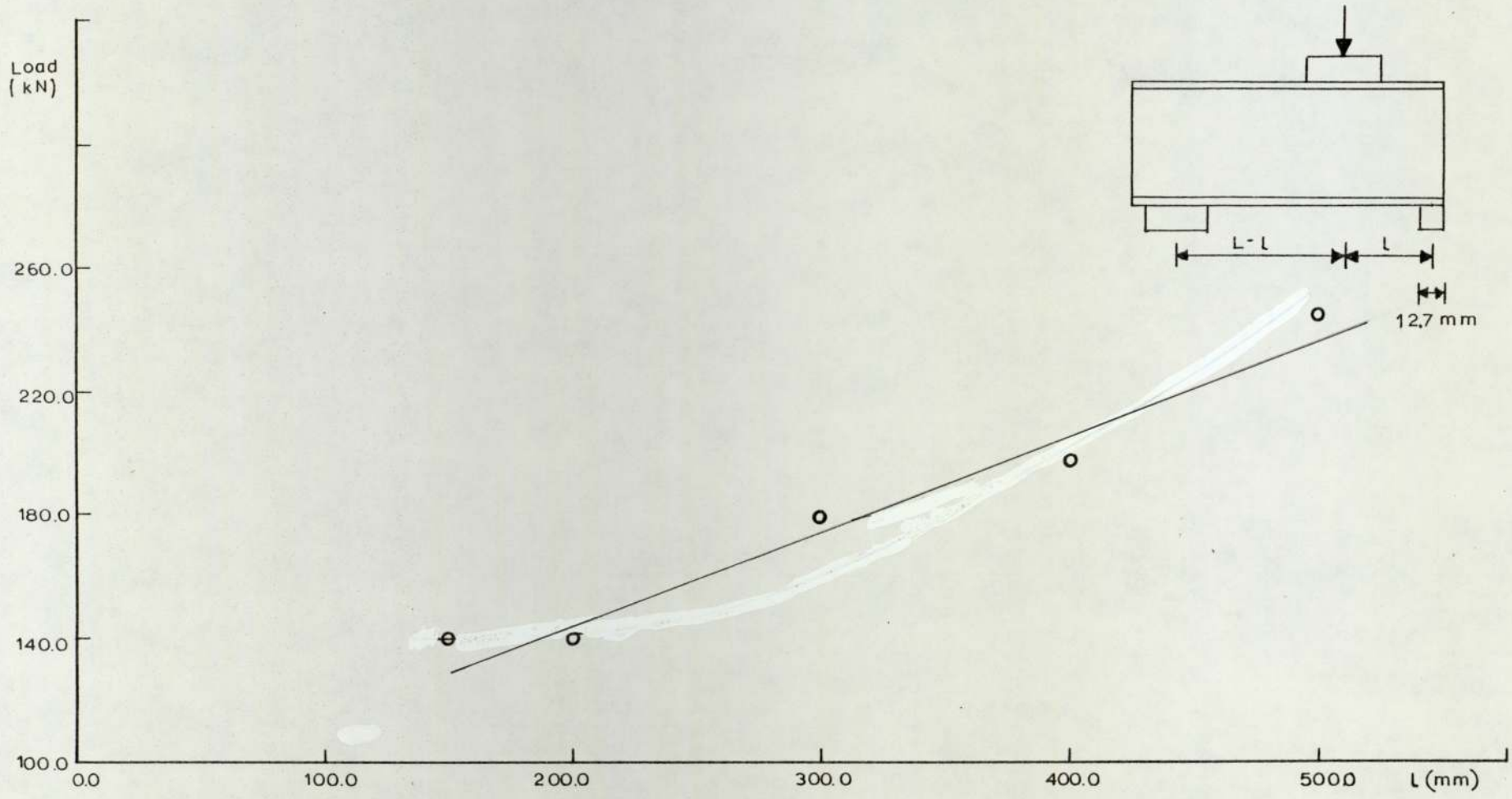

f. Series V

FIGURE 3.1 CONTINUED

Figure (3.1g, h), representing the failure loads for beams in series VI, shows that the failure load increases with the length of the applied load l_a and the curve appears to become flatter for long lengths of load. The variation of failure load with the flange width for different lengths of load is shown in figure (3.1i). The basic section size was 254 x 102 x 22 kg before alteration.

The influence of bending for beams in series VII is shown in figure (3.1f) for different beam serial sizes. Such a variation has also been obtained by reference (55), as shown in the same figure.

The variation of the failure load with the thickness of the loading plate for beams in series VIII is shown in figure (3.1k).

3.2.1 Modes of Failure

As has previously been mentioned a frame was introduced at both ends of the beams to prevent the top flange moving horizontally at right angles to the beams.

Whatever the location of failure the beams seemed to fail in a manner characterised by yielding of the flange and elastoplastic local buckling, or crushing of the web. Two modes of this type of failure were observed.

Failure Mode 1 - This failure mode is shown in plate (3.1a) and occurred to beams loaded or supported, depending on the location of failure, with relatively small or zero lengths of bearing. This failure mode is characterised by the out of plane deflections of the web, being confined to a small region of the beam in the vicinity of the applied load, or support. The largest out of plane deflection of the web seemed to occur at a depth about one

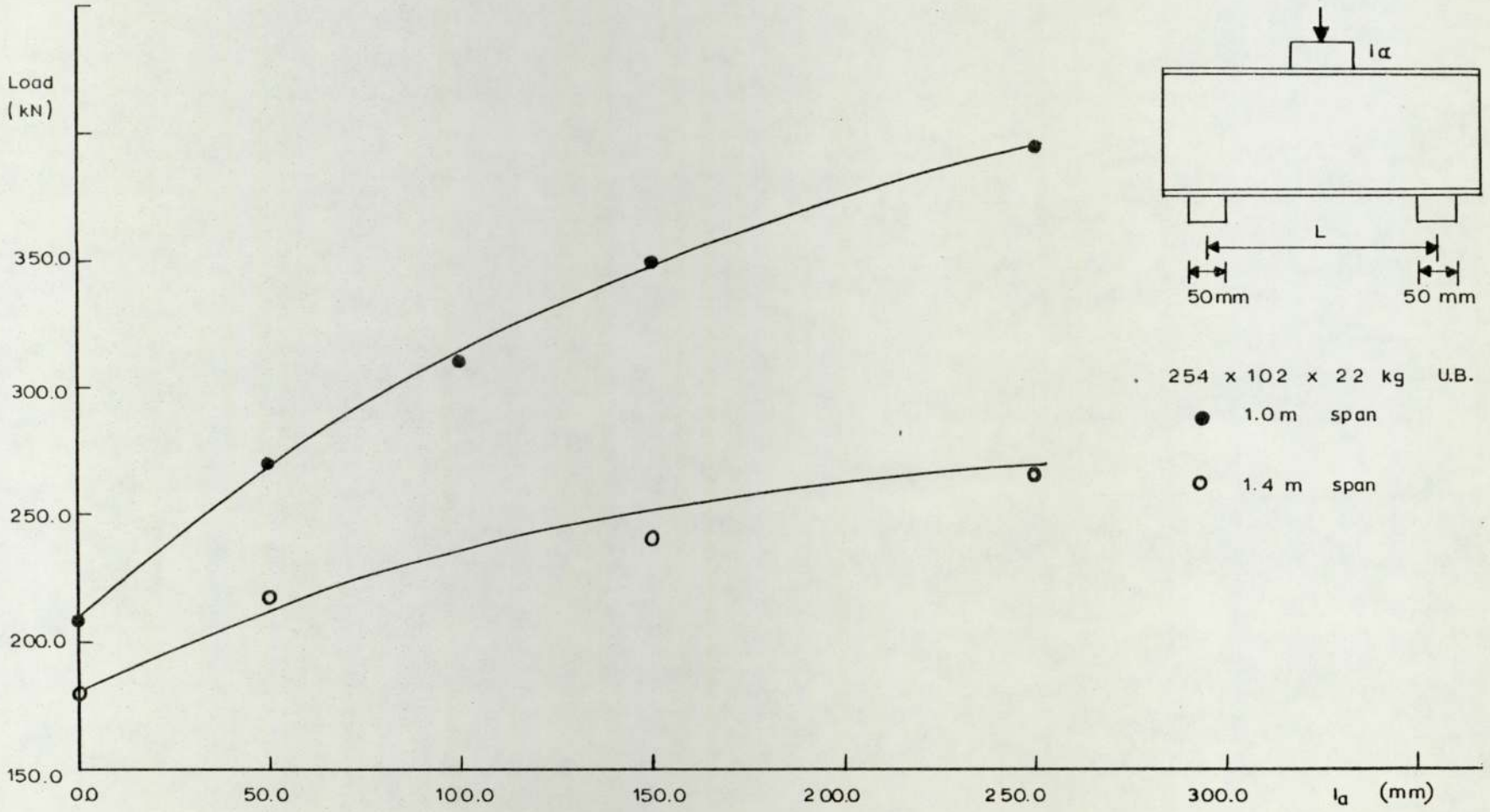

g. Series VI

FIGURE 3.1 CONTINUED

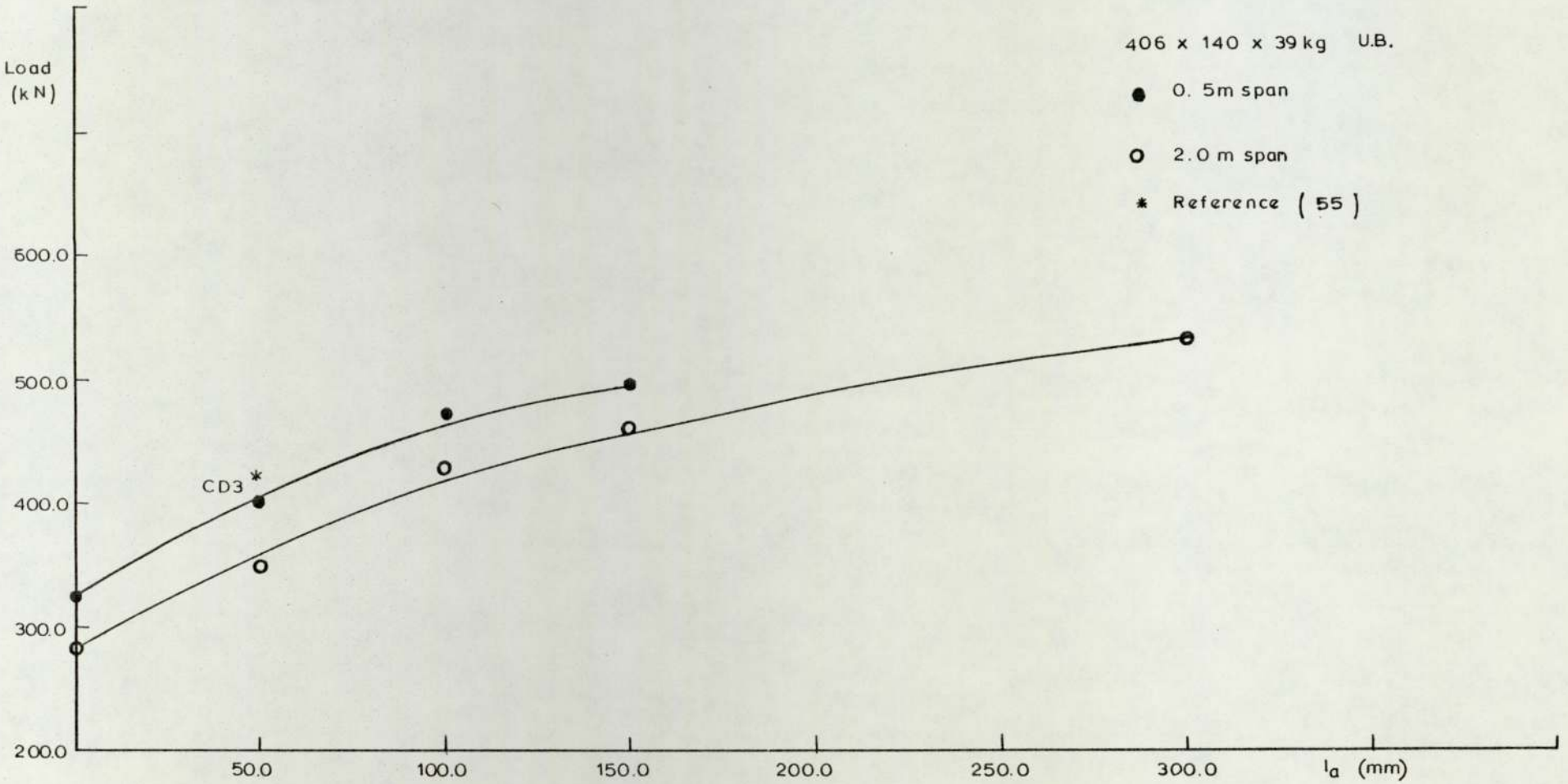

h. Series VI

FIGURE 3.1. CONTINUED

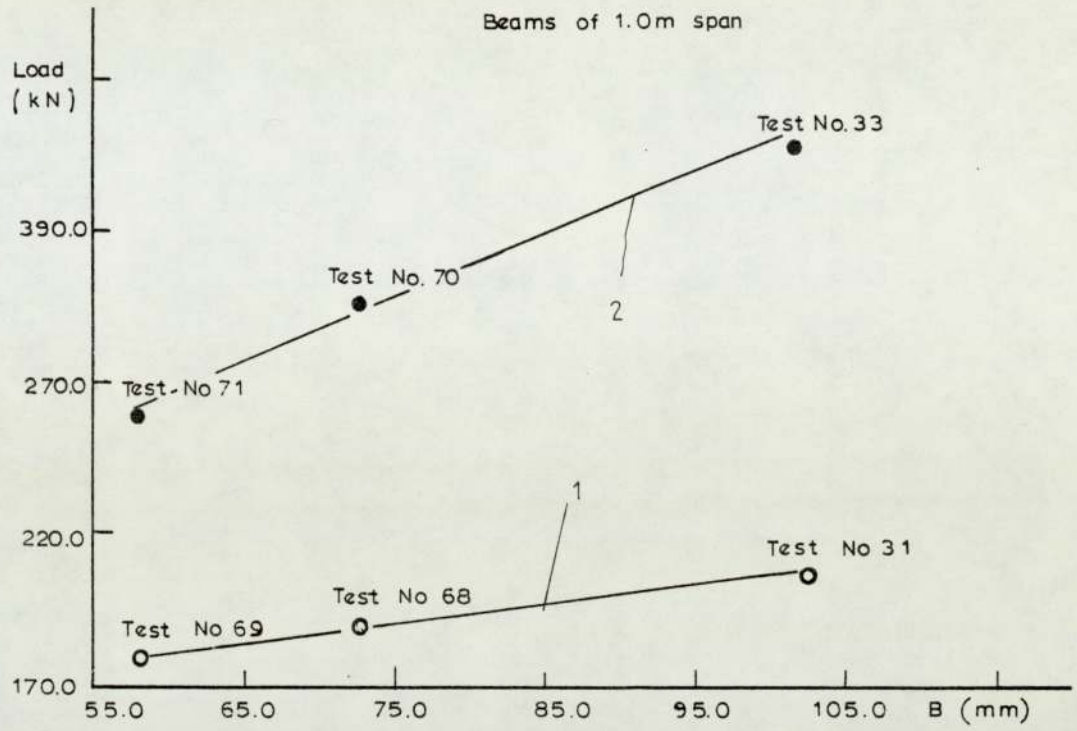

1 $l_a = 150$ mm

2 $l_a = 0$ mm

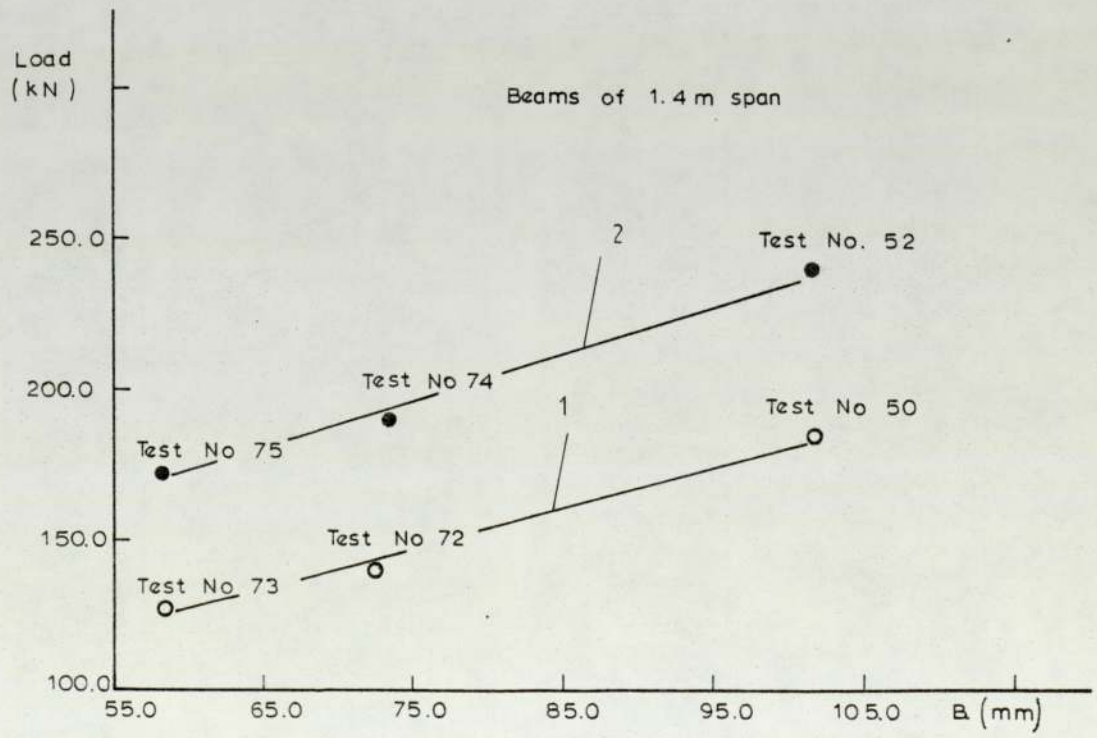

1. Series VI

FIGURE 3.1 CONTINUED

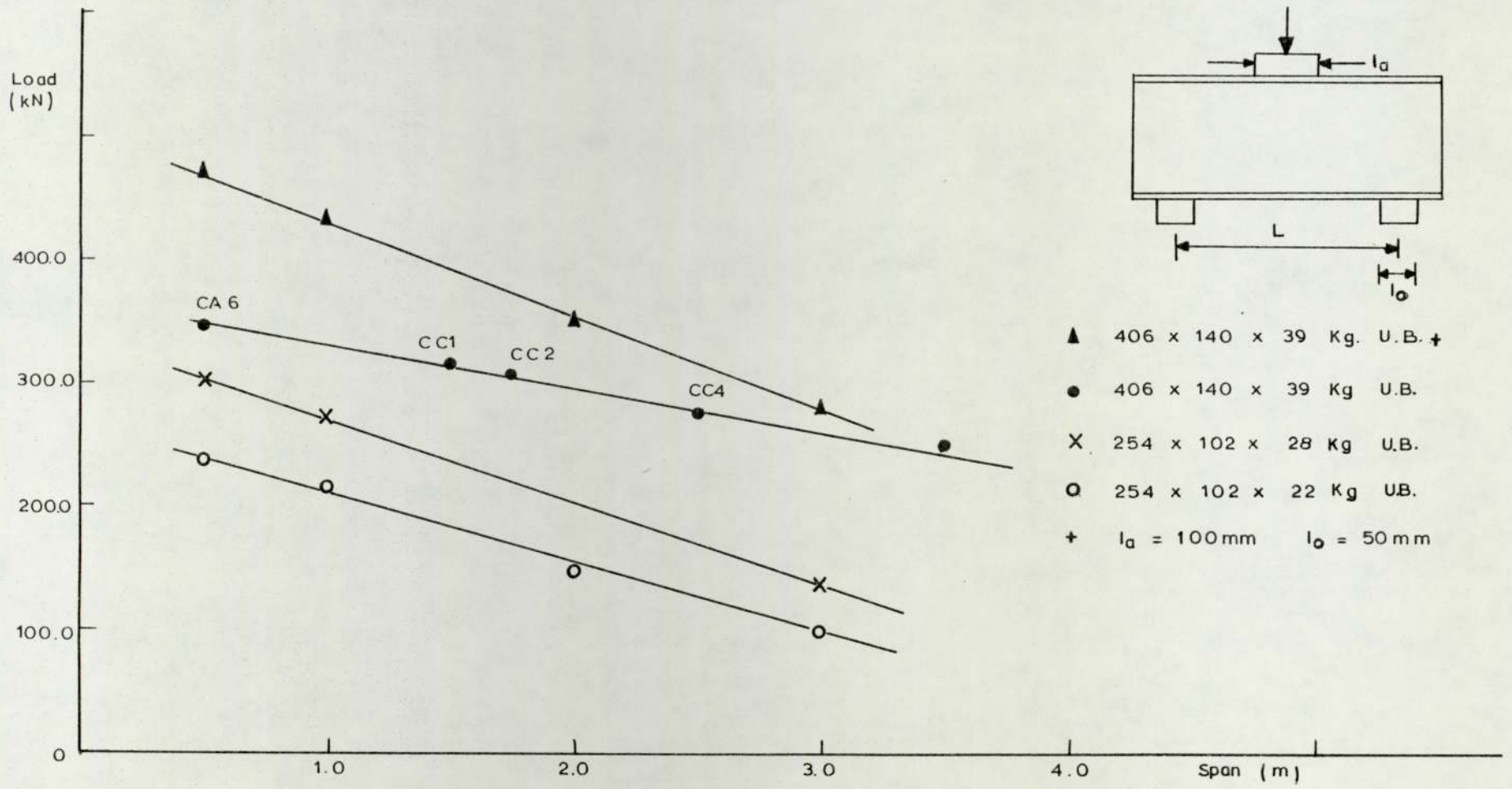

j Series VII

FIGURE 3.1 CONTINUED

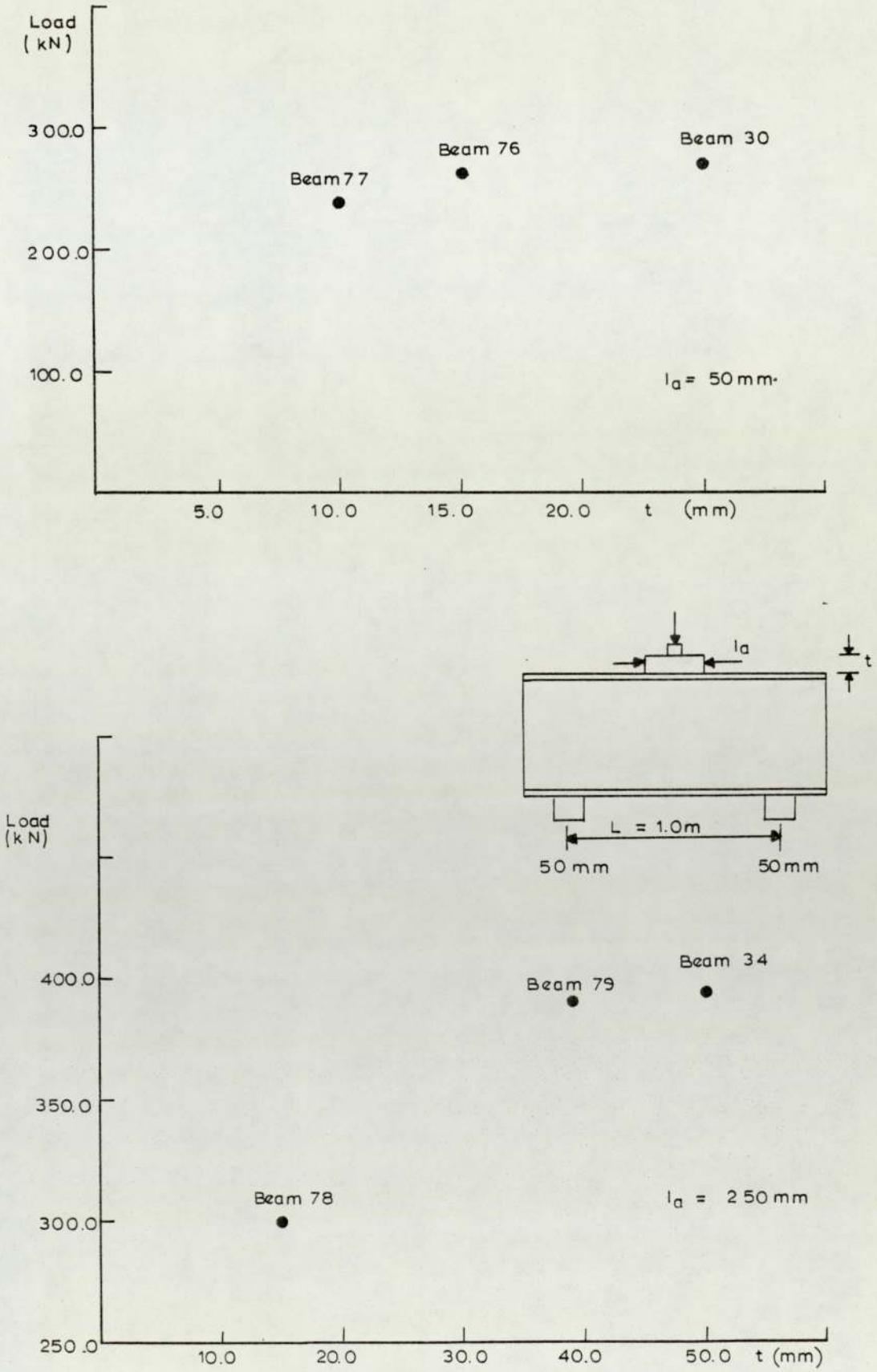

K. Series VII

FIGURE 3.1 CONTINUED

(a) Mode 1

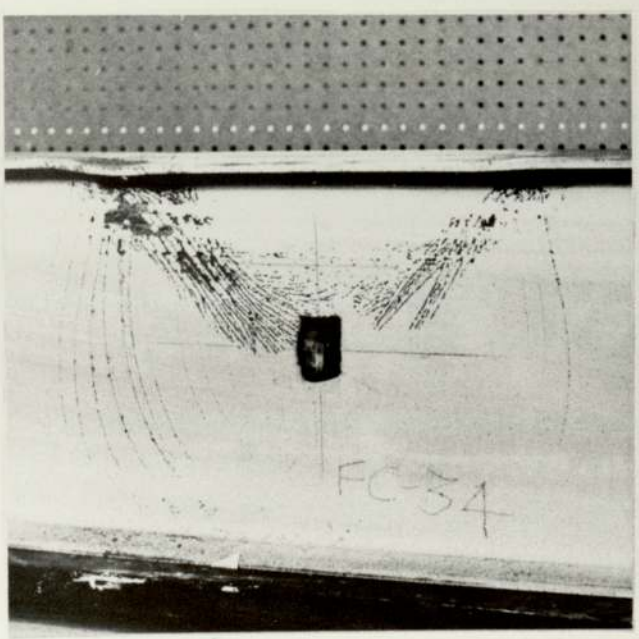

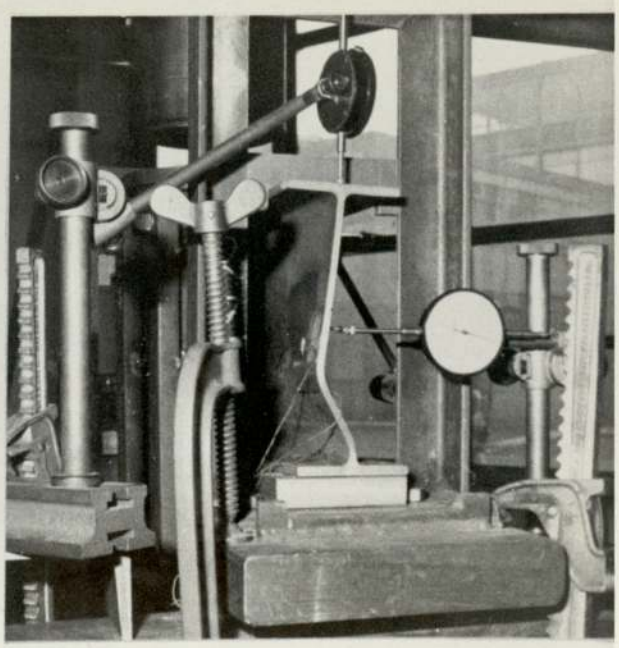

(b) Mode 2

PLATE 3.1 MODES OF FAILURE

third of the depth of the beam. A further feature, possibly due to the very local nature of the failure, is the transverse bending of the flanges which is such that contact with the support of load strip is only maintained directly over the web.

Failure Mode 2 - This failure mode is shown in plate (3.1b). The lateral deflection of the web had the same form as for mode 1, but they were larger; the maximum deflection occurred at about the same point, shown in plate (3.2a, b) for mode 1 and mode 2 respectively. This mode of failure was found to occur when the beams were loaded or supported with large lengths of bearing plate. The flanges were slightly distorted and it could be said that no significant transverse bending was noticed.

More information on the failure mode can be provided by examination of the loads attained for beams which were retested. Beams that had failed in mode 1, when retested, were attaining a load only slightly lower than the ultimate load. Figure (3.11) shows the effect of cycles of loading and unloading of beam No 35 which has failed in this mode. From figure (3.11) it is clear that the failure load reduces to 74% of the first loading after seven cycles. To the contrary beams that had failed in mode 2, when retested, could sustain a load a lot less than the ultimate load.

3.3 STRAIN RECORDINGS

Two ways were adopted in obtaining the strain distribution in the beams, as already has been mentioned in chapter 2. A general strain distribution was obtained from the flaking of the white-wash and a more accurate one from the readings of the attached strain gauges. The observations from these methods will be

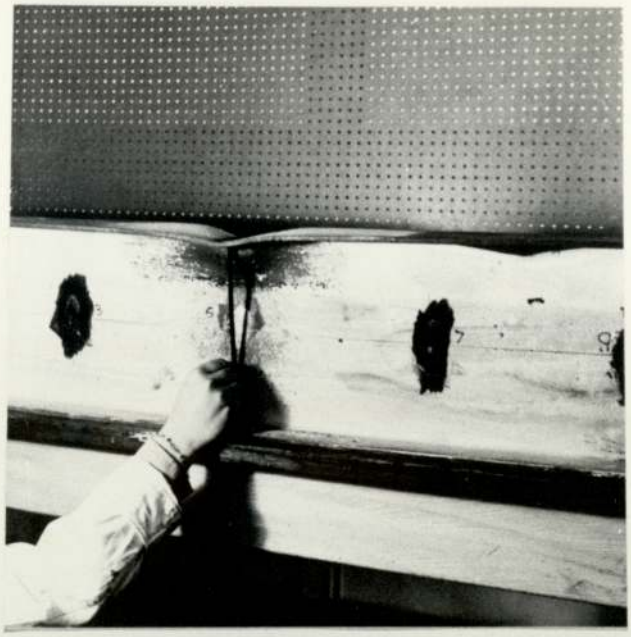

(a) Deflected Shape for Mode 1

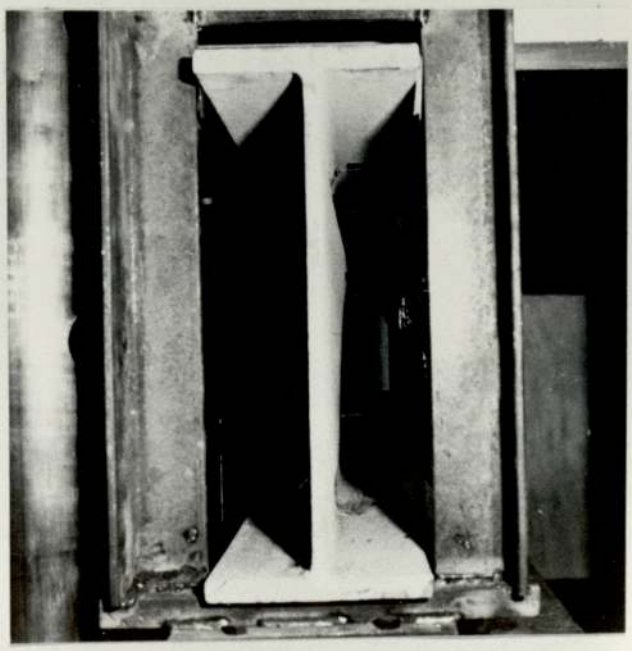

(b) Deflected Shape for Mode 2

PLATE 3.2 DEFLECTED SHAPE FOR BEAMS

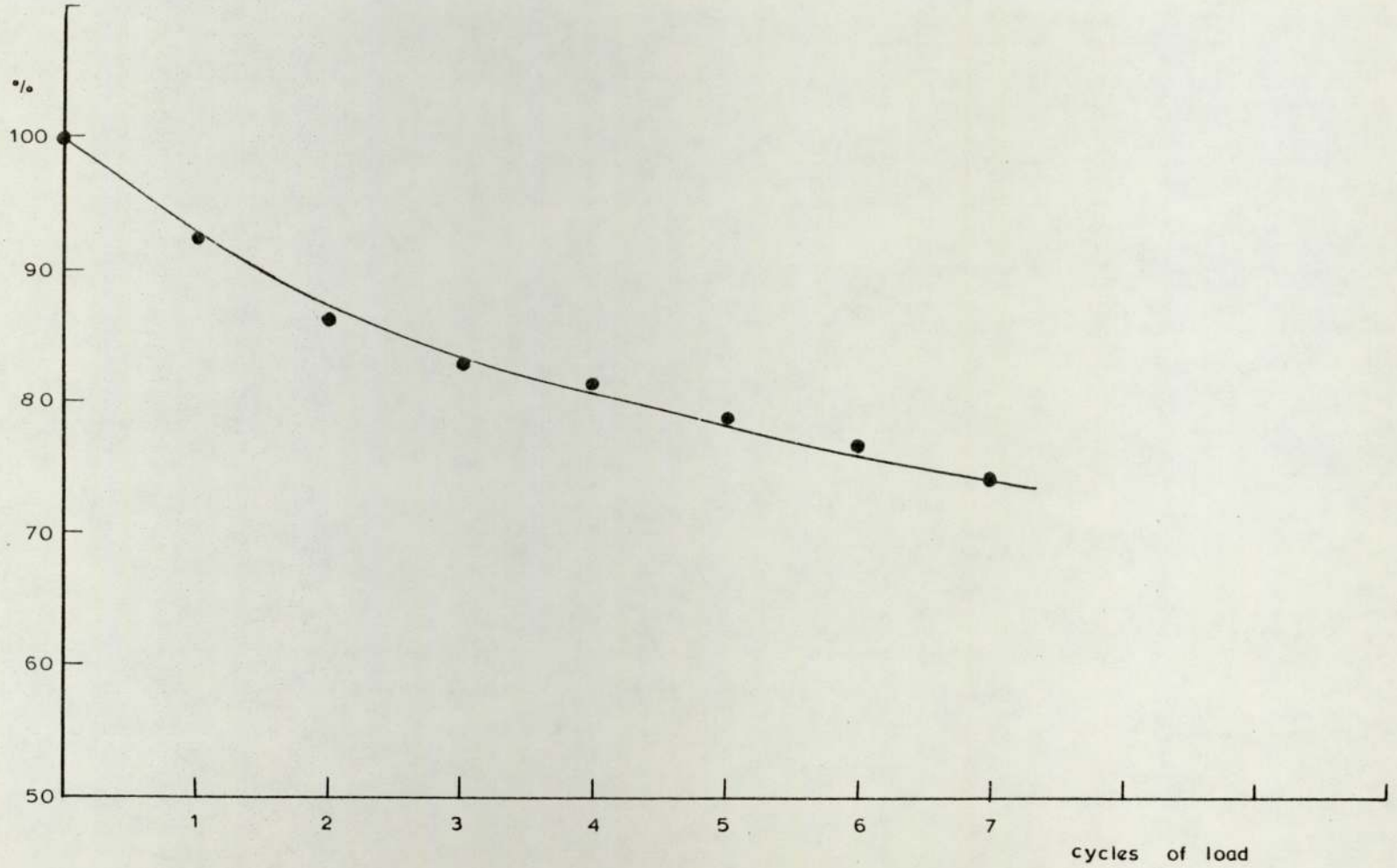

l. Reduction in Failure Load for Cycles of Load (Beam No 35)

FIGURE 3.1 CONTINUED

discussed individually as follows.

3.3.1 General Strain Distribution

It should be emphasized that the strain distribution obtained from the pattern of the crack lines in the white-wash is approximate. It is assumed that the crack lines are formed when the material yields.

It appears that the crack line patterns in the white-wash for beams which failed at the end are similar, despite the type of support. Typical patterns are shown in plate (3.3a, b), for beams 13b and 23a respectively. Areas of very high strain, such as at the support and in the vicinity of the applied load at mid-span, are indicated by the larger areas of flaked white-wash. In plate (3.3a) it could be seen that at the support, the angle the crack lines make with the plane of the flange, is in the region of 20° to 30°. Plate (3.3c) shows the crack lines in the white-wash in the region of the applied load for beam No 44. This was loaded and supported with12.7 mm long stiff bearings across the full width of the flanges. The span of this beam was 0.5 m and the large dark areas along the mid-depth line show the position of the strain gauges. As the span of the beam increases, the affected zone gets larger, this is well shown in plate (3.3d) for beam No 35. This had the same loading and supporting conditions as the former one and was of 1.0 m span. The angle, the crack lines make with the plane of the flange, for this case as displayed in plate (3.3d) is in the region of 40° to 50° and the total length of dispersion is about equal to the depth of the beam.

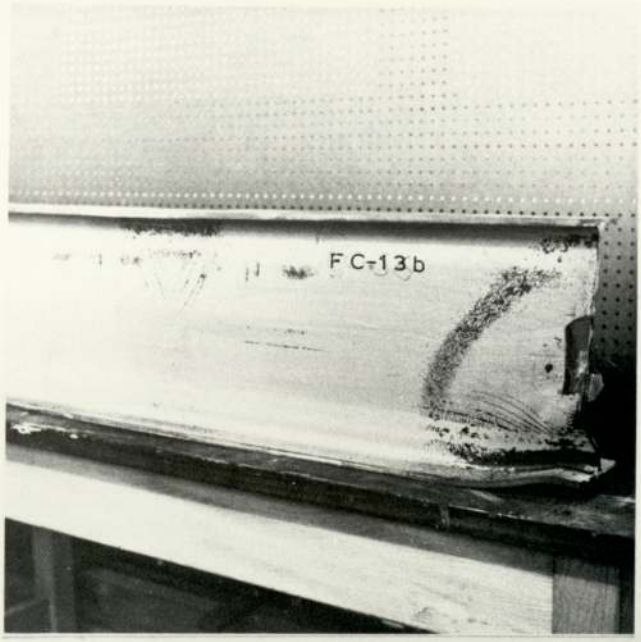

(a) Beam No 13b

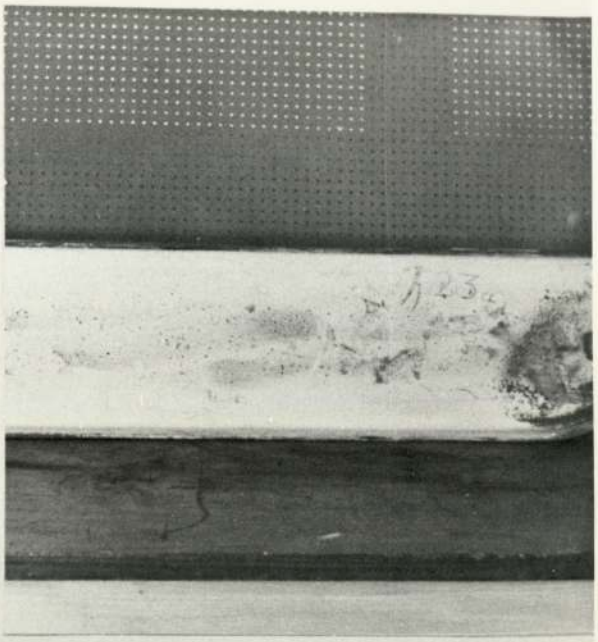

(b) Beam No 23a

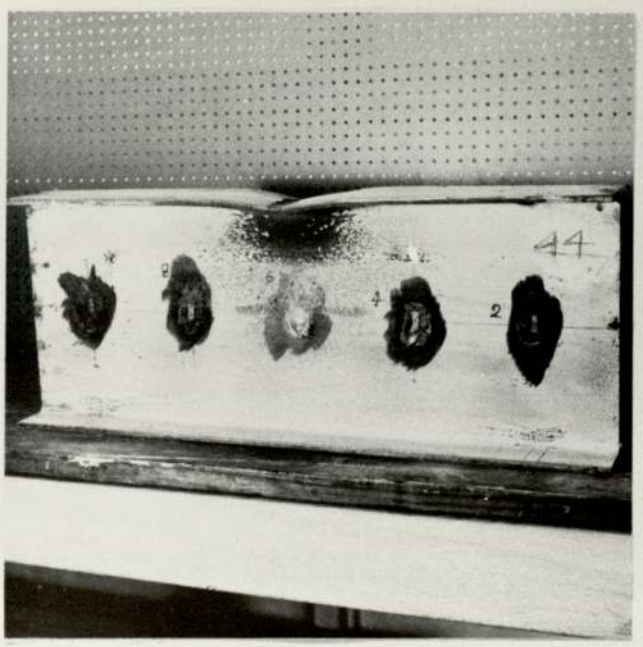

(d) Beam No 44

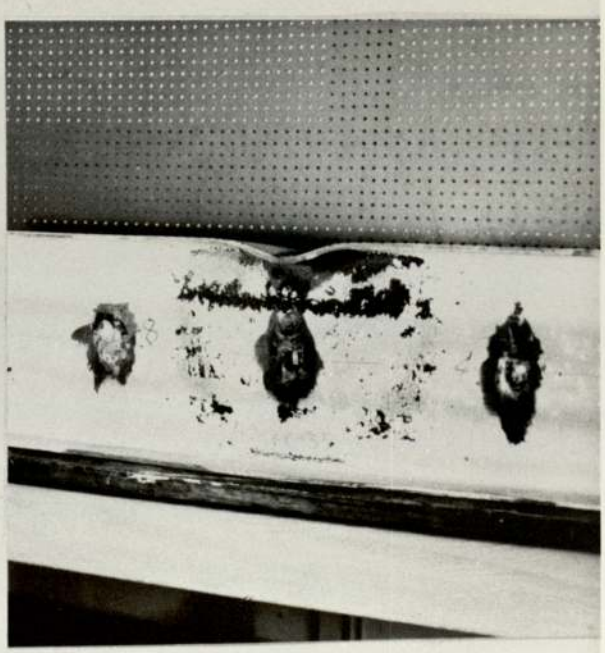

(c) Beam No 35

PLATE 3.3 CRACK LINES IN TESTED BEAMS

If the span of the beam is kept constant and the length of the applied load varies, then the strain distribution varies. This is shown in plate (3.4a) for beam No 66 and plate (3.4b) for beam No 67. These beams were loaded by 150 mm and 300 mm lengths of load respectively and as could be seen from the above mentioned plates the strain dispersion is greater for a shorter length of applied load. This statement is confirmed by plate (3.5a, b) for the beam Nos 60 and 61 respectively. These beams were loaded by 12.7 mm and 100 mm lengths of load respectively. Plate (3.5c) shows in greater detail the crack lines in the white-wash at the inside face of the top flange for beam No 60. The crack lines have a slight curvature away from the centre of the applied load. This was noticed for other cases and could also be seen in plates (3.4a, b).

3.3.2 Strain Gauge Readings

The strain gauge readings and the deflection gauge readings are given in table (A.1) in appendix 1. Strain readings which have exceeded the value of the 'yield strain' are shown with 'Y' alongside; the yield strain can be determined from the tensile test results.

The strain gauges, as previously mentioned, were always used in pairs, one each side of the web. The direct and bending strains can therefore be calculated, if required, from the semi-sum and semi-difference of the readings of the two strain gauges respectively. Figure (3.2a) shows the comparison of the direct strains for test No 8a and test No 10a of series I and series II respectively and figure (3.2b) shows the comparison of the bending strains for the same tests. The only difference in these

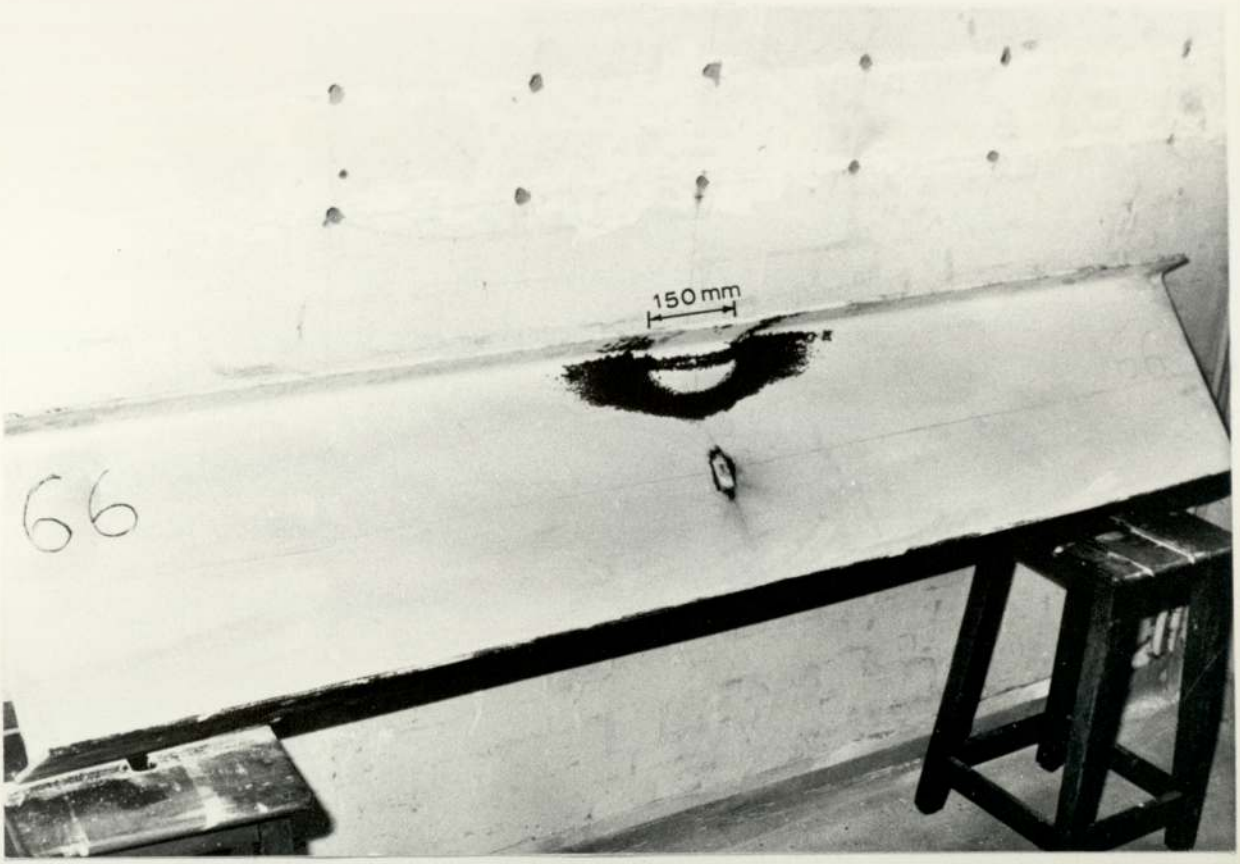

(a) **Beam** No 66

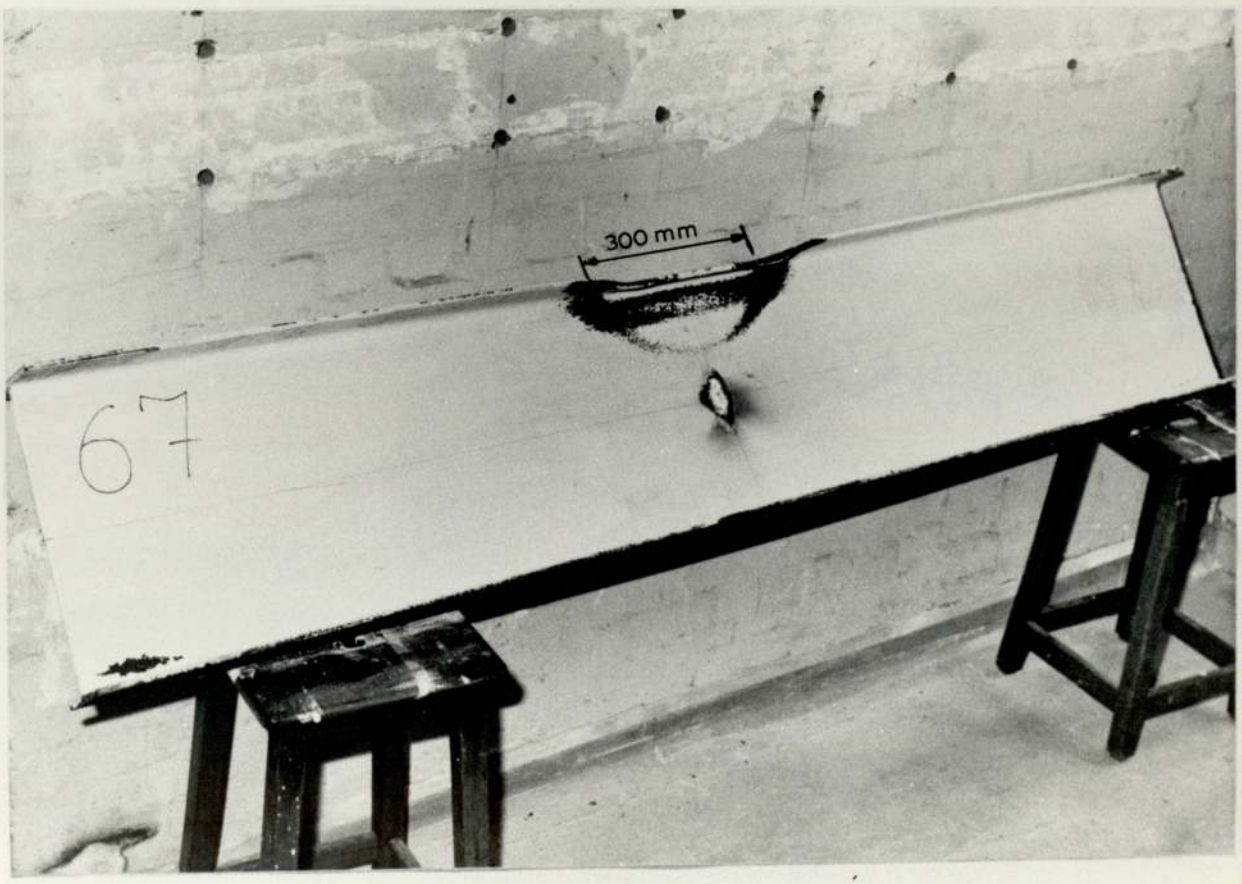

(b) Beam No 67

PLATE 3.4 CRACK LINES IN TESTED BEAMS

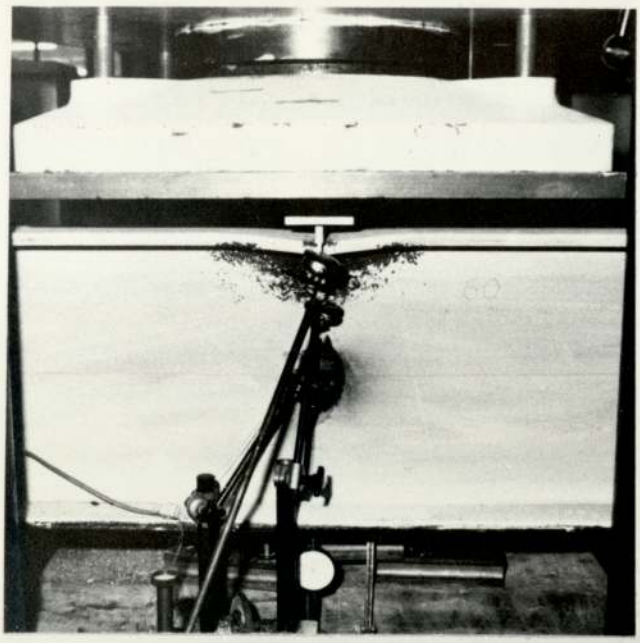

(a) Beam No 60

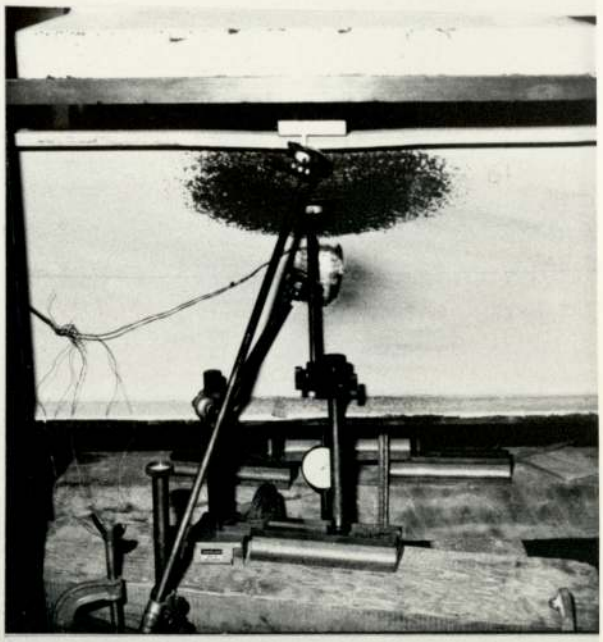

(b) Beam No 61

(c) Beam No 60

PLATE 3.5 CRACK LINES IN TESTED BEAMS

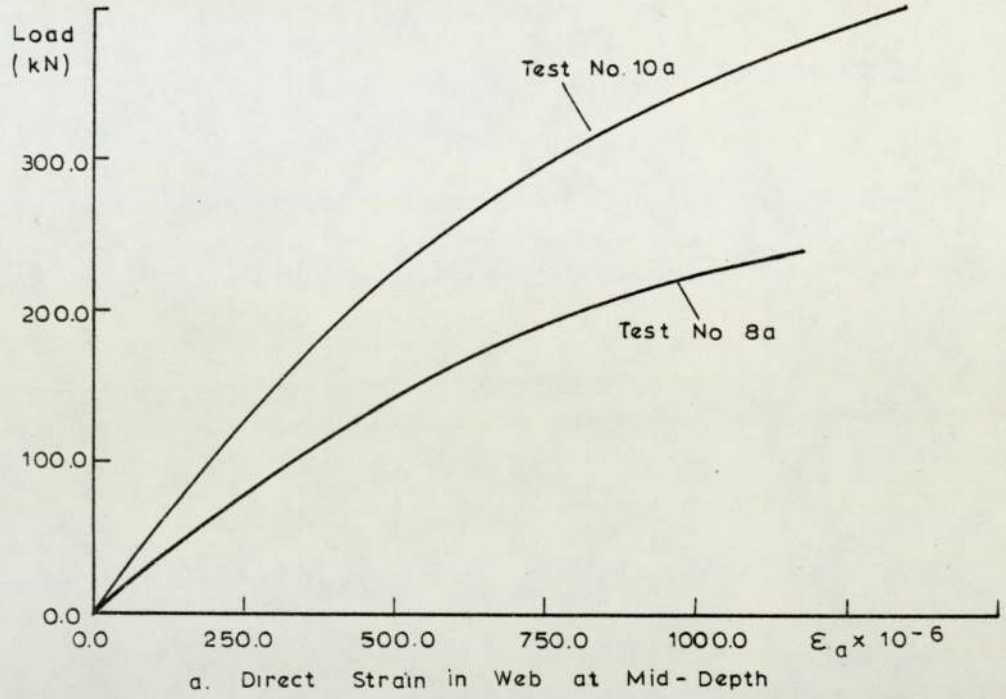

a. Direct Strain in Web at Mid-Depth

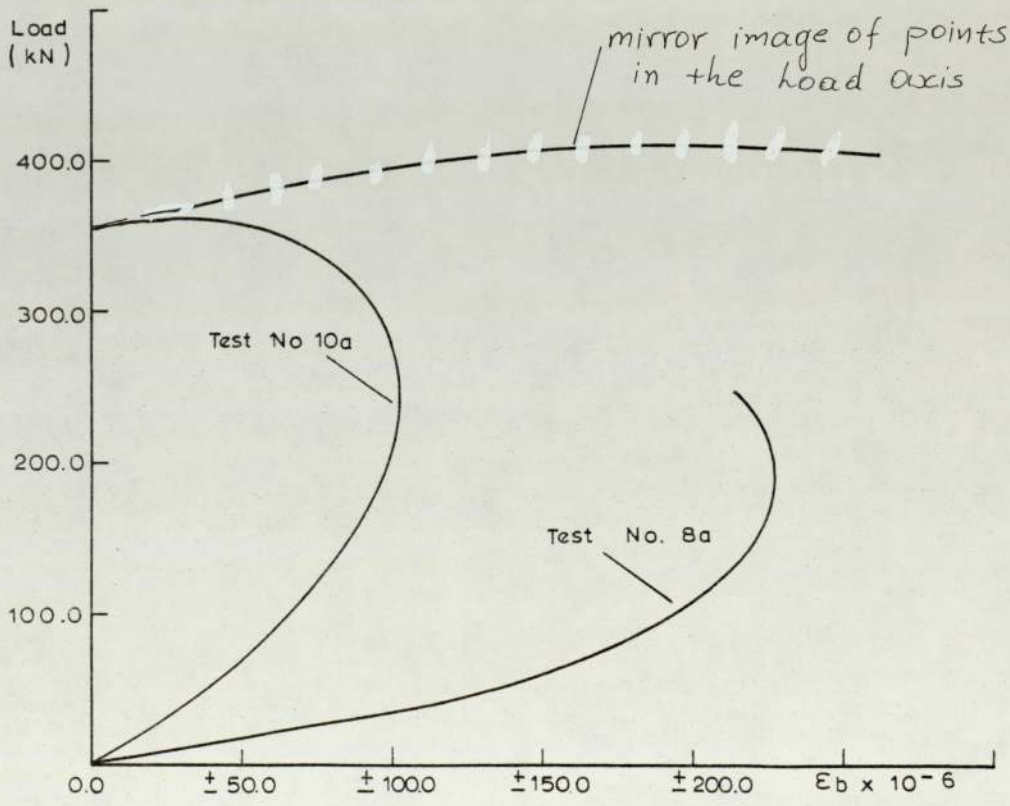

b. Bending Strain in Web at Mid-Depth

FIGURE 3.2 TYPICAL STRAIN IN WEB FOR SERIES I AND II

tests is the type of support, although the length of the bearing plate is the same. The direct strain distribution is similar but with higher strains for test No 8a, as one would expect. The bending strain distribution is rather peculiar. The strain increases with increasing loads and when the beam is near to failure it decreases and further it increases for test 10a. Figure (3.3a, b) shows a comparison between the strains for test No 13b and test No 25b of series III and series IV respectively. Each beam is identical, except for the type of support, but with the distance of the inner face of the bearing plate to the end of the beam approximately equal. The direct strains are quite comparable, with the strain being higher, at comparable loads, for test No 13b due to the smaller area of support. The bending strains show a similar distribution but not a uniform one. At small loads the strain reduces with an increase of load and suddenly near to failure point in increases. Certain beams in series III namely beam Nos 36, 37 and 38 had the width of the flanges reduced and figure (3.4) shows the direct and bending strain distributions. All these beams show very similar direct strain distributions except the strain for test No 13b, being slightly higher than the others at small loads. This is probably due to the large initial eccentricity of the web as can be seen from table (2.5) and the deflection readings given in table (A.1) in appendix 1. The comparison of the bending strains in figure (3.4b) shows that the strain is relatively small for test Nos 36, 37 and 38 and higher for test No 13b, for the reason given above. It appears that changes in flange width have little effect on the strain distribution in the web and further comparisons are not made. In series III,

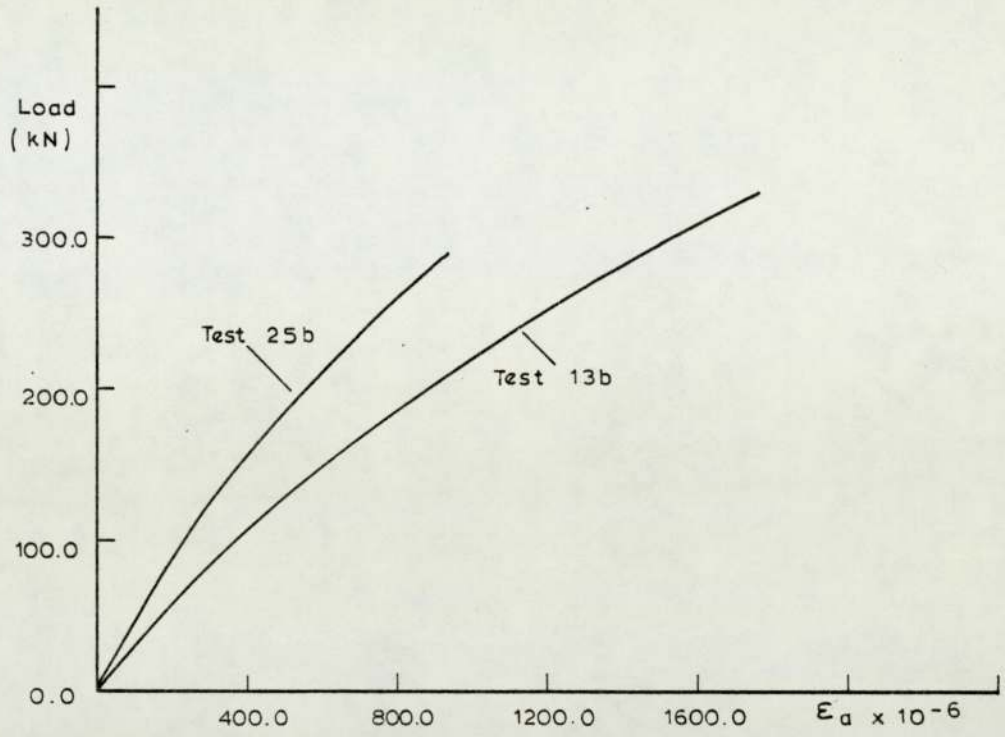

a. Comparison of Direct Strain

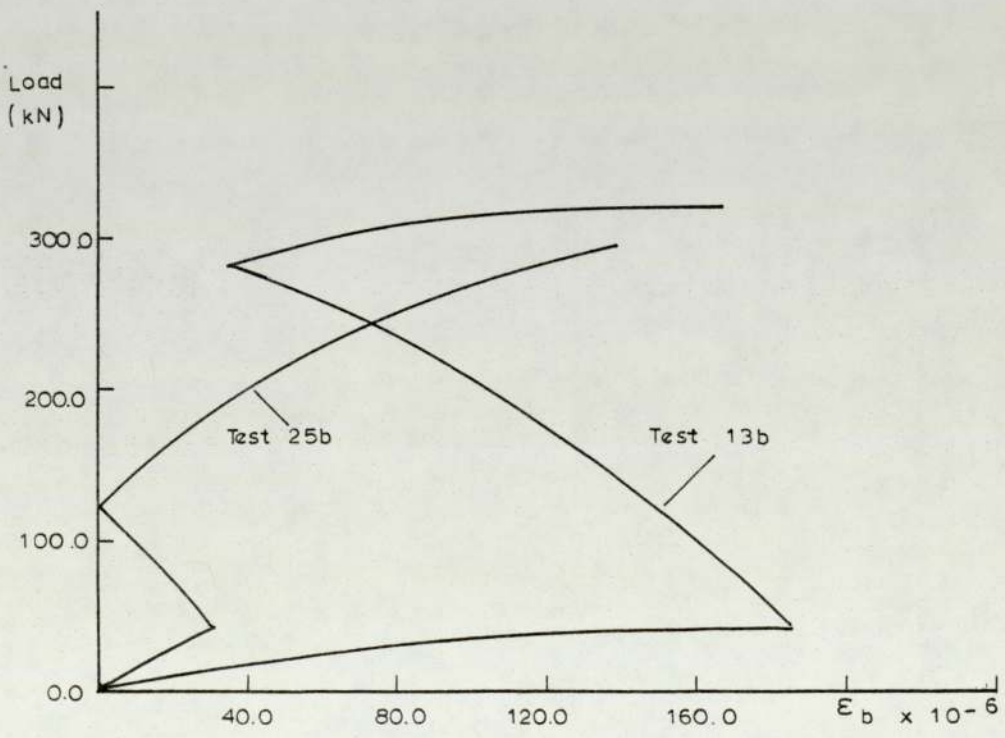

b. Comparison of Bending Strain

FIGURE 3.3 COMPARISON OF STRAIN FOR SERIES III AND IV

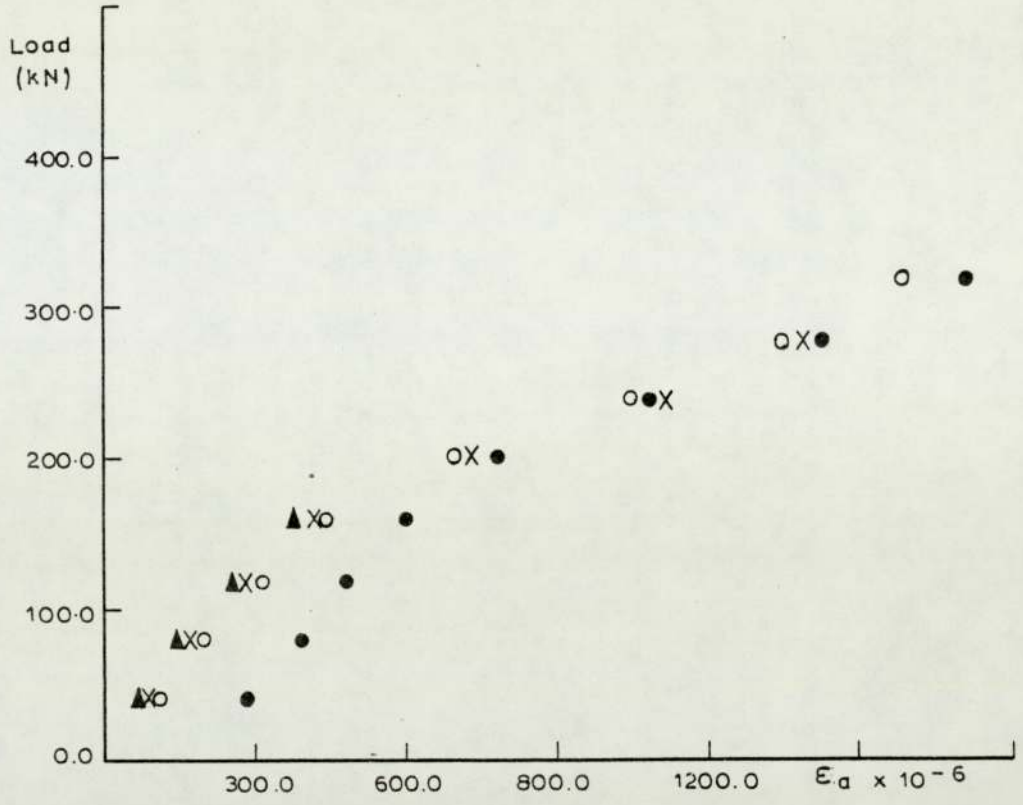

a. Direct Strain in the Web at Mid Depth

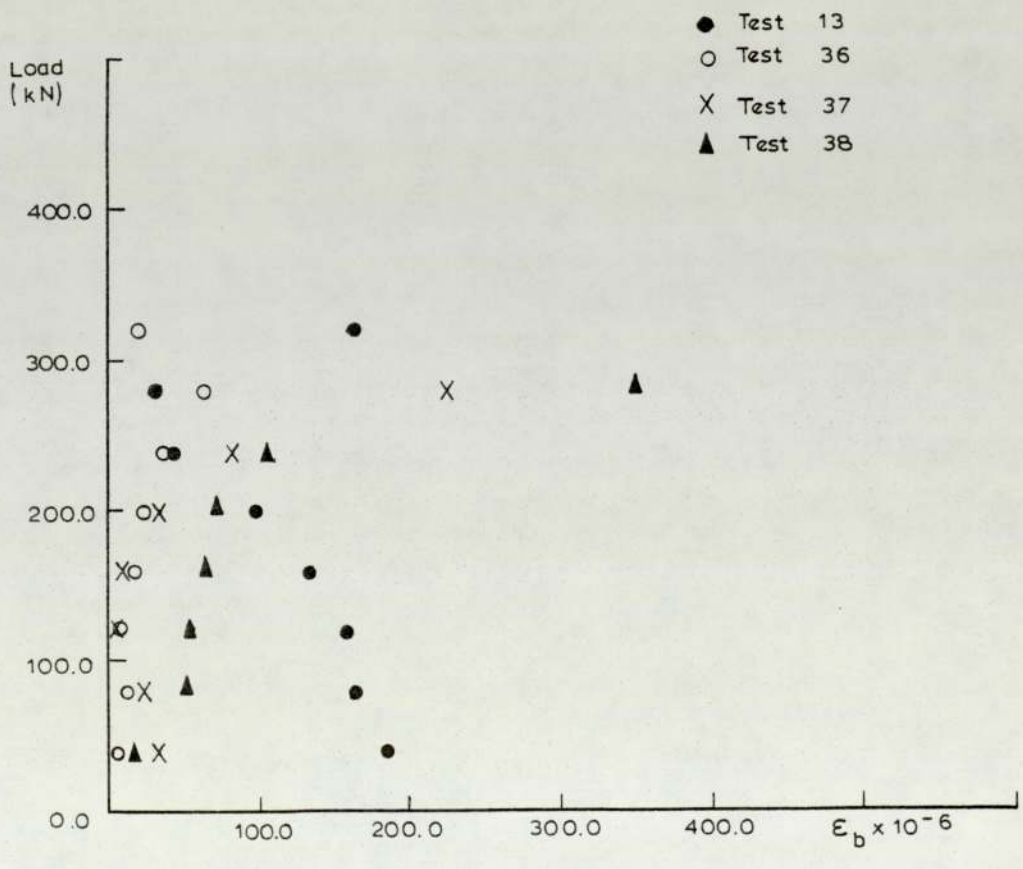

b. Bending Strain in the Web at Mid - Depth

FIGURE 3.4 TYPICAL STRAIN IN THE WEB FOR SERIES III

some beams had the thickness of the flanges reduced, namely beam Nos 39, 40, 41, 42 and 43. All beams show very similar direct strain distribution, as shown in figure (3.5a). As for the previous case the bending strain distribution is not very clear and any conclusions will be misleading.

The plot of the strain along the mid-depth line of the beam Nos 50, 51, 52 and 53 in series IV are shown in figure (3.6), at a load of 160 kN. All beams have the same span and are loaded at the top flange at mid-span through stiff loading plates of varying length. The direct strain curves, as one would expect, are flatter for increasing lengths of the applied load, higher in the vicinity of the applied load and decreasing away from it. Despite the differences of strain under the load point for different lengths of bearing the strains at the supports and the strains at a quarter span are similar for all tests.

Figure (3.7) shows the direct strain distribution on a vertical section of the web at the central point load at mid-depth and a quarter-depth from the top for beam Nos 50 and 53. Beam No 50 was loaded by a knife edge load and as could be seen from figure (3.7a) the strain is higher at a quarter depth than at mid-depth. For beam No 53 the load was distributed with a 250 mm long stiff bearing plate and the strain was about the same at a quarter and mid-depth. Near to the failure point though, as could be seen from figure (3.7b), the strains indicate a change of curvature of the web.

The state of strain in the web along the mid-depth line can be examined from the strain gauge readings for test No 44 in series VII, which was simply supported on two 12.7 mm long stiff bearings and loaded at mid-span through another. The strain distribution is

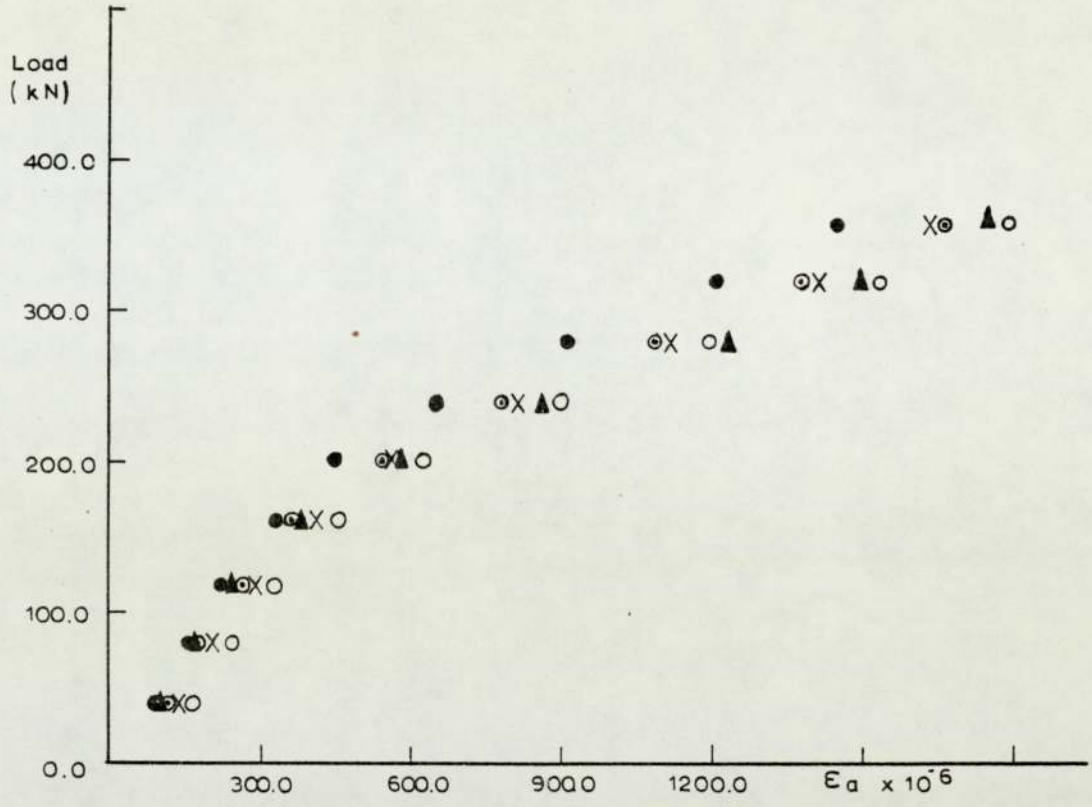

a. Direct Strain in Web at Mid-Depth

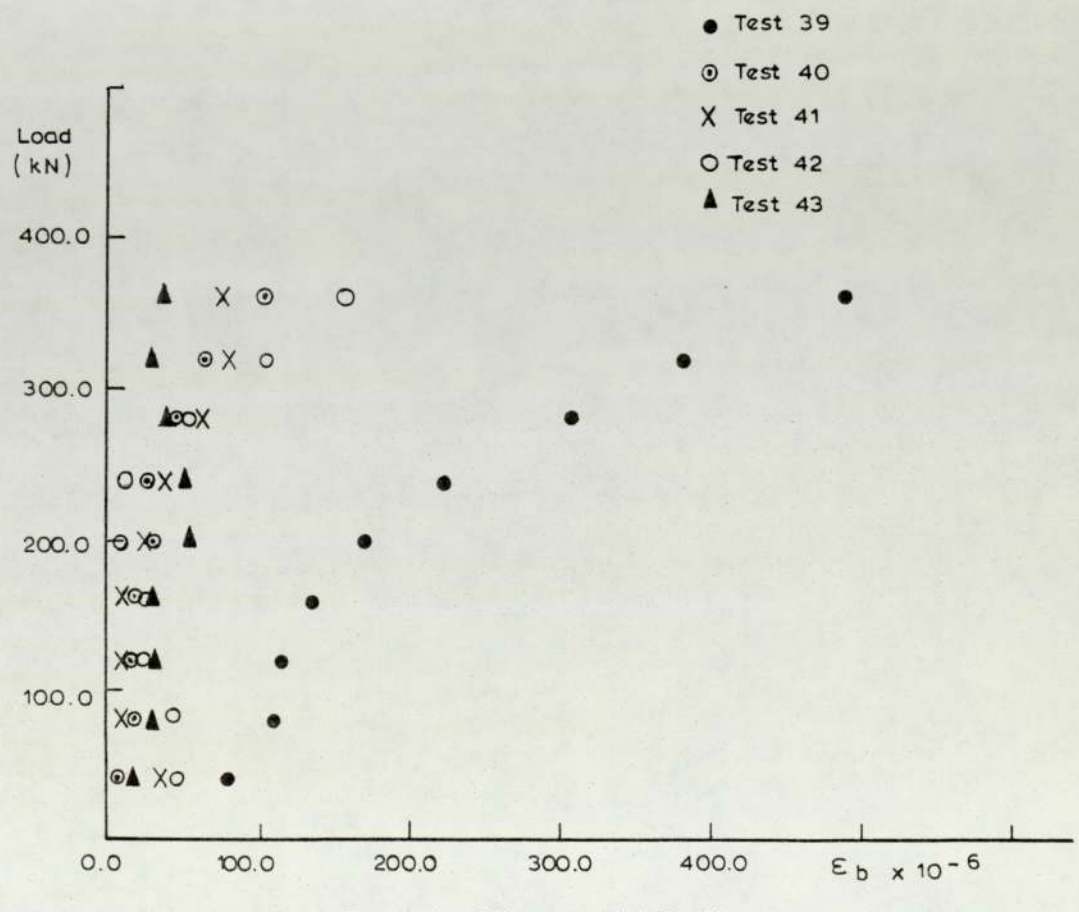

b. Bending Strain in Web at Mid-Depth

FIGURE 3.5 TYPICAL STRAIN DISTRIBUTION FOR BEAMS IN SERIES III

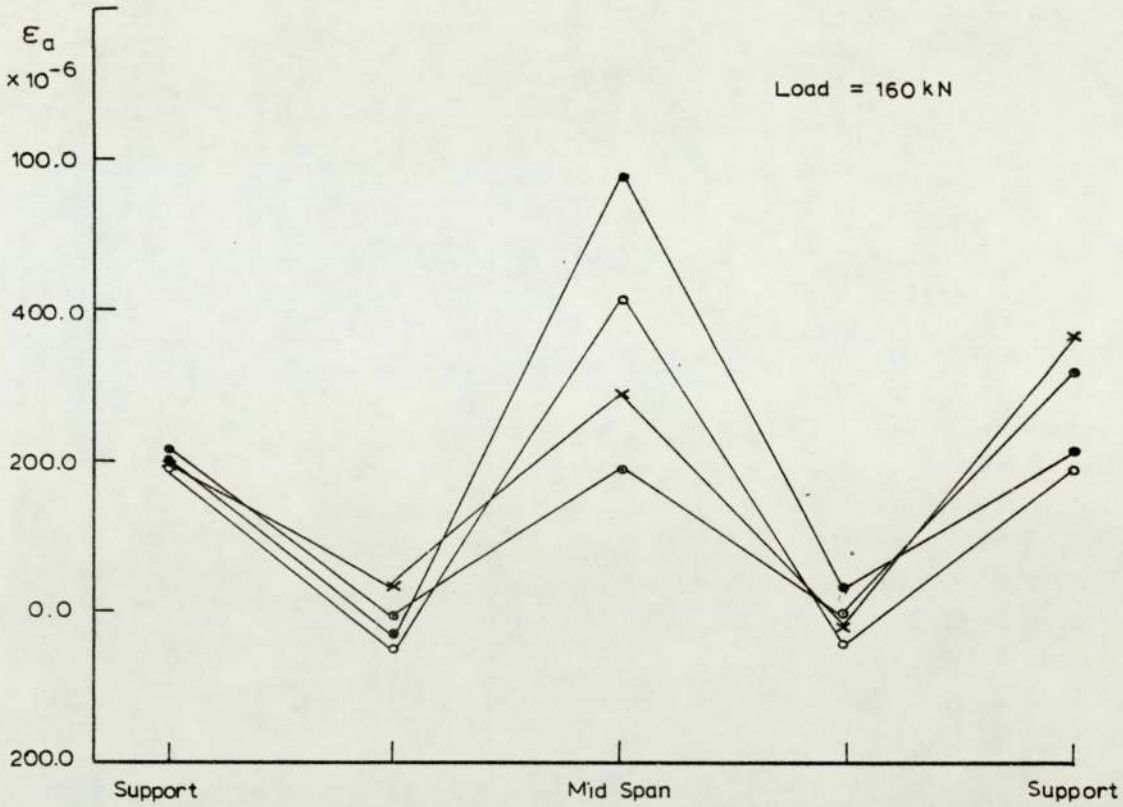

a. Comparison of Direct Strain

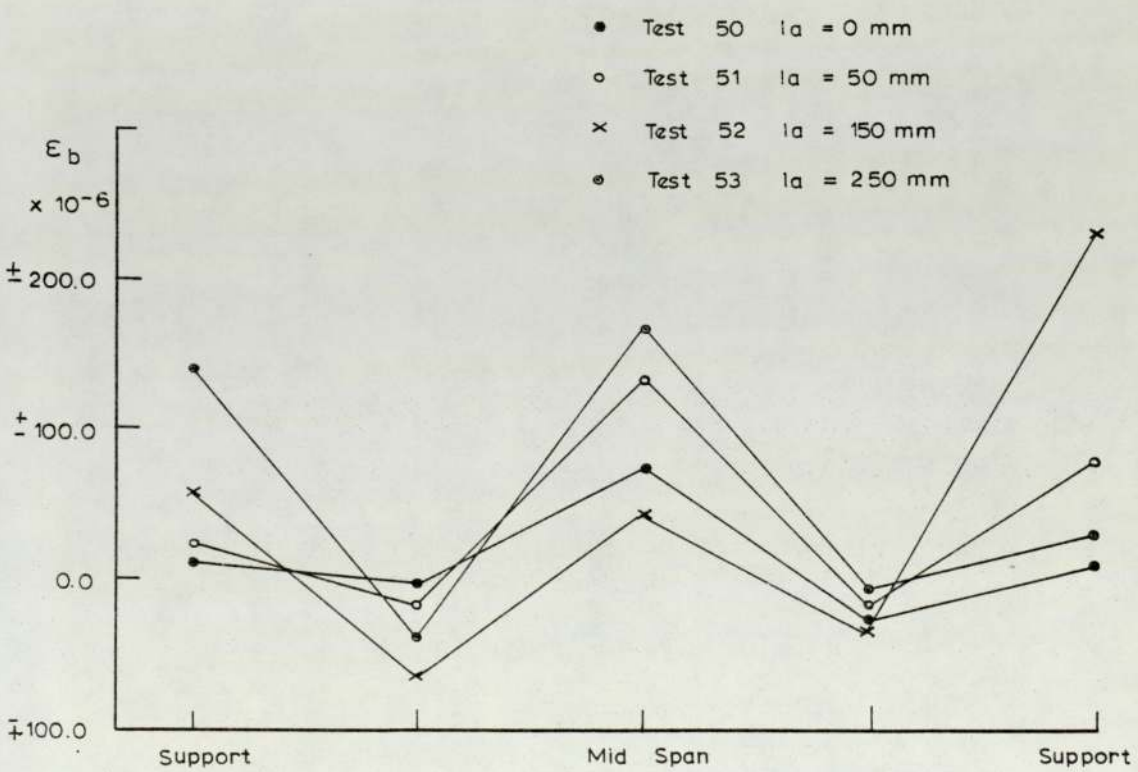

b. Comparison of Bending Strain

FIGURE .3.6 STRAIN DISTRIBUTION FOR SERIES VI

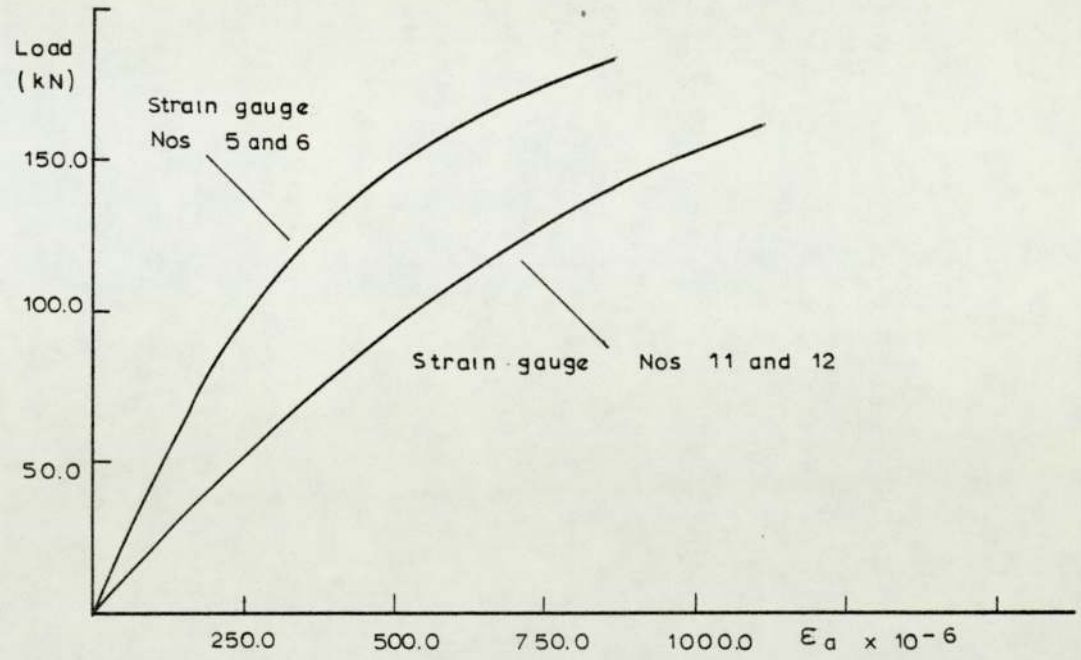

a. Direct Strain Distribution for Beam No. 50

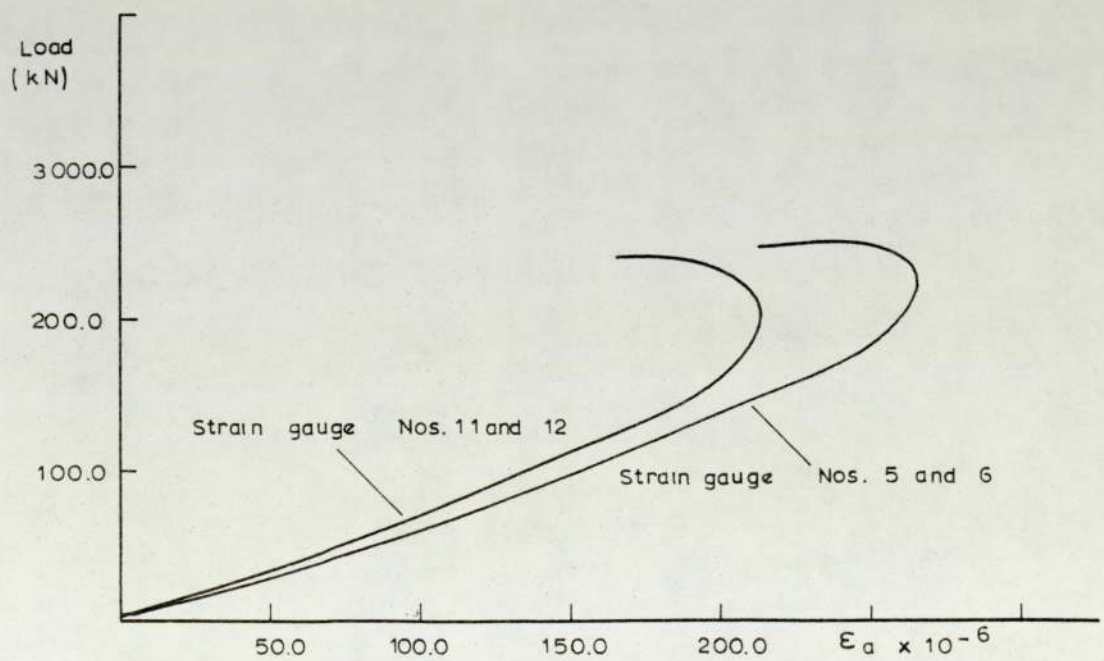

b. Direct Strain Distribution for Beam No. 53

FIGURE 3.7 DIRECT STRAIN DISTRIBUTION FOR SERIES IV

shown in figure (3.8). The direct strain is increasing with increasing loads,especially at mid-span and at the supports, this is possibly due to plastic yielding, and reduces between these two points at high loads, where by referring to figure (3.8b) is a region of high bending strains. Figure (3.9) shows the direct and bending strain distribution for beam Nos 44, 35, 45 and 46 all loaded in the manner explained above but for different lengths of span at a load of 80 kN. The effect of the initial eccentricity of the web of beam No 35 can be seen from these plots.

3.4 DEFLECTION GAUGE READINGS

The lateral web deflection along the mid-depth line at the location of failure was recorded for all the tests. For many tests the central deflection gauge showed a relatively large deflection of the web at a very small load. The deflections then increased very gradually, at a slower rate up to the point of failure when they increased at a very fast rate and became unreadable in some tests. These large initial deflections were mainly due to 'squaring up' of the flanges between the applied loads as the initial load increment was applied.

Typical load-deflection curves for beams tested for end failure are shown in figures (3.10) and (3.11) for test No 13a. Figure (3.10) shows the vertical deflection of the beam at mid-span and above the support. The lateral deflection of the top flange, at mid-span, is shown in figure (3.11a). At a very small load the movement is quite large and very small for further increments of load up to failure. Figure (3.11b) shows the lateral deflection of the web at the mid-depth line above the support. The deflection increases for small and intermediate increments

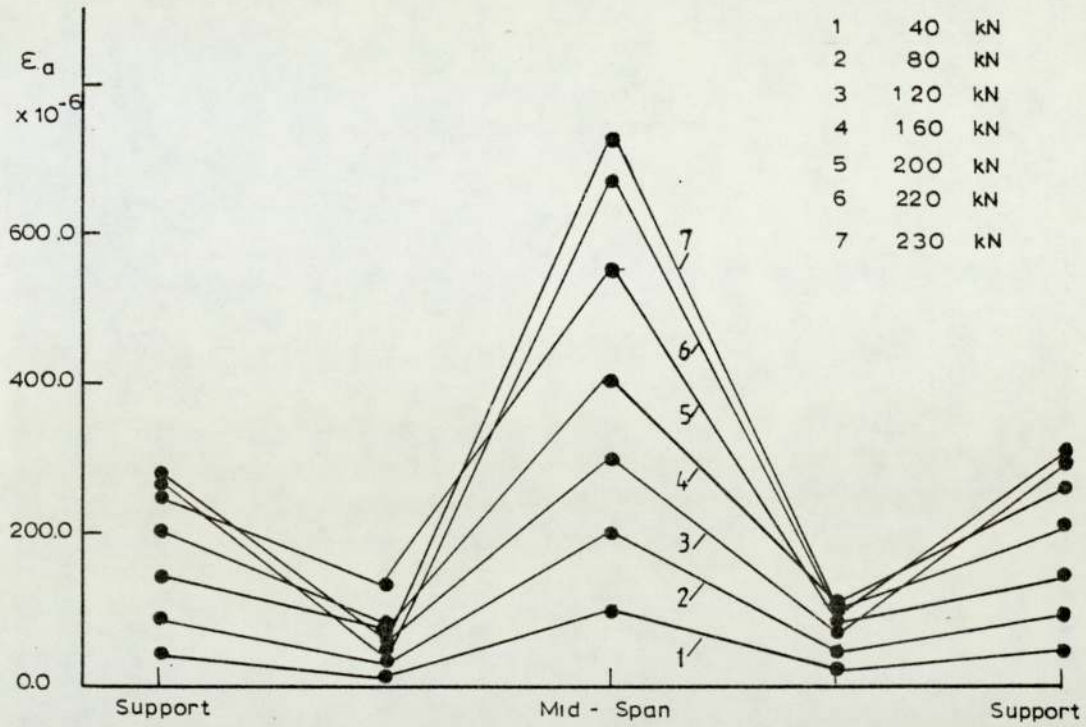

a. Direct Strain Distribution

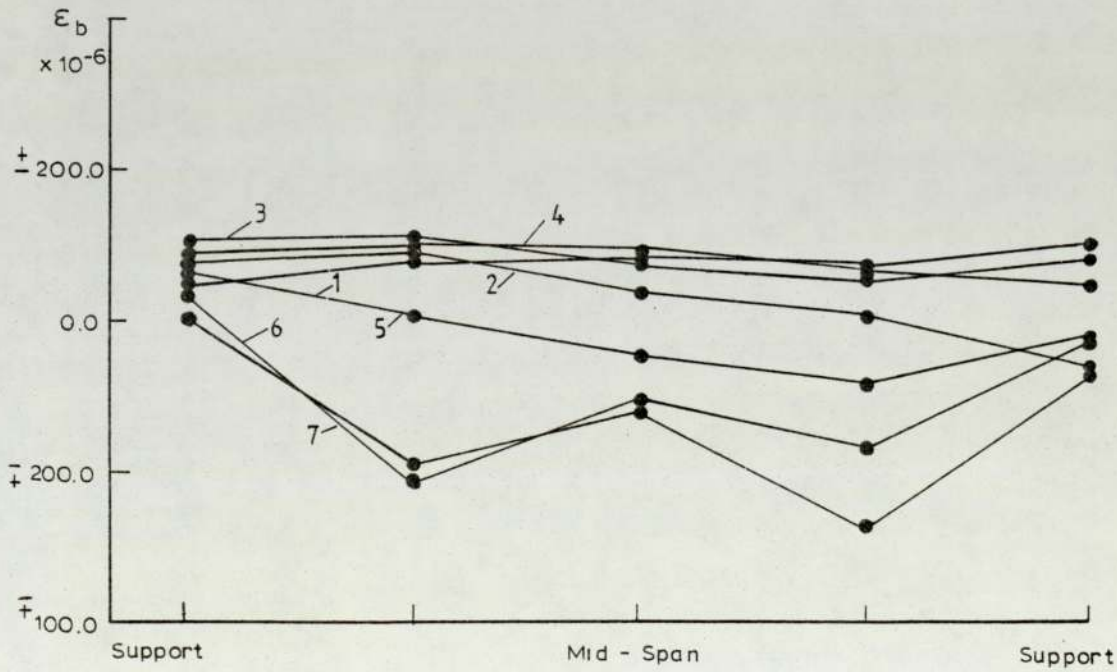

b. Bending Strain Distribution

FIGURE 3.8 STRAIN DISTRIBUTION FOR BEAM No. 44

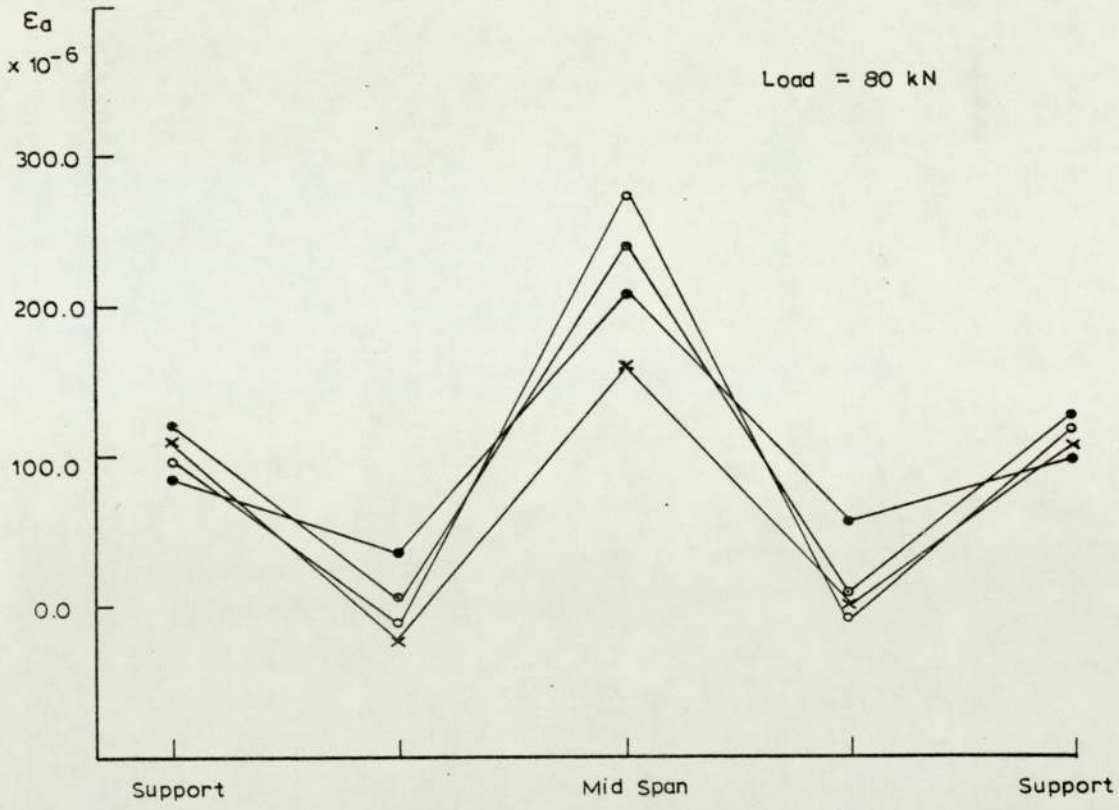

a. Direct Strain Distribution

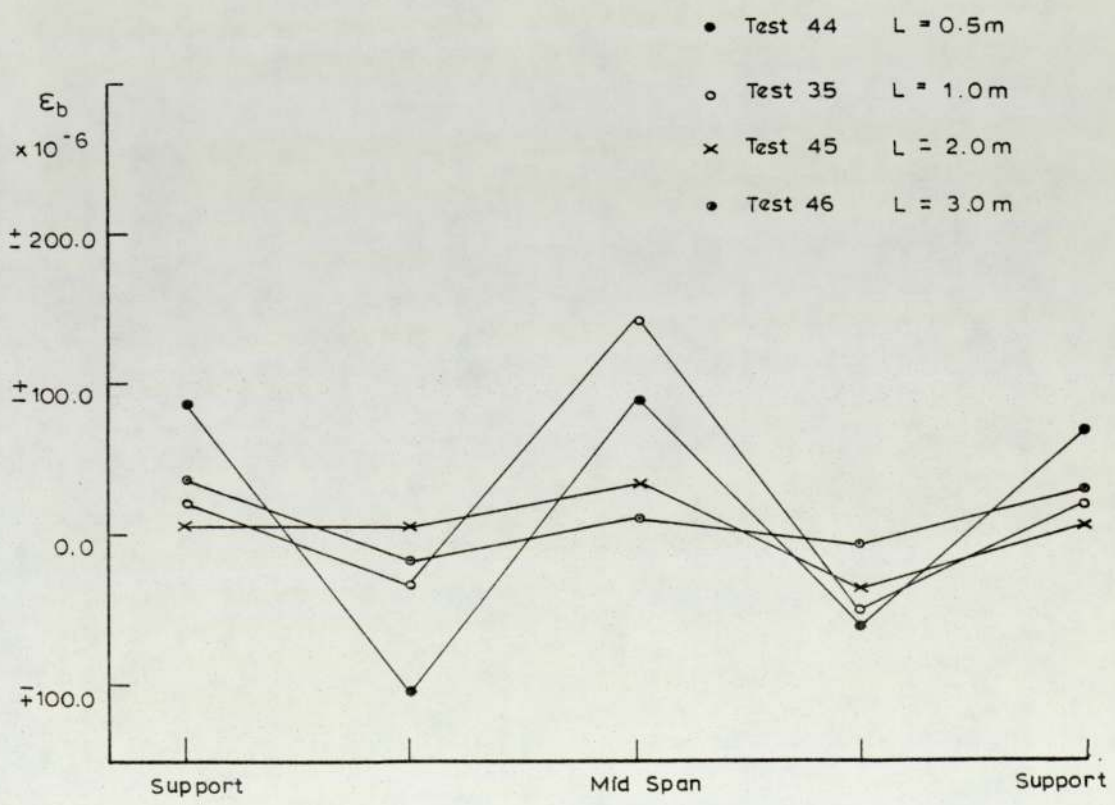

b. Bending Strain Distribution

FIGURE 3.9 STRAIN DISTRIBUTION FOR BEAMS IN SERIES VII

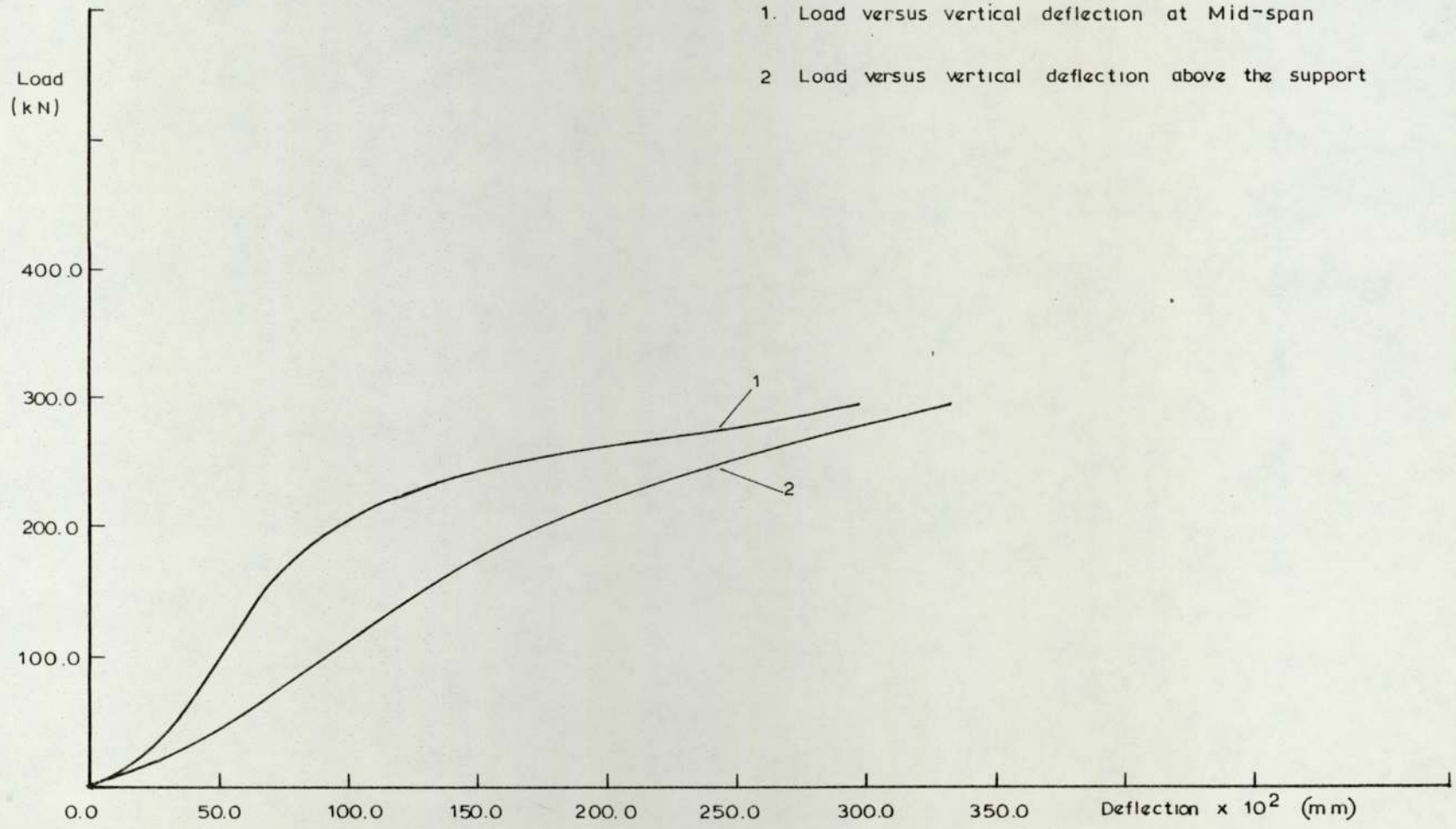

FIGURE 3.10 LOAD DEFLECTION PLOTS FOR BEAM 13a

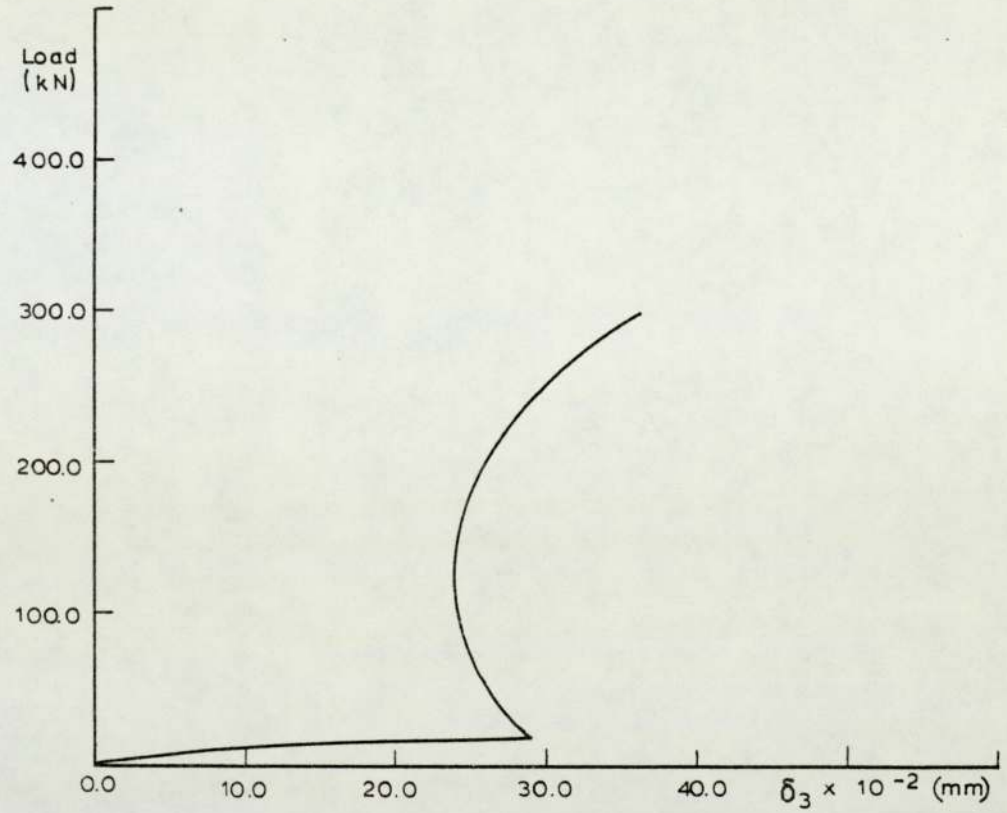

a. Flange Lateral Deflection for Beam 13a

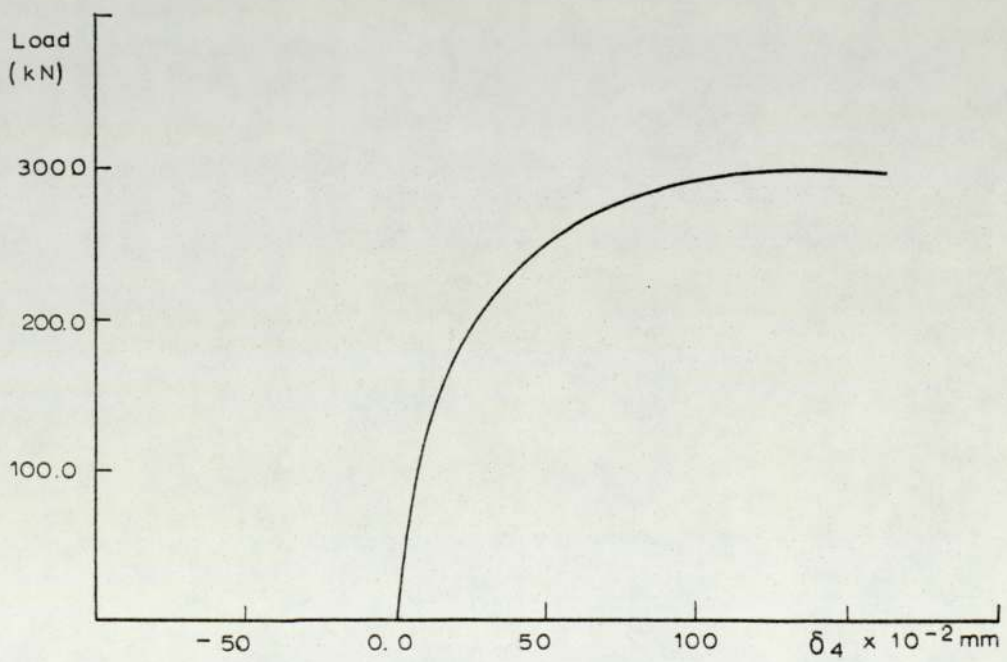

b. Web Lateral Deflection for Beam 13a

FIGURE 3.11 LOAD DEFLECTION PLOT FOR BEAM 13a

of load and near to failure it appears to become almost horizontal.

Figure (3.12) shows the variation of vertical deflection at the bottom flange of the beam with load for beam Nos 31, 30, 32, 33 and 34 for central failure. These beams had the same span and were loaded through stiff bearing plates of varying lengths. It could be said that at comparable loads the length of the stiff bearing has no influence on the vertical deflection of the beam at mid-span, until failure is imminent.

Figure (3.13) shows the influence of the length of the bearing plate on the lateral deflection of the web for beam Nos 64, 65, 56, 66 and 67. These had a span of 2.0 m long and loaded through different lengths of stiff plate . For small loads it appears that the deflection decreases with increasing lengths of loads and this could probably be due to initial lack of straightness. For further load increments no solid conclusions could be drawn out.

As the span increases, for a constant length of load, the vertical deflection of the beam, at mid-span, increases with increasing load. This is shown in figure (3.14) for beam Nos 44, 35, 45 and 46. Up to a span to depth ratio (L/d) of 4.0 the increase in the vertical deflection is relatively small and gets larger for ratios greater than 4.0. The same seems to happen with the lateral deflection of the web at mid-depth, as is shown in figure (3.15) for the same beams. That is, at comparable loads, the deflection increases with increasing spans.

Figures (3.16) and (3.17) show the lateral deflection over the web depth, for increments of load for beam Nos 60 and 61 respectively. These beams were identical except that the first mentioned beam was loaded through a 12.7 mm long stiff bearing and the other

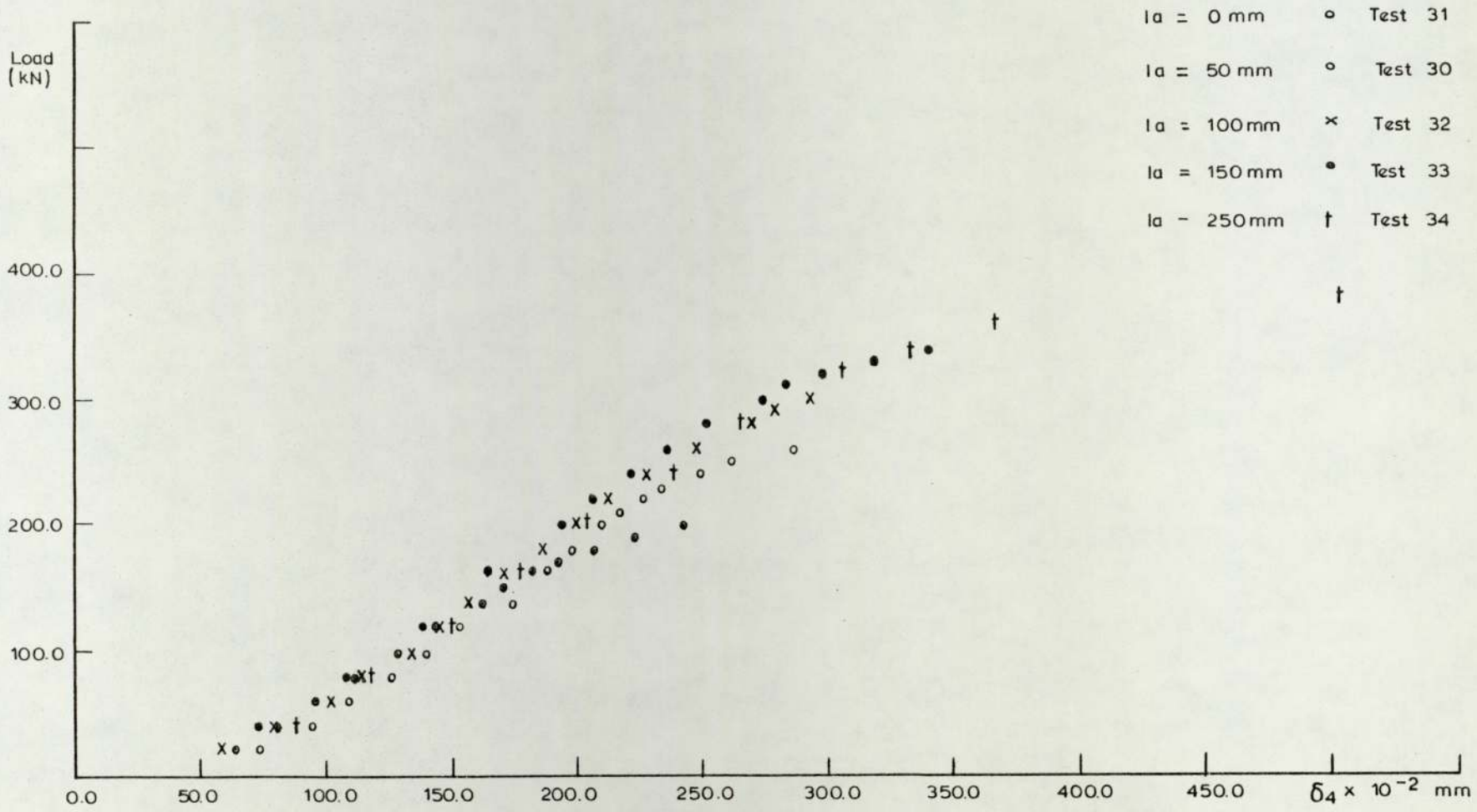

FIGURE 3.12 LOAD VERTICAL DEFLECTION PLOTS FOR BEAMS IN SERIES VI

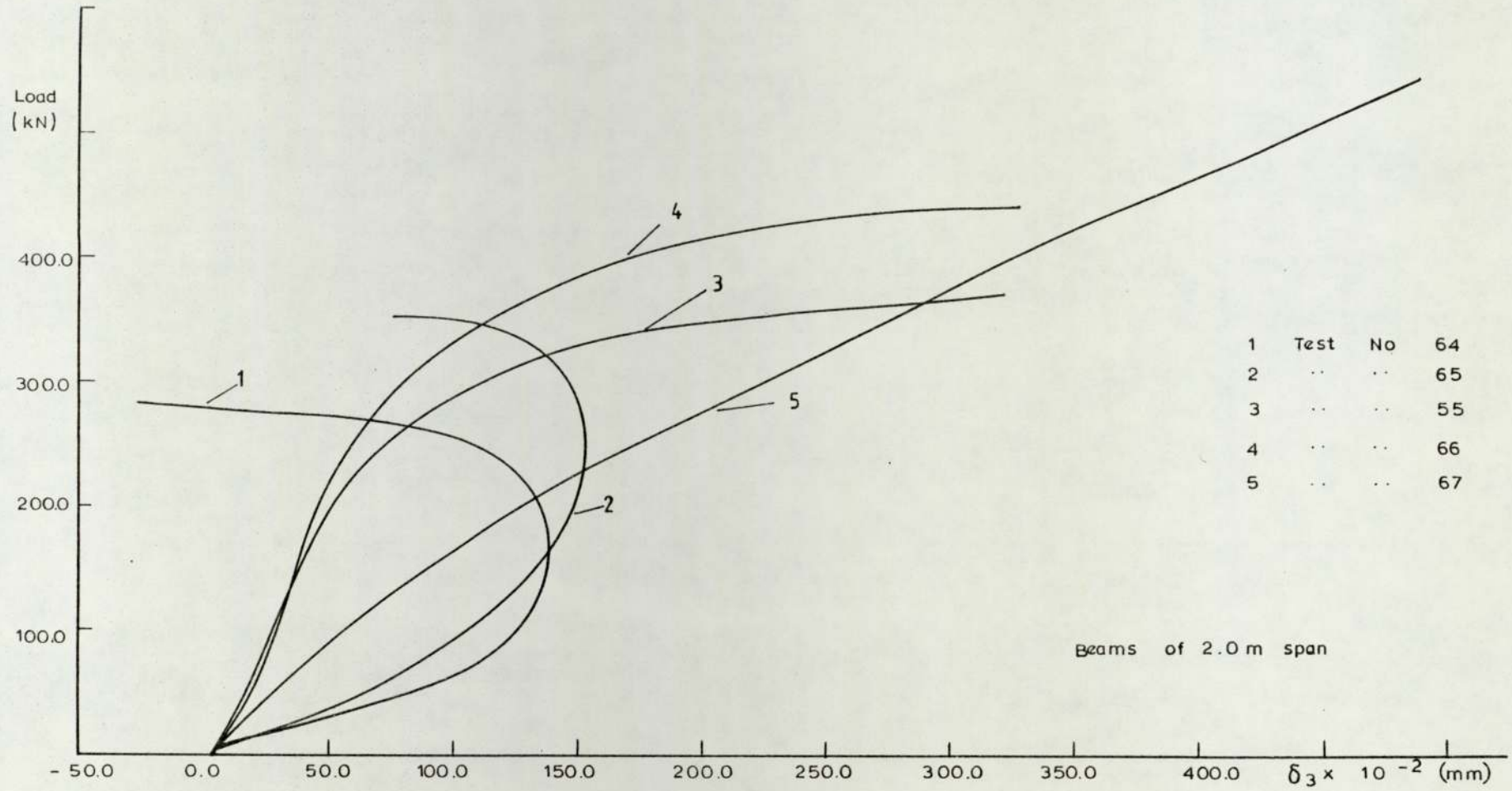

FIGURE 3.13 LOAD LATERAL DEFLECTION PLOTS FOR BEAMS IN SERIES VI

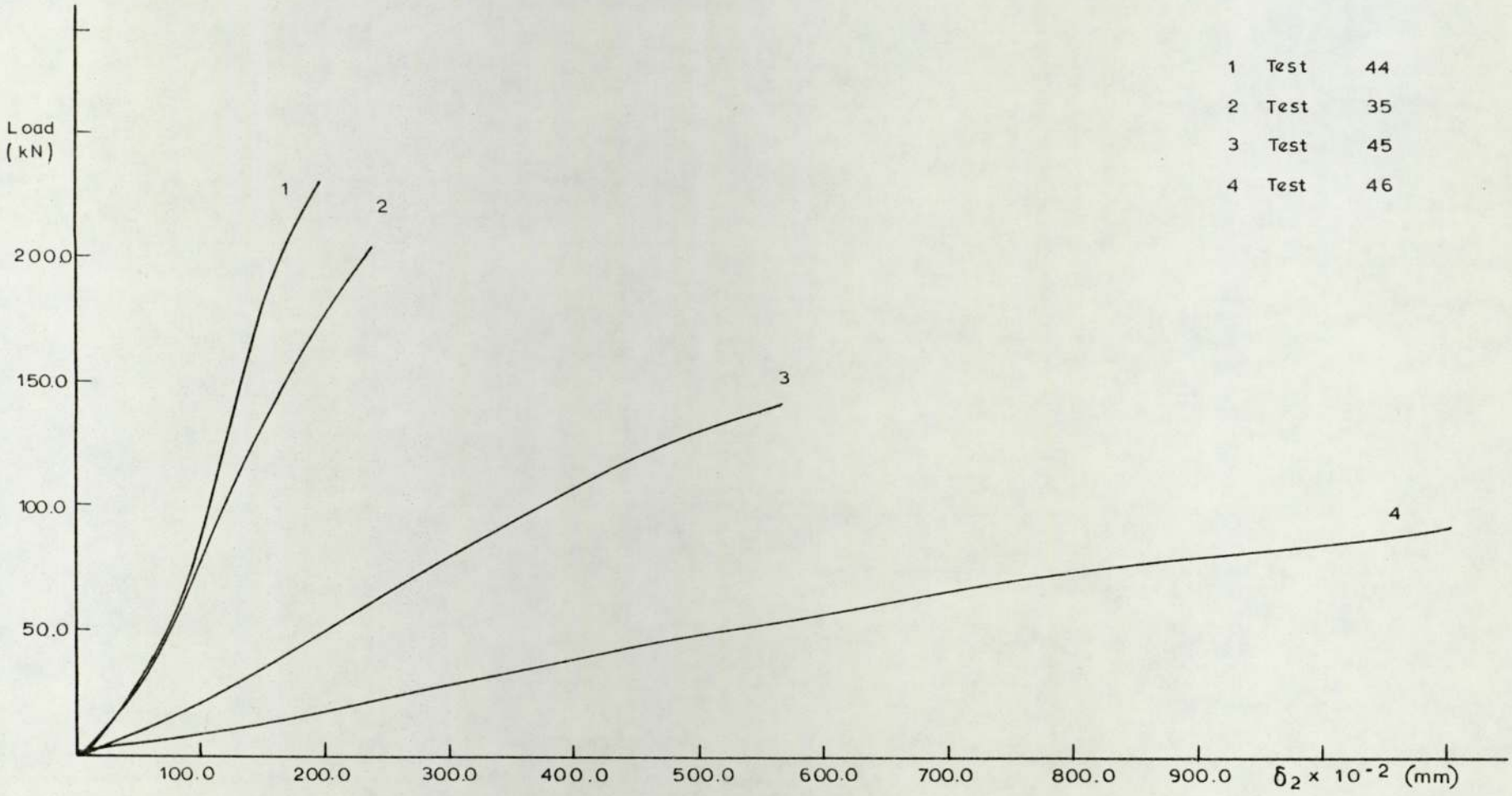

FIGURE 3.14 LOAD DEFLECTION PLOTS FOR BEAMS IN SERIES VII

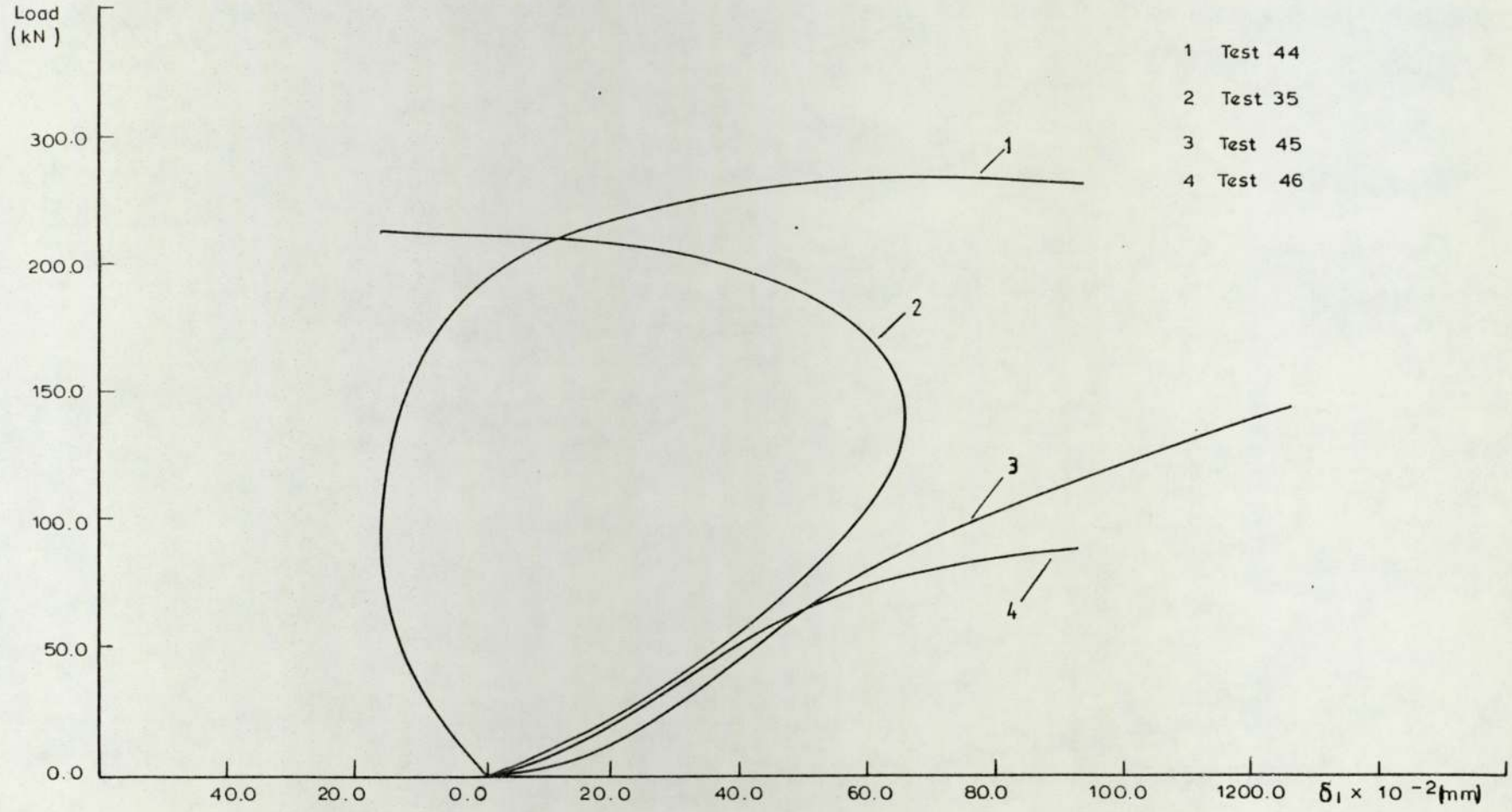

FIGURE 3.15 LOAD LATERAL DEFLECTION CURVES FOR BEAMS IN SERIES VII

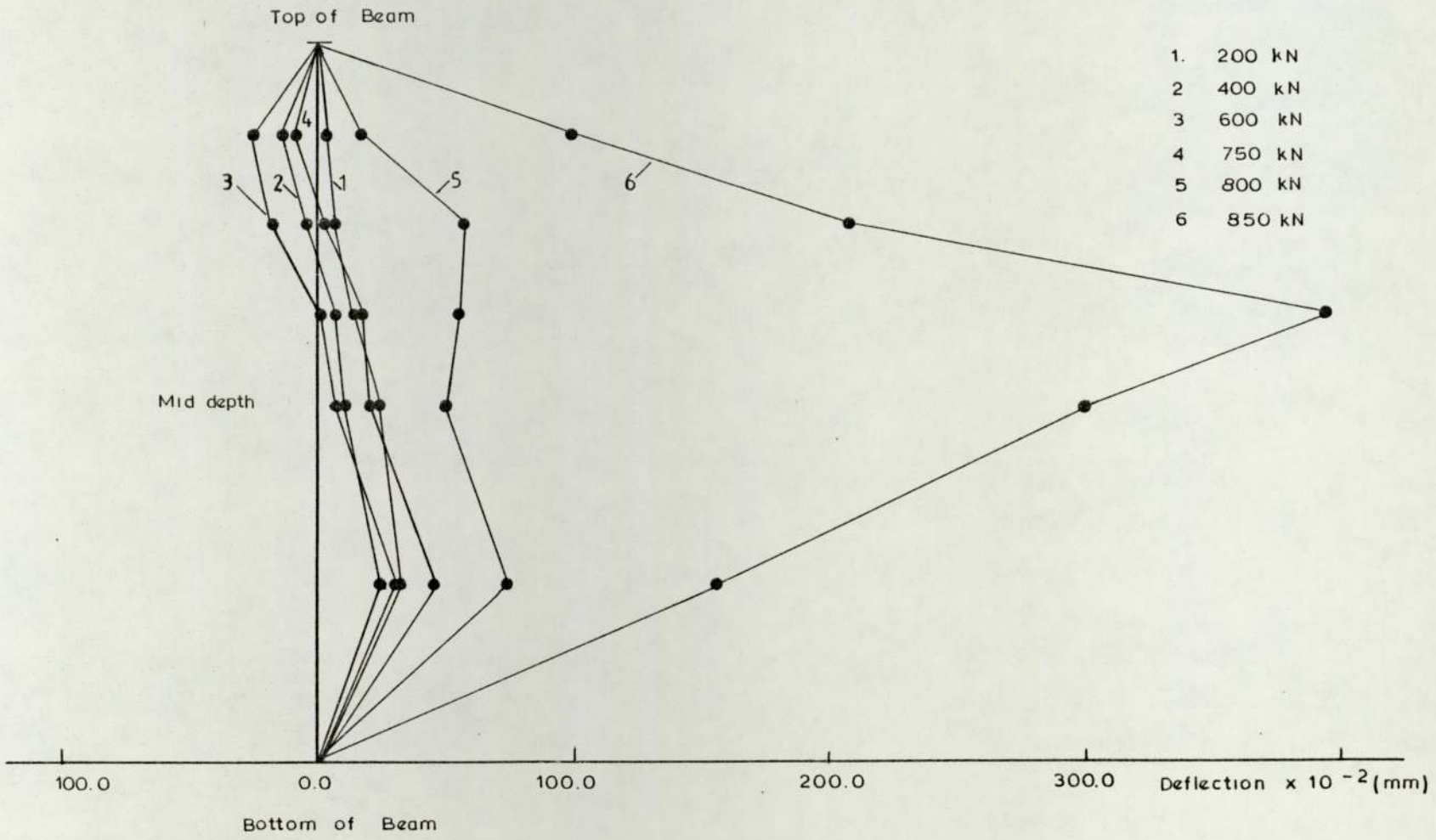

FIGURE 3.16 DEFLECTION CURVES FOR WEB UNDER LOAD POINT FOR BEAM No. 60

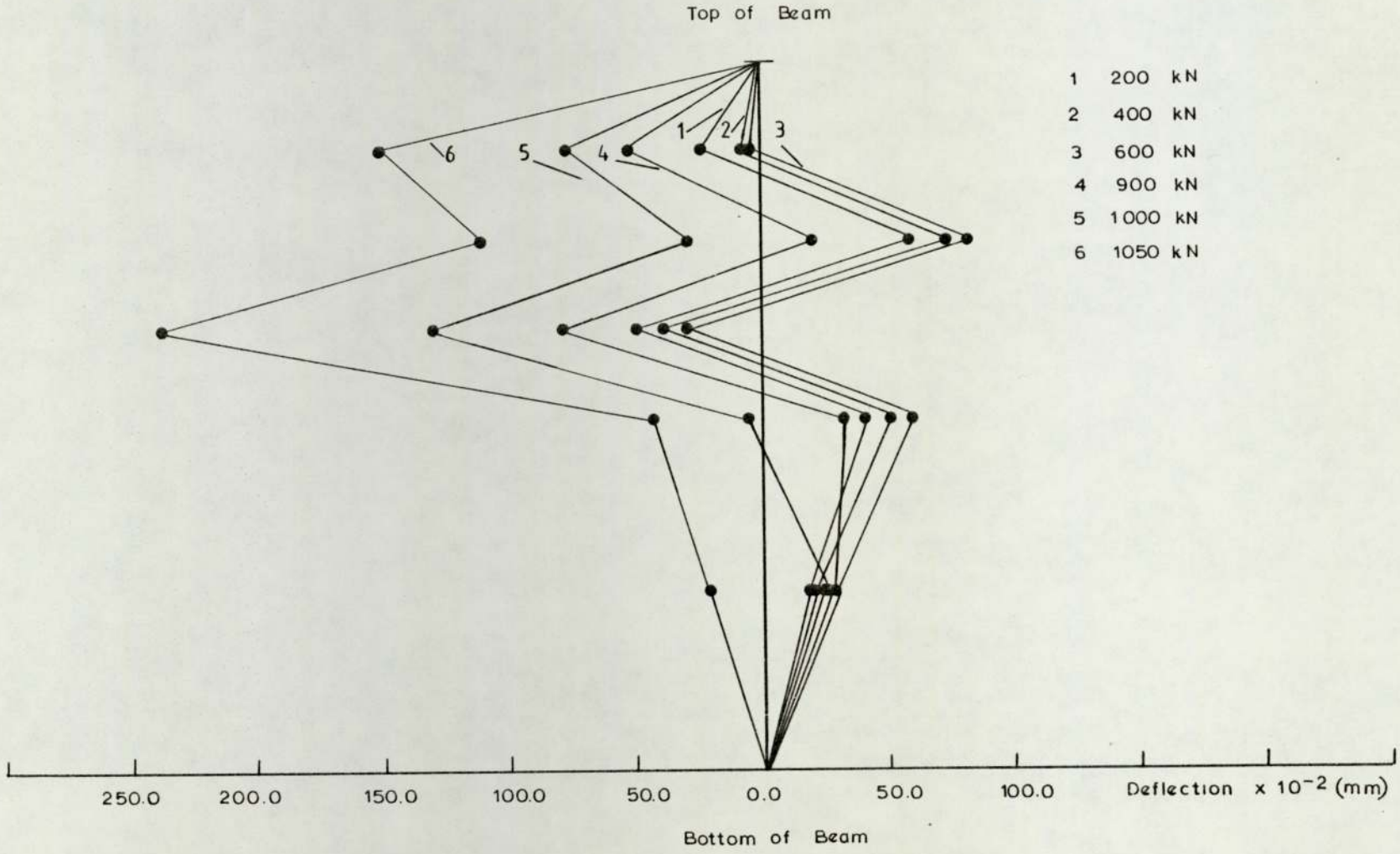

FIGURE 3.17 DEFLECTION CURVES FOR WEB UNDER LOAD POINT FOR BEAM No. 61

one through a 100 mm long stiff bearing. As could be seen from figure (3.16) the deflections are small for small and intermediate loads and become very large at loads near to failure point, as expected for buckling. The initial deflection due to small increments of loading is influenced by the initial curvature present before any loading is applied. As the load increases, the lateral deflection increases as well and the crest at which the deflection is maximum is above the mid-depth line of the web. The value of the maximum deflection decreases with increase in the length of the stiff bearing plate.

3.5 CONCLUSIONS FROM THE TEST RESULTS

The test results presented for certain types of loading for different beam serial sizes show similar behaviour patterns. However, for the test series where only one beam section size was tested, obviously, there will be doubts about the behaviour of other beam section sizes. Different beam section sizes were not possible to be included into the experimental program due to the large number of tests already conducted. This point will be referred to in the final chapter when considering suggestions for further research.

Some hypotheses were presented to explain the observations made during the tests for some beams. Later, when comparing the test results with analytical approaches the validity of these hypotheses will be discussed.

CHAPTER 4

CURRENT DESIGN CODES AND PUBLISHED THEORIES

4.1 INTRODUCTION

The design of steel beams is usually governed by limiting the stresses due to bending, shear, buckling, crushing etc., which are related to the known yield or ultimate stress of the material. The effects of 'web bearing', the failure which may result at concentrated loads if the vertical compression in the web is excessive and 'web buckling', the failure due to axial force and out of plane deflections of the web, as are considered in some current design codes, will be examined in this chapter.

Most of the current design standards, when considering the web buckling and web bearing behaviour of steel beams, use the technique of the load dispersion method. This is the distribution of the load through the flanges into the web. A large number of investigators have examined this subject, mostly in this country, America and Europe. However, there are variations in the angle of dispersion. These variations will be considered in the next section.

4.2 ANGLE OF DISPERSION

In Great Britain BS449(1969), the 'Specification for the Use of Structural Steel in Buildings' together with ammendment slip No 5, published 31 July 1975 (5), is widely used in design. When web-buckling is considered, a 45^{o} angle of dispersion is assumed. BS 153, 'Specification for Steel Girder Bridges' (6) is also in use and deals with the web buckling of rolled sections in the same way as BS 449. When a load is directly applied to the flange of a

beam both the BS 449 and BS 153 specifications consider that it is dispersed uniformly, through the flange to the connection of the flange to the web, at an angle of 30^{o} to the plane of the flange.

In America the A.I.S.C. specification (62) adopts a 45^{o} angle of dispersion for web-bearing. The same angle of dispersion is also assumed by Shedd (63) for the case of web buckling. Dispersion is taken through the root fillets or through the web flange welds and for both, British and American specifications, the angle of dispersion is constant and independent of the length of stiff bearing. Shedd's dispersion for buckling is for d/4.

In Holland Voorn (64), in a report written in Dutch, suggests that the angle of dispersion should vary with the length of bearing and that it is greater for short lengths of bearings than for long ones.

The BS 449 and BS 153 codes are considered in more detail, as it follows, since they are the most commonly used in this country.

4.2.1 Design to BS 449 and BS 153

For the purpose of the present work the clauses concerning web-buckling and web-bearing stresses, when the beam is subject to concentrated loads applied to the flanges or at points of support, are considered.

a) Web Buckling

The ultimate load due to web buckling P_B is calculated from equation (4.1), which assumes that a length of the web b is acting as a strut.

$$P_B = b \cdot t \ f_b \qquad 4.1$$

In the above expression t is the thickness of the web, f_b is the permissible stress, as given in table (17) in BS 449 or in part 3B, clause 9 in BS 153 for a slenderness ratio of $d\sqrt{3}/t$. This slenderness ratio has been derived by considering fully fixed conditions. If the loaded flange is allowed to rotate or is not restrained against lateral movement then the slenderness ratio should be increased accordingly. The f_b values of table (17) in BS 449 have been obtained by using the Perry formula for struts, given by equation (4.2), for a slenderness ratio $\frac{\ell}{r} \geq 30$. For $\frac{\ell}{r} < 30$, f_b is obtained from linear interpolation between the value of f_b for $\frac{\ell}{r} = 30$ by using equation (4.2) and a value of $f_b = 155$ N/mm^2 for $\frac{\ell}{r} = 0$.

$$k_1 f_b = \frac{f_y + (n+1) C_o}{2} - \sqrt{\left(\frac{f_y + (n+1) C_o}{2}\right)^2 - f_y C_o} \qquad 4.2$$

A factor of safety k_1 has been introduced and for BS 449 this factor has the value of 1.7. In the above expression f_y is the minimum yield stress and C_o is the Euler critical stress. The effective strut length b is defined as 'the length of stiff portion of the bearing (that portion which cannot deform appreciably in bending) plus the additional length given by dispersion at 45° angle to the level of the neutral axis plus the thickness of the seating angle (if any)'. It is also stated that the stiff portion of bearing should not be taken as greater than half the depth of the beam for simply supported beams and the full depth of the beam for beams continuous over a bearing.

b) Web-Bearing

The same argument holds for the bearing resistance of the web, but instead of a 45° angle of dispersion a 30° angle is considered

in this case. The ultimate load P_c can be calculated from:

$$P_c = b_c \, t \, f_y \qquad 4.3$$

In this expression b_c is the length of stiff bearing plus the length given by 30^o angle of dispersion up to the level of the junction of the web and the root radius. The thickness of any flange plate or seating angle may be included in the same way as for the previous case.

4.2.1.1 Comparison of the Test Results to BS 499 (1969)

In calculating the ultimate loads in accordance to BS 449, for the purpose of comparing them with the test failure loads, the yield stress obtained from the tensile tests is used.

The theoretical BS 449 ultimate loads, due to web-bearing and web-buckling, for all the 90 tests are shown in table (4.1). In the same table the failure loads are included as well as the ratio of the failure load to the minimum theoretical load . This ratio is less than 1.0 for 20 tests, which means that the BS 449 method gives a less than satisfactory safety factor at working load in these cases. Consequently, for 70 of the 90 tests the ratio is greater than 1.0 and so for these cases the BS 449 method is conservative by varying amounts.

The general observations from table (4.1) show that for zero or very short lengths of concentrated load and for short lengths of span, the method is conservative. For intermediate lengths of applied load and lengths of span, the method effects a suitable factor of safety against failure, and for long lengths of load and long lengths of span the method is unsatisfactory. It can be seen from table (4.1) that for all the tests, except for test No 67, this

Series	Beam No	Failure Load /kN	BS449 Bearing /kN	BS449 Buckling /kN	Lowest Mode	$\frac{P_{exp}}{P(BS449)}$
I	11a	255.0	159.10	446.46	C	1.603
	7a	260.0	154.02	434.76	C	1.688
	7b	270.0	154.02	434.76	C	1.753
	6b	257.5	153.12	507.73	C	1.682
	8a	260.0	314.20	503.23	C	0.827
	8b	285.0	314.20	503.23	C	0.907
	3	280.0	242.33	463.42	C	1.155
II	11a	255.0	159.10	446.46	C	1.603
	5a	310.0	168.21	446.17	C	1.842
	5b	320.0	187.20	461.58	C	1.709
	6a	339.0	223.63	488.31	C	1.516
	10a	410.0	273.96	623.15	C	1.497
	12a	450.0	311.65	649.76	C	1.444
	1	315.0	233.18	495.92	C	1.351
	2a	325.0	199.20	547.60	C	1.631
	2b	340.0	199.20	563.29	C	1.707
III	4b	245.0	142.22	442.24	C	1.723
	11b	265.0	193.17	473.86	C	1.372
	13a	297.5	231.03	502.46	C	1.288
	13b	340.0	265.75	533.96	C	1.355

C Indicates Bearing Failure

B Indicates Buckling Failure

TABLE 4.1 COMPARISON OF TEST RESULTS TO BS 449(1969)

Series	Beam No	Failure Load /kN	BS449 Bearing /kN	BS449 Buckling /kN	Lowest Mode	$\frac{P_{exp}}{P\ (BS449)}$
III	14	390.0	272.25	588.27	C	1.433
	15	400.0	269.87	642.96	C	1.482
	16	420.0	266.93	726.28	C	1.573
	18	440.0	265.98	866.01	C	1.654
	20	450.0	286.18	867.56	C	1.572
	22	455.0	282.95	887.79	C	1.608
	36	330.0	259.77	527.35	C	1.347
	37	310.0	249.68	487.12	C	1.322
	38	290.0	251.51	506.04	C	1.233
	39	407.5	299.95	592.08	C	1.425
	40	400.0	295.73	586.05	C	1.420
	41	397.5	287.33	573.11	C	1.453
	42	390.0	288.74	578.23	C	1.420
	43	385.0	277.07	559.23	C	1.462
IV	4b	245.0	152.70	442.24	C	1.604
	26a	258.0	180.37	447.19	C	1.430
	25a	270.0	214.63	463.88	C	1.258
	25b	320.0	252.00	493.22	C	1.270
	26b	340.0	294.33	537.76	C	1.155
	24b	350.0	329.10	560.05	C	1.064

TABLE 4.1 (CONTINUED)

Series	Beam No	Failure Load /kN	BS449 Bearing /kN	BS449 Buckling /kN	Lowest Mode	$\frac{P_{exp}}{P(BS449)}$
IV	27	390.0	388.73	646.44	C	1.003
	28	420.0	432.33	689.18	C	0.995
	R1b	295.0	208.00	525.57	C	1.418
	R1a	420.0	334.42	631.25	C	1.256
	R2	460.0	425.13	715.30	C	1.082
V	4b	245.0	142.22	442.24	C	1.722
	23b	198.0	134.57	371.29	C	1.471
	23a	180.0	115.34	318.24	C	1.561
	29a	140.0	95.34	263.45	C	1.468
	29b	140.0	89.74	247.95	C	1.560
VI	31	208.0	104.00	381.65	C	2.000
	30	270.0	202.60	480.48	C	1.333
	32	310.0	312.40	581.19	C	0.992
	33	350.0	412.33	659.35	C	0.849
	34	395.0	589.91	766.34	C	0.670
	50	185.0	105.20	377.39	C	1.759
	51	217.5	203.11	456.31	C	1.071
	52	240.0	389.63	584.71	C	0.616
	53	265.0	576.27	720.07	C	0.460
	63	322.5	165.10	429.07	C	1.953

TABLE 4.1 (CONTINUED)

Series	Beam No	Failure Load /kN	BS449 Bearing /kN	BS449 Buckling /kN	Lowest Mode	$\frac{P_{exp}}{P(BS\ 449)}$
VI	63	495.0	500.99	615.31	C	0.988
	60	860.0	340.96	1248.64	C	2.474
	61	1060.0	662.26	1519.89	C	1.607
	64	285.0	177.52	449.00	C	1.605
	65	350.0	280.03	507.74	C	1.250
	66	460.0	498.54	603.81	C	0.923
	67	530.0	846.23	810.35	B	0.626
	68	190.0	109.85	394.55	C	1.729
	69	180.0	109.49	396.55	C	1.644
	70	297.5	406.59	630.33	C	0.732
	71	260.0	404.13	624.61	C	0.643
	72	140.0	109.74	394.50	C	1.276
	73	127.5	109.57	394.52	C	1.164
	74	190.0	406.02	628.55	C	0.468
	75	172.5	407.14	630.58	C	0.424
VII	44	237.5	125.83	404.07	C	1.887
	35	215.0	136.82	455.16	C	1.571
	45	145.0	125.05	392.60	C	1.160
	46	100.0	125.26	393.49	C	0.798
	48	300.0	159.86	460.14	C	1.877
	47	272.5	159.37	458.75	C	1.710

TABLE 4.1 (CONTINUED)

Series	Beam No	Failure Load /kN	BS449 Bearing /kN	BS449 Buckling /kN	Lowest Mode	$\frac{P_{exp}}{P(BS\ 449)}$
VII	49	135.0	159.21	462.48	C	0.850
	58	250.0	205.26	468.45	C	1.218
	59	168.75	129.96	267.81	C	1.298
	54	470.0	413.81	596.10	C	1.136
	55	430.0	415.94	603.04	C	1.034
	56	350.0	421.91	621.79	C	0.830
	57	280.0	443.66	632.03	C	0.631
VIII	77	240.0	133.28	413.33	C	1.801
	76	260.0	207.75	472.39	C	1.252
	78	300.0	159.01	416.97	C	1.887
	79	390.0	600.38	779.11	C	0.650
	80	250.0	133.26	412.20	C	1.876

TABLE 4.1 (CONTINUED)

method indicates bearing failure. However, the calculated buckling load for test No 67 was quite near to the bearing load. It has been mentioned in chapter 3 that the beams seemed to fail in an elastoplastic manner and probably this is the reason why the method gives so conservative bearing loads.

For beams tested for end failure, that is for test series I to V, the method gives safe results except for two cases namely test Nos 8a and 8b in series I. The theoretical buckling loads are always unsatisfactory as well as the bearing loads for large lengths of the applied load.

For beams of series VI, tested for central failure, the method gives conservative bearing loads for short lengths of applied load and unsatisfactory results for large lengths of load. For both cases the theoretical buckling loads are unsatisfactory and for some cases the ratio of the failure load to the minimum theoretical load is below 0.5. This is shown in figure (4.1a) where typical theoretical failure loads are compared with the test failure loads of beams of the same serial section. Figure (4.1b) shows the comparison of typical test results with the theoretical loads for beams in series VII, namely beam Nos 44, 35, 45 and 46. The effect of bending, especially for relatively long lengths of span, can be seen as both, the theoretical bearing and buckling loads, are very unsafe. This is noticed for different beam serial sizes included in the same series.

4.2.1.2 Conclusions from the Comparison

It has been shown from the comparison that design according to BS 449, for web-bearing and web-buckling, gives a variable factor of safety against failure and in quite a few cases this factor is less than 1.0. For small lengths of the applied load and small

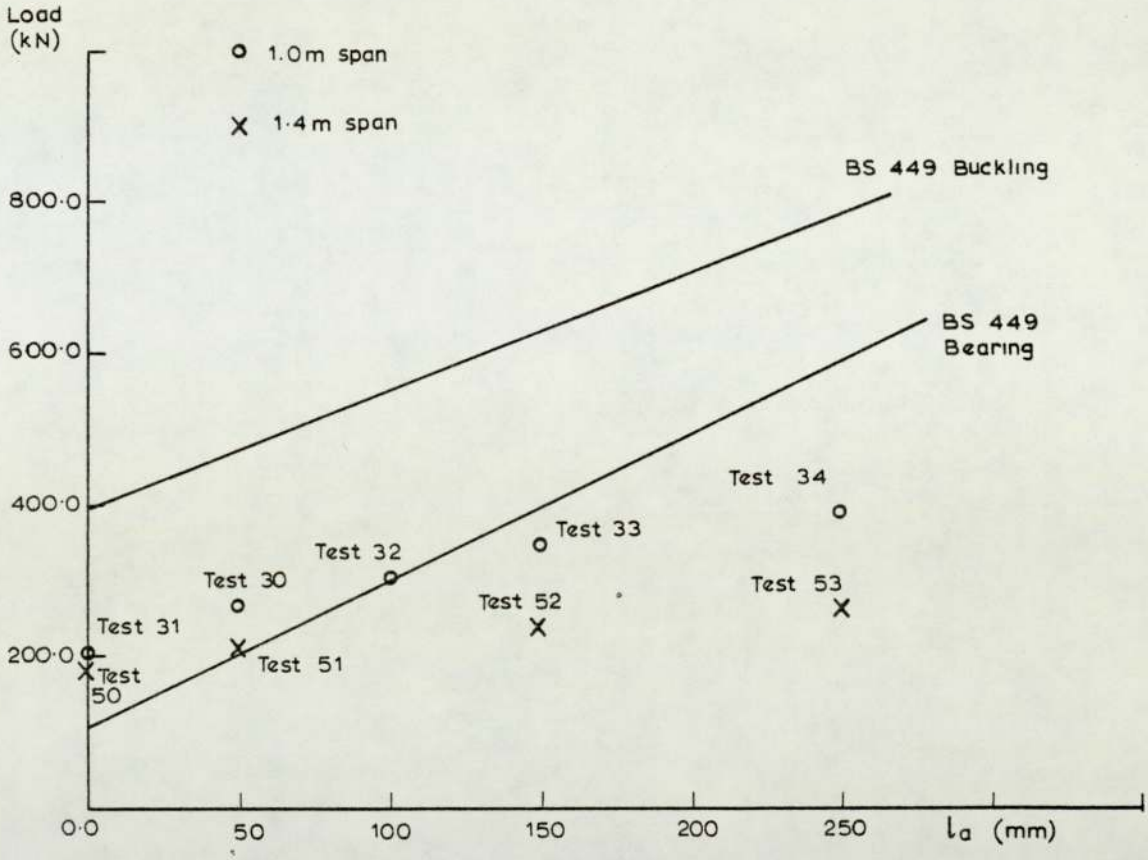

a. Series VI

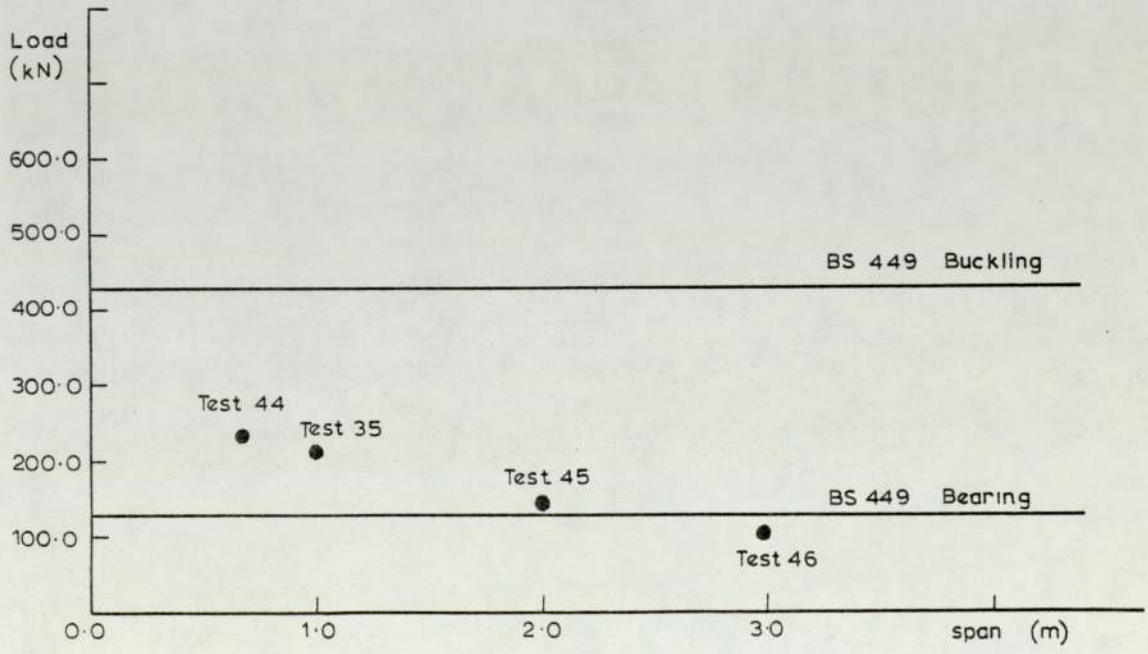

b. Series VII

FIGURE 4.1. COMPARISON OF FAILURE LOADS AND BS 449 ULTIMATE LOADS.

lengths of span the factor of safety is well above 1.0, but for long lengths of the applied load and long lengths of span this design method is unsatisfactory.

The test failure loads show clearly that the variation of the load with the length of the stiff bearing plate through which the load is applied is not linear, as the BS 449 method assumes by considering a constant angle of dispersion. As mentioned earlier fully fixed ended strut conditions are assumed by considering an effective length of $d\sqrt{3}/t$; this is erronious because the flange to web connection is insufficient to provide fixed ended strut condition even when full restraint to the flanges is attained. Therefore, as the comparison has indicated, the load dispersion approach is not a practical design method in its usual simple form and it would need to have many complicated modifications to cater for the variations investigated in the tests, to make it fully satisfactory.

4.2.2 Draft Standard Specification

As for the current code BS 449, the draft code limits the stresses at certain points in the web of the beam due to buckling and bearing when the beam is subjected to concentrated loads applied to the flanges or at the position of supports.

a) Web-Buckling

The buckling resistance P_w of the unstiffened web of the beam is obtained from:

$$P_w = (b_1 + n_1)\ t\ p_c$$

where

b_1 is the length of stiff bearing and it is that length which cannot

deform appreciably in bending. Dispersion of load through a steel bearing shall be taken at 45^{o}.

n_1 is the length obtained by dispersion at 45^{o} through half the depth of the member.

t is the web thickness

p_c is the compressive strength obtained from table (6.2.2) or figure (6.2.1) in the code with $a' = 5.5$ and slenderness ratio $\lambda' = 2.5d/t$, provided that the flange through which the load or reaction is applied, is effectively restrained against both rotation relative to the web, and lateral movement relative to the other flange. Alternatively p_c may be determined using a modified Perry Strut formula, as represented by equation (4.4), on which the above mentioned tables and figures are based. The compressive strength p_c shall be taken as the smallest root of:

$$(p_E - p_c)\ (p_y - p_c) = n\ p_E\ p_c \qquad 4.4$$

where

p_E is the Euler strength $(=\pi^2 E/\lambda'^2)$

p_y is the design strength $(=0.93\ f_y)$

n is the Perry factor $(= 0.001a(\lambda' - \lambda_o))$ but not less than zero.

a' is taken as 5.5

λ' is the slenderness ratio $(2.5\ d/t)$

λ_o is the limiting slenderness $(=0.2\sqrt{\pi^2 E/p_y})$

It is stated that when the load or support reaction is applied through a compression flange which is stressed to more than 60% of the capacity, the following inequality shall be satisfied.

$$\frac{F_w}{P_w} + \frac{M'}{M_p} + \frac{F_c}{A'p_y} \not> 1.6 \qquad 4.5$$

where

F_w is the applied force

P_w is the buckling resistance of the web

M' is the applied moment in the member

M_p is the moment capacity of the member

F_c is the axial compression in the member

A' is the area of the section

b) Web Bearing

The load capacity P_b of the web at its connection to the flange is given by:

$$P_b = (b_2 + n_2)\ t\ p_y \qquad 4.6$$

where

b_2 is the stiff length of bearing defined as before

n_2 is the length obtained by dispersion through the flange to the connection of the flange to the web at a slope of 1 to 2.5 to the plane of the flange.

4.2.2.1 Comparison of the Test Results to the Draft Code

The ultimate loads according to the draft code have been calculated for all the tested beams. Although it is specified in the code that the design strength p_y of the material should be used, the calculations were carried out using both the yield strength f_y and the design strength p_y. The value of the design strength of steel, complying with BS 4360, should be taken from table (5.7.1) of the code for the appropriate material thickness and grade of

steel. Alternatively p_y may be taken as 0.93 f_y but not greater than 0.73 f_{ult}, where f_{ult} is the ultimate tensile strength of the material.

The ultimate loads due to web-bearing and web-buckling for all the tested beams are shown with the test failure loads in table (4.2). In this table also the lowest mode is recorded as well as the ratio of the failure load to the minimum theoretical load, when the f_y and the p_y values are considered. As for the previous code, when the method indicates a bearing failure this is denoted by 'C' and when a buckling failure is indicated it is noted by 'B'.

For beams tested for end failure, that is for beams in series I to V, the proposed method, when the f_y values are considered, would fail to predict five of the results namely beam Nos 8a, 8b, 38, 27 and 28 by a small margin. For small lengths of stiff bearing the method is very conservative and for larger lengths of bearing the factor of safety varies, when the p_y values are considered the method failed to predict only one of these results namely beam No 8a.

For beams tested for central failure, that is beams in series VI to VIII the method failed to predict 18 test results when both the f_y and p_y values were considered and consequently the ratio of the failure load to the minimum theoretical load is less than 1.0. These cases, marked with an asterisk in table (4.2), were then checked for the condition given by equation (4.5) and only 9 cases give unsafe results when considering the f_y values and 8 cases when considering the p_y values. The values recorded in table (4.2) are those corresponding to these cases. It is worthwhile to notice that the code indicates buckling failure for 7 out of the 9 unsafe

Series	Test No	Failure Load /kN	Bearing Load		Buckling Load		Lowest Mode on f_y	$\frac{P_{exp}}{Pon\ f_y}$	Lowest Mode on p_y	$\frac{P_{exp}}{Pon\ p_y}$
			on f_y /kN	on p_y /kN	on f_y /kN	on p_y /kN				
I	11a	255.0	207.47	192.95	269.13	260.36	C	1.229	C	1.321
	7a	260.0	200.93	186.86	269.68	259.04	C	1.294	C	1.391
	7b	270.0	200.93	186.86	269.68	259.04	C	1.344	C	1.445
	6b	257.5	199.74	185.75	268.35	257.75	C	1.289	C	1.386
	8a	260.0	291.30	270.91	314.11	301.71	C	0.893	C	0.960
	8b	285.0	291.30	270.91	314.11	301.71	C	0.978	C	1.052
	3	280.0	204.07	189.78	262.21	254.07	C	1.372	C	1.475
II	11a	255.0	207.47	192.95	269.13	260.36	C	1.229	C	1.321
	5a	310.0	212.43	197.55	276.18	265.28	C	1.459	C	1.569
	5b	320.0	231.41	215.21	285.74	274.46	C	1.383	C	1.487
	6a	339.0	270.22	251.30	303.84	291.85	C	1.254	C	1.349
	10a	410.0	404.63	376.31	370.39	355.77	B	1.107	B	1.152
	12a	450.0	404.75	376.42	392.66	377.28	B	1.146	B	1.193
	1	315.0	204.07	189.78	284.64	272.22	C	1.544	C	1.660

TABLE 4.2 COMPARISON OF TEST RESULTS TO THE DRAFT CODE

Series	Test No	Failure Load /kN	Bearing Load		Buckling Load		Lowest Mode on f_y	$\frac{P_{exp}}{Pon\ f_y}$	Lowest Mode on p_y	$\frac{P_{exp}}{Pon\ p_y}$
			on f_y /kN	on p_y /kN	on f_y /kN	on p_y /kN				
II	2a	325.0	283.77	263.91	290.07	276.76	C	1.145	C	1.231
	2b	340.0	283.77	263.90	290.07	276.76	C	1.198	C	1.288
III	4b	245.0	199.11	185.17	275.63	263.10	C	1.230	C	1.323
	11b	265.0	241.54	224.63	285.64	276.34	C	1.097	C	1.180
	13a	297.5	279.63	260.05	303.54	293.66	C	1.063	C	1.144
	13b	340.0	308.22	286.65	317.32	303.67	C	1.103	C	1.186
	14	390.0	346.00	321.78	346.78	337.92	C	1.127	C	1.212
	15	400.0	367.18	341.47	390.97	378.48	C	1.089	C	1.171
	16	420.0	363.24	337.82	445.69	431.36	C	1.156	C	1.243
	18	440.0	361.87	336.54	465.39	450.43	C	1.216	C	1.307
	20	450.0	386.51	359.60	515.32	496.06	C	1.164	C	1.251
	22	455.0	384.93	353.98	533.02	512.84	C	1.182	C	1.285
	36	330.0	310.40	288.67	315.72	303.18	C	1.063	C	1.143
	37	310.0	300.64	279.59	293.41	283.30	B	1.056	B	1.094

TABLE 4.2 (CONTINUED)

Series	Test No	Failure Load /kN	Bearing Load		Buckling Load		Lowest Mode on f_y	$\frac{P_{exp}}{Pon\ f_y}$	Lowest Mode on p_y	$\frac{P_{exp}}{Pon\ p_y}$
			on f_y /kN	on p_y /kN	on f_y /kN	on p_y /kN				
III	38	290.0	302.96	281.75	299.92	287.68	B	0.967	C	1.029
	39	407.5	360.69	335.45	374.38	360.60	C	1.130	C	1.215
	40	400.0	352.96	328.25	366.83	353.16	C	1.133	C	1.219
	41	397.5	341.73	317.81	361.89	343.99	C	1.163	C	1.251
	42	390.0	343.32	319.29	358.52	344.99	C	1.136	C	1.221
	43	385.0	327.81	304.87	350.04	336.84	C	1.174	C	1.263
IV	4b	245.0	199.11	185.17	275.63	263.10	C	1.230	C	1.323
	26a	258.0	226.65	210.78	268.36	257.55	C	1.138	C	1.224
	25a	270.0	260.10	241.89	273.22	263.78	C	1.038	C	1.116
	25b	320.0	297.47	279.65	290.51	280.45	B	1.101	C	1.156
	26b	340.0	340.61	316.77	322.72	309.72	B	1.053	B	1.098
	24b	350.0	374.79	348.55	329.96	319.75	B	1.061	B	1.095
	27	390.0	437.56	406.93	396.49	381.33	B	0.983	B	1.023
	28	420.0	481.51	447.80	425.69	410.97	B	0.987	B	1.022
	R1b	295.0	262.86	244.46	327.92	312.11	C	1.122	C	1.207

TABLE 4.2 (CONTINUED)

Series	Test No	Failure Load /kN	Bearing Load		Buckling Load		Lowest Mode on f_y	$\frac{P_{exp}}{Pon\ f_y}$	Lowest Mode on p_y	$\frac{P_{exp}}{Pon\ p_y}$
			on f_y /kN	on p_y /kN	on f_y /kN	on p_y /kN				
V	R1a	420.0	389.28	362.03	393.85	374.87	C	1.079	C	1.160
	R2	460.0	481.26	447.57	446.19	414.12	B	1.031	B	1.111
V	4b	245.0	199.11	185.17	275.60	263.10	C	1.230	C	1.323
	23b	198.0	175.33	163.06	213.23	208.98	C	1.129	C	1.214
	23a	180.0	150.29	139.77	182.77	179.13	C	1.198	C	1.288
	29a	140.0	124.08	115.39	153.88	148.64	C	1.128	C	1.213
	29b	140.0	116.78	108.60	144.82	139.89	C	1.199	C	1.289
VI	31	208.0	150.12	139.61	225.22	216.09	C	1.385	C	1.490
	30	270.0	253.02	235.30	286.66	275.42	C	1.067	C	1.147
	32	310.0	361.17	335.89	288.91	283.66	B*	1.073	B*	1.093
	33	350.0	460.95	428.68	316.95	310.98	B*	1.104	B*	1.125
	34	395.0	636.72	572.18	358.52	353.55	B*	1.102	B*	1.117
	50	185.0	147.16	136.86	221.94	213.52	C	1.257	C	1.352
	51	217.5	242.37	225.40	204.98	199.93	B*	1.061	B*	1.088
	52	240.0	422.28	392.72	236.72	233.40	B*	1.014	B*	1.028

TABLE 4.2 (CONTINUED)

Series	Test No	Failure Load /kN	Bearing Load		Buckling Load		Lowest Mode on f_y	$\frac{P_{exp}}{Pon\ f_y}$	Lowest Mode on p_y	$\frac{P_{exp}}{Pon\ p_y}$
			on f_y /kN	on p_y /kN	on f_y /kN	on p_y /kN				
	53	265.0	602.91	560.71	270.94	266.56	B*	0.978	B*	0.994
	62	322.5	238.30	221.62	231.43	222.23	B	1.394	B	1.451
	63	495.0	574.95	534.70	289.69	281.55	B	1.708	B	1.758
	60	860.0	494.26	459.67	801.24	757.79	C	1.740	C	1.871
	61	1060.0	810.75	754.00	972.30	919.74	C	1.307	C	1.406
	64	285.0	239.15	232.45	227.49	219.55	B	1.253	B	1.298
	65	350.0	354.65	329.82	268.46	263.93	B	1.304	B	1.326
VI	66	460.0	572.52	532.44	315.50	308.20	B	1.458	B	1.493
	67	530.0	921.08	856.60	419.12	414.38	B	1.265	B	1.279
	68	190.0	158.55	147.45	234.90	222.91	C	1.198	C	1.289
	69	180.0	158.04	146.98	235.49	224.46	C	1.139	C	1.225
	70	297.5	455.27	423.40	256.95	251.14	B*	1.158	B*	1.184
	71	260.0	452.37	420.71	233.57	228.73	B*	1.113	B*	1.137
	72	140.0	158.40	147.32	188.61	183.65	C*	0.884	C*	0.950
	73	127.5	158.16	147.09	174.38	170.13	C*	0.806	C*	0.867

TABLE 4.2 (CONTINUED)

Series	Test No	Failure Load /kN	Bearing Load		Buckling Load		Lowest Mode on f_y	$\frac{P_{exp}}{P_{on}\ f_y}$	Lowest Mode on p_y	$\frac{P_{exp}}{P_{on}\ p_y}$
			on f_y /kN	on p_y /kN	on f_y /kN	on p_y /kN				
VI	74	190.0	454.66	422.83	255.19	248.56	B*	0.744	B*	0.764
	75	172.5	454.53	422.73	230.21	225.52	B*	0.749	B*	0.765
VII	44	237.5	172.88	160.78	242.17	232.42	C	1.374	C	1.477
	35	215.0	186.02	173.00	283.32	271.08	C	1.156	C	1.243
	45	145.0	169.83	157.94	154.02	151.78	B*	0.941	B*	0.955
	46	100.0	169.33	157.47	119.07	117.71	B*	0.840	B*	0.850
	48	300.0	217.32	202.10	286.41	275.60	C	1.380	C	1.484
	47	272.5	218.88	203.56	286.00	275.20	C	1.245	C	1.339
	49	135.0	218.58	203.28	153.44	151.40	B*	0.880	B*	0.892
	58	250.0	283.16	263.34	239.10	234.97	B	1.046	B	1.064
	59	168.75	174.95	162.71	174.91	172.82	B*	0.964	C	1.037
	54	470.0	492.50	458.03	305.11	301.72	B	1.540	B	1.558
	55	430.0	495.10	460.45	309.86	306.46	B	1.388	B	1.403
	56	350.0	502.48	467.31	320.61	313.72	B	1.092	B	1.116
	57	280.0	528.58	491.58	267.63	266.00	B*	1.046	B*	1.053

TABLE 4.2 (CONTINUED)

Series	Test No	Failure Load /kN	Bearing Load		Buckling Load		Lowest Mode on f_y	$\frac{P_{exp}}{Pon\ f_y}$	Lowest Mode on p_y	$\frac{P_{exp}}{Pon\ p_y}$
			on f_y /kN	on p_y /kN	on f_y /kN	on p_y /kN				
VIII	77	240.0	181.29	168.60	238.44	232.04	C	1.324	C	1.423
	76	260.0	256.14	238.21	277.64	273.94	C	1.015	C	1.091
	78	300.0	182.10	169.36	239.62	233.19	C	1.647	C	1.771
	79	390.0	648.70	603.29	363.23	367.72	B*	1.074	B*	1.060
	80	250.0	181.28	168.59	232.29	232.50	C	1.379	C	1.483

TABLE 4.2 (CONTINUED)

results and consequently bearing failures for the rest, two, namely beam Nos 72 and 73. For the buckling failures either the stiff bearing is small and the span relatively large or large lengths of stiff bearing and relatively small lengths of span. For the bearing failures the length of bearing and the span are both of small lengths.

4.2.2.2 Conclusions from the Comparison

The comparison of the failure loads of the tested beams and the theoretical ultimate loads according to the draft code, indicates that the proposed rules are over conservative for short lengths of bearing but inadequate for long lengths of bearing. This was noticed from the previous comparison of the test results to BS 449 (1969), although a different slenderness ratio, angle of load dispersion and a modified Perry formula is used for the draft code.

However, if the draft code will be used in future, some alterations should be made in the proposed rules; if the 'Perry formula' will be used, in calculating the f_b values, a new expression for the effective length should be formulated.

4.2.3 American Specification

The only limitation the American code A.I.S.C. (1973) places on the prevention of web buckling is on the clear distance between the flanges h of beams and plate girders is

$$h \leq \frac{14000}{\sqrt{f_y (f_y + 16.5)}}\ t \qquad 4.6$$

where

t is the web thickness in inches

f_y is the yield stress of the compression flange;

otherwise stiffeners should be introduced.

For web-crushing the compressive stress at the web toe of the fillets, resulting from concentrated load, not supported by bearing stiffeners, shall not exceed the value of 0.75 f_y; otherwise bearing stiffeners shall be provided. The governing formulas are:

For interior loads,

$$\frac{R}{t(N + 2k)} \leq 0.75\ f_y \qquad 4.7.1$$

For end reactions,

$$\frac{R}{t(N + k)} \leq 0.75\ f_y \qquad 4.7.2$$

where

R is concentrated load or reaction

t is the web thickness

N is the length of bearing

k is the distance from the outer face of flange to web toe or fillet.

4.2.3.1 Comparison of the Test Results to the American Specification and Conclusions from the Comparison

Equations (4.7.1) and (4.7.2) can be written as:

For interior load

$$R \leq 0.75\ f_y\ t\ (N + 2k) \qquad 4.8.1$$

For end reaction

$$R \leq 0.75\ f_y\ t\ (N + k) \qquad 4.8.2$$

The crushing loads for all the beams have been calculated, utilising the above equations, and all the values are shown in table (4.3).

As could be seen from the comparison this method is over conservative for small lengths of stiff bearings and very unsafe for

Series	Beam No	Failure Load /kN	$R_{(Amer.\ specif)}$ /kN	$\frac{P_{exp}}{R}$
I	11a	255.0	84.75	3.009
	7a	260.0	81.98	3.172
	7b	270.0	81.98	3.293
	6b	257.5	116.75	2.206
	8a	260.0	151.20	1.720
	8b	285.0	151.20	1.885
	3	380.0	120.63	3.150
II	11a	255.0	84.75	3.009
	5a	310.0	102.06	3.037
	5b	320.0	130.54	2.451
	6a	339.0	187.25	1.810
	10a	410.0	281.71	1.455
	12a	450.0	279.98	1.607

Series	Beam No	Failure Load /kN	$R_{(Amer.\ specif)}$ /kN	$\frac{P_{exp}}{R}$
	1	315.0	132.07	2.385
	2a	325.0	133.27	2.437
	2b	340.0	149.40	2.276
III	4b	245.0	40.67	6.024
	11b	265.0	110.30	2.403
	13a	297.5	130.88	2.273
	13b	340.0	130.88	2.598
	14	390.0	134.07	2.909
	15	400.0	133.27	3.001
	16	420.0	131.77	3.187
	18	440.0	131.36	3.350
	20	450.0	129.13	3.485
	22	455.0	128.48	3.541

TABLE 4.3 COMPARISON OF THE TEST RESULTS TO AMERICAN SPECIFICATION

Series	Beam No	Failure Load /kN	$R_{(Amer.\ specif)}$ /kN	$\frac{P_{exp}}{R}$
III	36	330.0	127.12	2.596
	37	310.0	123.18	2.517
	38	290.0	124.10	2.337
	39	407.5	154.53	2.637
	40	400.0	150.17	2.664
	41	397.5	144.18	2.757
	42	390.0	144.76	2.694
	43	385.0	136.57	2.819
IV	4b	245.0	40.67	6.024
	26a	258.0	51.09	5.050
	25a	270.0	64.24	4.203
	25b	320.0	78.25	4.089
	26b	340.0	93.83	3.624

Series	Beam No	Failure Load /kN	$R_{(Amer.\ specif)}$ /kN	$\frac{P_{exp}}{R}$
IV	24b	350.0	107.08	3.269
	27	390.0	128.32	3.039
	28	420.0	144.54	2.906
	R1b	295.0	58.39	5.052
	R1a	420.0	105.80	3.970
	R2	460.0	136.79	3.363
V	4b	245.0	40.67	6.024
	23b	198.0	71.91	2.753
	23a	180.0	61.64	2.920
	29a	140.0	50.96	2.747
	29b	140.0	47.96	2.919
VI	31	208.0	45.04	4.618
	30	270.0	120.42	2.242

TABLE 4.3 (CONTINUED)

Series	Beam No	Failure Load /kN	$R_{(Amer. specif)}$ /kN	$\frac{P_{exp}}{R}$
VI	32	310.0	199.44	1.554
	33	350.0	274.48	1.275
	34	395.0	408.94	0.966
	50	185.0	44.15	4.190
	51	217.5	115.09	1.890
	52	240.0	251.30	0.955
	53	265.0	387.15	0.684
	62	322.5	71.49	4.511
	63	495.0	322.49	1.535
	60	860.0	171.48	5.015
	61	1060.0	370.74	2.859
	64	285.0	73.92	3.855
	65	350.0	156.68	2.234
VI	66	460.0	321.02	1.433
	67	530.0	581.17	0.912
	68	190.0	47.57	3.994
	69	180.0	47.41	3.796
	70	297.5	270.15	1.101
	71	260.0	268.62	0.968
	72	140.0	47.52	2.946
	73	127.5	47.45	2.687
	74	190.0	269.75	0.704
	75	172.5	270.39	0.638
VII	44	237.5	62.68	3.789
	35	215.0	67.45	3.187
	45	145.0	61.59	2.354

TABLE 4.3 (CONTINUED)

Series	Beam No	Failure Load /kN	$R_{(Amer. specif)}$ /kN	$\frac{P_{exp}}{R}$
VII	46	100.0	61.46	1.627
	48	300.0	76.56	3.918
	47	272.5	76.99	3.539
	49	135.0	76.97	1.754
	58	250.0	98.21	2.545
	59	168.75	62.39	2.705
	54	470.0	254.11	1.849
	55	430.0	255.36	1.684
	56	350.0	258.83	1.352
	57	280.0	272.04	1.029
VIII	77	240.0	95.17	2.522
	76	260.0	121.22	2.144
	78	300.0	110.46	2.716
	78	390.0	415.73	0.938
	80	250.0	64.10	3.900

TABLE 4.3 (CONTINUED)

relatively long lengths of stiff bearings. For 8 out of the 90 tests the method is very unsatisfactory, namely for beam Nos 34, 52, 53, 67, 71, 74, 75 and 79. These beams failed at the centre and the load was applied through relatively large lengths of bearing . For the beams which failed at the end the American specification is more conservative than the British specification.

4.3 OTHER INVESTIGATORS' WORK

4.3.1 Shedd

Shedd in 1934 gave some design guides concerning web vertical buckling and web-bearing in rolled steel beams. These guides have been adopted in the A.I.S.C. specification as Hrenrikoff (2) refers.

Vertical or column buckling is the type of web failure in which the section of web vertically above the bearing plate at the reaction or below a concentrated load is subjected to column action and tends to buckle under it. Shedd recommended that the height of web for investigating this column action over reaction, depends on the effectiveness of the restraint against relatively lateral movement of the two flanges. If the top and bottom flanges of the beam are restrained against lateral movement or rotation the web must act as a fixed-end column and if only the bottom flange is held in position it may act as a column having one end fixed and the other hinged. These cases are shown in figure (4.2a, b) and the lengths which may be used in applying the column formula is half of the depth and two-thirds of the depth. For the latter case Shedd suggests that buckling may also occur as indicated by figure (4.2c) and some other designers as indicated by figure (4.2d), where the top flange will be kept in a horizontal plane due to the restraint provided by the load and the stiffness of the flange.

Shedd suggested that for the web over the reaction the area

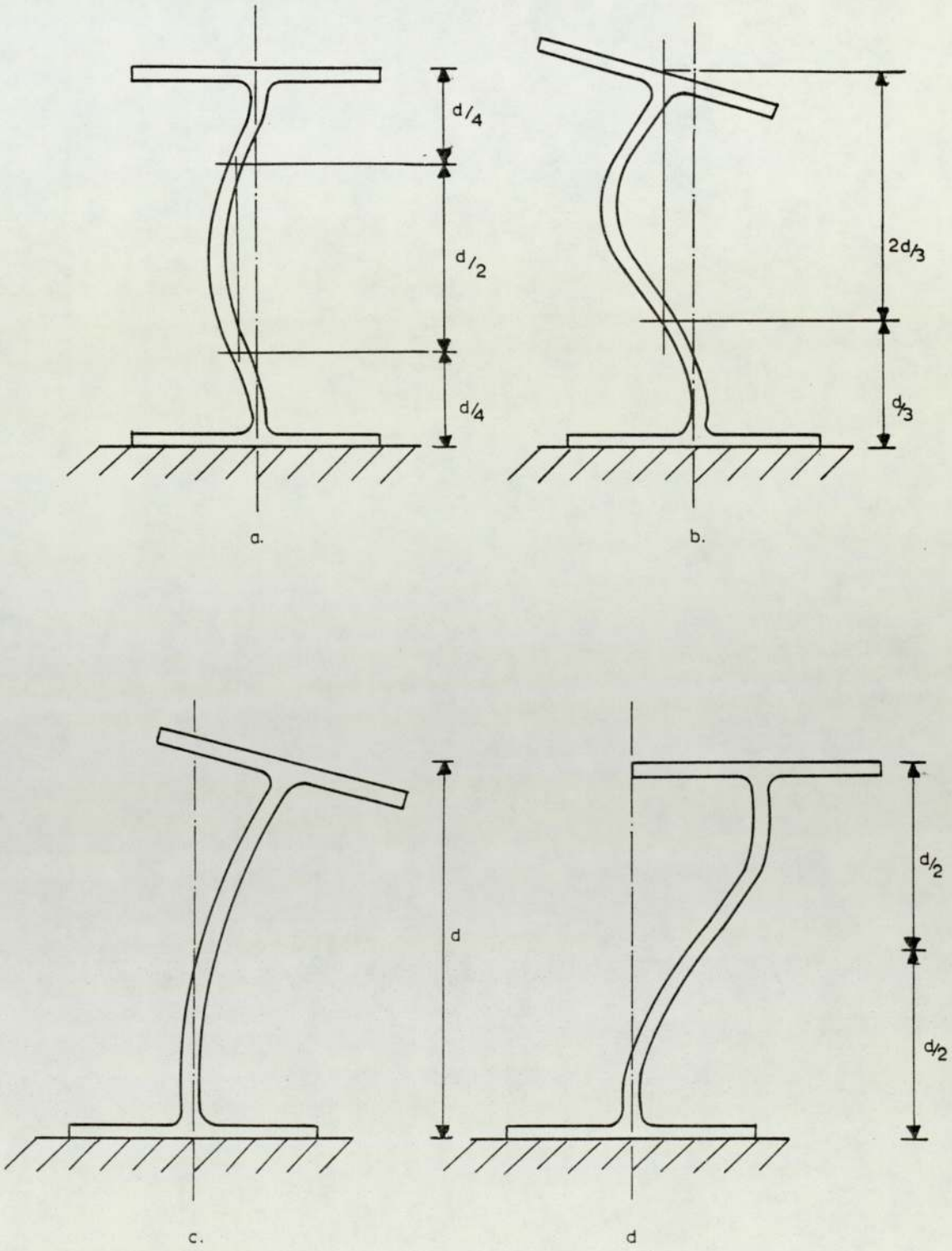

FIGURE 4.2 BUCKLING TYPES CONSIDERED BY SHEDD

of the simulate column section should be taken as

$$A_1 = t\ (N_r + D/4) \qquad 4.8.1$$

and for the web under a concentrated load as

$$A_2 = t\ (N_p + D/2) \qquad 4.8.2$$

where

N_r is the length of bearing at end reaction

N_p is the length of bearing for internal load.

From the expression (4.8.1) and (4.8.2) it is clear that a 45^o angle of dispersion is taken, similarly to BS 449, but only allowed up to one quarter of the overall depth of the section. For web bearing he did not recommend any angle of dispersion from the point of load application. He accepted that the direct stress are resisted by the length of the web directly below the load.

By comparing the failure loads of the tested beams with the ultimate loads given by the above expressions this method for end failure is very conservative. For beams tested for central failure, in general, is unsatisfactory for small lengths of span , loaded by small lengths of load and for long lengths of span and long lengths of the applied load.

4.3.2 Winter and Pian

When beams are cold formed, the depth to thickness ratio of their webs are in general greater than 50 and in such cases stiffeners cannot be easily introduced. So besides bending and shear examination it it necessary to design these webs against local failure at points where loads are applied or at reactions.

Winter and Pian investigated this problem by performing some 136 tests on double and single webbed sections. The loading and

supporting conditions of these beams are shown in figure (4.3). Failure occurred either under the applied load or at the supports. It is noticed from the test results that there was only a little difference in the average failure load for double and single webbed sections. The failure load for end failure was also half of the failure load for span failure. They represented their results by two simple empirical formulas for span and end failure respectively as

$$P = (15 + 3.25 \sqrt{la/t})\ t^2\ f_y \qquad 4.9.1$$

and

$$P = (10 + 1.25 \sqrt{la/t})\ t^2\ f_y \qquad 4.9.2$$

where

P is the failure load

la is the length of bearing

t is the thickness of single web

From these two expressions it is clear that the crushing strength consists of two parts: a) the resistance the web could offer for zero length of bearing and b) the added resistance due to an increase in the length of bearing. It should be noticed that the depth of the section is not included in these expressions and since the sections used were made from metal of uniform thickness the contributions of the web and flange thicknesses in the above expressions cannot be detected.

Although the test results of the present work are not directly comparable with the predicted ultimate loads using the above expressions, the comparison for the beams in series VI and VII, for central failure, and beams in series IV, for end failure, are shown in table (4.4). If the quantity $\sqrt{la/t}$ is plotted against $P_{exp}/t^2 f_y$

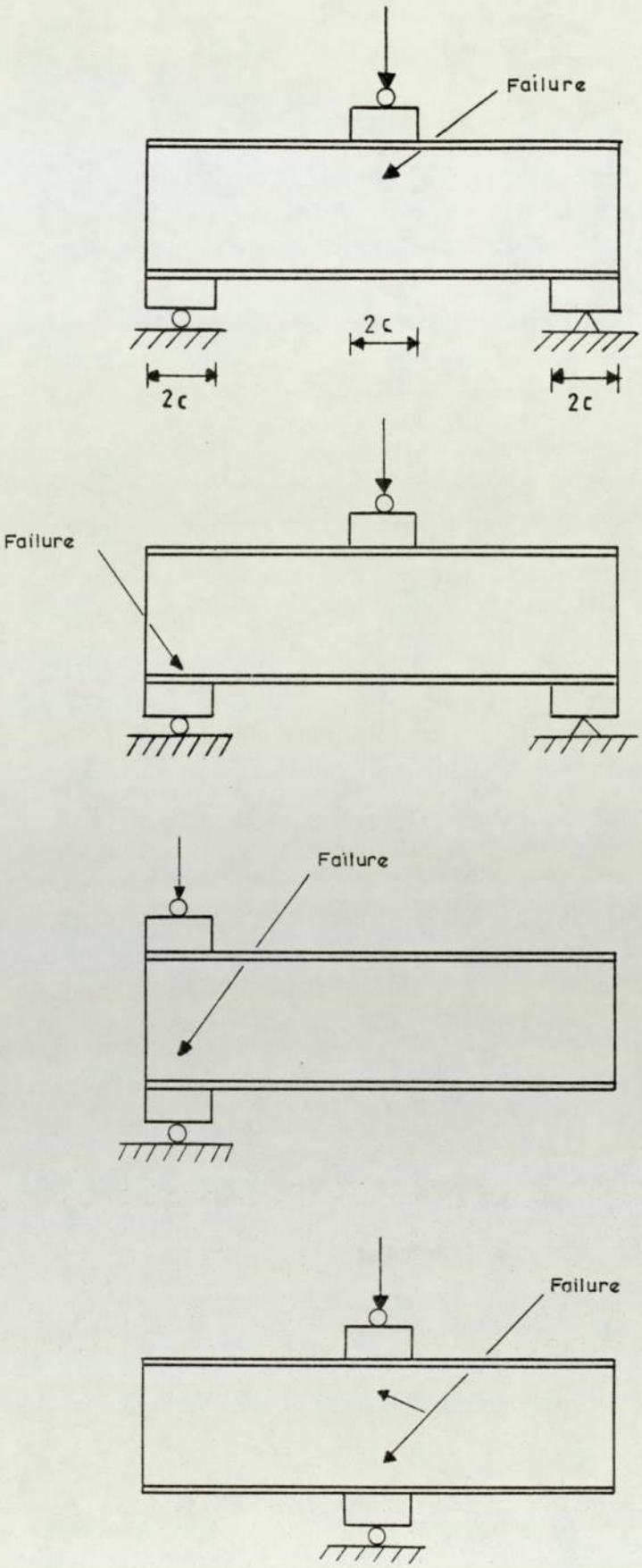

FIGURE 4.3 LOADING AND SUPPORTING CONDITIONS FOR TESTS PERFORMED BY WINTER AND PIAN

SERIES VI	Beam	31	30	32	33	34	50	51	52	53	60	61		
	$\sqrt{l_a/t}$	0	2.856	3.994	4.900	6.455	0	2.882	5.042	6.531	0	2.936		
	P/t^2fy	18.199	22.256	24.425	27.754	33.987	16.534	19.181	22.035	24.664	23.586	30.014		
SERIES VII	Beam	44	35	45	46	48	47	49	58	59	54	55	56	54
	$\sqrt{l_a/t}$	1.449	1.397	1.461	1.460	1.395	1.397	1.392	1.383	1.660	3.843	3.835	3.812	3.829
	P/t^2fy	20.738	16.214	13.090	8.997	23.112	21.123	10.337	16.242	19.877	29.373	26.636	21.180	16.282
SERIES IV	Beam	4b	26a	25a	25b	26b	24	27	28	R1b	R1a	R2		
	$\sqrt{l_a/t}$	1.414	1.814	2.240	2.586	2.868	3.154	3.315	3.527	1.738	2.748	3.232		
	P/t^2fy	10.202	11.170	12.084	14.322	14.721	15.406	15.383	16.258	10.754	15.055	16.100		

TABLE 4.4 COMPARISON OF TEST RESULTS TO WINTER AND PIAN FORMULAS

and if Winter and Pians' assumed variables were correct then the lines represented by equation (4.8.1) and (4.8.2) should have been the best fitted lines through these points.

By referring to figures (4.4) and (4.5) it could be said that Winter and Pians' formulas compared to the test results, for both types of failure, are conservative for small lengths of bearing and unsafe for larger lengths of bearing.

4.3.3 Delesques

In 1974 Delesques came to some conclusions concerning the buckling of webs of slender beams when they are subjected to concentrated loads on the upper flange. He gathered his information from tests performed by Bergfelt (65) Bergfelt and Hovick (66) and some by Marinoto and Velez, Lyse and Godfrey. Bergfelt and Hovick used very slender beams, the depth to thickness ratio varied from 50 to 350 which covers a large range of practical applications.

Following Hoglund's procedure, who expressed the resistance of the web p as $p \propto 850\ t^2$, Delesques expressed p as a function of Et^2, where E is the modulus of elasticity of the section. He carried out an investigation of the possible influence of different parameters in a graphical form and came to the conclusion that:

1) the elastic limit of the web,
2) the aspect ratio of the beam panel,
3) the stiffness of the beam flange and conditions for supporting the loads,
4) the depth to thickness ratio of the web do not have any appreciable influence on the failure load. He concluded that for all the beams tested, whatever the slenderness ratio of the

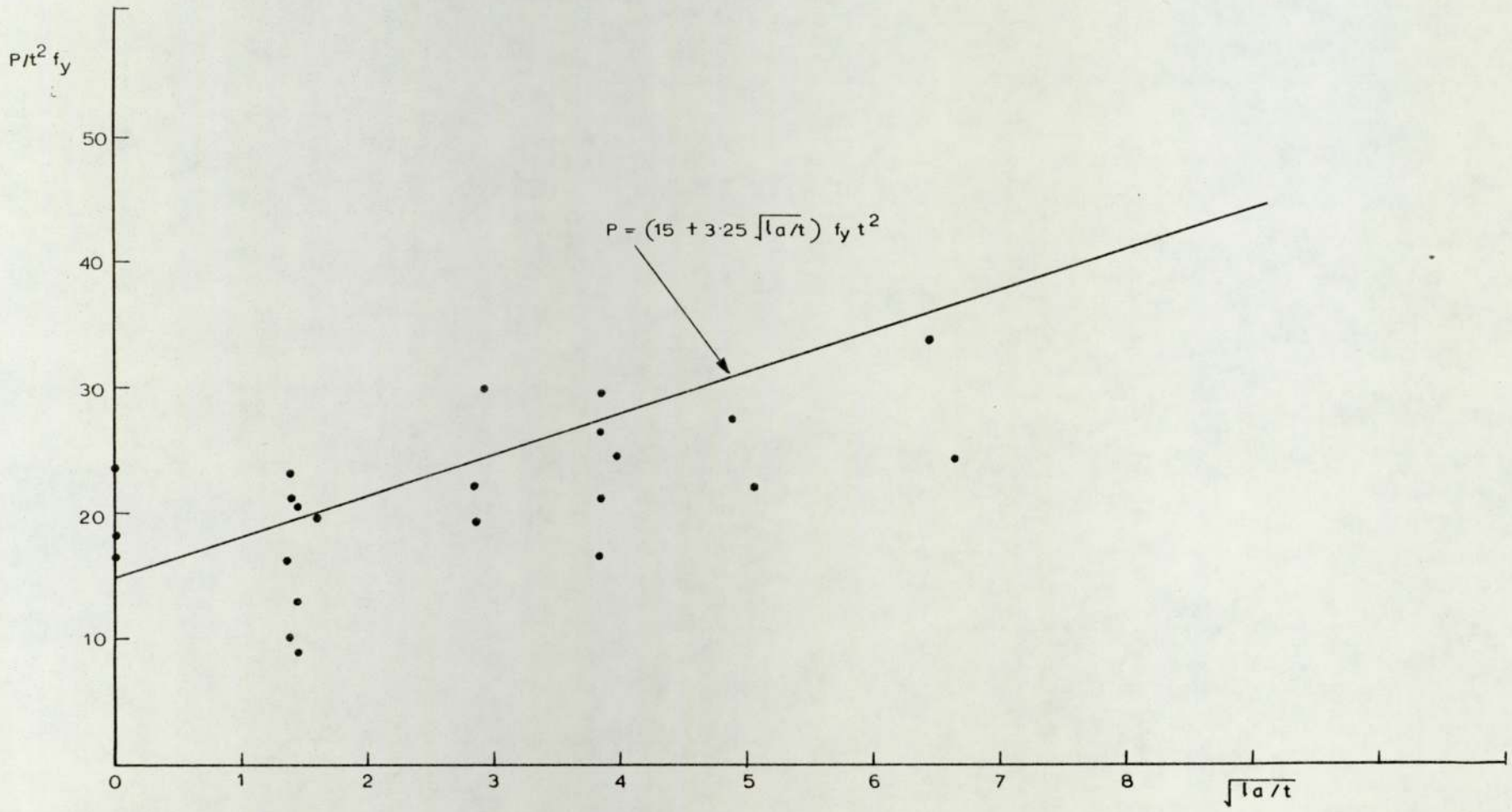

FIGURE 4.4 COMPARISON OF TEST RESULTS FOR CENTRAL FAILURE WITH THE WINTER AND PIAN FORMULA

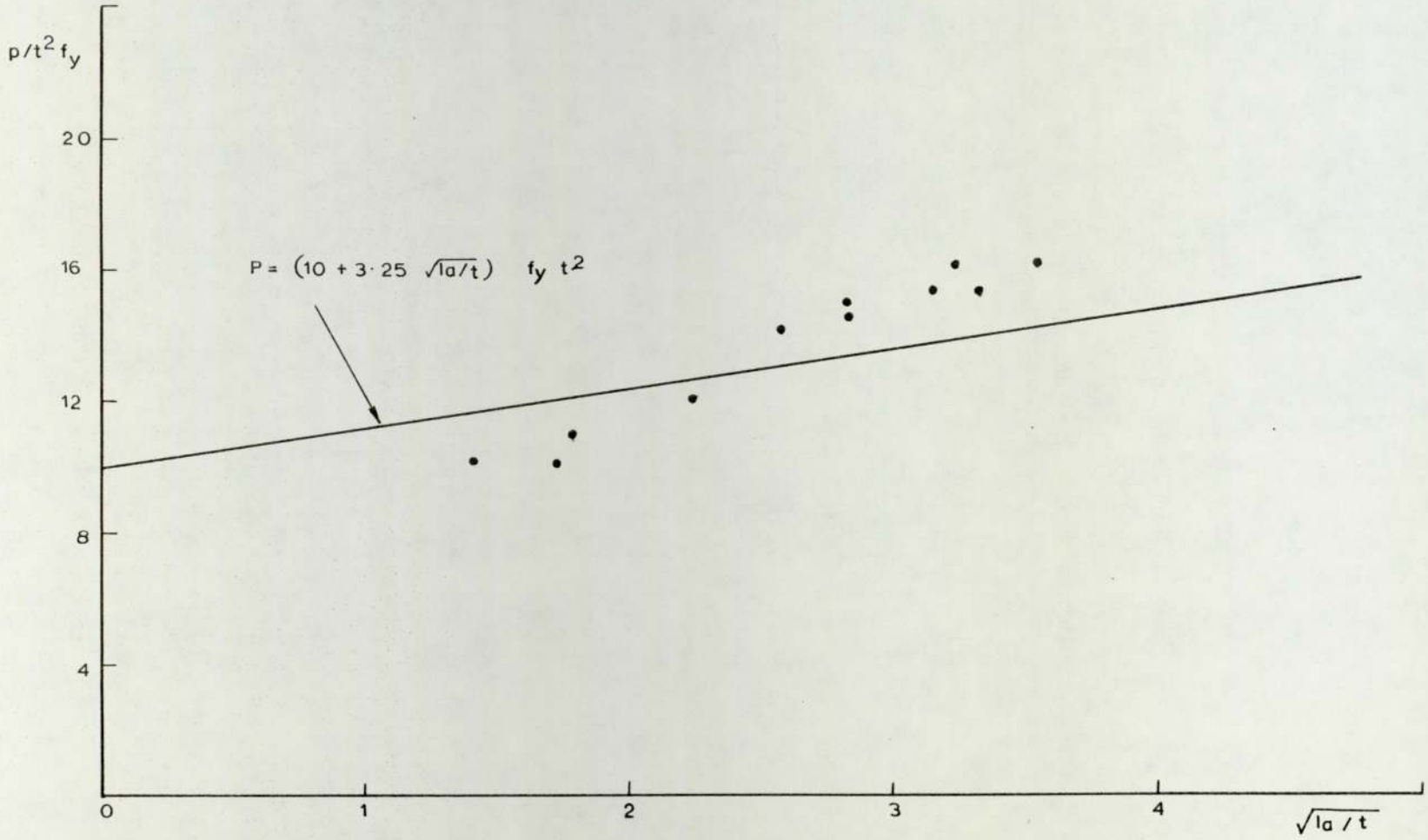

FIGURE 4.5 COMPARISON OF TEST RESULTS FOR END FAILURE WITH THE WINTER AND PIAN FORMULA

web in which buckling takes place, under the load the resistance p was greater than $0.04\ Et^2$.

All the tests for the present work have been performed on rolled steel universal beams. The depth to thickness ratio of the web (d/t) for the whole range varies from 26.9 to 56.7. Therefore, the results of these tests are not comparable with the work of Delesques, since this is based on very slender beams; such sections could behave in a different way under loading than the universal beam sections. However, as it has been shown from the test results some of these factors investigated by Delesques do have an influence on the failure load of the tested beams.

4.3.4 C.I.R.I.A. Project R.P. 219

In the C.I.R.I.A. project 'Web Buckling of Rolled Steel Beams'R.P 219, carried out in the Civil Engineering Department at Aston University, the investigators, using the concept of an equivalent strut, have shown that the axial load W_a, for span failure, is given by the expression

$$W_a = \frac{b_e\ t\ f_{br}}{1 + \frac{L\ D^3\ t}{28 b_e\ I}} \qquad 4.11$$

where

b_e is the equivalent width of strut; for this elastoplastic type of failure it is given by:

$b_e = 0.0125\ \frac{h}{r}\ D + 1a$, where $\frac{h}{r}$ is the slenderness ratio, taken for this case as $0.75 \times 2\sqrt{3}\ d/t$.

D is the overall depth of the section

1a is the length of the stiff bearing

f_{br} is the buckling stress, obtained by using the formula in the

appendix B of BS 449 (1969)

L is the span of the beam

I is the second moment of area of the section about the axis of bending.

By using equation (4.11), the theoretical failure loads for the beams in series VI and VII have been calculated and the comparison with the test failure load is shown in table (4.4). As could be seen from this comparison, this method gives unsatisfactory results for large lengths of stiff bearing and long lengths of span.

4.4 CONCLUSIONS

The various design methods considered here were shown to be conservative for certain loading conditions and very unsuitable for others.

Most of these methods use the load dispersion theory for calculating the effective bearing length which in its present form gave unsatisfactory results, especially for cases involving long spans and long lengths of bearing.

The conclusions that many investigators have drawn from these tests mainly concern beams more slender than universal beams which behave in a different manner under load.

Series	Beam No	Span /m	la /mm	P_{exp} /kN	P_{th} /kN	$\frac{P_{exp}}{P_{th}}$
	31	1.00	0	208.0	201.03	1.035
	30	1.00	50.0	270.0	251.94	1.072
	32	1.00	100.0	310.0	306.93	1.010
	33	1.00	150.0	350.0	353.65	0.990
	34	1.00	250.0	395.0	419.77	0.941
	50	1.40	0	185.0	181.27	1.021
	51	1.40	50.0	217.5	222.96	0.975
	52	1.40	150.0	240.0	297.90	0.806
	53	1.40	250.0	265.0	375.59	0.705
	62	0.50	0	322.5	299.56	1.077
VI	63	0.50	150.0	495.0	386.97	1.279
	60	1.25	12.0	860.0	799.59	1.055
	61	1.25	100.0	1060.0	981.81	1.084
	64	2.00	0	285.0	239.12	1.192
	65	2.00	50.0	350.0	307.39	1.139
	66	2.00	150.0	460.0	352.68	1.304
	67	2.00	300.0	530.0	446.36	1.187
	68	1.00	0	190.0	188.60	1.007
	69	1.00	0	180.0	179.66	1.002
	70	1.00	150.0	297.5	318.65	0.934

TABLE 4.5 COMPARISON OF TEST RESULTS TO CIRIA FORMULA

Series	Beam No	Span /m	la /mm	P_{exp} /kN	P_{th} /kN	$\frac{P_{exp}}{P_{th}}$
VI	71	1.00	150.0	260.0	302.90	0.858
	72	1.00	0	140.0	166.56	0.841
	73	1.00	0	127.5	155.67	0.819
	74	1.00	150.0	190.0	287.20	0.662
	75	1.00	150.0	172.5	271.08	0.636
VII	44	0.50	12.7	237.5	250.74	0.947
	35	1.00	12.7	215.0	231.38	0.929
	45	2.00	12.7	145.0	165.70	0.875
	46	3.00	12.7	100.0	136.38	0.733
	48	0.50	12.7	300.0	296.58	1.012
	47	1.00	12.7	272.5	257.88	1.057
	49	3.00	12.7	135.0	170.87	0.790
	58	3.50	12.7	250.0	243.77	1.026
	59	0.75	12.7	168.75	129.31	1.305
	54	0.50	100.0	470.0	343.58	1.368
	55	1.00	100.0	430.0	396.56	1.084
	56	2.00	100.0	350.0	354.79	0.986
	57	3.00	100.0	280.0	322.33	0.869

TABLE 4.5 (CONTINUED)

CHAPTER 5

ELASTIC BUCKLING THEORY

5.1 INTRODUCTION

In chapter 4 the current design practices mentioned assume that the failure of the rolled steel beams could be either due to local crushing in the vicinity of the applied load, or, due to overall elastic buckling of the web in which part of the web is considered as a uniformly loaded strut.

In this chapter an elastic buckling analysis of the web plate of a universal beam is presented to investigate what relationship, if any, exists between elastic buckling theory and ultimate strength of the beam. This theory is mainly concerned with the conditions and loading which best represent the actual behaviour of the web plate. In this buckling analysis, consideration has also been given to the bending; the forces, longitudinal and vertical are assumed to be proportional to each other.

5.2 ELASTIC BUCKLING ANALYSIS

The web plate of a universal beam could be considered as a rectangular plate, subjected to different types of loading and boundary conditions. The influence of the restraint provided by the flanges is, of course, very important in the analysis of the plate as it is for a strut. According to the amount of restraint at its ends, a strut of length b will have an elastic critical load of between $\pi^2 EI/b^2$ and $4\pi^2 EI/b^2$. This elastic critical load is usually written in the form:

$$P_{cr} = K \frac{\pi^2 EI}{b^2} \qquad 5.1$$

where K is referred to as an elastic buckling coefficient. Similarly for plates the critical load per unit length N_{cr} could be obtained from the following expression:

$$N_{cr} = K_1 \frac{\pi^2 D_1}{b^2} \qquad 5.2$$

where K_1 is an elastic buckling coefficient and D_1 is the modulus of rigidity of the plate and is given by $D_1 = Et^3/12(1-v^2)$. The total critical load P_{cr} can be obtained from:

$$P_{cr} = N_{cr}\, a = K_1 \frac{\pi^2 D_1}{b} \cdot \frac{a}{b} \qquad 5.3.1$$

and by substituting $K = K_1 \frac{a}{b}$, then

$$P_{cr} = K \frac{\pi^2 D_1}{b} \qquad 5.3.2$$

Where convenient, for presenting results, both K_1 and K will be used.

When no body forces are present, the St. Venant differential equation can be used for the analysis as presented by Timoshenko (12) et al.

$$D_1 \nabla^4 \omega = N_x \frac{\partial^2 \omega}{\partial x^2} + N_y \frac{\partial^2 \omega}{\partial y^2} + 2N_{xy} \frac{\partial^2 \omega}{\partial x \partial y} \qquad 5.4$$

The elastic critical load could be obtained by solving the above equation for various boundary conditions. The solution of this equation becomes more difficult when the N_x, N_y and N_{xy} forces are not constant throughout the plate, due to variable coefficients. The energy method is an alternative in solving equation (5.4). This enables the stability of the plate to be examined in a very direct and simple way. According to this method, the strain energy

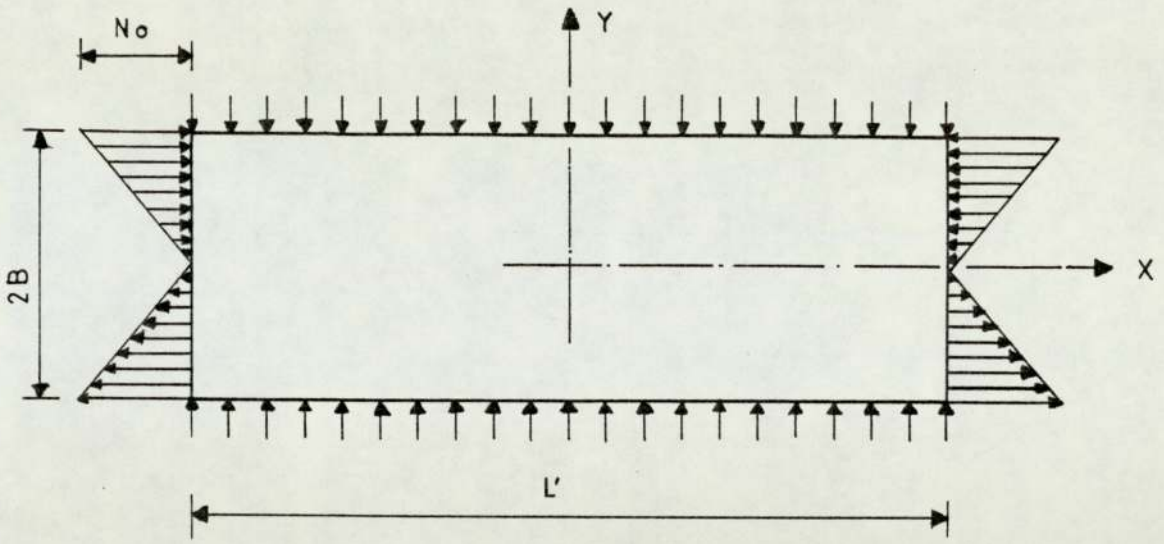

a.

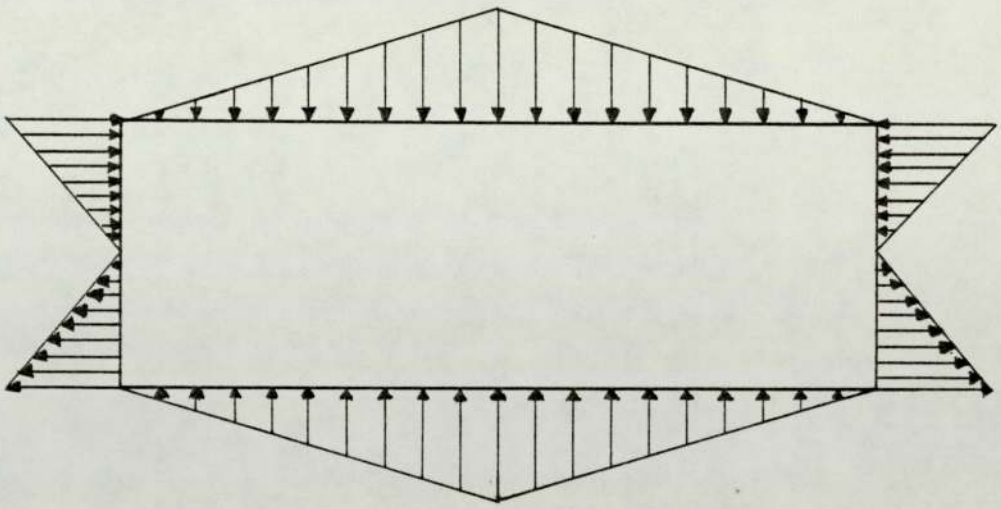

b.

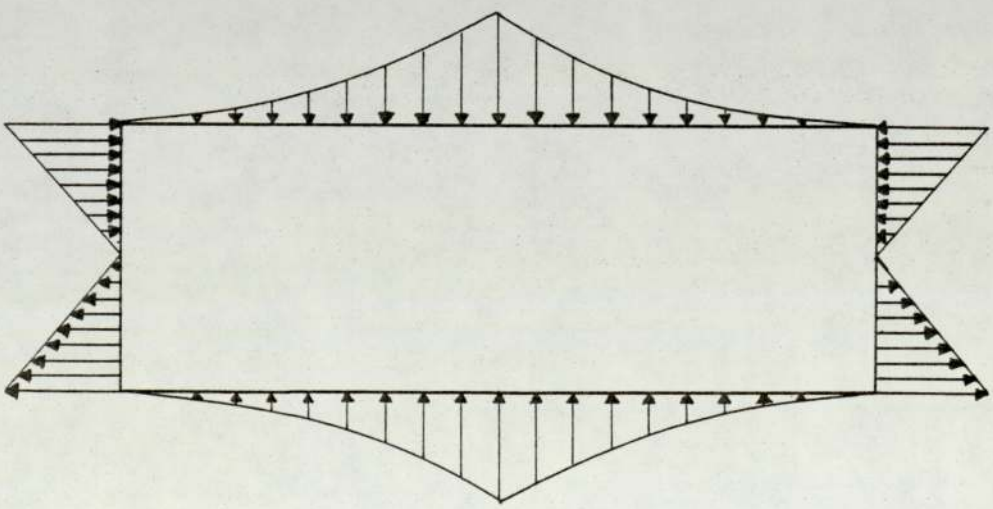

c.

FIGURE 5.1 PLATE SUBJECTED TO VARIOUS TYPES OF LOADING

of bending is equated to the work done by the forces acting in the middle plane of the plate. The general energy equation is presented as:

$$-\frac{1}{2}\iint\left(N_x\left(\frac{\partial\omega}{\partial x}\right)^2+N_y\left(\frac{\partial\omega}{\partial y}\right)^2+2N_{xy}\frac{\partial\omega}{\partial x}\frac{\partial\omega}{\partial y}\right)dx\,dy$$

$$=\frac{D_1}{2}\iint\left(\left(\frac{\partial^2\omega}{\partial x^2}+\frac{\partial^2\omega}{\partial y^2}\right)^2-2(1-\nu)\left(\frac{\partial^2\omega}{\partial x^2}\frac{\partial^2\omega}{\partial y^2}-\left(\frac{\partial^2\omega}{\partial x\partial y}\right)^2\right)\right)dx\,dy \qquad 5.5$$

An expression for the lateral deflection of the plate ω must be found to satisfy the boundary conditions and to make the variation of the energy equation a minimum. For more complicated loadings and boundary conditions an approximate method of analysis such as Rayleigh-Ritz method can be used.

5.2.1 Web Plate of Universal Beam Subjected to Various Loading and Boundary Conditions

In this section the theoretical determination of the elastic buckling load of a rectangular plate, for three different types of loading and various boundary conditions is presented. The applied load is one of the following forms:

1) Uniformly Distributed
2) Triangularly Distributed
3) Parabolically Distributed

and it is applied on the two opposite longitudinal edges. The vertical edges are subjected to bending forces. The three loading cases are shown in figure (5.1); the analysis for the cases shown in figure (5.1a, b) is given in Appendix 2.

The web plate of the universal beam will be considered as a

rectangular plate with the two vertical edges simply supported or free and the longitudinal edges simply supported or fixed, due to the restraint provided by the flanges.

5.2.1.1 Web Plate of a Universal Beam Subjected to a Parabolically Distributed Load

Consider the plate shown in figure (5.1c), loaded, in the y direction, in the middle plane by a force parabolically distributed. This force is given by:

$$N_y = N_o \gamma \left[\frac{x^2}{A^2} + \frac{2x}{A} + 1\right] \qquad -A \leqslant x \leqslant 0 \qquad 5.6.1$$

$$N_y = N_o \gamma \left[\frac{x^2}{A^2} - \frac{2x}{A} + 1\right] \qquad 0 \leqslant x \leqslant A \qquad 5.6.2$$

The force distribution in the x-direction N_{bx} is given by:

$$N_{bx} = N_o \left[1 - \alpha_o \frac{B-y}{2B}\right] \qquad 5.7$$

where

N_y is the vertical compressive force per unit length acting on plate middle plane

N_o is the maximum compressive/tensile value of N_b at the edge of the plate (estimated by elementary means)

N_x is the longitudinal compressive force per unit length acting on plate middle plane

N_{bx} is the sum of the longitudinal loadings N_x and N_b

γ is a numerical factor to be defined later

α_o is a numerical factor

Various longitudinal force distributions can be obtained by altering α_o in expression (5.7). For example by setting $\alpha_o = 0$ the case of uniformly distributed force is obtained. The case of pure bending is obtained by setting $\alpha_o = 2$ and a combination of bending and compression or bending and tension by setting $\alpha_o < 2$ or $\alpha_o > 2$

respectively. Different boundary conditions will be considered, as follows.

a) All Edges Simply Supported

The plate in this case is assumed to be simply supported along its edges so that out of plane deflection along its edges is not prevented. Along any perpendicular to the longitudinal edges the plate is free to move in its own plane. The out of plane deflection of the plate ω must satisfy the boundary conditions along its edges $x = \pm A$ and $y = \pm B$. These boundary conditions are:

$$\omega = 0 \quad \text{at} \quad x = \pm A \quad \text{and} \quad y = \pm B \tag{5.8.1}$$

$$\frac{\partial^2 \omega}{\partial x^2} + \nu \frac{\partial^2 \omega}{\partial y^2} = 0 \quad \text{at } x = \pm A \tag{5.8.2}$$

$$\frac{\partial^2 \omega}{\partial y^2} + \nu \frac{\partial^2 \omega}{\partial x^2} = 0 \quad \text{at} \quad y = \pm B \tag{5.8.3}$$

This is for $2A = L'$, where L' is the overall length of the plate. It should be noted that the length $2A$ is an undetermined parameter. It could be greater, equal or less than L'. In cases, where the length is greater than L', such as for short plates, this has no meaning and the limit should be taken as L'. The length $2A$ is less than L' for cases of very long plates. An approximate expression for the deflection ω which satisfies the above mentioned boundary conditions and the experimental observations is taken as $(\cos \frac{\pi y}{2B} + \lambda \sin \frac{\pi y}{B})$ in the y-direction, which is not symmetrical about the x-direction, and as a half cosine curve in the x-direction. The numerical factor λ is obtained from the deflected experimental shape; for the purpose of the present work it is taken as 0.25 .

The deflection ω is given therefore by the following expression.

$$\omega = \omega_o \cos \frac{\pi x}{2A} \left(\cos \frac{\pi y}{2B} + \lambda \frac{\sin \pi y}{B}\right) \quad -A \leqslant x \leqslant A \qquad 5.9.1$$

$$\omega = 0 \qquad -\frac{L'}{2} \leqslant x \leqslant -A \qquad 5.9.2$$

$$\omega = 0 \qquad A \leqslant x \leqslant \frac{L'}{2} \qquad 5.9.3$$

where ω_o is the initial deflection in the plate; the deflected shape is shown in figure (5.2a). By introducing the correct limits of integration into equation (5.5) this becomes:

$$-\frac{1}{2}\int_{-B}^{B}\int_{-A}^{A} [N_x (\frac{\partial \omega}{\partial x})^2 + N_y (\frac{\partial \omega}{\partial y})^2] dx\, dy = \frac{D_1}{2}\int_{-B}^{B}\int_{-A}^{A} (\frac{d^2\omega}{dx^2} + \frac{d^2\omega}{dy^2})^2 -$$

$$2(1-\nu)[\frac{\partial^2 \omega}{\partial x^2} \cdot \frac{\partial^2 \omega}{\partial y^2} - (\frac{\partial^2 \omega}{\partial x \cdot \partial y})^2]) \; dx \cdot dy \qquad 5.10$$

By substituting now equations (5.6.1), (5.6.2), (5.7) and (5.9.1) into equation (5.10) and after evaluating and simplifying N_o can be obtained from:

$$N_o = K \frac{\pi^2 D_1}{(2B)^2} \qquad 5.11$$

where K is a buckling coefficient given by

$$K = \frac{(\frac{B}{A})^2 (1 + \lambda^2) + (\frac{A}{B})^2 (1 + 16\lambda^2) + 2 (1 + 4\lambda^2)}{\frac{64\lambda}{9\pi^2} + (\frac{A}{B})^2 \gamma \frac{(1 + 4\lambda^2)(6 + \pi^2)}{3\pi^2}} \qquad 5.12$$

At this stage the numerical factor γ has to be determined. From the simple theory of bending N_o can be obtained from

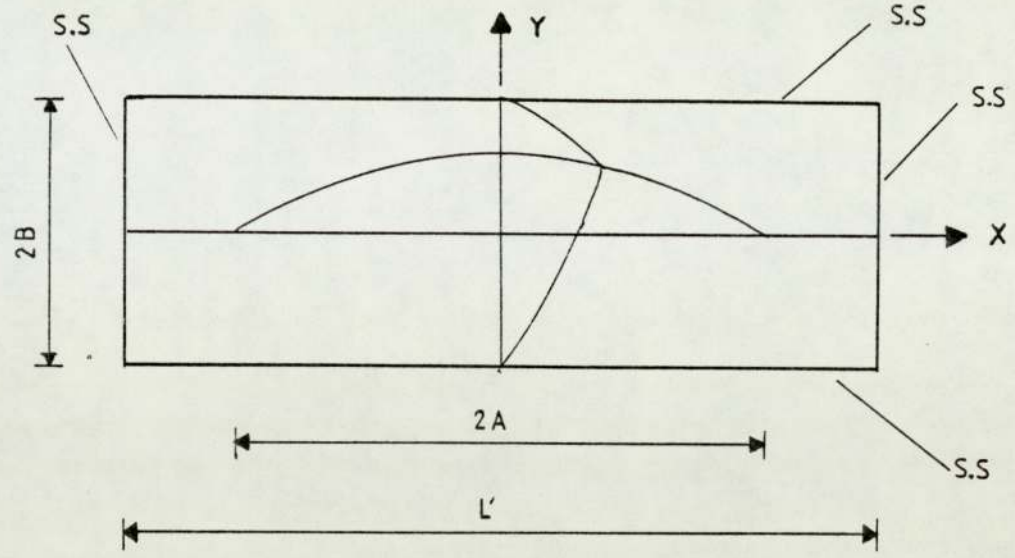

a. Deflected shape

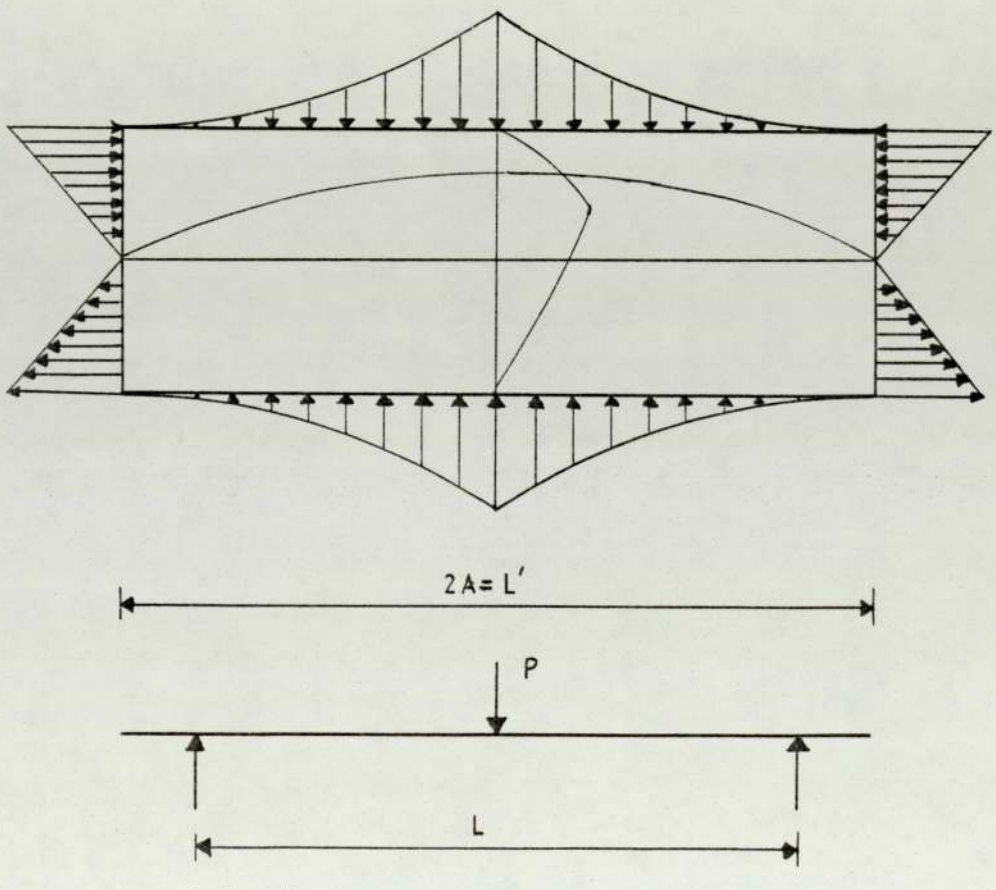

b. Loading

FIGURE 5.2 DEFLECTED SHAPE AND LOADING OF PLATE UNDER INVESTIGATION

$$N_o = \frac{P\ L\ d\ t}{8I} \qquad 5.13$$

where P is the applied critical load and L is the span of the beam, as shown in figure (5.2b). In equation (5.13) P is unknown and could be obtained by integrating the expression giving the load, that is

$$P = 2N_o\ \gamma \int_0^A \left(\frac{x^2}{A^2} - \frac{2x}{A} + 1\right) dx$$

which gives $$P = \frac{2}{3} N_o\ A\ \gamma \qquad 5.14$$

By substituting this value of P in to equation (5.13) and rearranging

$$\gamma = \frac{1}{A}\ \ \frac{12I}{Ldt} \qquad 5.15$$

and therefore equation (5.12) becomes:

$$K = \frac{\left(\frac{B}{A}\right)^2 (1+\lambda^2) + \left(\frac{A}{B}\right)^2 (1 + 16\ \lambda^2) + 2\ (1 + 4\ \lambda^2)}{\frac{64\lambda}{9\pi^2} + \left(\frac{A}{B}\right)^2 \frac{(1+4\lambda^2)\ (6+\pi^2)}{3\pi^2}\ \ \frac{12I}{LdtB}} \qquad 5.16$$

b) Longitudinal Edges Fixed and Vertical Edges Simply Supported

The loading remains the same as for the previous case, but the edges $y = \pm B$ are now fixed; the edges $x = \pm A$, as before, simply supported. An expression for the deflection ω must be formulated which satisfies the boundary conditions. The deflected shape and the edge conditions are shown in figure (5.3a); the new boundary conditions are

$\omega = 0$ at $x = \pm A$ and $y = \pm B$ 5.17.1

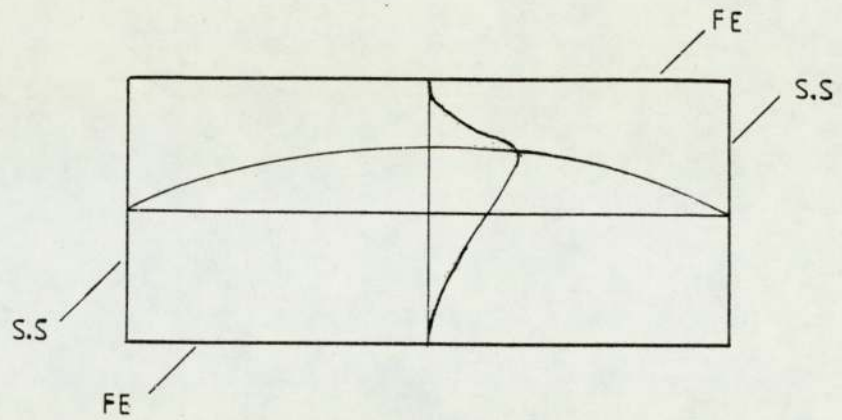

a. Deflected shape for case (b)

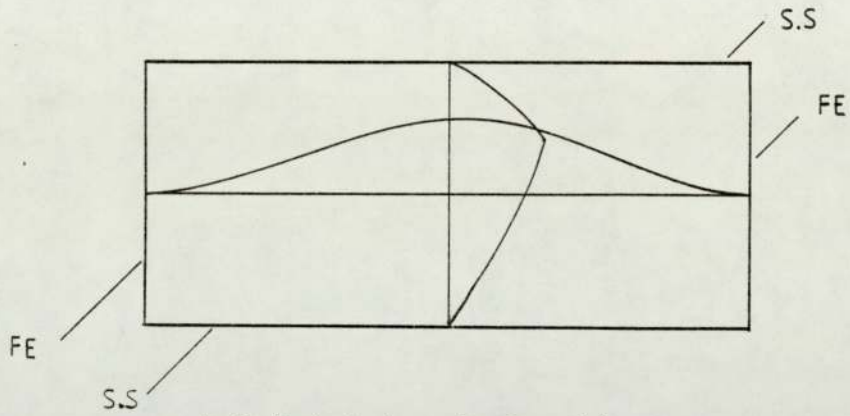

b. Deflected shape for case (c)

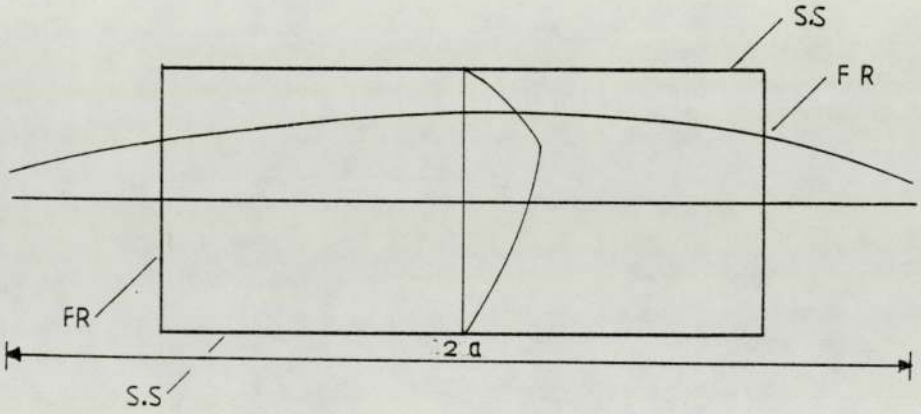

c. Deflected shape for case (d)

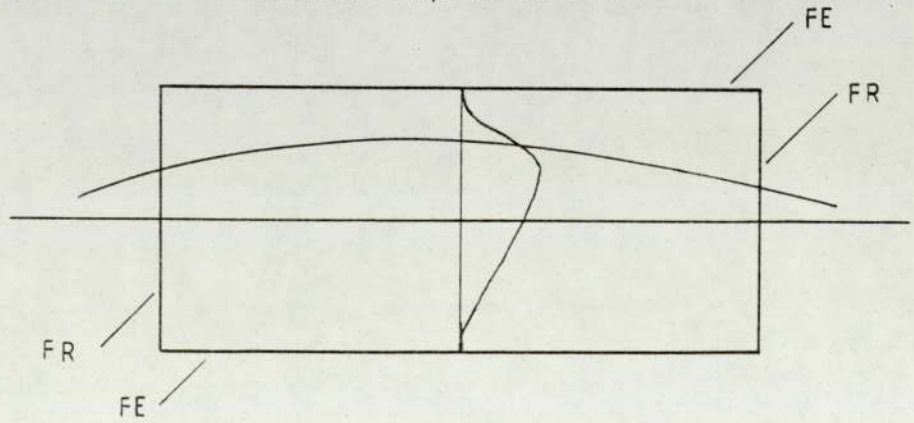

d. Deflected shape for case (e)

FIGURE 5.3 DEFLECTED SHAPES

$$\frac{\partial^2 \omega}{\partial x^2} + \nu \frac{\partial^2 \omega}{\partial y^2} = 0 \qquad \text{at} \quad x = \pm A \qquad 5.17.2$$

$$\frac{\partial \omega}{\partial y} = 0 \qquad \text{at} \quad y = \pm B \qquad 5.17.3$$

An expression for ω, which satisfies the above conditions is

$$\omega = \omega_o \cos \frac{\pi x}{2A} \left(\cos \frac{\pi y}{2B} + \lambda \sin \frac{\pi y}{B}\right)^2 \qquad -A \leqslant x \leqslant A \qquad 5.18.1$$

$$\omega = 0 \qquad -\frac{L'}{2} \leqslant x \leqslant -A \qquad 5.18.2$$

$$\omega = 0 \qquad A \leqslant x \leqslant \frac{L'}{2} \qquad 5.18.3$$

By following the same procedure as for case (a) the buckling coefficient K is given by.

$$K = \frac{\left(\frac{B}{A}\right)^2 \left(\frac{3}{4}+3\lambda^2+\frac{3}{4}\lambda^4\right) + \left(\frac{A}{B}\right)^2 \left(4+82\lambda^2+64\lambda^4\right) + 2\left(1+16\lambda^2-\frac{2}{11\pi}\lambda^2+4\lambda^4\right)}{\frac{4}{11025\pi^2}\left(9016\lambda+29184\lambda^3\right) + \left(\frac{A}{B}\right)\frac{(\pi^2+6)\ (1+10\lambda^2+4\lambda^4)}{3\pi^2}\frac{12I}{LdtB}}$$

5.19

c) Longitudinal Edges Simply Supported and Vertical Edges Fixed

As for the previous two cases the loading remains the same. The edges $y = \pm B$ are now simply supported and the edges $x = \pm A$ are fixed. The expression for the deflected shape must satisfy the new boundary conditions which are:

$$\omega = 0 \qquad \text{at} \quad x = \pm A \quad \text{and} \quad y = \pm B \qquad 5.20.1$$

$$\frac{\partial \omega}{\partial x} = 0 \qquad \text{at } x = \pm A \qquad 5.20.2$$

$$\frac{\partial^2 \omega}{\partial y^2} + \nu \frac{\partial^2 \omega}{\partial x^2} = 0 \qquad \text{at } y = \pm B \qquad 5.20.3$$

Such an expression can be written in the form

$$\omega = \omega_o \cos^2 \frac{\pi x}{2A} \left(\cos \frac{\pi y}{2B} + \lambda \sin \frac{\pi y}{B}\right) \qquad -A \leqslant x \leqslant A \qquad 5.21.1$$

$$\omega = 0 \qquad -\frac{L'}{2} \leqslant x \leqslant -A \qquad 5.21.2$$

$$\omega = 0 \qquad A \leqslant x \leqslant \frac{L'}{2} \qquad 5.21.3$$

and the deflected shape is shown in figure (5.3b). By following the same procedure as before the buckling coefficient K can be written as

$$K = \frac{\left(\frac{B}{A}\right)^2 (1+\lambda^2) + \left(\frac{A}{B}\right)^2 \frac{(1+16\lambda^2)}{8} + \frac{(1+4\lambda^2)}{2}}{\frac{16\lambda}{9\pi^2} + \left(\frac{A}{B}\right) \frac{(4+\pi^2)(1+4\lambda^2)}{4\pi^2} \cdot \frac{3I}{LdtB}} \qquad 5.22$$

d) Longitudinal Edges Simply Supported and Vertical Edges Free

For this case the longitudinal edges, that is $y = \pm B$, are simply supported and the vertical edges $x = \pm A$ are now free. The deflected shape can be expressed as:

$$\omega = \omega_o \cos \frac{\pi x}{2a} \left(\cos \frac{\pi y}{2B} + \lambda \sin \frac{\pi y}{B}\right) \qquad 0 \leqslant A \leqslant a \qquad 5.23$$

where 2a is the wavelength as shown in figure (5.3c). The quantity 2a is not yet determined; by following the same procedure as for the previous cases and by introducing the correct limits when integrating, the buckling coefficient K could be written as

$$K = \frac{(A+\frac{a}{\pi}\sin\frac{\pi A}{a})\ (\frac{B^2}{4a^4}\ (1+\lambda^2) + \frac{1}{4B^2}\ (1+16\lambda^2) + \frac{1}{2a^2}\ (1+4\lambda^2))}{\frac{1}{4a^2}\ (A-\frac{a}{\pi}\sin\frac{\pi A}{a})\ \frac{64\lambda}{9\pi^2} + \frac{\gamma}{4B^2}\ (1+4\lambda^2)\ (\frac{A}{3} - \frac{2a^3}{A^2\pi^3}\sin\frac{\pi A}{a} + \frac{2a^2}{A\pi^2})} \qquad 5.24$$

It should be emphasized at this point that the correct limits of integration in the x-direction, -A and A, are the actual dimensions of the plate, that is 2A = L'; this means that the applied load is considered as acting along the whole length of the plate. It is worthwhile noting that for a = A equation (5.24) becomes identical to equation (5.12), for the case (a) when all the edges are simply supported and the wavelength is equal to the length of the plate. By denoting $F = \frac{a}{B}$ and $D = \frac{A}{B}$ then equation (5.24) can be rewritten as:

$$K = \frac{(D+\frac{F}{\pi}\sin\frac{\pi D}{F})\ (\frac{(1+\lambda^2)}{4F^4} + \frac{(1+16\lambda^2)}{4} + \frac{(1+4\lambda^2)}{2F^2})}{\frac{1}{4F^2}\ (D-\frac{F}{\pi}\sin\frac{\pi D}{F})\ \frac{64\lambda}{9\pi^2} + \frac{G}{4D}(1+4\lambda^2)\ (\frac{D}{3} + \frac{2F^2}{D\pi^2} - \frac{2F^3}{D^2\pi^3}\sin\frac{\pi D}{F})} \qquad 5.25$$

where G = 12I/BLdt and therefore γ, given by equation (5.15) could be written in the form:

$$\gamma = \frac{1}{A}\frac{12I}{Ldt} = \frac{G}{D} \qquad 5.26$$

e) Longitudinal Edges Fixed and Vertical Edges Free

The loading conditions remains the same as for the previous cases, the only difference being that the longitudinal edges are now fixed and the vertical edges free. An expression for the deflected shape which satisfies these new boundary conditions can be written in the form:

$$\omega = \omega_o \cos \frac{\pi x}{2a} \left(\cos \frac{\pi y}{2B} + \lambda \sin \frac{\pi y}{B}\right)^2 \qquad 0 \leq A \leq a \qquad 5.27$$

and it is shown in figure (5.3d). The limits of integration for the wavelength a are the same as for case (d) and the expression obtained for the buckling coefficient K is given by:

$$K = \frac{P_o \quad Q_o}{T_o} \qquad 5.28.1$$

where

$$P_o = \left(A + \frac{a}{\pi} \sin \frac{\pi A}{a}\right) \qquad 5.28.2$$

$$Q_o = \left(\frac{4B^2}{16a^4} \left(\frac{3}{4} + 3\lambda^2 + \frac{3}{4}\lambda^4\right) + \frac{1}{4B^2} \left(4 + 28\lambda^2 + 64\lambda^4\right) + \right.$$

$$\left. \frac{2}{4a^2} \left(1 + 16\lambda^2 - \frac{2\lambda^2}{11\pi} + 4\lambda^4\right)\right) \qquad 5.28.3$$

$$T_o = \left(\frac{1}{4a^2} \left(A - \frac{a}{\pi} \sin \frac{\pi A}{a}\right) \frac{4}{11025\pi^2} \left(9016\lambda + 29184\lambda^3\right) + \right.$$

$$\left. \frac{\gamma}{4B^2} \left(\frac{A}{3} - \frac{2a^3}{A^2\pi^3} \sin \frac{\pi A}{a} + \frac{2a^2}{A\pi^2} \left(1 + 10\lambda^2 + 4\lambda^4\right)\right)\right) \qquad 5.28.4$$

By substituting a = A in the above expression it becomes identical to equation (5.19), for the case when the vertical edges are simply

supported and the loaded edges are fixed; the wavelength is equal to the length of the plate, that is $2a = 2A = L'$ similarly to the latest case, setting $F = \frac{a}{A}$ and $D = \frac{A}{B}$ and by substituting back into equation (5.28) this becomes:

$$K = \frac{P\,Q}{T} \qquad 5.29.1$$

where

$$P = \left(D + \frac{F}{\pi} \sin \frac{\pi D}{F}\right) \qquad 5.29.2$$

$$Q = \left(\frac{1}{4F^4} \left(\frac{3}{4} + 3\lambda^2 + \frac{3}{4}\lambda^4\right) + \frac{1}{4}\left(4 + 82\lambda^2 + 64\lambda^4\right) + \right.$$

$$\left. \frac{1}{2F^2}\left(1 + 16\lambda^2 - \frac{2\lambda^2}{11\pi} + 4\lambda^4\right)\right) \qquad 5.29.3$$

$$T = \left(\frac{1}{4F^2}\left(D - \frac{F}{\pi} \sin \frac{\pi D}{F}\right) \frac{4}{11025\pi^2}\left(9016\lambda + 29184\lambda^3\right) + \right.$$

$$\left. \frac{G}{4D}\left(\frac{D}{3} - \frac{2F^3}{D^2\pi^3} \sin \frac{\pi D}{F} + \frac{2F^2}{D\pi^2}\right)\left(1 + 10\lambda^2 + 4\lambda^4\right)\right) \qquad 5.29.4$$

5.3 DETERMINATION OF THE BUCKLING COEFFICIENT

It is obvious that the buckling coefficient K for a particular plate, that is when the quantity 2B has a fixed value, is a function of the wavelength and in order to determine the smallest possible buckling load it is necessary to minimize K with respect to the wavelength. The resultant expression obtained for K can be written in the form

$K = \frac{\text{Numerator}}{\text{Denominator}}$ and by differentiating this with respect to F and setting $\frac{\partial k}{\partial F} = 0$, a value for F and therefore for the wavelength a can be obtained for which K is a minimum, that is

$$\frac{\partial K}{\partial F} = \text{Denominator} \times \frac{\partial}{\partial F}(\text{Numerator}) - \text{Numerator} \times \frac{\partial}{\partial F}(\text{Denominator}) = 0$$

The resulting expressions, after differentiation are given in Appendix 2 with the flow chart of a computer program, written to solve this problem.

5.4 CALCULATION OF THE ELASTIC CRITICAL LOAD

As could be seen from equations (5.25) and (5.28) the buckling coefficient K can be obtained for various aspect ratios D(= A/B) of the plate and for different values of bending stresses by altering the quantity G(=12I/LdtB).

A universal beam section, namely 406 × 140 × 39 kg has been chosen for demonstrating the procedure for calculating the elastic critical load. The first step is to keep the bending stresses constant and obtain the variation of K with the aspect ratio A/B, say for simply supported conditions, using equation 5.25, for a 0.5 m span. The aspect ratio A/B versus the buckling coefficient K plot is marked, in dotted line, as (a) in figure (5.4). As has been mentioned before there is a limitation in the value of the wavelength a, therefore, the case when the vertical edges of the plate are simply supported will be considered as well. For the same values of aspect ratio A/B and the quantity G a plot of the aspect ratio versus the buckling coefficient, using equation 5.16 is obtained and it is marked, in dotted line, as (b) in figure

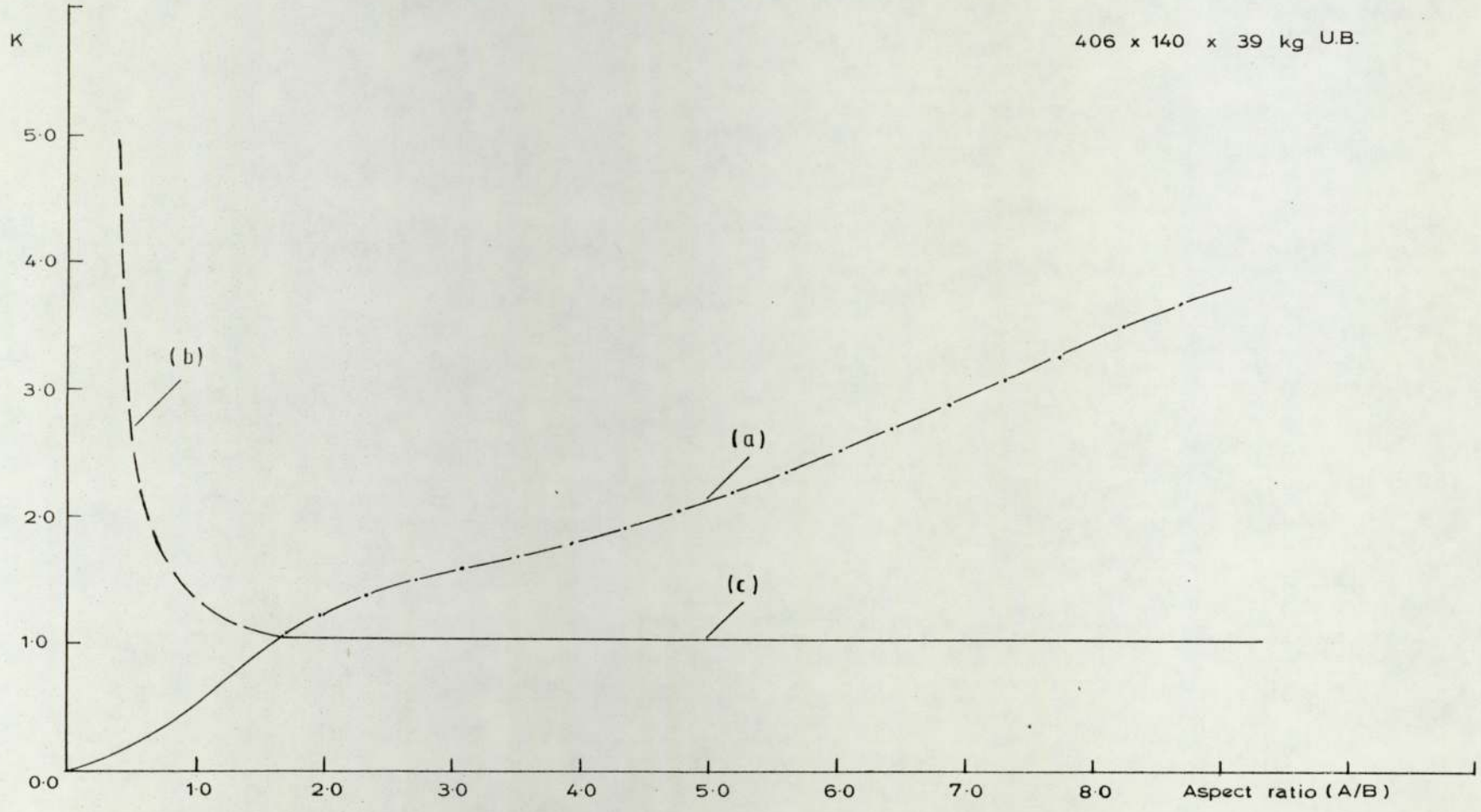

FIGURE 5·4 BUCKLING CURVES FOR 0·5m SPAN BEAM OF 406 x 140 x 39 kg U.B.

(5.4). Now these two curves, marked (a) and (b) are combined and the resultant curve is marked, in solid line, as (c) in the same figure.

Exactly the same procedure is repeated for different lengths of span, obtaining a series of graphs. The next step is to represent in a graphical form the variation of the critical load P with the span L. Rearranging equation (5.13), P can be obtained from:

$$P = N_o \cdot \frac{8I}{Ldt} \qquad 5.30$$

where N_o is given by the expression below

$$N_o = \frac{D_1 \pi^2}{(2B)^2} K$$

and equation (5.3), therefore, becomes:

$$P = \frac{D_1 \pi^2}{(2B)^2} \cdot \frac{8I}{dt} \cdot \frac{K}{L} \qquad 5.31$$

If the overhang at each end of the beam is denoted by x_o then the total length of the plate will be $L + 2x_o$ (=2A). By considering the curve (c) in figure (5.4), the buckling coefficient for this particular case is obtained utilising equation (5.31), and the elastic critical load can be calculated. The same steps are repeated for the other case when the longitudinal edges are fixed and the vertical edges free and simply supported for the proper limits. Finally the two theoretical extreme curves corresponding to the cases when the longitudinal edges are simply supported and fixed are obtained. These two curves are shown in figure (5.5). In the first case the restraint provided by the flanges is zero and in the other case the flanges provide infinitely large restraint.

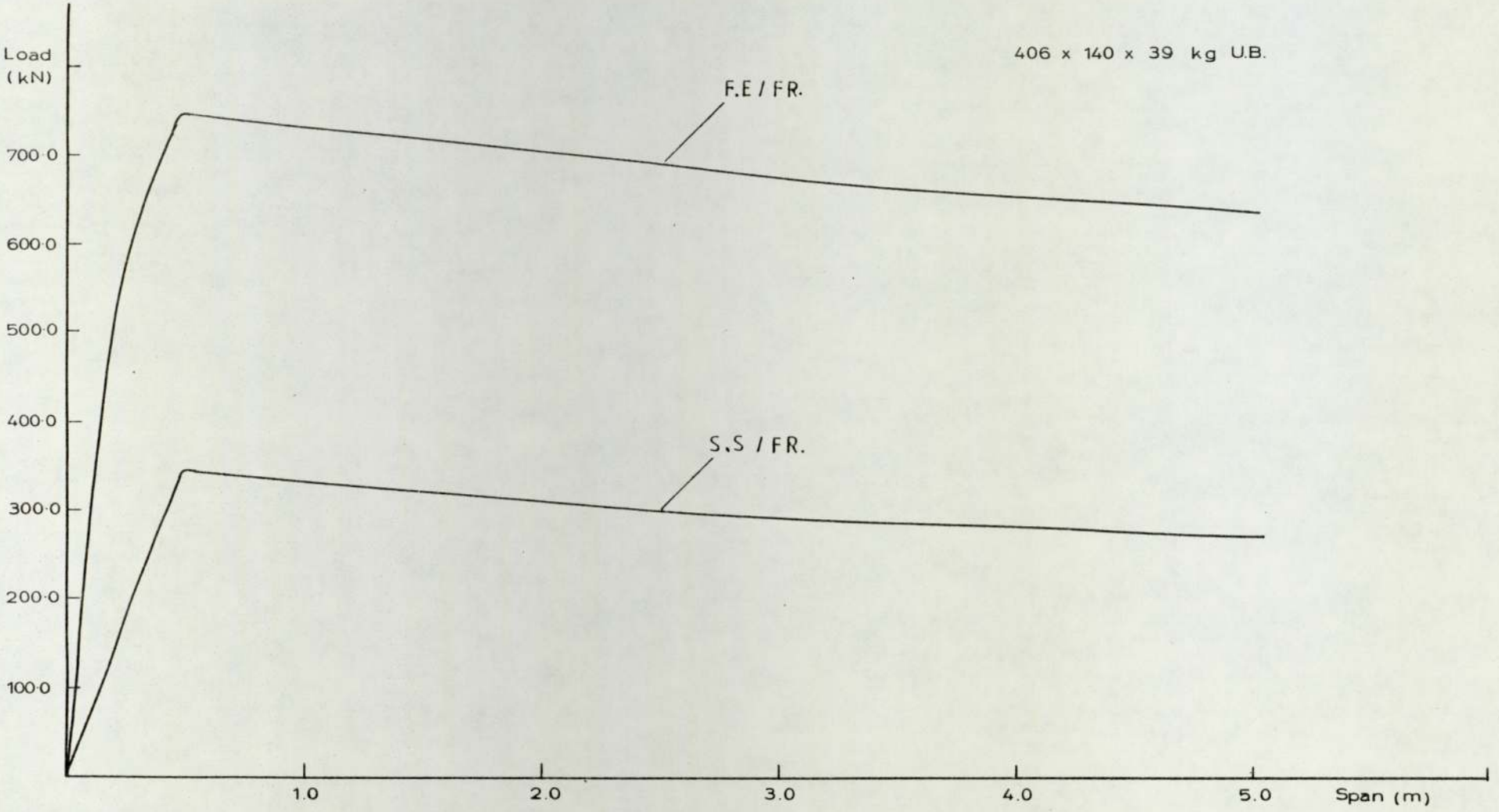

FIGURE 5.5 THEORETICAL EXTREME BUCKLING CURVES FOR 406 x 140 x 39 kg U.B.

The same procedure is followed for determining the two theoretical extreme curves for other beam sections. For the purpose of this work theoretical curves are shown only for those sections used for testing.

5.5 EXPERIMENTAL CRITICAL ELASTIC LOAD

In the previous sections the theoretical elastic buckling load for various boundary conditions has been determined. For the purpose of any comparison, the load at which the web of each beam attained its elastic critical load must be established. There are two possible ways of achieving the above by utilising the test observations. The first one is from the strain behaviour and the other one from the deflection behaviour in the web of the beam. These ways will be discussed in more detail, as follows.

5.5.1 Web Behaviour from Strain Recordings

If the web plate of the beam is considered as an isolated plate, it is then a stable symmetrical system. Such systems when they reach their critical elastic load have an alternative equilibrium position to the flat position, a similar behaviour to struts when they reach their critical load they have an alternative equilibrium position to the flat one. At this stage the out of plane deflections, especially at the vicinity of the applied load, increase considerably and such increases would influence the membrane stress, obtained by the strain gauge recordings, attached to the extreme fibres. It can be seen from the deflection and strain observations of the tested beams, presented in chapter 3 and the strain and deflection recordings in Appendix 1, that the only time that sudden changes in these readings were obtained was at failure.

Hence, from the strain gauge recordings of the beams it appears that these did not attain their elastic critical load before the overall failure load.

5.5.2 Critical Load Using Southwell Plot

Southwell (67) in 1932 devised a method of obtaining the critical load from observations of applied loads and lateral deflections from tests; these tests were conducted on struts having small imperfections. He verified that equation (5.32) below, as it is given also by reference (12) is true

$$\omega_n = \frac{\bar{\omega}_n}{1-\frac{P_n}{P}} \qquad 5.32$$

where

ω_n is any initial lateral deflection present at the centre of the strut.

$\bar{\omega}_n$ is the additional deflection at a load.

P_n is the nth critical load for the perfect strut, the smallest is P_{cr}.

P is the axial force

ω_n and $\bar{\omega}_n$ are represented by a Fourier series. As P_n approaches its critical value the first term of deflection, ω_1, becomes predominant and the deflection δ at the centre of the strut can be represented by a rectangular hyperbola as

$$\delta \simeq \omega_1 = \frac{\bar{\omega}_1}{1 - \frac{P_{cr}}{P}} \qquad 5.33$$

This hyperbola has asymptotes the P-axis and the line $P = P_{cr}$,

as is shown in figure (5.6a). Equation (5.33) can be expressed as

$$P_{cr} \frac{\delta}{P} = \delta - \overline{\omega}_1$$

Hence by measuring P and δ during testing P_{cr} can be estimated from the inverse slope of the best straight line fitted through the points of the δ versus δ/P plot. It should be borne in mind, though, that this Southwell approach for calculating the elastic critical load of an imperfect structure is based on small deflection theory. The deflections should also be large enough to be significant and more predominant than the initial deflections.

The Southwell approach has been adopted by other investigators (68), (69), (70) for considering cases with shells, plates and frameworks. In such cases the load/deflection curve is affected by the large initial geometrical imperfections and the critical load obtained from the Southwell plot must be considered with the post-critical behaviour of the structure. In these cases the load/deflection plots are not rectangular hyperbolas but have perfect equilibrium curves as asymptotes, as it is shown in figure (5.11b). The plot of δ versus δ/P gives rise to a curve line in the post critical region and it is termed by Roorda (71) as Southwell lines.

When the initial deflection is large and therefore more dominant than the deflections under load, this initial deflection can be avoided by shifting the origin of the rectangular hyperbola. In such cases the resulting plot proved to yield a better straight line. Southwell in his original paper refers to the change in slope of the plot when the restraint to the loaded ends is changed.

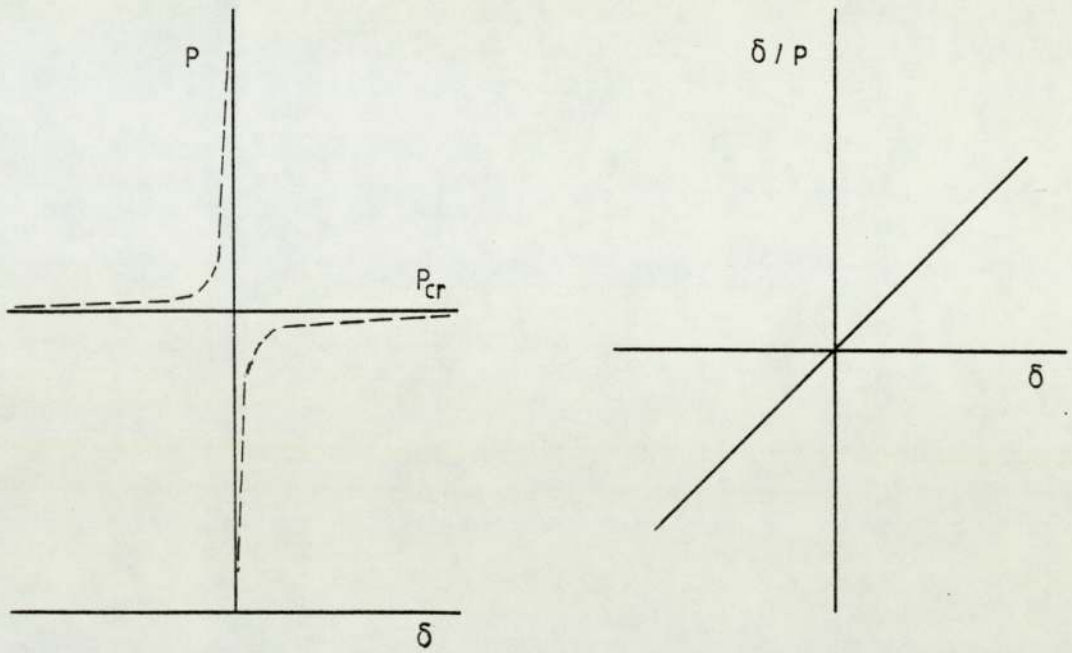

a. Neutral

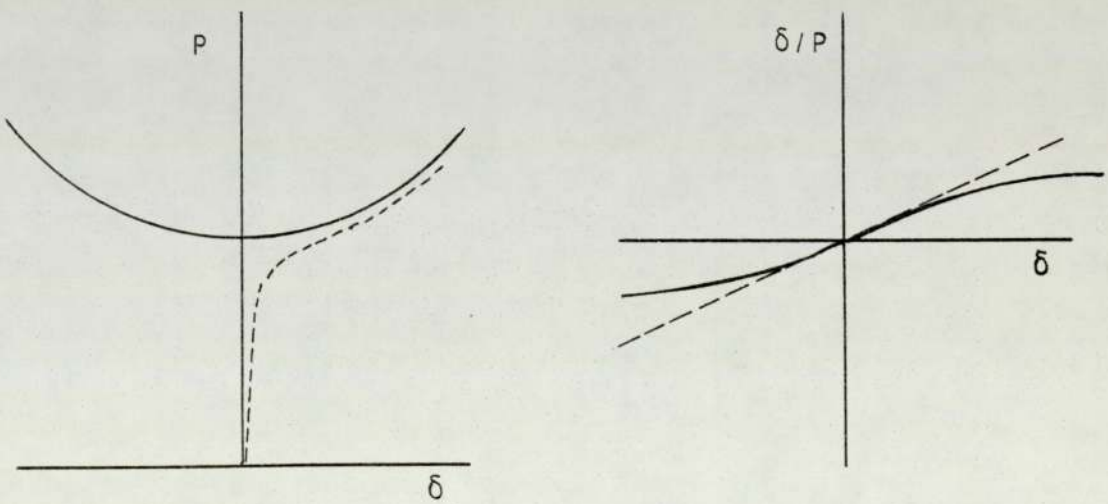

b. Stable Symmetric

FIGURE 5.6 BUCKLING TYPES AND SOUTHWELL LINES

5.5.2.1 Southwell Plot for the Beams Tested

It was observed from the test results that yielding occurred in the web of the beam in the vicinity of the applied load, for a large number of beams; and this of course, will affect the applicability of the Southwell plot procedure in these cases.

There are many complications when performing the Southwell plot, such as the 'squaring up' of the flanges. This effect produces, in many cases, initial deflection to the web which is more dominant than the deflection under load. In such cases, if this effect of initial deformation of the web is avoided by shifting the origin, the Southwell plot yields more satisfactory results. Also the lateral movement of the flanges under load reduces the restraint provided to the web and, therefore, affects the applicability of the Southwell plot.

Figure (5.7) shows typical Southwell plots for beam Nos 25a and 26b in series IV, tested for end failure. These plots show an initial curve followed by an ill-defined straight line. It was found that for many beams which failed at the end, the Southwell plot could not work.

Figures (5.8) and (5.9) show typical Southwell plots for beam Nos 54, 55 and 56 respectively in series VII, which were tested for central failure. These plots show well defined straight lines, giving critical loads quite near to the test failure load of the beams.

In general, the Southwell approach for determining the critical elastic load was found to be inapplicable to the beams of the present work and further comments at this point would be of little use.

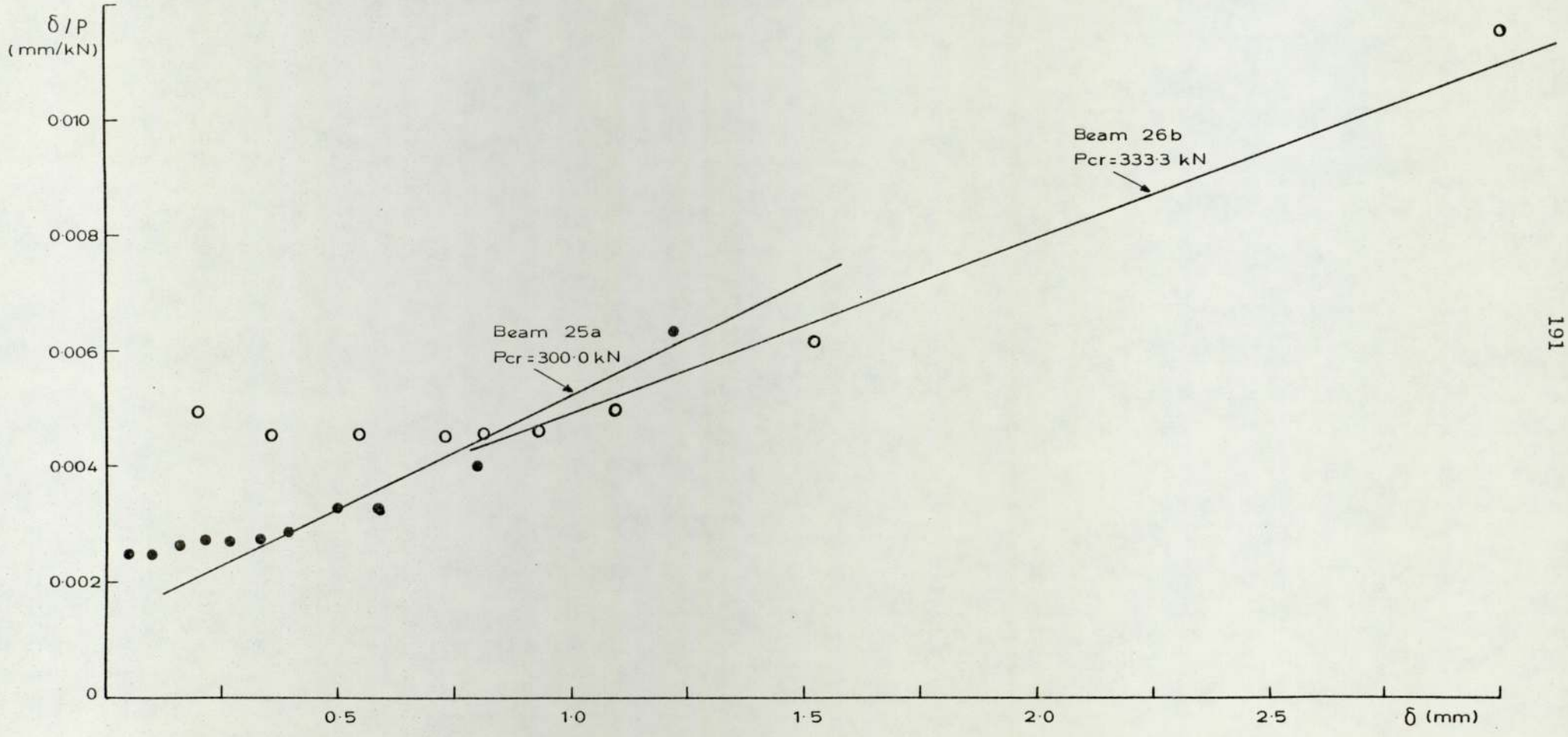

FIGURE 5·7 SOUTHWELL PLOT FOR BEAM NOS. 25a AND 26b

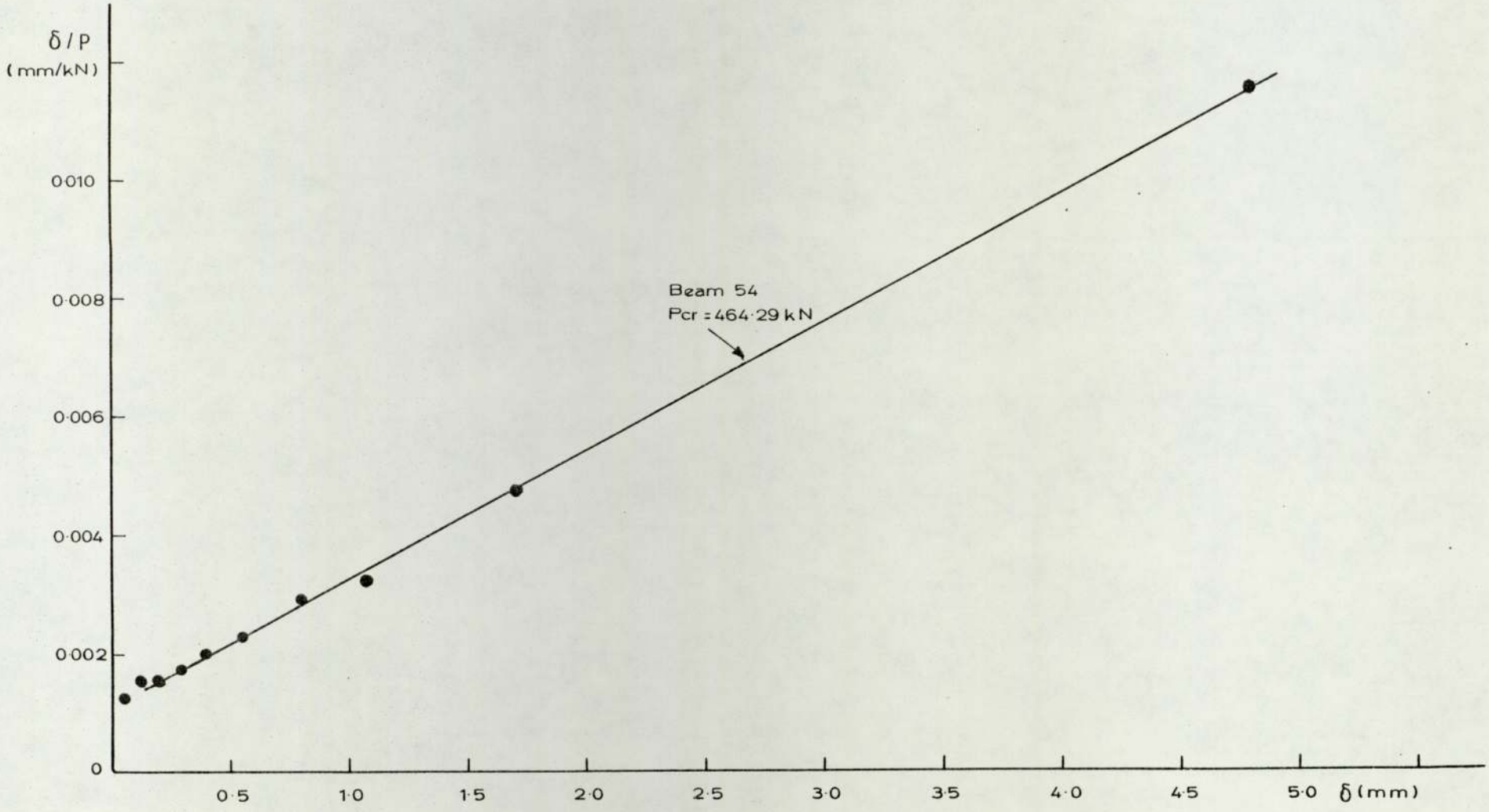

FIGURE 5·8 SOUTHWELL PLOT FOR BEAM NO. 54

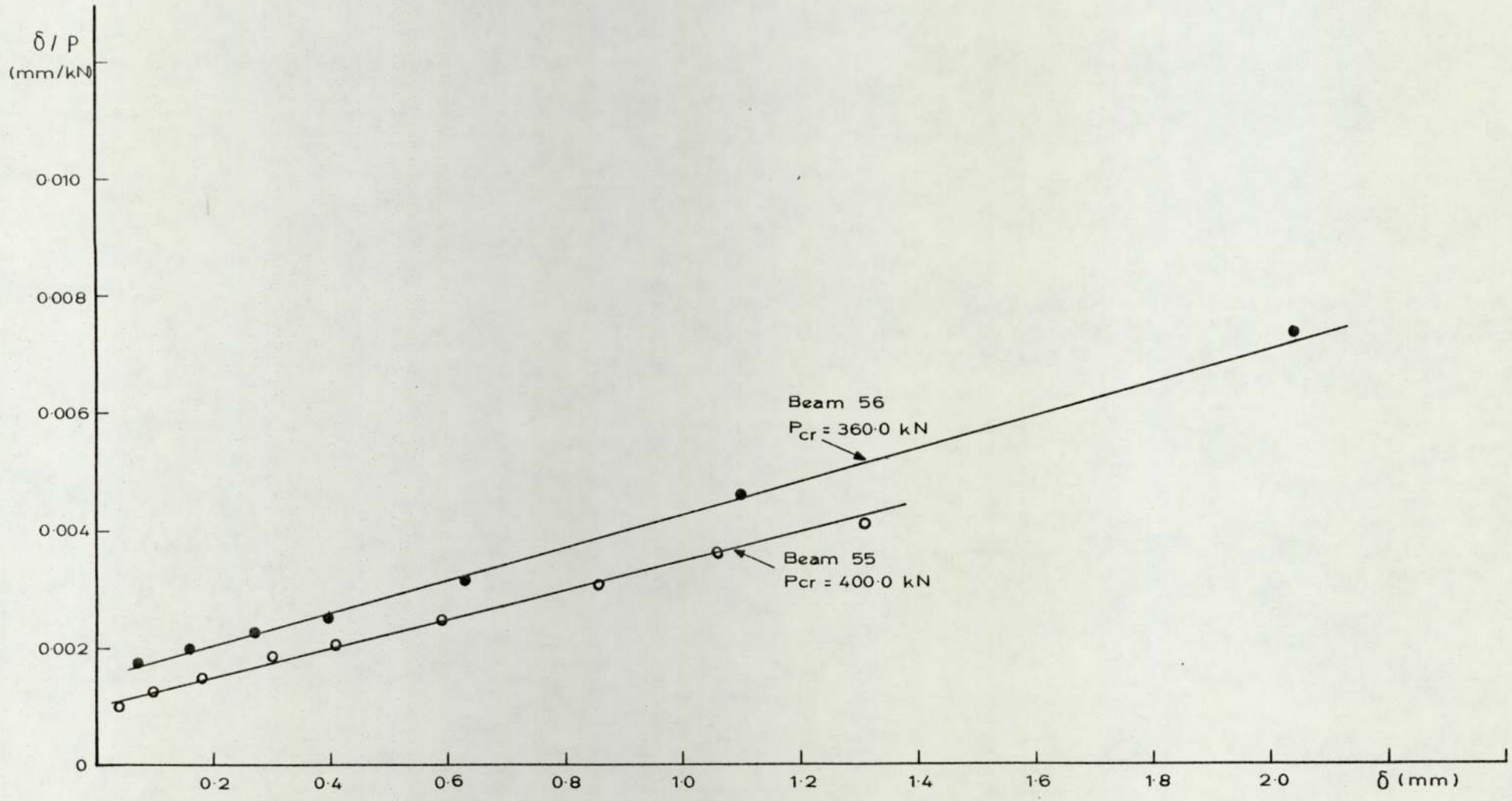

FIGURE 5·9 SOUTHWELL PLOTS FOR BEAM NOS. 55 AND 56

5.6 COMPARISON OF THE DEVELOPED THEORY WITH OTHER PUBLISHED ANALYSES

The results achieved by the elastic theory cannot be directly compared with other results, since to the author's knowledge such a loading type has not been considered before. However, if the bending forces, acting along the longitudinal sides of the plate, are ignored, then the case of a plate compressed by two equal and opposite forces acting in the plane of the plate is obtained; these forces are parabolically distributed and the case when all edges of the plate are simply supported is considered. As has been mentioned earlier in this chapter, similar cases to this have been examined by Timoshenko (12) and Leggett (26), and it is worthwhile comparing them.

Table (5.1) shows the values for the buckling coefficient K, for different aspects ratios, obtained by Timoshenko, Leggett and by the author. These values are also presented in a graphical form in figure (5.10). From the results of the calculation for various values of the aspect ratio, the critical load P for a square plate obtained by the theory is $2.766\,\pi^2 D_1/b$, while that obtained by Leggett is $2.456\,\pi^2 D_1/b$ and by Timoshenko $1.907\,\pi^2 D_1/b$. The fact that the results obtained by this theory are higher by about 11.17% and 31.06% of those obtained by Leggett and Timoshenko respectively can be seen from a consideration of the loading. For this case it is assumed that the load is applied along the whole length of the plate and not as a concentrated one. As the aspect ratio increases this difference in the value of K reduces, and for an aspect ratio of 2 this theory gives lower results than those by the other two investigators.

Aspect Ratio	Timoshenko's Results	Leggett's Results	Author's Results
1.0	1.907	2.457	2.766
1.5	1.416	-	1.652
2.0	1.310	1.507	1.338
2.5	1.282	1.470	1.207
3.0	1.276	1.460	1.139
∞	1.274	-	-

TABLE 5.1 VALUES OF THE BUCKLING COEFFICIENT

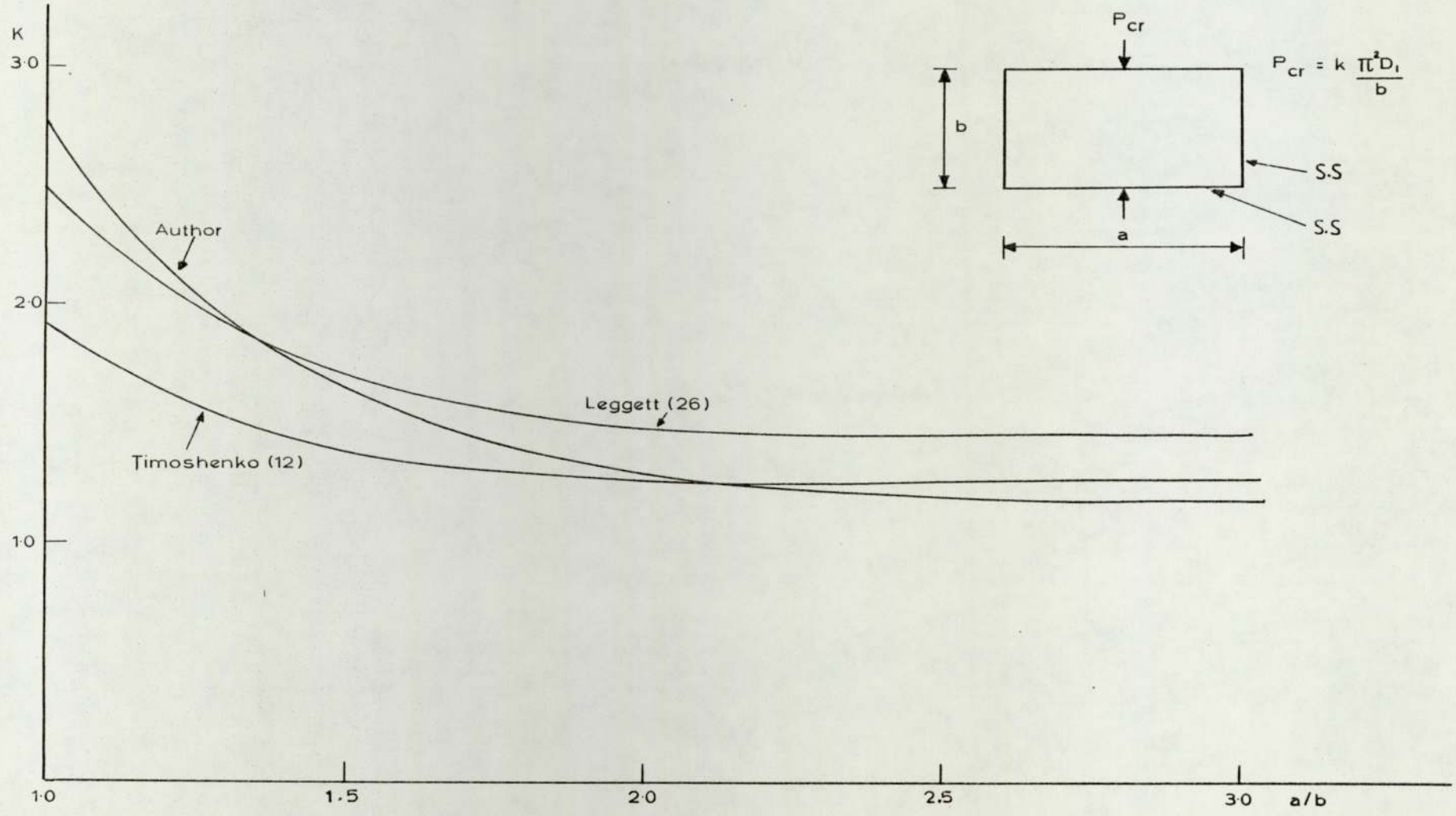

FIGURE 5·10 VALUES OF BUCKLING COEFFICIENT BY VARIOUS INVESTIGATORS

The applicability of this theory is discussed in more detail in the next section, where it is compared to the test results of the beams.

5.7 COMPARISON OF THE DEVELOPED THEORY AND THE TEST RESULTS

It has been shown earlier that the elastic critical load of the beams could not be determined from the test observations, and, therefore, the test ultimate loads of the beams attained are used, when the developed elastic theory is compared to the test results.

Figures (5.11) to (5.15) show the extreme theoretical curves for the beam section sizes used in the tests and the test ultimate loads of the beams.

Figure (5.11) considers the 406 × 140 × 39 kg U.B. section and the failure load of all the beams of this section, tested for central failure, in series VI and VII. Theoretically, if the failure of these beams was an elastic one, and the initial assumptions fully applied, the test ultimate loads should lie between the two extreme curves. Unfortunately this does not happen for some cases; this can be explained by the fact that these had a relatively long length of span and were loaded through small lengths of stiff bearing. For short lengths of span the flanges provide larger restraint to the web than for long lengths of span. Similarly, when the load is applied through large lengths of stiff bearing the flange provides more restraint to the web than when it is applied through zero or small lengths of load, where in such a case the beam is more likely to crush under the load point. As has been observed from the tests, the area of the web at its

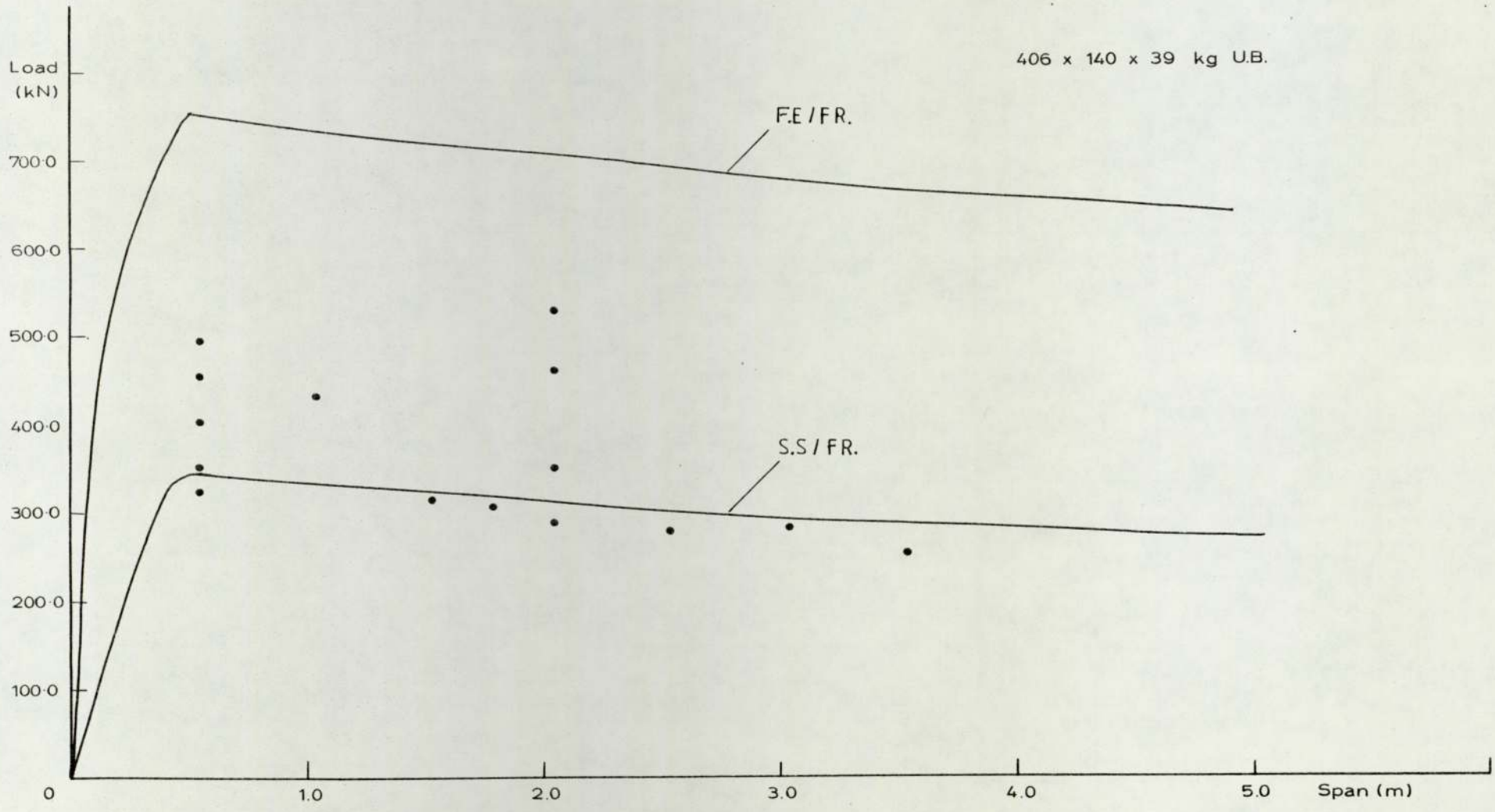

FIGURE 5.11 ELASTIC BUCKLING CURVES FOR 406 x 140 x 39 kg U.B.

junction with the root radius, under the load point, yields at relatively low loads and thus reduces the restraint of the loaded edge.

Figure (5.12) considers the 245 × 102 × 22 kg U.B. section and as can be seen only two of the test results lie between the theoretical extreme curves, namely beam Nos 34 and 79. These had 1.0 m span and loaded through a 250 mm long stiff bearing. The rest of the test results lie below the lower extreme curve and could be explained in the same way as for the previous section.

Figure (5.13) considers the 254 × 102 × 28 kg U.B. section and as could be seen all the test results for these beams lie below the lower extreme curve. These beams were of different length of span and loaded through a 12.7 mm long stiff bearing.

Figure (5.14) considers the 457 × 191 × 98 kg U.B. section, for the beam Nos 60 and 61. These were of the same span and loaded through a 12.7 mm and 100 mm long stiff bearing respectively; both results lie below the lower extreme curve.

Figure (5.15) shows the extreme curves for the section 254 × 102 × 22 kg U.B. section and considers the beams which failed at the end. The ultimate loads shown are those attained by the beams, that is the total loads. As could be seen from this figure the majority of the test results lie below the lower extreme as these beams were supported by relatively small lengths of stiff bearing.

5.8 CONCLUSIONS FROM THE COMPARISON

It appears, from the comparison of the developed theory to the test results, that only a few beams failed elastically. Figures (5.11) to (5.15) show that the restraint provided by the flanges

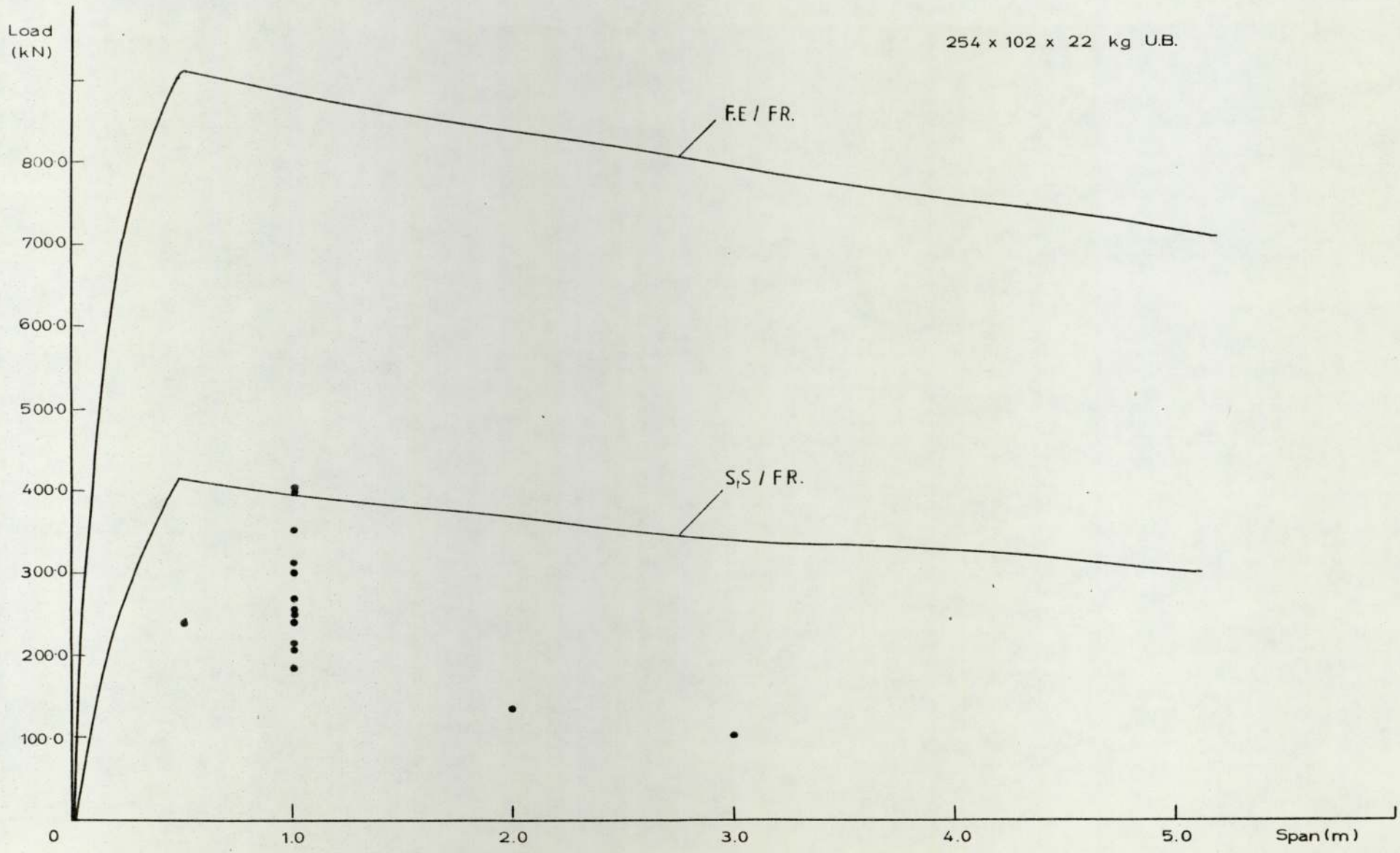

FIGURE 5.12 ELASTIC BUCKLING CURVES FOR 254 x 102 x 22 kg U.B.

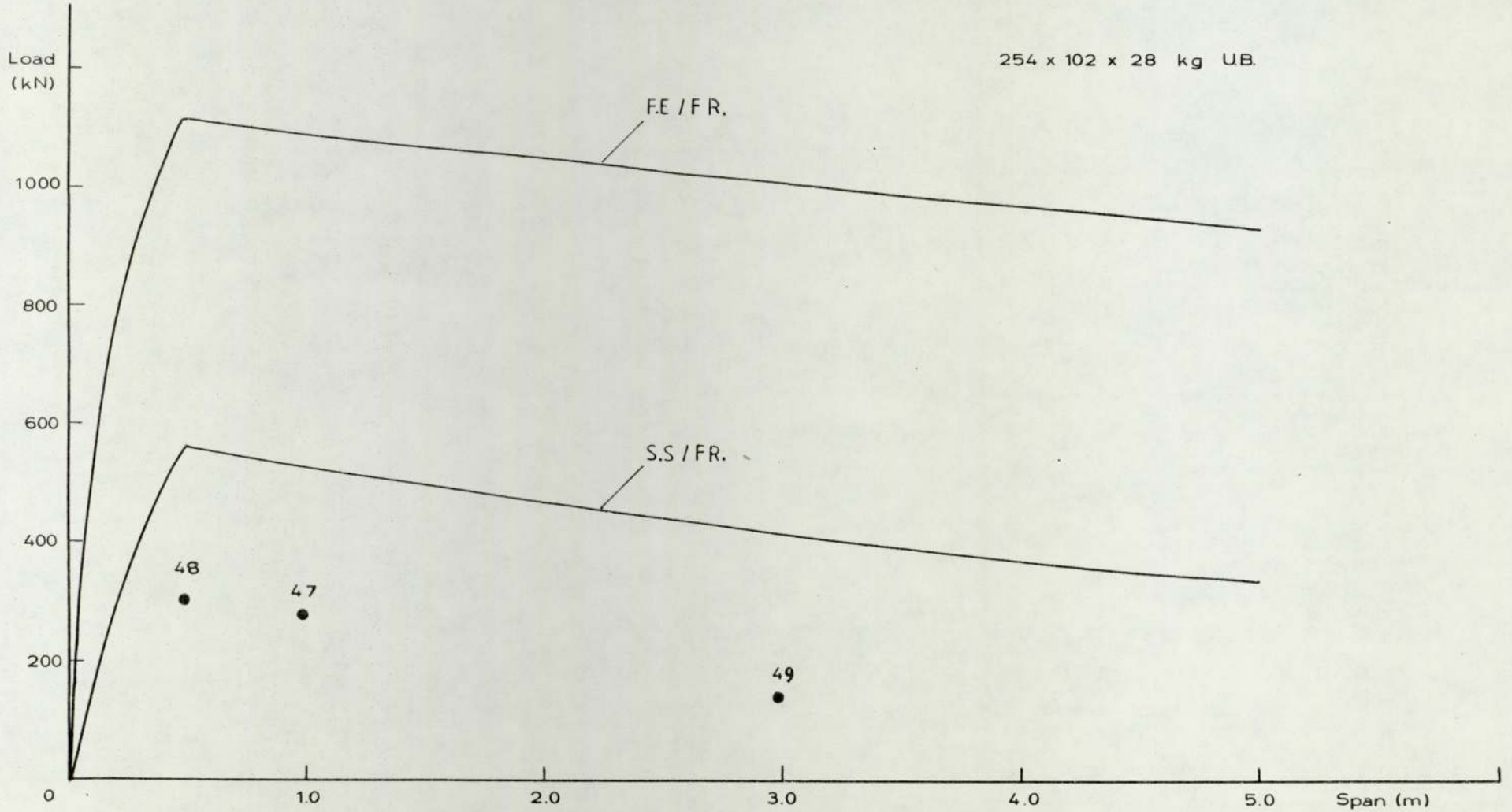

FIGURE 5.13 ELASTIC BUCKLING CURVES FOR 254 x 102 x 28 kg U.B.

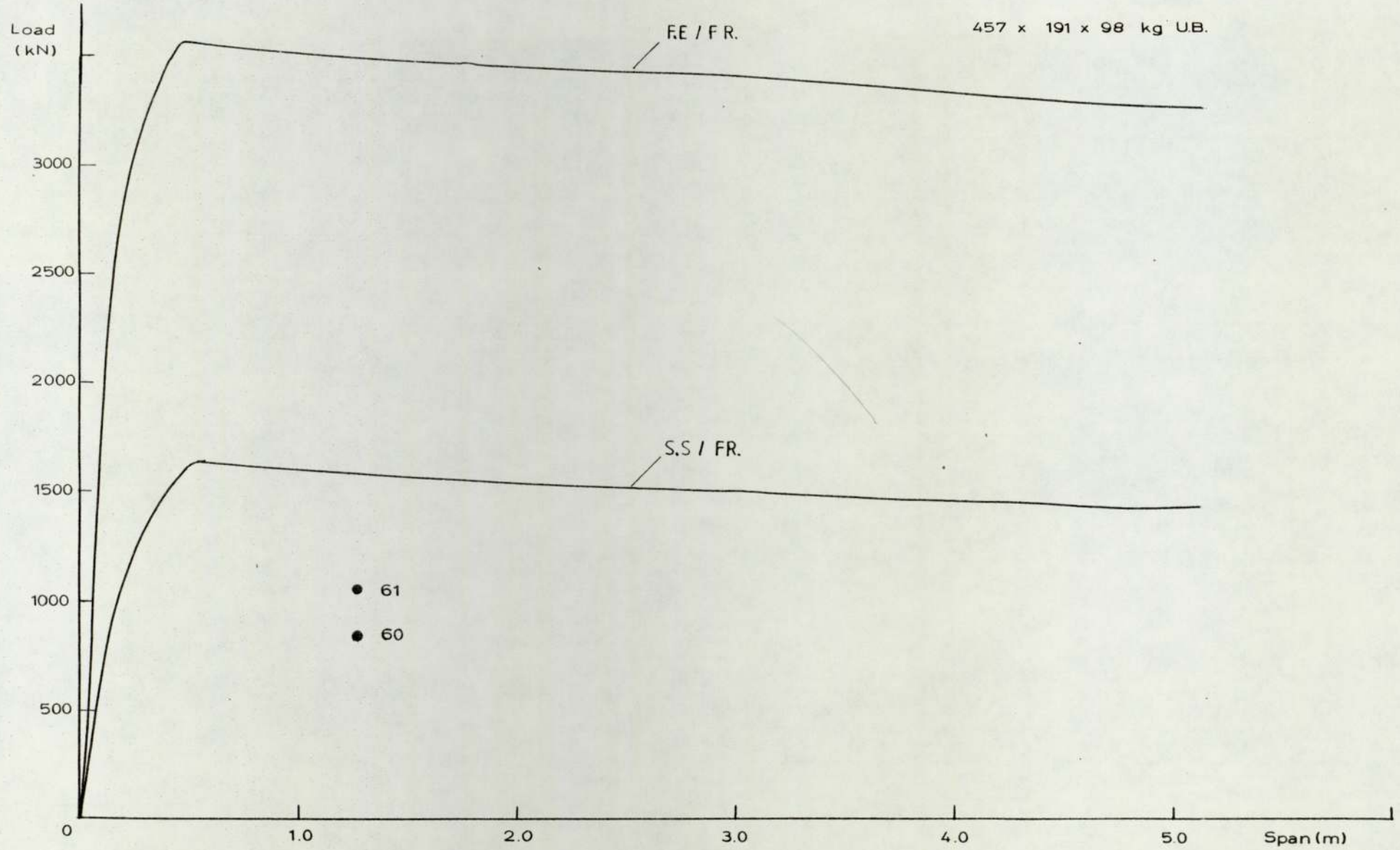

FIGURE 5.14 ELASTIC BUCKLING CURVES FOR 457 x 191 x 98 kg U.B.

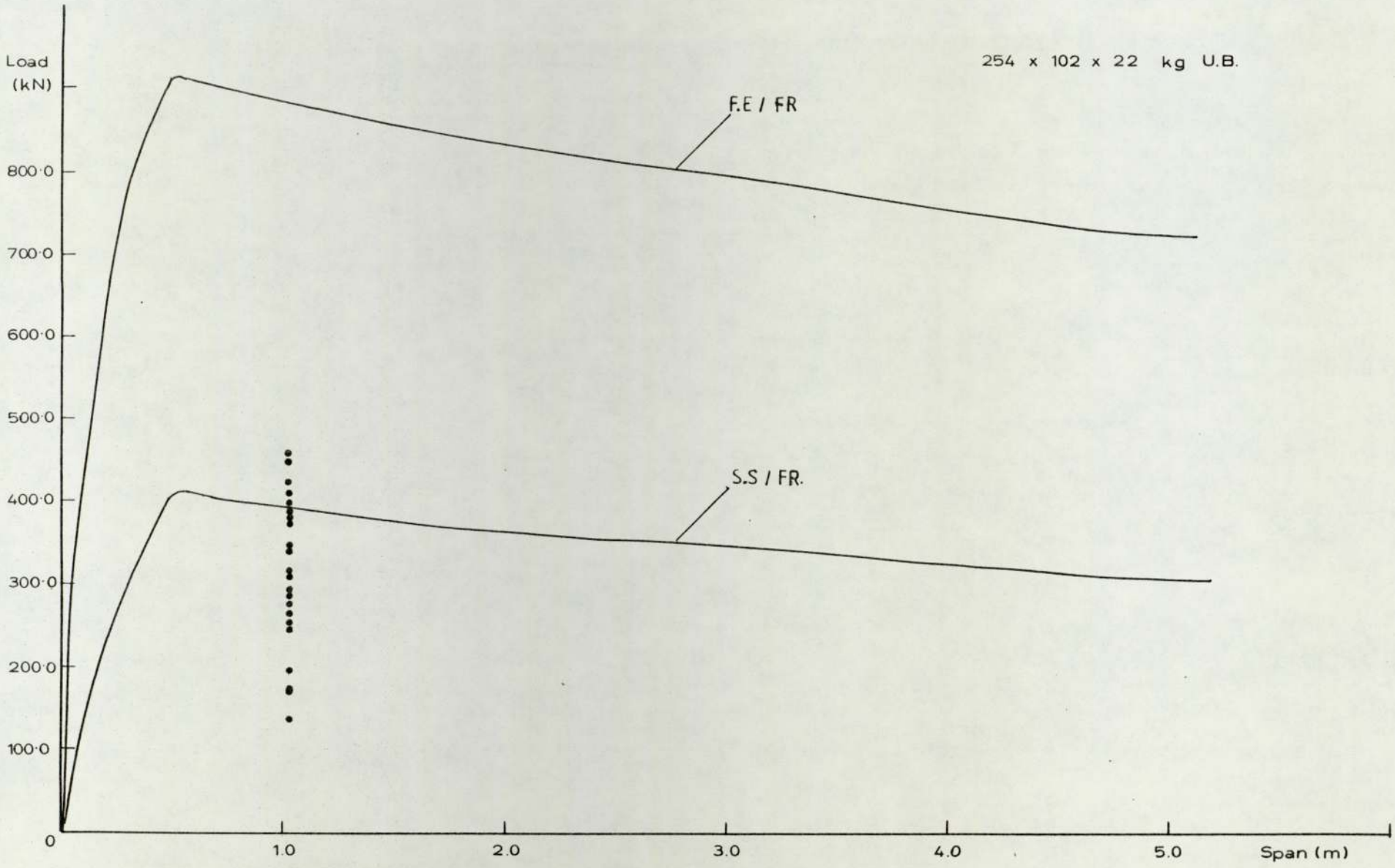

FIGURE 5.15 ELASTIC BUCKLING CURVES FOR END FAILURE 254 x 102 x 22 kg U.B.

is more for the slender beams than for the less slender ones. However, despite the fact that slender beams have thicker flanges than the less slender, namely beam section 406 × 140 × 39 kg which has the highest slenderness ratio of all the universal beam sections, these flanges are far smaller than necessary to provide sufficient restraint to the loaded edges.

It was noticed that beams indicating elastic buckling failure were of the 406 × 140 × 39 kg U.B. section, mainly of small lengths of span and loaded through relatively large lengths of stiff bearing. Such type of loading provides more restraint to the loaded edge and represents best the loading and conditions assumed in deriving the theory. The other less slender beam sections used in the present work do not appear to indicate an elastic buckling failure, particularly when the beams were loaded through small lengths of stiff bearing or knife edge load. In these cases the restraint of the loaded edge is reduced at low loads, due to the effect of yielding at the area of the web at its junction with the root radius.

Even so, in cases where a beam appeared to have an elastic buckling failure, this was accompanied by a local crushing and flange yielding in the vicinity of the applied load.

CHAPTER 6

LOCAL CRUSHING THEORY

6.1 INTRODUCTION

When a universal beam is subjected to concentrated loads on its flanges in the plane of the web, yielding occurs at the junction of the web and the root radius in the vicinity of these loads. This local failure probably initiates the failure of the beam as a whole; it could either be an elastic buckling failure, due to the reduction in the restraint provided by the flanges to the web, or a local crushing failure, as the flanges are distorted and the web undergoes large out of plane deflections reaching its yield stress at the outer fibres at a load much lower than the elastic critical load.

In this chapter a local crushing in the flanges accompanied by a yield line pattern in the web is examined. Most current design practices, when considering local crushing, assume that the beam fails when yielding occurs at the junction of the web with the flange, without considering the flange strength or web resistance in the area which has not yielded. Also no consideration has been given to the bending of the beam as a whole. The theory developed considers such factors and its applicability is examined when compared to the test results.

Also in this chapter an expression for the minimum thickness of the load spreader is formulated, since in the derived theory it is assumed that the load is applied through stiff bearing plates.

6.2 LOCAL CRUSHING THEORY FOR CENTRAL FAILURE

The local crushing failure and the flange yielding mechanism assumed to form is shown in figure (6.1). The applied load P has moved through a vertical distance Δ, causing distortion in the flange and thus formation of the plastic hinges due to rotation. At the same time the web, at the region of the root radius has yielded a total length of $2L_1 + 1_a$, where L_1 is to be defined later and 1_a is the length of the stiff bearing plate.

According to the principle of virtual work, the work done by the external forces will be equal to the work done by the internal forces.

$$P.\Delta = 2\, M_{PF}\, \theta + 2\, M_{PT}\, \theta + 2\, w\, L_1\, \frac{\Delta}{2} + w\, 1_a\, \Delta \qquad 6.1$$

The displacements and rotations are assumed to be small. The axial stresses in the flange due to bending are assumed to be small enough to not significantly affect the plastic moment of resistance of the flange. In equation (6.1) M_{PF} is the plastic moment of resistance of the flange under the applied load and M_{PT} is the plastic moment of resistance of the flange at the ends of the failed zone and could be written as $M_{PT} = \alpha M_{PF}$, where α is a factor describing the shape of the 'T-section' of the flange and web taking part. The value of this factor will be determined empirically and it could be said at this point that considering the effect of bending stresses in calculating M_{PF} and M_{PT} would only change the value of α. As the angle θ is small it could be written that $\theta \simeq \tan \theta = \Delta/L_1$ and equation (6.1) after simplification becomes

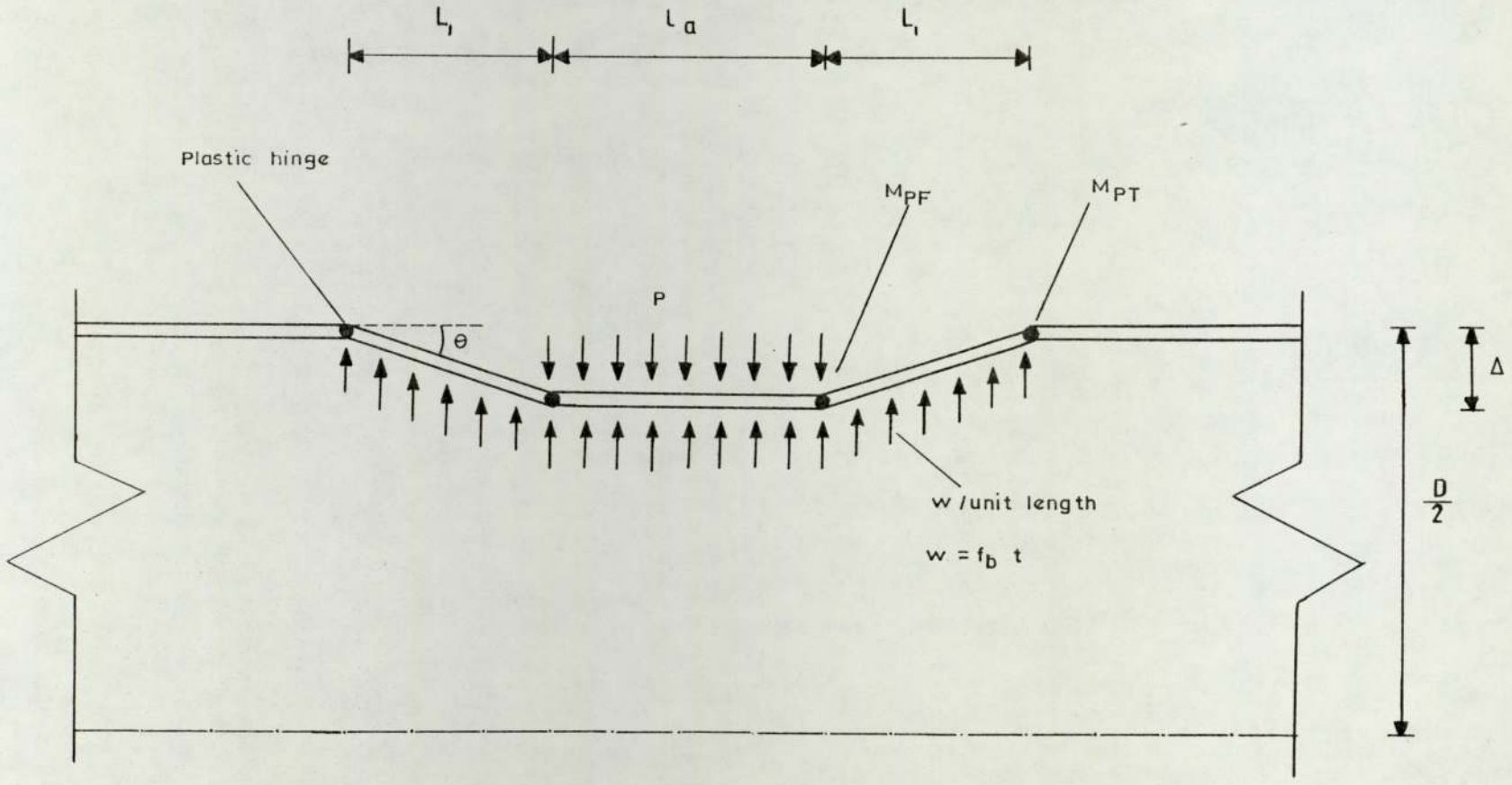

FIGURE 6.1 FAILURE MECHANISM FOR CENTRAL FAILURE

$$P = \frac{2(M_{PF} + M_{PT})}{L_1} + wL_1 + wl_a \qquad 6.2$$

In this expression the only variable is the quantity L_1 and the failure load will be a minimum when

$$\frac{\partial P}{\partial L_1} = 0 = \frac{-2(M_{PF} + M_{PT})}{L_1^2} + w$$

and rearranging, L_1 is obtained from:

$$L_1 = \sqrt{\frac{2(M_{PF} + M_{PT})}{w}} \qquad 6.3$$

By substituting this value of L_1 and the corresponding one for M_{PT} into equation (6.2)

$$P = \sqrt{2w\, M_{PF}\, (1+\alpha)} + w\, l_a \qquad 6.4$$

As shown in figure (6.1) $w = f_b t$, where f_b is the compressive stress, assumed to be uniform. This stress cannot exceed the value of $\beta\, f_{yr}$, where β is a factor and f_{yr} is the yield stress of the section at the root radius. The value of the factor β depends on the overall bending in the section, that is on the longitudinal compression and on the length of the applied load and it will be determined in the following section. By substituting $M_{PF} = \frac{1}{4} BT^2 f_{yf}$ and $w = \beta\, t\, f_{yr}$ into equation (6.4).

$$P = T\sqrt{2B\beta t\, (1+\alpha) f_{yr} f_{yf}} + \beta t f_{yr}\, l_a \qquad 6.5$$

In this expression both the factors α and β are unknown and by rearranging, α is obtained in terms of β, thus

$$\alpha = \frac{P - \beta t f_{yr} l_a}{2T^2 B \beta t f_{yr} f_{yf}} - 1 \qquad 6.6$$

6.2.1 Determination of the β-Factor

The β factor may have values greater than, equal to or less than 1.0. For zero or small lengths of stiff bearing, the limit to be defined later, β is greater than 1.0 and it is obtained from the Distortion Energy theory or Von Mises yield criterion. For large lengths of stiff bearing β is obtained from a yield line analysis.

6.2.1.1 Von Mises Yield Criterion

According to Von Mises yield criterion yielding begins when the distortion strain energy equals the distortion strain energy at yield in simple tension. For the general case of stresses σ_1 σ_2 and σ_3 the condition for yielding is

$$(\sigma_1 - \sigma_2)^2 + (\sigma_2 - \sigma_3)^2 + (\sigma_1 - \sigma_3)^2 = 2f_y^2 \qquad 6.7$$

In this particular case, considering two dimensions only, $\sigma_3 = 0$ and equation (6.7), by substituting $\sigma_1 = f_{bc}$ and $\sigma_2 = f_b$, becomes

$$f_{bc}^2 - f_{bc} f_b + f_b^2 = f_y^2 \qquad 6.8$$

where f_{bc} is the bending stress in the beam. After substituting for f_b and rearranging, β can be obtained from

$$\beta = \frac{f_{bc}}{2f_{yr}} + \sqrt{1 - \frac{3}{4}\left(\frac{f_{bc}}{f_{yr}}\right)^2} \qquad 6.9$$

and thus the α factor can be examined utilising equation (6.6).

6.2.1.2 Yield Line Pattern 1

Consider the yield line pattern formed in the web of the beam, as is shown in figure (6.2); this yield line pattern depends on the length of the applied load. The work W_1, done by the yield lines in bending, is given by:

$$W_1 = (l_a + \frac{d}{3} \tan a_1)\ 3\ \theta\ M_w + 2d\ \psi\ M_w \qquad 6.10$$

where M_w is the ultimate moment of resistance in bending per unit length of the web, that is $M_w = f_{yw} t^2/4$. The work W_2, done by the bending stress f_{bc} at top to move a horizontal distance Δ_H at top, is

$$W_2 = \frac{1}{3} f_{bc}\ t\ d\ \Delta_H \qquad 6.11$$

and the work W_3, done by the applied load to move through a vertical distance Δ, as is shown in figure (6.2), is

$$W_3 = f_b\ t\ (l_a + \frac{d}{3} \tan a_1)\ \Delta \qquad 6.12$$

Equating the work done by the external forces to the work done by the section in bending along the yield lines, that is $W_2 + W_3 = W_1$

$$f_b t\ (l_a + \frac{d}{3} \tan a_1)\ \Delta + \frac{1}{3} f_{bc}\ t\ d\ \Delta_H =$$

$$(l_a + \frac{d}{3} \tan a_1)\ 3\ \theta M_w + 2d\psi M_w \qquad 6.13$$

By substituting $f_b = \beta\ f_{yr}$, $\theta = 6\omega_1/d$, $\psi = \theta/\tan a_1$ and $M_w = f_{yw}\ t^2/4$ into equation (6.13) and rearranging

$$fy_r\ (1a + \frac{d}{3} \tan a_1) + \frac{1}{3} f_{bc}\ d\ \frac{\Delta_H}{\Delta} =$$

$$\frac{9}{2}\ \frac{t}{d}\ fy_w\ (l_a + \frac{d}{3} \tan a_1)\ \frac{\omega_1}{\Delta} + \frac{3f_{yw}}{\tan a_1} t\ \frac{\omega_1}{\Delta} \qquad 6.14$$

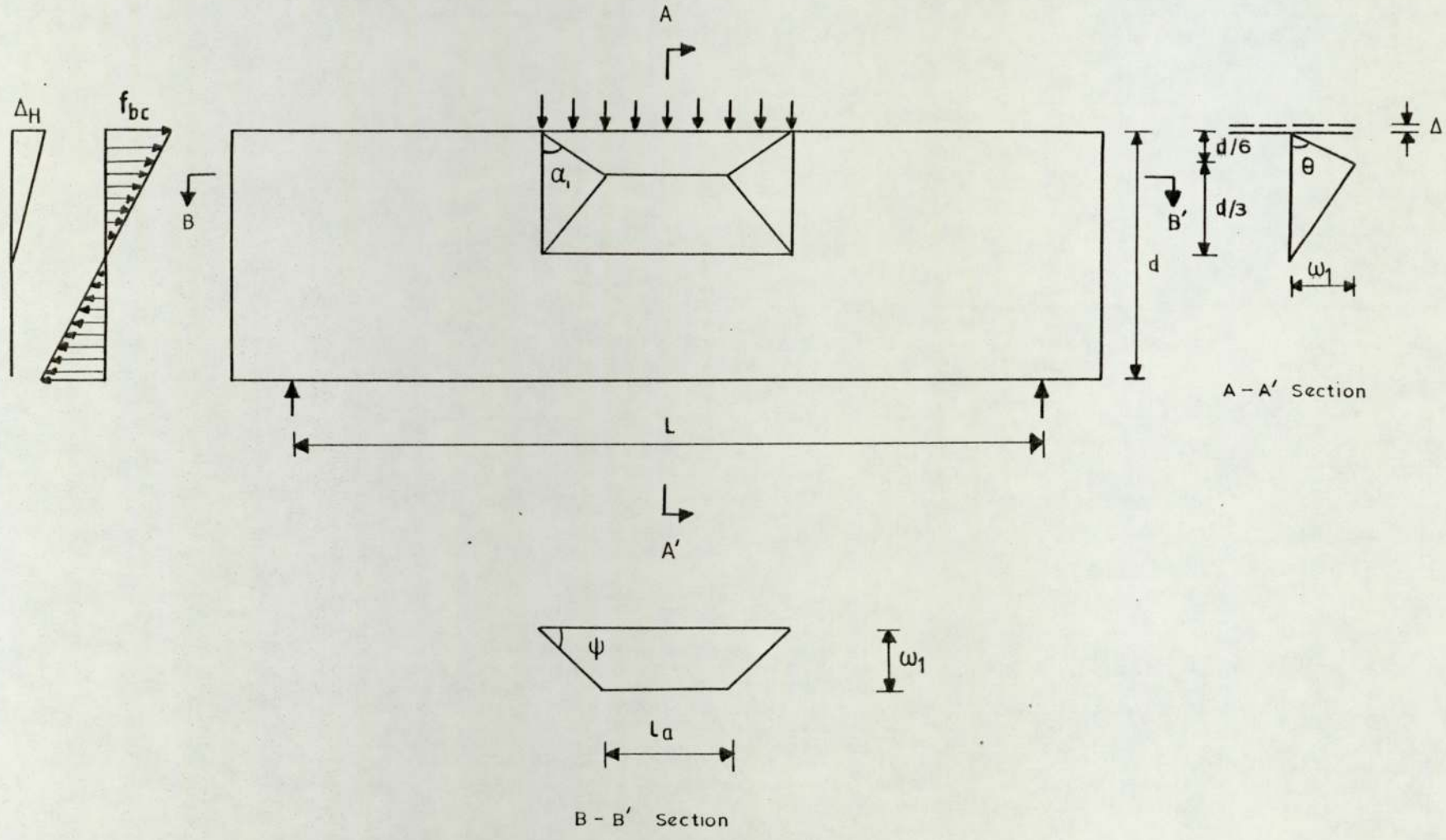

FIGURE 6.2 YIELD LINE PATTERN I FOR CENTRAL FAILURE

From the derived theory in section 6.2 it was found that the length L_1 is given by

$$L_1 = \sqrt{\frac{2(M_{PF} + M_{PT})}{w}} = T\sqrt{\frac{B(1+\alpha)f_{yf}}{2\beta f_{yr} t}}$$

and by considering figure (6.3) this length should be identical to the length L_2, that is

$$L_1 = T\sqrt{\frac{B(1+\alpha)f_{yf}}{2\beta f_{yr} t}} = \tan \alpha_1 \quad \frac{d}{6} \qquad 6.15$$

If the quantity $T\sqrt{\frac{B(1+\alpha)f_{yf}}{2f_{yr} t}}$ is denoted by M then tan a_1 can be obtained from

$$\tan a_1 = \frac{6}{d} \frac{M}{\sqrt{\beta}} \qquad 6.16$$

By substituting this expression into equation (6.14) and re-arranging

$$l_a \beta^{3/2} + (2M + \frac{1}{2} t d \frac{f_{yw}}{f_{yr}} \frac{1}{M} \frac{\omega_1}{\Delta}) \beta +$$

$$(\frac{1}{3} d \frac{f_{bc}}{f_{yr}} \frac{\Delta H}{\Delta} - \frac{9}{2} \frac{t}{d} \frac{f_{yw}}{f_{yr}} l_a \frac{\omega_1}{\Delta}) \beta^{\frac{1}{2}} - 9 \frac{t}{d} \frac{f_{yw}}{f_{yr}} M \frac{\omega_1}{\Delta} = 0 \qquad 6.17$$

The only unknown in this expression is β and can be solved by using any convenient method. For the present case the Newton Raphson method is used to solve the equation, which can be written in the form

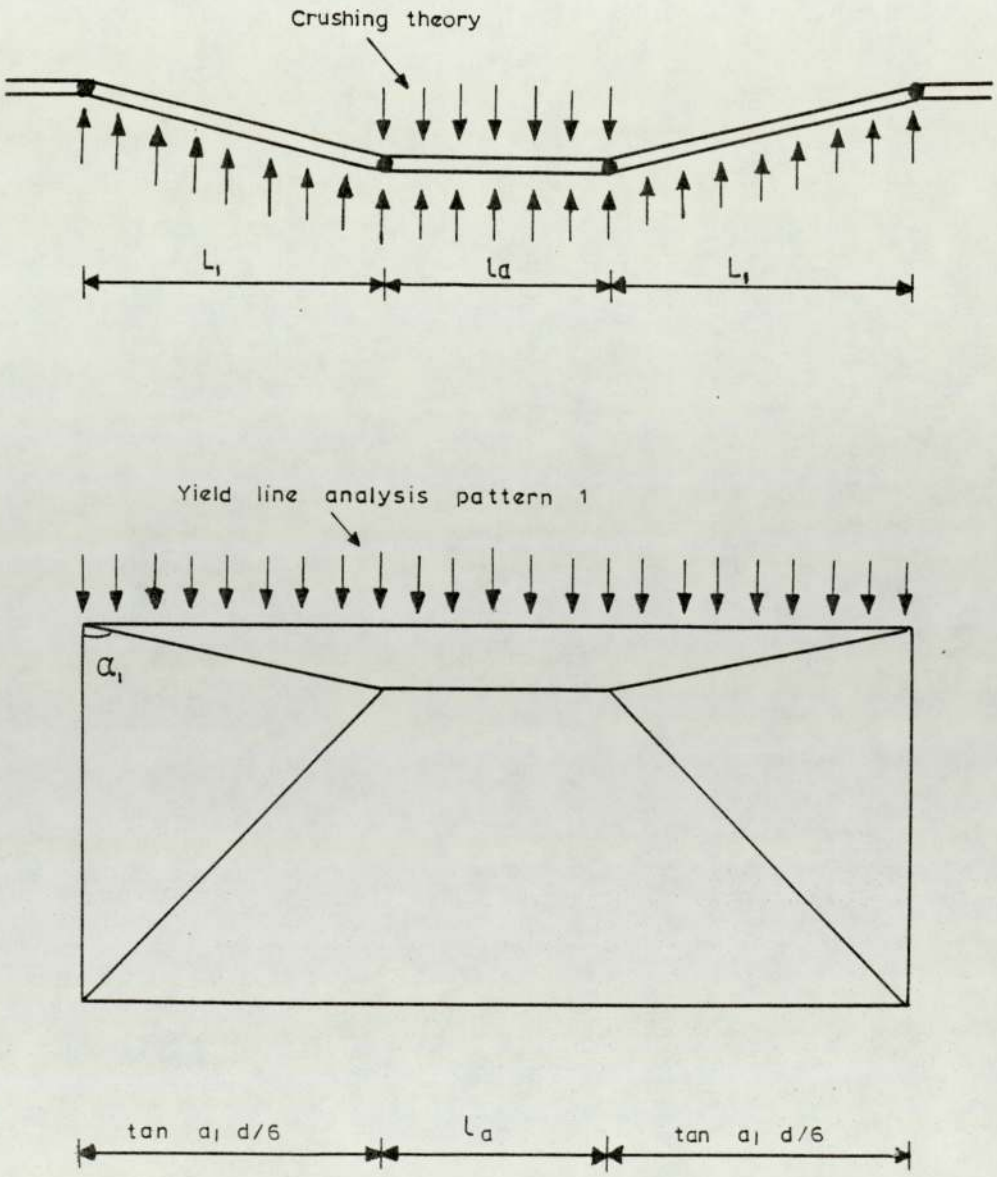

FIGURE 6.3 DETERMINATION OF THE LENGTH OF THE FAILED ZONE

$$A_o x^3 + A_1 x^2 + A_2 x + A_3 = 0 \qquad 6.18.1$$

where

$$A_o = l_a \qquad 6.18.2$$

$$A_1 = 2M + \frac{1}{2} t\, d\, \frac{f_{yw}}{f_{yr}}\, \frac{1}{M}\, \frac{\omega_1}{\Delta} \qquad 6.18.3$$

$$A_2 = \frac{1}{3} d\, \frac{f_{bc}}{f_{yr}}\, \frac{\Delta H}{\Delta} - \frac{9}{2} \frac{t}{d}\, \frac{f_{yw}}{f_{yr}}\, l_a\, \frac{\omega_1}{\Delta} \qquad 6.18.4$$

$$A_3 = - 9\, \frac{t}{d}\, \frac{f_{yw}}{f_{yr}}\, M\, \frac{\omega_1}{\Delta} \qquad 6.18.5$$

Equation (6.17) can further be simplified, since in practice it can be assumed that $f_{yf} = f_{yw} = f_y$. By substituting this into equation (6.17)

$$l_a\, \beta^{3/2} + \left(2M + \frac{1}{2} t\, d\, \frac{1}{M} \frac{\omega_1}{\Delta} \right) \beta + \left(\frac{1}{3} d\, \frac{f_{bc}}{f_y}\, \frac{\Delta_H}{\Delta} - \frac{9}{2} \frac{t}{d}\, l_a\, \frac{\omega_1}{\Delta} \right) \beta^{\frac{1}{2}}$$

$$- 9\, \frac{t}{d}\, M\, \frac{\omega_1}{\Delta} = 0 \qquad 6.19.1$$

and

$$A_o = l_a \qquad 6.19.2$$

$$A_1 = 2M + \frac{1}{2} td\, \frac{1}{M}\, \frac{\omega_1}{\Delta} \qquad 6.19.3$$

$$A_2 = \frac{1}{3} d\, \frac{f_{bc}}{f_y}\, \frac{\Delta_H}{\Delta} - \frac{9}{2} \frac{t}{d}\, l_a\, \frac{\omega_1}{\Delta} \qquad 6.19.4$$

$$A_3 = - 9\, \frac{t}{d}\, M\, \frac{\omega_1}{\Delta} \qquad 6.19.5$$

where M now is given by $M = T\sqrt{\frac{\beta\ (1+\alpha)}{2\ t}}$. For the purpose of

comparing the theory with the test results, equation (6.17) will be used since this gives more accurate results.

6.2.1.3 Yield Line Pattern 2

Consider the yield line pattern shown in figure (6.4). This is similar to the previous one, with the only difference being that the span of the beam is taken into account. The section shown in figure (6.4) is that one drawn through the line of action of the applied load.

The work W_1 done by the section along the yield lines is

$$W_1 = (l_a + 2x_1 + 2L_1)\ 3\theta M_w + 2d\ \phi M_w \qquad 6.20$$

and the work W_2, done by the bending stress f_{bc} at top to move a horizontal distance Δ_H, is

$$W_2 = \frac{1}{3} f_{bc}\ t\ d\ \Delta_H \qquad 6.21$$

Finally the work W_3, done by the applied load to move a vertical distance Δ is

$$W_3 = f_b\ t\ (l_a + 2L_1)\ \Delta \qquad 6.22$$

By equating the external work done to the internal work done, that is $W_2 + W_3 = W_1$

$$f_b\ t\ (l_a + 2L_1)\ \Delta + \frac{1}{3} f_{bc}\ t\ d\ \Delta_H =$$

$$(l_a + 2x_1 + 2L_1)\ 3\ \theta M_w + 2d\ \phi M_w \qquad 6.23$$

From the geometry of the figure,

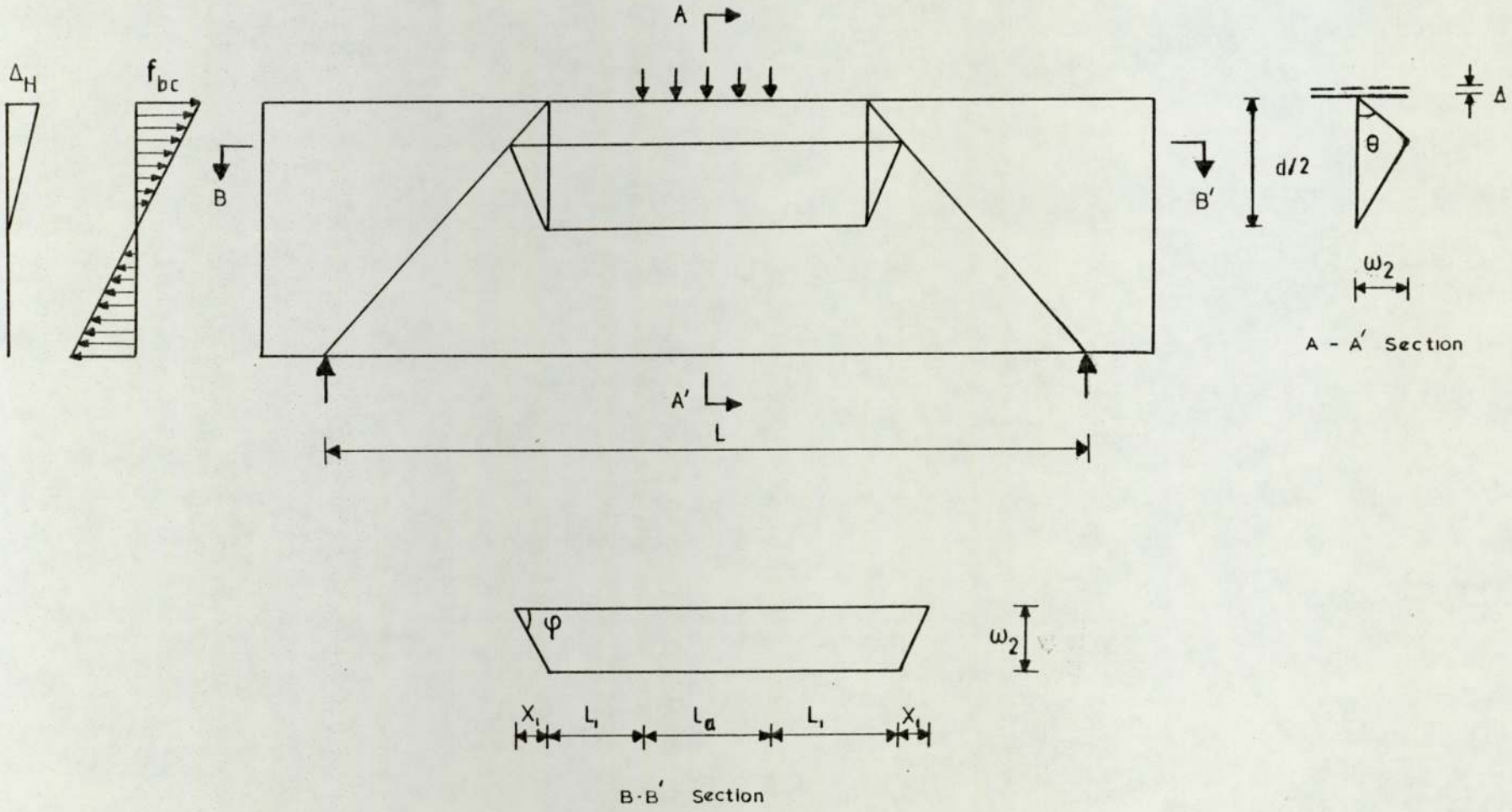

FIGURE 6.4 YIELD LINE PATTERN 2 FOR CENTRAL FAILURE

$$x_1 = \frac{L - l_a - 2L_1}{12}, \quad \theta = \frac{6\omega_2}{d} \quad \text{and} \quad \phi = \frac{12\omega_2}{L-l_a-2L_1}$$

and as for the previous case $f_b = \beta f_{yr}$ and $M_w = f_{yw} t^2/4$.

After substitution of these parameters into equation (6.23) this becomes

$$(l_a + 2L_1)\beta + \frac{1}{3} d \frac{f_{bc}}{f_{yr}} \frac{\Delta_H}{\Delta} = \frac{3}{4}\frac{t}{d}(5l_a + L + 10L_1) \frac{f_{yw}}{f_{yr}} \frac{\omega_2}{\Delta}$$

$$+ 6 \frac{d\ t}{L-l_a-2L_1} \frac{f_{yw}}{f_{yr}} \frac{\omega_2}{\Delta} \qquad 6.24$$

As for the yield line pattern 1, the length L_1, obtained from the theory in section 6.2, is $L_1 = M/\sqrt{\beta}$, shown in figure (6.5), and by substituting into above equation and rearranging.

$$l_a(L-l_a)\beta^2 + 2(L-2l_a) M\beta^{3/2} - \left(4M^2 - (L-l_a)\frac{d}{3}\frac{f_{bc}}{f_{yr}} \frac{\Delta_H}{\Delta}\right.$$

$$\left. + \frac{3}{4}(4 l_a L + L^2 - 5 l_a^2)\frac{t}{d}\frac{f_{yw}}{f_{yr}}\frac{\omega_2}{\Delta} + 6\, d\, t \frac{f_{yw}}{f_{yr}}\frac{\omega_2}{\Delta}\right)\beta$$

$$- \left(\frac{2}{3} d M \frac{f_{bc}}{f_{yr}} \frac{\Delta_H}{\Delta} + 3(2L - 5 l_a)\frac{t}{d} M \frac{f_{yw}}{f_{yr}} \frac{\omega_2}{\Delta}\right)\beta^{1/2}$$

$$+ 15 \frac{t}{d} M^2 \frac{f_{yw}}{f_{yr}} \frac{\omega_2}{\Delta} = 0 \qquad 6.25$$

The unknown in this equation is β and can be obtained by any convenient method of solution. As for the previous case this expression can be written as

$$B_o x^4 + B_1 x^3 + B_2 x^2 + B_3 x + B_4 = 0 \qquad 6.26.1$$

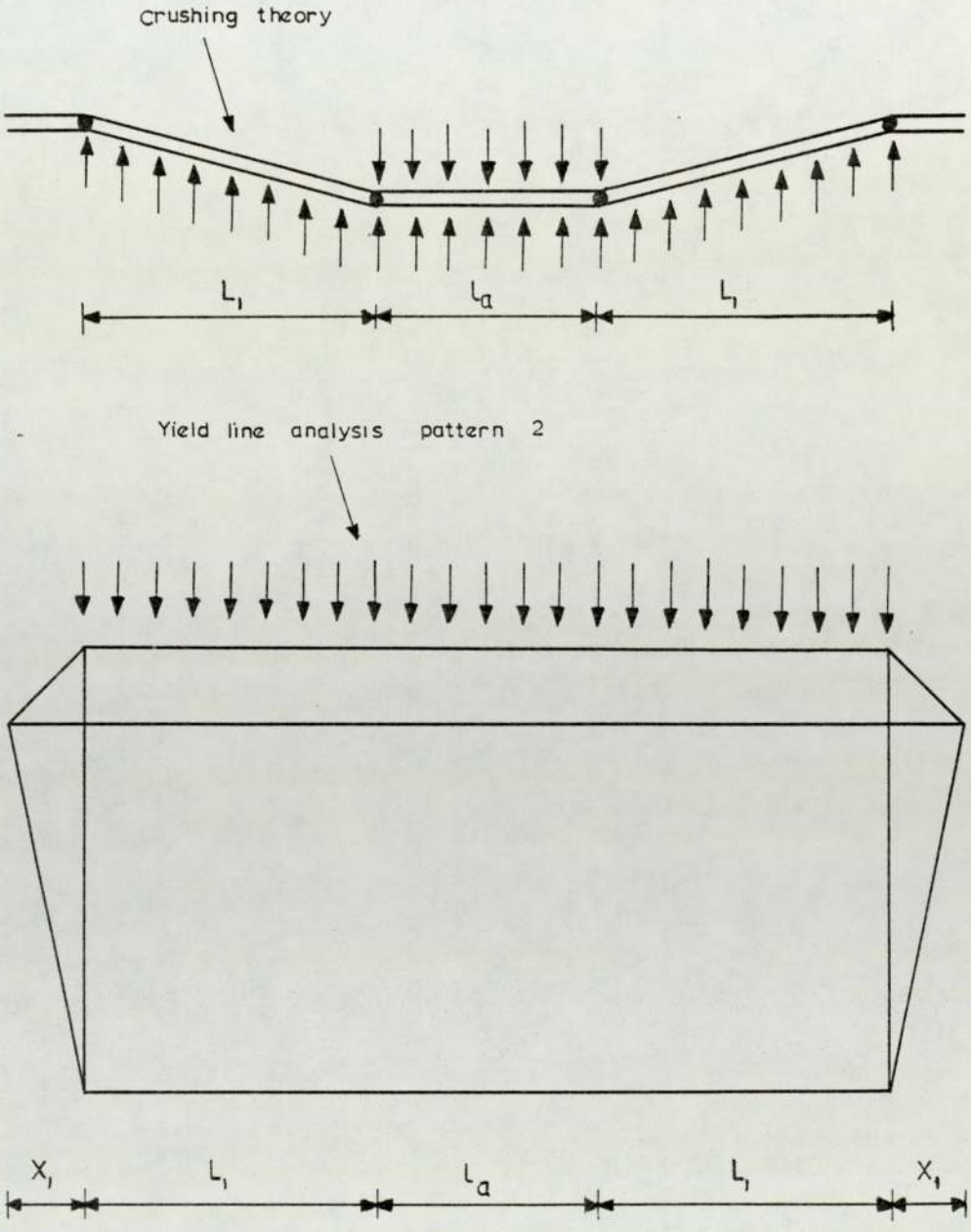

FIGURE 6.5 DETERMINATION OF THE LENGTH OF THE FAILED ZONE

where

$$B_o = l_a(L-l_a) \qquad 6.26.2$$

$$B_1 = 2(L-2l_a)\, M \qquad 6.26.3$$

$$B_2 = -\Big(4M^2 - (L-l_a)\frac{d}{3}\frac{f_{bc}}{f_{yr}}\frac{\Delta_H}{\Delta} + \frac{3}{4}(4l_a L + L^2 - 5l_a{}^2)\cdot$$

$$\frac{t}{d}\frac{fy_w}{fy_r}\frac{\omega_2}{\Delta} + 6\,d + \frac{f_{yw}}{f_{yr}}\frac{\omega_2}{\Delta}\Big) \qquad 6.26.4$$

$$B_3 = -\left(\frac{2}{3}\,d\,M\frac{f_{bc}}{fy_r}\frac{\Delta_H}{\Delta} + 3\,(2L_a - 5l_a)\frac{t}{d}M\frac{f_{yw}}{f_{yr}}\frac{\omega_2}{\Delta}\right) \qquad 6.26.5$$

$$B_4 = 15\,\frac{t}{d}M^2\,\frac{f_{yw}}{f_{yr}}\,\frac{\omega_2}{\Delta} \qquad 6.26.6$$

and can further be simplified by assuming $f_{yr} = f_{yw} = f_{yf} = f_y$ for design purposes.

6.3 LOCAL CRUSHING THEORY FOR END FAILURE

The mechanism assumed to form in this case is shown in figure (6.6). By following the same procedure as for central failure, that is by equating the work done by the external forces to the work done by the internal forces

$$P_1\Delta = M_{PF}\,\theta + M_{PT}\,\theta + wL_1\frac{\Delta}{2} + wl_a\Delta$$

and after substituting and rearranging

$$P_1 = \frac{(M_{PF} + M_{PT})}{L_1} + \frac{1}{2}\,w\,L_1 + wl_a \qquad 6.27$$

The crushing load P_1 will be a minimum when $\frac{\partial P_1}{\partial L_1} = 0$. After

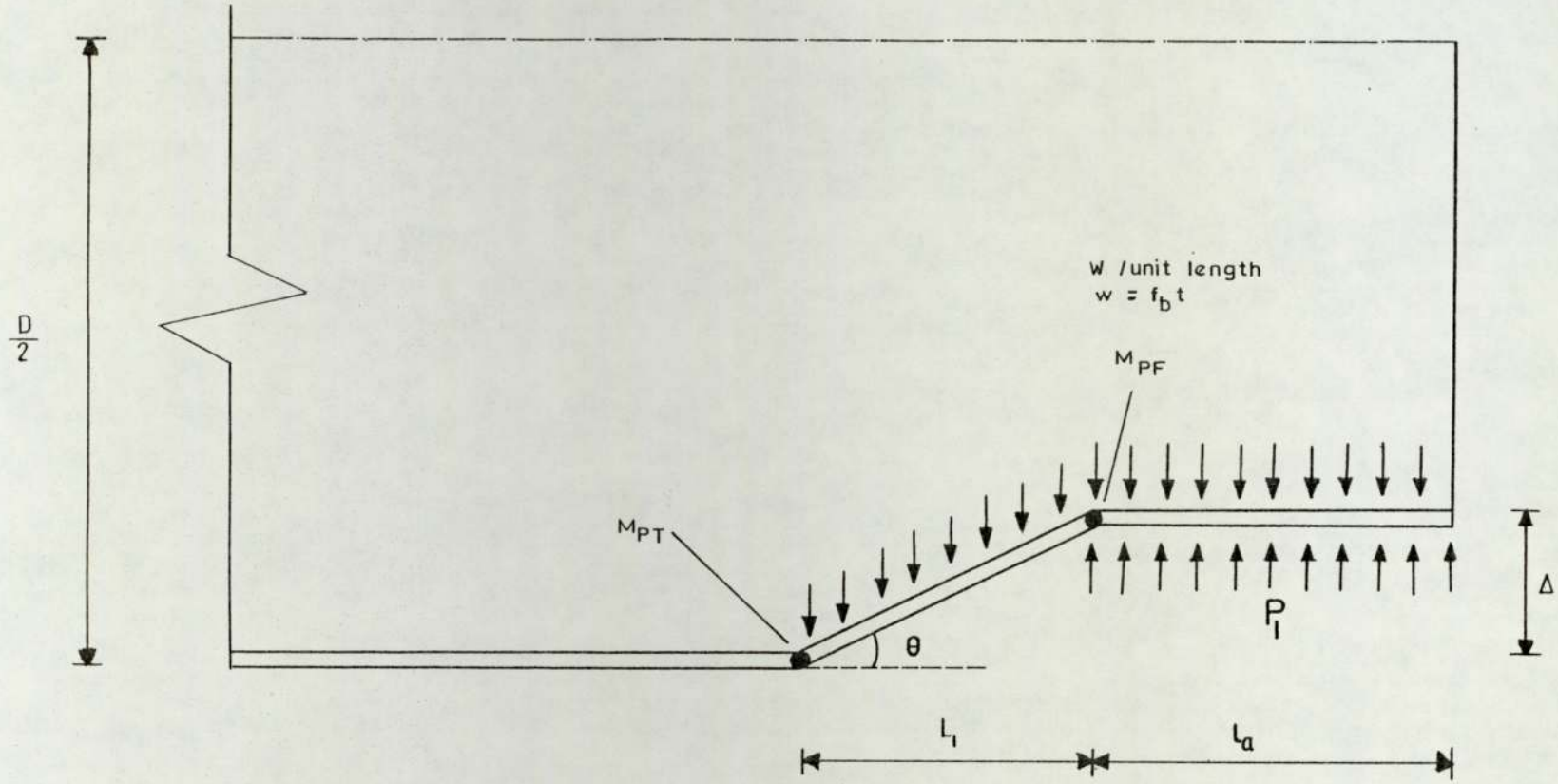

FIGURE 6.6 FAILURE MECHANISM FOR END FAILURE

differentiation and back substitution for $L_1 = \sqrt{\frac{2(M_{PF} + M_{PT})}{w}}$

equation (6.27) becomes

$$P_1 = T\sqrt{0.5B\beta\ t\ (1+\alpha)\ f_{yr}\ f_{yf}} + \beta t l_a\ f_{yr} \qquad 6.28$$

In equation (6.28) l_a, generally, is the distance from the inner face of the bearing plate to the end of the beam.

6.3.1 Determination of the β Factor

As for central failure the β factor for end failure is obtained according to the length of the bearing plate. For small lengths of bearing it is obtained using Von Mises yield criterion and for longer lengths from a yield line analysis.

6.3.1.1 Von Mises Yield Criterion

For this type of failure the bending stresses are very small and the value of β, obtained from equation (6.9) is about 1.0, as f_{bc} tends to zero. For the sake of accuracy though, the exact value of β will be calculated for comparing the theory with the test results. For design purposes it could be assumed as 1.0.

6.3.1.2. Yield Line Pattern 1

Consider the yield line pattern, formed at the end of the beam, shown in figure (6.7). The work W_1 done by the section in bending along the yield lines is

$$W_1 = 3\ M_w\ \left(\frac{6l_a}{d} + \tan a_2 + \frac{4}{\tan a_2}\right)\ \omega_3 \qquad 6.29$$

and the work W_2, done by the compressive stress to move through a vertical distance Δ, is

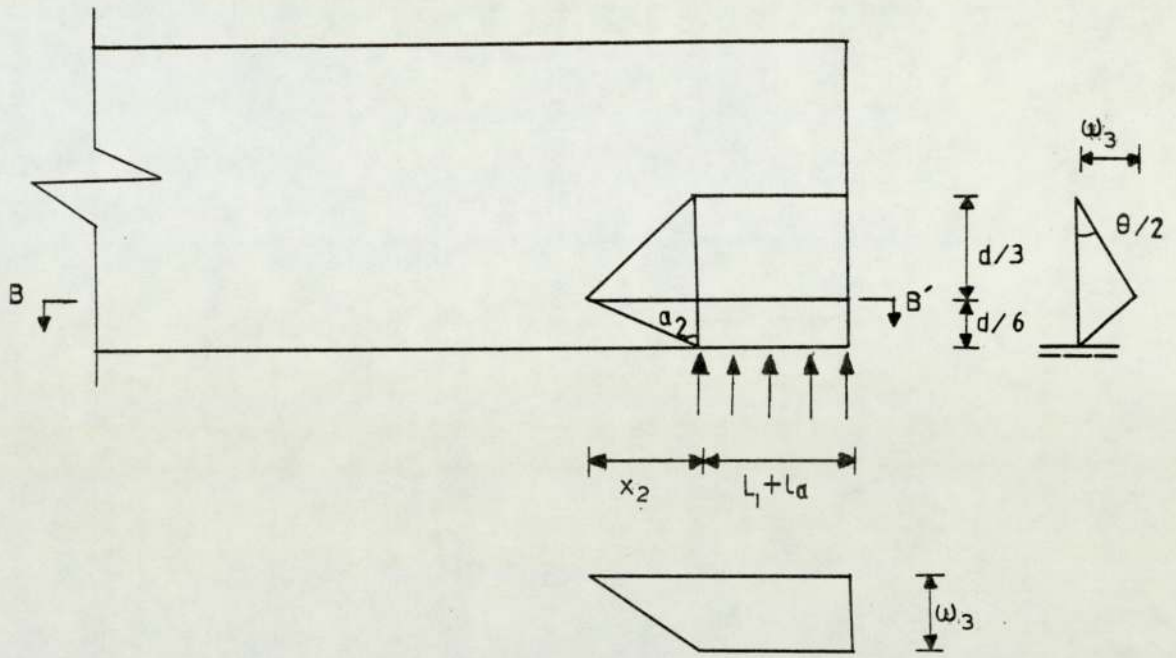

B-B' Section

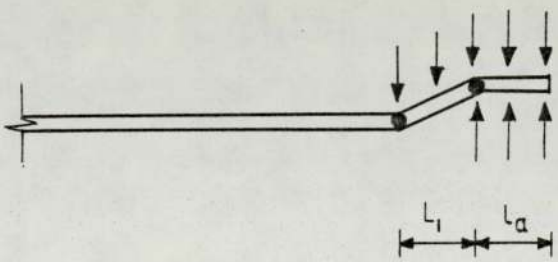

FIGURE 6.7. YIELD LINE PATTERN 1 FOR END FAILURE

$$W_2 = f_b \; t \; (l_a + L_1) \; \Delta \qquad 6.30$$

By equating the work done by the external forces to the work done by the section in bending along the yield lines, that is $W_1 = W_2$ and setting $f_b = \beta \, f_{yr}$

$$\beta \, f_{yr} (l_a + L_1) t \Delta = 3 \, M_w \left(\frac{6l_a}{d} + \tan a_2 + \frac{4}{\tan a_2}\right) \omega_3$$

or

$$\beta \, f_{yr} \, (l_a + L_1) = \frac{3}{4} \, f_{yw} \, t \left(\frac{6l_a}{d} + \tan a_2 + \frac{4}{\tan a_2}\right) \frac{\omega_3}{\Delta} \qquad 6.31$$

In equation (6.31) the angle a_2 is unknown and can be expressed in a similar way as for central failure, that is by equating the length L_1 from crushing theory and x_2 for the present case. Therefore,

$$\frac{\tan a_2}{6} = \sqrt{\frac{2(M_{PT} + M_{PF})}{w}} \quad \text{or} \quad \tan a_2 = \frac{6}{d} \, \frac{M}{\sqrt{\beta}} \quad \text{where M has}$$

been defined before. By substituting the above for $\tan a_2$ back into equation (6.31), after simplifying and rearranging

$$4(l_a + M) \, \beta^{3/2} - 2t \, \frac{d}{M} \, \frac{f_{yw}}{f_{yr}} \, \frac{\omega_3}{\Delta} \, \beta - 18 \, \frac{t}{d} \, l_a \, \frac{f_{yw}}{f_{yr}} \, \frac{\omega_3}{\Delta} \, \beta^{1/2}$$

$$- 18 \, \frac{t}{d} \, M \, \frac{f_{yw}}{f_{yr}} \, \frac{\omega_3}{\Delta} = 0 \qquad 6.32$$

By setting $\sqrt{\beta} = x$ as before equation (6.32) can be written as

$$C_o \, x^3 + C_1 \, x^2 + C_2 \, x + C_3 = 0 \qquad 6.33.1$$

where

$$C_0 = 4\ (l_a + M) \qquad 6.33.2$$

$$C_1 = -2t\ \frac{d}{M}\ \frac{f_{yw}}{f_{yr}}\ \frac{\omega_3}{\Delta} \qquad 6.33.3$$

$$C_2 = -18\ \frac{t}{d}\ l_a\ \frac{f_{yw}}{f_{yr}}\ \frac{\omega_3}{\Delta} \qquad 6.33.4$$

$$C_3 = -18\ \frac{t}{d}\ M\ \frac{f_{yw}}{f_{yr}}\ \frac{\omega_3}{\Delta} \qquad 6.33.5$$

and further be simplified by assuming $f_{yr} = f_{yf} = f_{yw} = f_y$ as for the previous cases.

6.3.1.3 Yield Line Pattern 2

Consider the yield line pattern shown in figure (6.8). Although this yield line pattern looks the same as yield line pattern 1, the analysis differs because the span of the beam is taken into account for this case.

The work W_1, done by the section in bending along the yield lines, is

$$W_1 = 6\ M_w\ \left(\frac{2l_a + L + L_1}{d} + \frac{4d}{L - l_a - 2L_1}\right)\ \omega_4 \qquad 6.34$$

and the work W_2, done by the compressive stress f_b to move through a vertical distance Δ, is

$$W_2 = f_b\ t\ (l_a + L_1)\ \Delta \qquad 6.35$$

By equating the external work done to the internal work done and by substituting $L_1 = M/\sqrt{\beta}$, as has previously been obtained, after simplifying and rearranging, the factor β is finally obtained from.

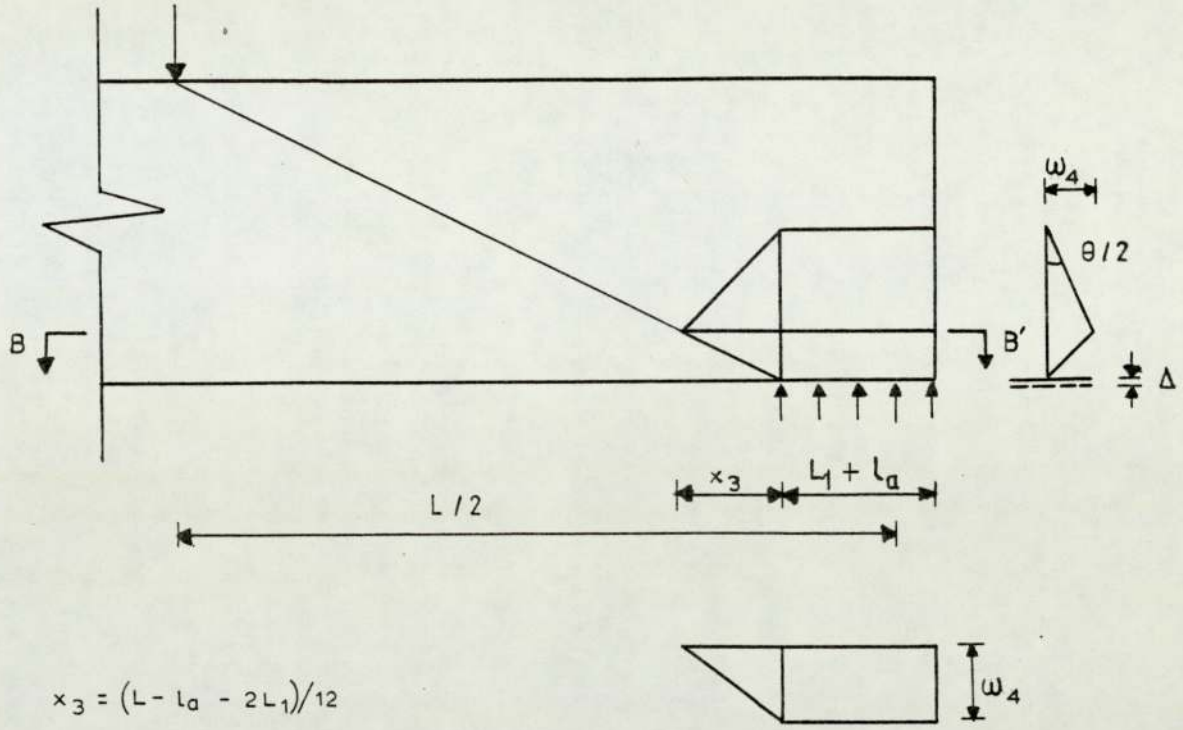

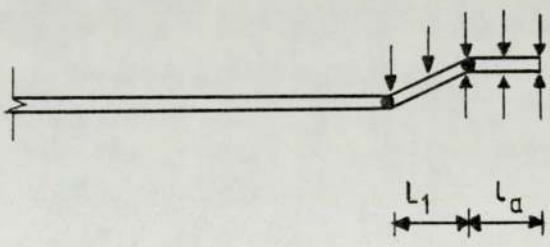

FIGURE 6.8 YIELD LINE PATTERN 2 FOR END FAILURE

$$l_a\,(L-l_a)\beta^2 + M(L-3l_a)\beta^{3/2} - \left(\frac{3}{2}\frac{t}{d}\frac{f_{yw}}{f_{yr}}(2l_a + L)\,(L-l_a)\,\frac{\omega_4}{\Delta}\right.$$

$$\left.-6\,t\,d\,\frac{f_{yw}}{f_{yr}}\,\frac{\omega_4}{\Delta} + 2M^2\right)\beta - \frac{3}{2}\frac{t}{d}M\,\frac{f_{yw}}{f_{yr}}(5l_a + L)\,\frac{\omega_4}{\Delta}\,\beta^{\frac{1}{2}} + \frac{2M^2}{d}\,\frac{\omega_4}{\Delta} = 0$$

6.36

As previously, by substituting $\sqrt{\beta} = x$, equation (6.36) can be written in the form

$$D_0x^4 + D_1\,x^3 + D_2\,x^2 + D_3\,x + D_4 = 0 \qquad 6.37.1$$

where

$$D_0 = l_a(L-l_a) \qquad 6.37.2$$

$$D_1 = M(L-3l_a) \qquad 6.37.3$$

$$D_2 = -\left(\frac{3}{2}\frac{t}{d}\frac{f_{yw}}{f_{yr}}(2l_a + L)\,(L-l_a)\,\frac{\omega_4}{\Delta} - 6\,t\,d\,\frac{f_{yw}}{f_{yr}}\,\frac{\omega_4}{\Delta} + 2M^2\right) \qquad 6.37.4$$

$$D_3 = -\frac{3}{2}\,\frac{t}{d}M\,\frac{f_{yw}}{f_{yr}}\,(5l_a + L)\,\frac{\omega_4}{\Delta} \qquad 6.37.5$$

$$D_4 = \frac{2M^2}{d}\,\frac{\omega_4}{\Delta} \qquad 6.37.6$$

These terms, as before can further be simplified, by writing $f_{yr} = f_{yf} = f_{yw} = f_y$, as it is more likely to happen in design.

6.4 MINIMUM THICKNESS OF LOADING PLATE

In the theory, derived in the previous section, it was assumed that the loading plate is stiff, that it cannot bend and can distribute the load satisfactorily. To satisfy these requirements in this section a formula for the minimum thickness of the loading

plate is derived.

6.4.1 Minimum Thickness of Loading Plate for Central Failure

In the theory developed in section 6.2 it was assumed that the loading plate, used to spread the applied load is stiff and the mechanism formed has been shown in figure (6.1). A theory will be developed for the case when the load is applied through thin spreaders, which may yield at failure, as shown in figure (6.9a).

Consider the local crushing failure and flange yielding mechanism formed, as is shown in figure (6.9a). The notation remains the same, as explained in section 6.2 and c is the width of the secondary member. By equating the work done by the external forces to the work done by the internal forces in the system

$$P_3\Delta = 2M_{PF}\theta + 2M_{PT}\theta + 2M_{PP}\theta + 2wL_1\frac{\Delta}{2} + wc\,\Delta \qquad 6.38$$

where M_{pp} is the plastic moment of resistance of the plate $M_{pp} = b\,t_p^2\,f_{yp}/4$ and b is the length, t_p is the thickness and f_{yp} is the yield stress of the plate. Since rotations and displacements are assumed to be small, after substitution, equation (6.38) becomes

$$P_3 = \frac{2(M_{PT} + M_{PF} + M_{PP})}{L_1} + w\,(L_1 + c) \qquad 6.39$$

and P_3 will be a minimum when $\frac{\partial P_3}{\partial L_1} = 0$, thus

$$\frac{\partial P_3}{\partial L_1} = 0 = -\frac{2}{L_1^2}(M_{PT} + M_{PF} + M_{PP}) + w \text{ and therefore}$$

$$L_1 = \sqrt{\frac{2(M_{PT} + M_{PF} + M_{PP})}{w}} \qquad 6.40$$

By substituting now the above value of L_1 into equation (6.39) and the corresponding values for w, M_{PT}, M_{PF} and M_{PP}, P_3 is finally given by

$$P_3 = \sqrt{2\beta t f_{yr}}\ \sqrt{B T^2 f_{yf}(1+\alpha) + b\, t_p^2\, f_{yp}} + \beta\, t\, c\, f_{yr} \qquad 6.41$$

When the spreader is stiff it was found that the crushing load is given by

$$P = T\sqrt{2B\beta t\ (1+\alpha)\ f_{yr}\ f_{yf}} + \beta\, t\, l_a\, f_{yr}$$

At the point when the spreader will just start bending the crushing load is given by equation (6.41). By equating therefore the expressions for P and P_3, that is

$$T\sqrt{2B\beta\ t\ (1+\alpha)\ f_{yr}\ f_{yf}} + \beta\, t\, l_a\, f_{yr} =$$

$$\sqrt{2\ \beta t\ f_{yr}}\ \sqrt{BT^2(1+a) f_{yf} + bt^2_p\ f_{yp}} + \beta t\ c\ f_{yr} \qquad 6.42$$

The thickness of the plate t_p can be determined by simplifying and rearranging the above equation as

$$t_p = \sqrt{\frac{2T(l_a - c)\ \sqrt{2B\beta t(1+\alpha)\ f_{yr}\ f_{yf}} + \beta t\ (l_a - c)^2\ f_{yr}}{2\ b\ f_{yp}}} \qquad 6.43$$

In the case when the applied load is a knife edge load t_p is obtained by setting c = 0 into equation (6.43), thus

$$t_p = \sqrt{\frac{2Tl_a\sqrt{2B\beta t(1+\alpha)\ f_{yr}\ f_{yf}} + \beta\, t\, l_a^2\, f_{yr}}{2b\ f_{yp}}} \qquad 6.44$$

6.4.2 Minimum Thickness of Loading Plate at Support for End Failure

When the spreader at the supports of the beam is stiff and failure occurs at the end it was previously found that the crushing load is given by equation (6.28). When the spreader is thin, which may yield at failure, the failure mechanism formed is shown in figure (6.9b). By equating the work done by the external forces to the work done by the internal forces it is obtained,

$$P_4 \Delta = (M_{PT} + M_{PF} + M_{PP}) \theta + w L_1 \frac{\Delta}{2} + wc\Delta$$

or

$$P_4 = \frac{(M_{PT} + M_{PF} + M_{PP})}{L_1} + \frac{1}{2} w L_1 + wc \qquad 6.45$$

The crushing load P_4 will be a minimum when

$$\frac{\partial P_4}{\partial L_1} = 0 = - \frac{(M_{PT} + M_{PF} + M_{PP})}{L_1^2} + \frac{1}{2} w \qquad 6.46$$

and therefore

$$L_1 = \sqrt{\frac{2(M_{PT} + M_{PF} + M_{PP})}{w}} \qquad 6.47$$

Back substitution of the above expression for L_1 into equation (6.45) and the corresponding values for w, M_{PF}, M_{PT} and M_{PP} gives

$$P_4 = \sqrt{0.5\beta t f_{yr}} \sqrt{BT^2(1+\alpha) f_{yf} + bt_p^2 f_{yp}} + \beta t c f_{yr} \qquad 6.48$$

As for central failure, the crushing load given by equation (6.48) above will be equal to the load given by equation (6.28), at the

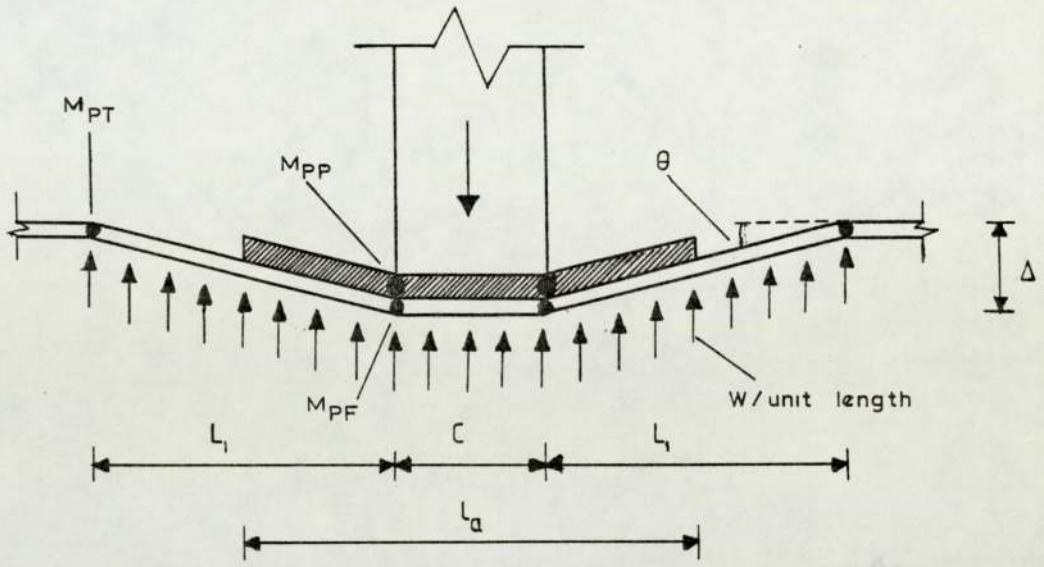

a. Central failure

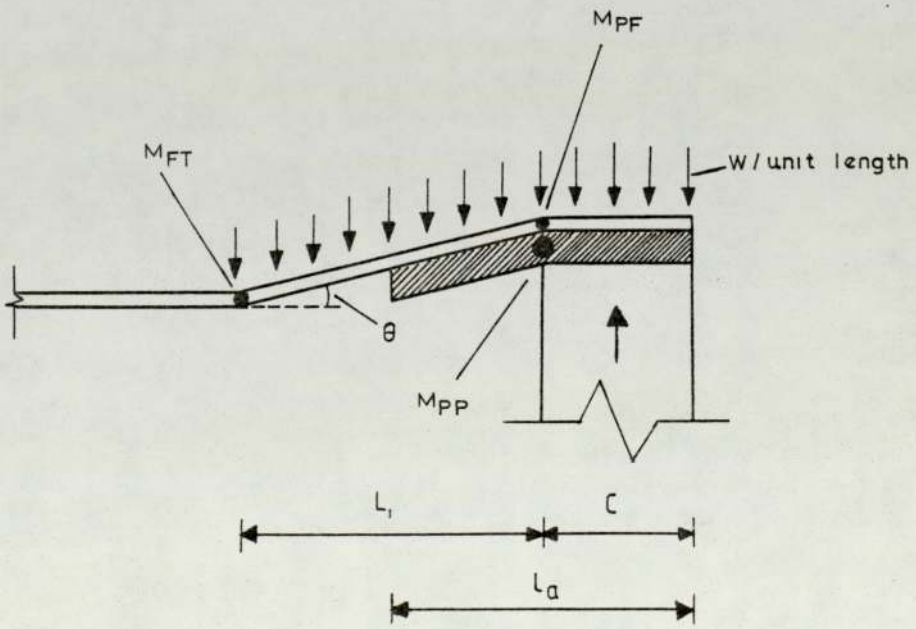

b. End failure

FIGURE 6.9. MINIMUM THICKNESS OF LOADING PLATE

point when the plate just starts to bend. Thus,

$$T\sqrt{0.5B\beta\ t(1+\alpha)f_{yr}\ f_{yf}} + \beta t\ l_a\ f_{yr} =$$

$$\sqrt{0.5\beta t\ f_{yr}}\ \sqrt{BT^2(1+\alpha)\ f_{yf} + bt_p^2\ f_{yp}} + \beta t\ c\ f_{yr} \qquad 6.49$$

After simplifying and rearranging the above equation, the minimum thickness of the plate is given by

$$t_p = \sqrt{\frac{2T(l_a-c)\sqrt{0.5B\beta t(1+\alpha)\ f_{yr}\ f_{yf}} + \beta t(l_a-c)^2\ f_{yr}}{0.5\ b\ f_{yp}}} \qquad 6.50$$

and for the case when the beam is supported by a knife edge support that is c = 0, t_p is obtained from

$$t_p = \sqrt{\frac{2Tl_a\sqrt{0.5B\beta t(1+\alpha)\ f_{yr}\ f_{yf}} + \beta t\ l_a^2\ f_{yr}}{0.5\ b\ f_{yp}}} \qquad 6.51$$

6.5 SUITABILITY OF CRUSHING THEORY AND DETERMINATION OF OTHER FACTORS

a) Central Failure

The suitability of the crushing theory can be examined after determining the various factors involved. It was stated previously in this chapter that, according to the length of the stiff bearing, the β factor is obtained using different methods. The determination of the α factor is dependant upon the method used for the calculation of β. The limit for the length of stiff bearing will be decided from the comparison of the experimental ultimate load

and the theoretical crushing load of the tested beams.

The value of α for beams loaded with zero or small lengths of bearing, that is when β is obtained by Von Mises yield criterion, can be obtained empirically. The variation of α, obtained from equation (6.6), was examined with different variables such as $\frac{d}{l_a}$, $\frac{l_a}{L}$ and $\left(\frac{f_{bc}}{fy}\right)^n$ for various values on n; finally it was found that α varies best with the $\left(\frac{f_{bc}}{fy}\right)^6$ ratio. This variation of α is given by the following expression

$$\alpha = 5.35 - 3.2\left(\frac{f_{bc}}{fy}\right)^6 \qquad 6.52.1$$

for a web depth to web thickness ratio up to 45. For $d/t > 45$ α is obtained from

$$\alpha = \left(5.35 - 3.2\left(\frac{f_{bc}}{fy}\right)^6\right)\frac{d}{L} \qquad 6.52.2$$

and for both cases the maximum value of α is taken 3.75, that is

$$0 \leqslant \alpha \leqslant 3.75 \qquad 6.52.3$$

In cases where the above expression for α gives a negative value, this value should be taken as zero. A negative value of α indicates that the outer hinges are formed outside the span of the beam, as shown in figure (6.10), and such a situation cannot exist. By taking $\alpha = 0$ it is assumed that these hinges are formed at the points of support.

At this stage the theoretical crushing loads can be compared with the test results. The crushing loads for all the beams tested for central failure, that is beams in series VI, VII and VIII,

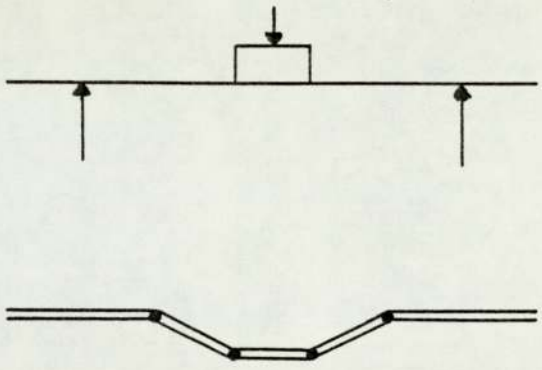

a. Case with $\alpha > 0$

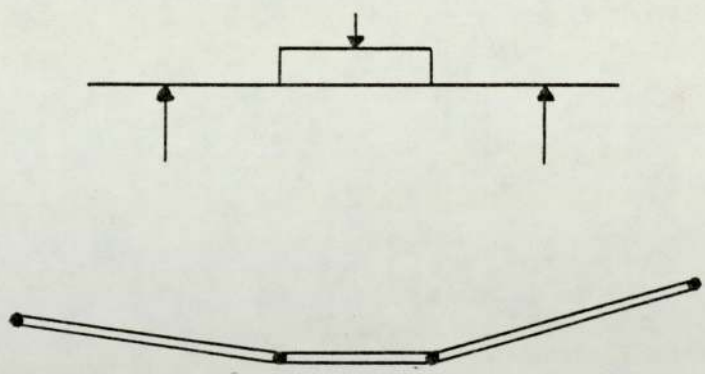

b. Case with $\alpha < 0$

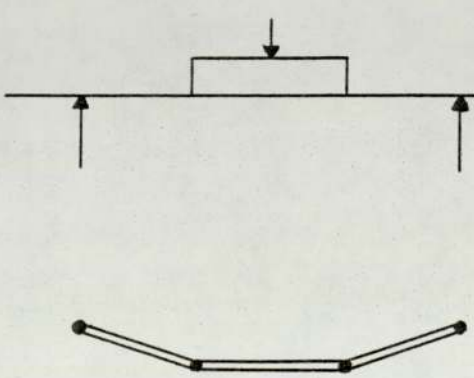

c. Case with $\alpha = 0$

FIGURE 6.10 TYPICAL POSITION OF PLASTIC HINGES

are shown in the fourth column in table (6.1). The β factor is obtained by Von Mises yield criterion. It can be seen from the comparison that the theory gives quite satisfactory results for beams loaded with zero or small lengths of bearing and unsatisfactory results for beams loaded with relatively large lengths of bearing. For these cases, as previously suggested, the β factor is obtained from a yield line analysis. When the yield line pattern 1 is considered the α factor is obtained from equation (6.53) below

$$\alpha = \left(7.24 \frac{d}{l_a} - 1.01 \frac{L}{d}\right) \quad \text{for } \frac{l_a}{d} \geq 1.0 \qquad 6.53.1$$

and

$$\alpha = \left(7.24 \frac{d}{l_a} - 1.01 \frac{L}{d}\right) 0.85 \frac{l_a}{d} \quad \text{for } \frac{l_a}{d} < 1.0 \qquad 6.53.2$$

and for both cases the maximum value of α is taken 5.75 and the minimum value is zero, as explained before; therefore

$$0 \leq \alpha \leq 5.75 \qquad 6.53.3$$

Exactly the same equations are used for determining α when the yield pattern 2 is considered.

When the yield line patterns are considered for determining the β factor, two variables other than α are involved and must be determined. These variables are the $\frac{\omega}{\Delta}$ and $\frac{\Delta_H}{\Delta}$ ratio as have been defined in the theory. As for the α factor, these variables are empirically derived. When the yield line pattern 1 is considered the $\frac{\omega_1}{\Delta}$ ratio is given by

$$\frac{\omega_1}{\Delta} = \left(14.75 - 5.6125 \frac{l_a}{d}\right) \quad \text{for } \frac{L}{d} \leq 5.0 \qquad 6.54.1$$

and

$$\frac{\omega_1}{\Delta} = (14.75 - 5.6125 \frac{l_a}{d}) \, 4.0 \times \frac{d}{L} \quad \text{for } \frac{L}{d} > 5 \qquad 6.54.2$$

When the yield pattern 2 is considered the $\frac{\omega_2}{\Delta}$ ratio is given by

$$\frac{\omega_2}{\Delta} = (5.95 - 0.6174 \frac{L}{d}) \quad \text{for } \frac{L}{d} > 3.0 \qquad 6.55.1$$

and

$$\frac{\omega_2}{\Delta} = (5.95 - 0.6174 \frac{L}{d}) \, 0.3 \frac{L}{d} \quad \text{for } \frac{L}{d} \leq 3.0 \qquad 6.55.2$$

The $\frac{\Delta_H}{\Delta}$ ratio for both yield line patterns is given by the expression

$$\frac{\Delta_H}{\Delta} = 0.3 - 0.185 \left(\frac{f_{bc}}{fy} \right)^4 \qquad 6.56$$

The determination of the factors α, $\frac{\omega}{\Delta}$ and $\frac{\Delta_H}{\Delta}$ is purely empirical within the ranges of beam sizes tested.

b) End Failure

As for central failure, different methods have been employed for calculating the β factor for end failure. When the beam is loaded with zero or small lengths of bearing and consequently β is calculated by Von Mises yield criterion α is given by the following expression

$$\alpha = (1.35 + 0.29 \frac{d}{l_a}) \qquad 6.57.1$$

and the maximum value of α for this case is 4.5, thus

$$0 \leqslant \alpha \leqslant 4.5 \qquad 6.57.2$$

For larger lengths of stiff bearing, when β is obtained from a yield line analysis, α is calculated from the same expressions, that is from equation (6.57) above. For this case the $\frac{\omega}{\Delta}$ ratio, for both yield line patterns is constant and it is expressed by

$$\frac{\omega_3}{\Delta} = \frac{\omega_4}{\Delta} = 1.75 \qquad 6.58$$

For end failure, in general, as l_a was taken the distance of the inner face of the stiff bearing to the end of the beam and the failure mechanism formed is that shown in figure (6.11a). As the stiff bearing moves towards the centre of the beam and consequently l_a increases the failure mechanism is as given in figure (6.11b). For both mechanisms the crushing load P_1 is obtained from

$$P_1 = T\sqrt{0.5B\beta t\ (1+\alpha)\ f_{yr}\ f_{yf}} + \beta t\ l_a\ f_{yr} \qquad 6.59$$

Where $l_a = l_a' + l_e$

For further increases in the value of l_a a stage is reached where the above mentioned mechanism cannot be formed. Instead of that the yield mechanism shown in figure (6.11c) is assumed to form and the crushing load P_2 for this case is given by

$$P_2 = T\sqrt{2B\beta t\ (1+\alpha)\ f_{yr}\ f_{yf}} + \beta t\ l_a\ f_{yr}$$

where $l_a = l_a'$

Therefore, for large lengths of l_e both expressions should be examined and that one which yields the lowest crushing load should be used in design.

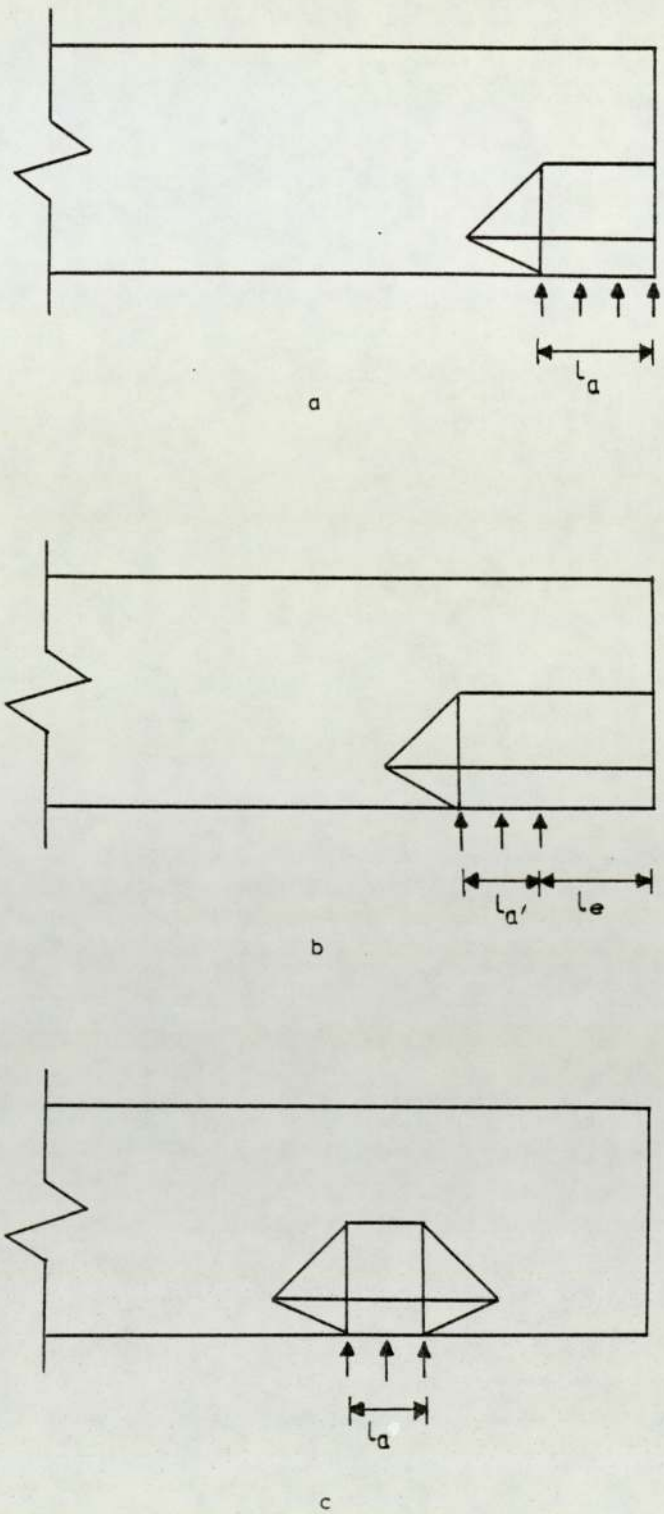

FIGURE 6.11. FAILURE MECHANISM FOR END FAILURE

6.6 COMPARISON OF LOCAL CRUSHING THEORY TO THE TEST RESULTS

The theoretical crushing loads, calculated using the developed theory, are shown in table (6.1), with the test ultimate load, for all the beams. As can be seen from this table three values of theoretical load are obtained for all beams. The three values are obtained for different values of the β factor using 1) Von Mises yield criterion, 2) yield line pattern 1 and 3) yield line pattern 2.

For beams loaded through relatively large lengths of stiff bearing, as explained in the previous section, the β factor is obtained from a yield line analysis; the crushing loads are calculated when both yield line patterns are considered. Included in the same table is the ratio of the experimental failure load to the theoretical crushing load of the beams to be taken for design purposes. This theoretical load has been calculated considering the various methods for obtaining β, depending on the d/l_a ratio.

It can be seen from table (6.1) that the theoretical load for the beams in series I to V which failed at the end, is close to the test failure load and in a few cases only the theory failed, by a small margin, to predict the test ultimate load. When the β factor is obtained by Von Mises yield criterion, the theory gives safe results for beams supported by small lengths of bearing and unsafe results for beams supported by relatively large lengths of bearing. For these cases when the β factor is obtained from the yield line patterns, the calculated theoretical loads given by this method are quite safe.

Series	Beam No	P_{exp} /kN	P_1 by V.M /kN*	P_2 by Y.L.1 /kN†	P_3 by Y.L.2 /kN††	$\frac{P_{exp}}{P_1}$	$\frac{P_{exp}}{P_2}$	$\frac{P_{exp}}{P_3}$	$\frac{d}{l_a}$	P_{th} /kN	$\frac{P_{exp}}{Pth}$
I	11a	255.0	224.91	164.46	257.18	1.134	1.551	0.992	17.677	224.91	1.134
	7a	260.0	228.39	168.11	260.94	1.138	1.547	0.996	17.677	228.39	1.138
	7b	270.0	229.55	168.11	260.94	1.176	1.606	1.035	17.677	229.55	1.176
	6b	257.5	216.65	164.64	251.89	1.188	1.564	1.022	17.677	216.65	1.188
	8a	260.0	218.98	167.21	257.24	1.188	1.555	1.011	17.677	218.86	1.188
	8b	285.0	219.98	167.21	257.24	1.295	1.704	1.108	17.677	219.98	1.295
	3	280.0	233.89	162.43	249.32	1.197	1.724	1.123	17.677	233.89	1.197
II	11a	255.0	224.91	164.46	257.18	1.134	1.551	0.992	17.677	224.91	1.134
	5a	310.0	235.22	168.92	260.88	1.318	1.835	1.188	13.731	235.22	1.318
	5b	320.0	270.75	173.79	265.29	1.181	1.841	1.206	10.515	270.75	1.181
	6a	339.0	329.08	180.67	250.52	1.030	1.876	1.353	7.161	329.08	1.030
	10a	410.0	364.90	204.32	291.28	1.124	2.007	1.407	5.429	364.90	1.124
	12a	450.0	359.64	211.86	295.78	1.251	2.124	1.521	4.372	211.86	2.124

* V.M. Indicates Von Mises Yield Criterion
† Y.L.1 Indicates Yield Line Pattern 1
†† Y.L.2 Indicates Yield Line Pattern 2
P_{th} Theoretical Load for Design According to the d/l_a ratio

TABLE 6.1 COMPARISON OF THE CRUSHING THEORY TO THE TEST RESULTS

Series	Beam No	P_{exp} /kN	P_1 by V.M /kN	P_2 by Y.L.1 /kN	P_3 by Y.L.2 /kN	$\frac{P_{exp}}{P_1}$	$\frac{P_{exp}}{P_2}$	$\frac{P_{exp}}{P_3}$	$\frac{d}{l_a}$	P_{th} /kN	$\frac{P_{exp}}{Pth}$
II	1	315.0	270.54	297.17	259.74	1.164	1.060	1.213	17.677	270.54	1.164
	2a	325.0	271.77	299.17	261.03	1.196	1.196	1.245	7.161	271.77	1.196
	2b	340.0	272.81	306.28	283.11	1.246	1.110	1.201	7.161	272.81	1.246
III	4b	245.0	215.50	165.07	246.70	1.137	1.484	0.993	17.677	215.50	1.137
	11b	265.0	261.96	173.16	282.95	1.012	1.530	0.937	10.515	261.96	1.012
	13a	297.5	284.55	190.72	280.59	1.045	1.560	1.060	7.161	284.55	1.045
	13b	340.0	314.91	200.40	286.85	1.080	1.696	1.185	5.429	314.91	1.080
	14	390.0	359.56	234.80	280.34	1.085	1.661	1.391	4.844	359.56	1.085
	15	400.0	400.84	370.93	330.73	0.998	1.078	1.209	3.384	370.93	1.078
	16	420.0	540.14	365.49	349.84	0.778	1.149	1.201	2.330	365.49	1.149
	18	440.0	582.61	356.57	355.76	0.755	1.234	1.237	2.111	356.57	1.234
	20	450.0	740.92	379.59	387.87	0.607	1.185	1.160	1.777	379.59	1.185
	22	455.0	783.10	377.56	389.36	0.581	1.205	1.168	1.534	377.56	1.205

TABLE 6.1 (CONTINUED)

Series	Beam No	P_{exp} /kN	P_1 by V.M /kN	P_2 by Y.L.1 /kN	P_3 by Y.L.2 /kN	$\frac{P_{exp}}{P_1}$	$\frac{P_{exp}}{P_2}$	$\frac{P_{exp}}{P_3}$	$\frac{d}{l_a}$	P_{th} /kN	$\frac{P_{exp}}{Pth}$
III	36	330.0	307.38	200.12	350.85	1.074	1.649	0.941	5.429	307.38	1.074
	37	310.0	285.99	183.03	321.71	1.084	1.694	0.964	5.429	285.99	1.084
	38	290.0	277.26	232.79	312.42	1.046	1.246	0.928	5.429	277.26	1.046
	39	407.5	371.43	216.22	483.09	1.097	1.885	0.844	5.429	371.43	1.097
	40	400.0	355.42	214.39	405.34	1.125	1.866	0.987	5.429	355.42	1.184
	41	397.5	335.76	203.63	384.14	1.184	1.952	1.035	5.429	335.76	1.184
	42	390.0	327.81	215.64	385.08	1.189	1.809	1.013	5.429	327.81	1.189
	43	385.0	303.49	199.33	353.76	1.268	1.931	1.088	5.429	303.49	1.268
IV	4b	245.0	215.50	165.07	246.70	1.137	1.484	0.993	17.677	215.50	1.137
	26a	258.0	256.26	175.28	268.97	1.007	1.472	0.959	11.225	256.26	1.007
	25a	270.0	276.13	178.09	262.71	0.978	1.516	1.028	7.483	276.13	0.978
	25b	320.0	315.08	148.83	183.43	1.016	2.150	1.745	5.613	315.08	1.016
	26b	340.0	342.24	201.26	283.31	0.993	1.689	1.200	4.490	201.26	1.689

TABLE 6.1 (CONTINUED)

Series	Beam No	P_{exp} /kN	P_1 by V.M /kN	P_2 by Y.L.1 /kN	P_3 by Y.L.2 /kN	$\frac{P_{exp}}{P_1}$	$\frac{P_{exp}}{P_2}$	$\frac{P_{exp}}{P_3}$	$\frac{d}{l_a}$	P_{th} /kN	$\frac{P_{exp}}{Pth}$
IV	24b	350.0	377.88	320.61	283.63	0.962	1.092	1.234	3.742	320.61	1.092
	27	390.0	439.25	351.20	323.53	0.888	1.110	1.205	3.207	351.20	1.110
	28	420.0	472.70	354.56	336.80	0.889	1.185	1.247	2.806	354.56	1.185
	R1b	295.0	313.16	204.71	313.09	0.942	1.441	0.942	11.225	313.16	0.942
	R1a	420.0	396.11	283.50	330.53	1.060	1.481	1.271	4.490	283.50	1.481
	R2	460.0	478.70	397.26	375.81	0.960	1.158	1.224	3.207	397.26	1.158
V	4b	245.0	215.50	165.07	246.70	1.137	1.484	0.993	17.677	215.50	1.137
	23b	198.0	198.50	153.80	231.53	0.998	1.287	0.855	17.677	198.50	0.998
	23a	180.0	170.15	131.82	198.45	1.058	1.365	0.907	17.677	170.15	1.058
	29a	140.0	140.13	115.35	173.65	0.999	1.214	0.806	17.677	140.13	0.999
	29b	140.0	131.89	108.56	163.44	1.061	1.289	0.856	17.677	131.89	1.061
VI	31	208.0	174.25	148.27	205.82	1.194	1.403	1.011	∞	174.25	1.194
	30	270.0	266.35	218.00	251.69	1.014	1.239	1.073	4.490	218.00	1.239

TABLE 6.1 (CONTINUED)

Series	Beam No	P_{exp} /kN	P_1 by V.M /kN	P_2 by Y.L.1 /kN	P_3 by Y.L.2 /kN	$\frac{P_{exp}}{P_1}$	$\frac{P_{exp}}{P_2}$	$\frac{P_{exp}}{P_3}$	$\frac{d}{l_a}$	P_{th} /kN	$\frac{P_{exp}}{Pth}$
VI	32	310.0	366.14	307.33	286.76	0.847	1.009	1.081	2.245	307.33	1.009
	33	350.0	420.87	369.66	360.32	0.832	0.947	0.971	1.497	369.66	0.947
	34	395.0	594.56	383.31	410.11	0.664	1.030	0.963	0.898	383.31	1.030
	50	185.0	166.00	140.41	168.13	1.114	1.318	1.100	∞	166.00	1.114
	51	217.5	204.32	185.54	190.13	1.064	1.172	1.144	4.490	185.54	1.172
	52	240.0	296.08	209.31	219.20	0.811	1.147	1.095	1.497	209.31	1.147
	53	265.0	575.07	259.99	233.96	0.461	1.019	1.133	0.898	259.99	1.091
	62	322.5	269.51	201.73	259.89	1.197	1.599	1.241	∞	269.51	1.197
	63	495.0	598.24	410.62	489.59	0.827	1.205	1.011	2.383	410.62	1.205
	60	860.0	853.99	931.14	1018.30	1.007	0.924	0.845	31.843	853.99	1.007
	61	1060.0	1157.53	1122.38	1013.70	0.916	0.944	1.046	4.044	1122.38	0.944
	64	285.0	182.54	191.57	207.20	1.561	1.488	1.375	∞	182.54	1.561
	65	350.0	239.35	253.79	262.98	1.462	1.379	1.331	7.148	239.35	1.462
	66	460.0	425.82	319.87	262.32	1.080	1.438	1.736	2.383	319.87	1.483

TABLE 6.1 (CONTINUED)

Series	Beam No	P_{exp} /kN	P_1 by V.M /kN	P_2 by Y.L.1 /kN	P_3 by Y.L.2 /kN	$\frac{P_{exp}}{P_1}$	$\frac{P_{exp}}{P_2}$	$\frac{P_{exp}}{P_3}$	$\frac{d}{l_a}$	P_{th} /kN	$\frac{P_{exp}}{Pth}$
	67	530.0	656.34	389.87	338.81	0.808	1.359	1.564	1.191	389.87	1.359
	68	190.0	146.90	111.79	182.91	1.293	1.699	1.039	∞	146.90	1.293
	69	180.0	128.12	93.11	183.11	1.405	1.933	0.983	∞	128.12	1.405
	70	297.5	321.77	295.87	343.29	0.925	1.006	0.867	1.497	295.87	1.006
VI	71	260.0	295.96	259.52	338.48	0.878	1.002	0.768	1.497	259.52	1.002
	72	140.0	146.80	113.32	199.59	0.954	1.235	0.701	∞	146.80	0.954
	73	127.5	127.56	91.96	155.18	1.000	1.386	0.822	∞	127.56	1.000
	74	190.0	384.37	203.53	187.91	0.494	0.934	1.011	1.497	203.53	0.934
	75	172.5	296.54	184.25	193.04	0.582	0.936	0.894	1.497	184.25	0.936
	44	237.5	206.33	180.82	230.18	1.151	1.313	1.032	17.677	206.33	1.151
	35	215.0	215.00	181.64	225.62	1.000	1.184	0.953	17.677	215.00	1.000
VII	45	145.0	143.56	136.24	61.44	1.010	1.064	2.360	17.677	143.56	1.010
	46	100.0	116.56	116.18	75.50	0.858	0.861	1.324	17.677	116.56	0.858
	48	300.0	265.92	284.99	279.82	1.128	1.053	1.072	17.677	265.92	1.128

TABLE 6.1 (CONTINUED)

Series	Beam No	P_{exp} /kN	P_1 by V.M /kN	P_2 by Y.L.1 /kN	P_3 by Y.L.2 /kN	$\frac{P_{exp}}{P_1}$	$\frac{P_{exp}}{P_2}$	$\frac{P_{exp}}{P_3}$	$\frac{d}{l_a}$	P_{th} /kN	$\frac{P_{exp}}{Pth}$
VII	47	272.5	265.05	274.94	242.38	1.028	0.991	1.124	17.677	265.05	1.028
	49	135.0	129.32	178.99	98.25	1.044	0.754	1.374	17.677	129.32	1.044
	58	250.0	173.91	192.88	97.96	1.437	1.296	2.552	28.142	173.91	1.437
	59	168.75	207.27	261.39	91.98	0.814	0.646	1.835	9.283	207.29	0.814
	54	470.0	824.47	402.33	416.11	0.570	1.168	1.130	3.574	402.33	1.168
	55	430.0	506.26	378.79	423.06	0.849	1.135	1.016	3.574	378.79	1.135
	56	350.0	459.61	333.74	315.74	0.762	1.049	1.109	3.574	333.74	1.049
	57	280.0	465.81	271.54	125.08	0.601	1.031	2.239	3.574	271.54	1.031
VIII	77	240.0	189.43	160.18	247.30	1.267	1.498	0.970	4.490	160.18	1.498
	76	260.0	281.41	161.16	249.96	0.924	1.613	1.040	4.490	161.16	1.613
	78	300.0	604.27	232.91	381.48	0.496	1.288	0.786	0.898	232.91	1.288
	79	390.0	620.19	385.79	400.65	0.629	1.011	0.973	0.898	385.79	1.011
	80	250.0	264.22	173.14	224.26	0.946	1.444	1.115	4.490	173.14	1.444

TABLE 6.1 (CONTINUED)

Series	Beam No	P_{exp} /kN	P_1 by V.M /kN	P_2 by Y.L.1 /kN	P_3 by Y.L.2 /kN	$\frac{P_{exp}}{P_1}$	$\frac{P_{exp}}{P_2}$	$\frac{P_{exp}}{P_3}$	$\frac{d}{l_a}$	P_{th} /kN	$\frac{P_{exp}}{P_{th}}$
†	CA6	345.0	330.99	263.80	287.93	1.042	1.308	1.198	28.142	330.99	1.042
†	CC1	312.0	239.79	236.54	321.62	1.301	1.319	0.970	28.142	239.79	1.301
†	CC2	305.0	232.39	235.79	385.04	1.312	1.294	0.792	28.142	232.39	1.312
†	CC4	275.0	214.40	244.16	361.3	1.283	1.126	0.761	28.142	214.40	1.283
†	CD3	400.0	399.44	327.02	324.66	1.001	1.223	1.232	7.148	399.44	1.001
†	CH1	280.0	249.77	187.09	280.44	1.121	1.497	0.988	5.506	249.77	1.121
**	97	311.3	268.75	309.74	328.31	1.157	1.005	0.948	∞	268.75	1.157
**	98	385.0	467.61	373.71	413.13	0.823	1.030	0.932	3.574	373.71	1.030

† Reference (55)
** Reference (56)

TABLE 6.1 (CONTINUED)

Examining the latter cases, the ratio of the depth of the section between the root radius to the length of the stiff bearing is greater than 4.5; this is taken as the criterion for choice of calculating the β factor and is obtained by inspection of the results. Therefore, for beams having $d/l_a \leq 4.5$ the β is less than 1.0 and is calculated using a yield line analysis.

Similarly, the theoretical loads calculated for the beams in series VI, VII and VIII, which were tested for central failure, when the β factor is obtained by Von Mises yield criterion, are safe for small lengths of bearing and unsafe when the load is applied through large lengths of stiff bearing. The factor of safety for the latter cases increases when the yield line analysis is used in obtaining the β factor. From the two yield line patterns examined that one which gives the minimum theoretical load should be considered further; although it was found that for most of the cases the results given by the two yield line patterns are quite close. However, yield pattern 1 appears to give more satisfactory results and is recommended for design.

The beams in series VIII were loaded through thin spreaders, of different thicknesses and as can be seen from table (6.1) the factor of safety varies by different amounts.

The same criterion for choice of the Von Mises yield criterion or the yield line analysis for calculating the β factor applies for central failure as for end failure. Therefore, for cases where $d/l_a > 4.5$ the β factor is obtained from the Von Mises yield criterion and for cases with $d/l_a \leq 4.5$ a yield line analysis is used. The above limit has been imposed empirically.

In table (6.1) the test results in references (55) and (56)

are included and as could be seen from the comparison the developed theory predicts safe results for these beams.

It is worth noting that where the developed theory failed to predict safe results this is by only a small margin, except for two cases namely beam Nos 46 and 59. The ratio of the experimental failure load to the theoretical crushing load is 0.858 and 0.814 respectively. Beam No 46 was of 3.0 m span and loaded through a 12.7 mm long stiff bearing and beam No 59 was of 0.75 m span, loaded in the same way as the former one.

During testing of beam No 46 a horizontal movement of the beam was noticed under the load probably initiated due to the initial eccentricity of the web, being 0.5 mm, and that it was carrying almost the full plastic moment. These factors possibly caused a premature failure of the beam.

Beam No 59 was of the 152 x 98 x 17.09 kg joist section, the only beam tested from this serial size. The values of the yield stress, obtained from the tensile test for this beam, are relatively high and this is probably the reason the theory over-estimates the crushing load for this beam. The short piece used in the test was a straight piece cut from an otherwise bent beam. The tensile test pieces may have been affected by cold working of the bent part of the beam.

6.7 CONCLUSIONS FROM THE COMPARISON

Assumptions made when deriving this theory include small rotations and deflections. However, this is not quite true since the flanges were severely distorted, especially in cases where the load was applied through small lengths of stiff bearing.

When the β factor is obtained from the yield line analysis, the yield line patterns were assumed to have vertical yield lines in the web. In fact such yield lines cannot be formed unless the web provides enough restraint away from them; this could only happen when the beam is sufficiently long.

The various factors, that is α, $\frac{\omega}{\Delta}$ and $\frac{\Delta_H}{\Delta}$, included in the theory and considered in section 6.5 are purely empirical. It should be emphasized that the satisfactory results for the loading and beam section sizes relate specifically to this work, as these factors for other types of loading and beam serial sizes may vary.

The current design practices assume that there is a linear variation between the length of the stiff bearing and the crushing load. From the test results it was found that such a variation does not appear to be true, particularly for relative large lengths of bearing. The theory developed deals with this point, as the factors α and β are expressed in terms of this variable.

If the assumptions considered in this theory are correct, then the values of the ratio of the test ultimate load to the minimum theoretical load, given in table (6.1) should be consistent.

CHAPTER 7

A SIMPLIFIED APPROACH TO THE CRUSHING THEORY

7.1 INTRODUCTION

In the preceding chapter a theory was developed for predicting the crushing load of the beams. Certain factors in the final expressions had to be determined and in cases where relatively long lengths of stiff bearings are considered, the calculations involved are rather lengthy.

Although the results obtained from this theory are quite satisfactory, especially for cases where the current design codes fail to do so, this theory is not likely to be used as a basis for design of beams unless it is recast in a reasonably simple form, easily used by designers.

In the present chapter an attempt is made to express the crushing theory in a much more simple form, which at the same time gives quite satisfactory results, as is shown in a following section.

7.2 SIMPLIFICATION OF THE CRUSHING THEORY

a) Central Failure

When developing the crushing theory in chapter 6, it was assumed that the outer hinges of the failed zone have a plastic moment $M_{PT} = \alpha M_{PF}$ and the α factor had to be determined by considering various expressions. The resistance w provided by the web was taken as $w = \beta t f_{yr}$. This analysis can be simplified, somehow, by assuming $\alpha = 1$, that is all the formed plastic hinges have the same plastic moment M_{PF}. The resistance provided by the web is taken as $w = t p_c$, where p_c is the compressive strength, calculated according to the Draft Standard Code (8).

The failure mechanism assumed to form is shown in figure (7.1a). By equating the work done by the external forces to the work done by the internal forces it is obtained

$$P.\Delta = 4M_{PF}\,\theta + 2\,w\,L_1\,\frac{\Delta}{2} + w\,l_a\,\Delta$$

and after substituting for Δ and θ the above expression becomes:

$$P = 4\,\frac{M_{PF}}{L_1} + w\,L_1 + w\,l_a \qquad 7.1$$

The crushing load P will be a minimum when $\frac{\partial P}{\partial L_1} = 0$. By differentiating, therefore, equation (7.1) with respect to L_1 and setting $\frac{\partial P}{\partial L_1} = 0$, L_1, is obtained from

$$L_1 = 2\sqrt{\frac{M_{PF}}{w}} \qquad 7.2$$

By substituting for L_1 and w into equation (7.1), the crushing load P is obtained from

$$P = 2T\sqrt{B\,t\,f_{yf}\,P_c} + t\,p_c\,l_a \qquad 7.3$$

Equation (7.3) can be written in a more general form as

$$P = 2Z_1\,T\sqrt{B\,t\,f_{yf}\,P_c} + Z_2\,t\,P_c\,l_a \qquad 7.4$$

The inserted factors Z_1 and Z_2 are determined in a following section.

b) End Failure

The same argument holds when considering failure at the end. The failure mechanism assumed to form in this case is shown in figure (7.1b). Following the same assumptions and procedure, as

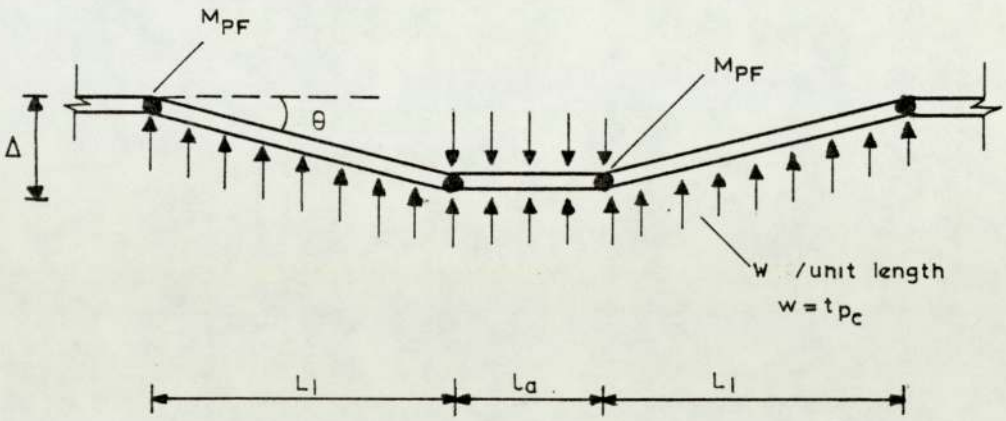

a. Central failure

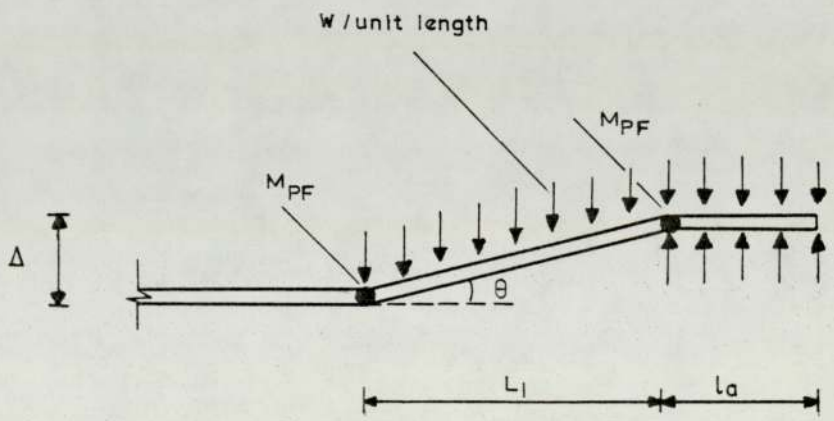

b. End failure

FIGURE 7. 1. FAILURE MECHANISM

for the previous case, the crushing load P_1 is obtained from

$$P_1 = T\sqrt{B\ t\ f_{yf}\ p_c} + t\ p_c\ l_a \qquad 7.5$$

By introducing the factors Z_3 and Z_4, equation (7.5) can be written in a general form as

$$P_1 = Z_3\ T\sqrt{B\ t\ f_{yf}\ p_c} + Z_4\ t\ p_c\ l_a \qquad 7.6$$

The factors Z_3 and Z_4, as the factors Z_1 and Z_2, are determined in a following section, empirically.

7.3 MINIMUM THICKNESS OF LOADING PLATE IN A SIMPLIFIED FORM

a) Central Failure

The theory derived in chapter 6 for the minimum thickness of the loading plate can further be simplified, in a similar manner to the simplification of the theory made in section 7.2.

The failure mechanism assumed to form is shown in figure (7.2a). By assuming, therefore, that $\alpha = 1$ and the resistance provided by the web as $w = t p_c$ and by equating the work done by the external forces to the work done by the internal forces it is obtained.

$$P_3\ \Delta = 4M_{PF}\ \theta + 2M_{PP}\ \theta + 2\ w\ L_1\ \frac{\Delta}{2} + w\ c\ \Delta \qquad 7.7$$

Following the same procedure as before and substituting for the various variables into equation (7.7), P_3 is obtained from the following expression.

$$P_3 = \sqrt{t\ p_c}\ \sqrt{4\ BT^2\ f_{yf} + 2\ t_p^{\,2}\ b\ f_{yp}} \qquad 7.8$$

When the loading plate is stiff, the crushing load was found to be

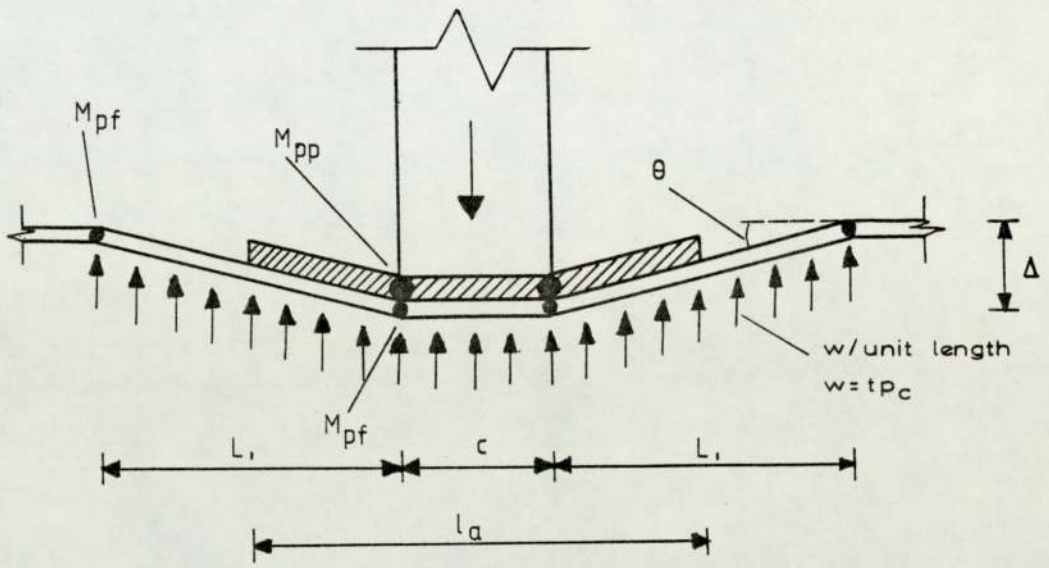

a. Central failure

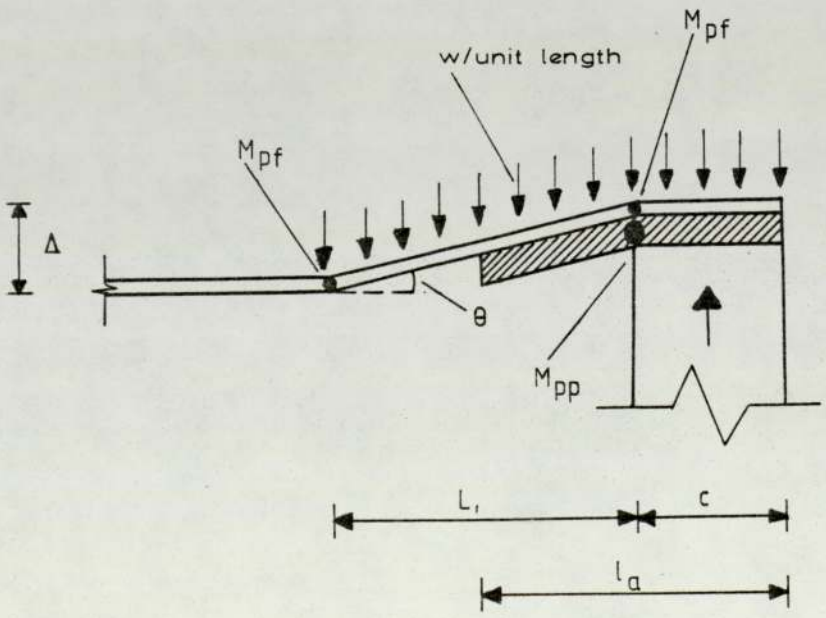

b. End failure

FIGURE 7.2 MINIMUM THICKNESS OF LOADING PLATE FOR SIMPLIFIED THEORY

given by equation (7.3), that is

$$P = 2T\sqrt{B\ t\ f_{yf}\ p_c} + t\ p_c\ l_a$$

and when the plate is thin the load is given by equation (7.8). At the point, therefore, when the loading plate will just start bending the two values for the crushing load, given by equations (7.3) and (7.8), should be equal. Thus.

$$2T\sqrt{B\ t\ f_{yf}\ p_c} + t\ p_c\ l_a = \sqrt{t\ p_c}\ \sqrt{4\ B\ T^2\ f_{yf} + 2t_p^{\,2}\ b\ f_{yp}} \qquad 7.9$$

Rearranging, the minimum thickness of the loading plate t_p is obtained from

$$t_p = \sqrt{\frac{4T(l_a-c)\sqrt{B t f_{yf}\ p_c} + t\ p_c\ (l_a-c)^2}{2\ b\ f_{yp}}} \qquad 7.10$$

and by inserting a factor Z_5 into the above expression this becomes

$$t_p = Z_5\sqrt{\frac{4T(l_a-c)\sqrt{B t f_{yf}\ p_c} + t\ p_c (l_a-c)^2}{2\ b\ f_{yp}}} \qquad 7.11$$

b) End Failure

The failure mechanism assumed to form, when failure is obtained at the end, is shown in figure (7.2b). By following exactly the same procedure as for the previous case, the minimum thickness of the loading plate t_p is given by

$$t_p = \sqrt{\frac{2T\,(l_a-c)\sqrt{B\,t\,f_{yf}\,p_c} + t\,p_c\,(l_a-c)^2}{0.5\,b\,f_{yp}}} \qquad 7.12$$

and by introducing a factor Z_6 into the above expression this becomes:

$$t_p = Z_6\sqrt{\frac{2T\,(l_a-c)\sqrt{B\,t\,f_{yf}\,p_c} + t\,p_c\,(l_a-c)^2}{0.5\,b\,f_{yp}}} \qquad 7.13$$

7.4 EMPIRICAL ASSESSMENT OF INSERTED FACTORS

The introduced factors Z_1, Z_2, Z_3, Z_4, Z_5 and Z_6 are determined empirically in this section. It must be emphasized, though, that the expressions representing the above mentioned factors give satisfactory results for the beam serial sizes and loading conditions considered in the present work.

The Z_1 factor is determined by considering beams loaded by knife edge loads, so eliminating the Z_2 factor in equation (7.4). This factor found to vary best with the d/L ratio, as given by the following expression

$$Z_1 = (25\,\frac{d}{L} - 3.4) \qquad \text{for } L/d > 3.0 \qquad 7.14.1$$

and

$$Z_1 = (25\,\frac{d}{L} - 3.4)\,12\,\frac{d}{t} \qquad \text{for } L/d \leq 3.0 \qquad 7.14.2$$

The Z_2 factor is determined from beams having constant span and different lengths of stiff bearing. It was found that this factor varies with the l_a/L ratio as it is given by equation (7.15).

$$Z_2 = \left(1 - 0.5 \frac{l_a}{L}\right) \qquad \text{and} \quad 0.5 \leqslant Z_2 \leqslant 1.0 \qquad 7.15$$

For end failure, the introduced factors Z_3 and Z_4 were found to have a constant value and are taken as

$$Z_3 = 2.5 \quad \text{and} \quad Z_4 = 1.0 \qquad \text{for} \ \frac{d}{l_a} > 3.0 \qquad 7.16.1$$

and

$$Z_3 = 2.5 \quad \text{and} \quad Z_4 = 0.85 \qquad \text{for} \ \frac{d}{l_a} \leqslant 3.0 \qquad 7.16.2$$

For the cases, where the loading plate was thin, it was found that for the case of central failure when $Z_5 = Z_2$ and for the case of end failure when $Z_6 = Z_4$, satisfactory results are obtained. The Z_5 and Z_6 factors are obtained from equations (7.11) and (7.13) respectively.

The applicability and validity of these factors will be indicated when the test results are compared to the simplified crushing theory as follows.

7.5 COMPARISON OF THE SIMPLIFIED CRUSHING THEORY TO THE TEST RESULTS

The theoretical crushing loads of all the beams, calculated according to the simplified crushing theory, are shown with the experimental ultimate loads in table (7.1). As can be seen from this table of results, the loads predicted by the theory are quite safe and the factor of safety varies by different amounts.

The crushing loads calculated using the theory for beams in series I to VI, which were tested for end failure, are safe for all the beams except for one case, beam No R1b. The theory for this case overestimates the test failure load by 3.17%.

Series	Beam No	P_{exp} /kN	P_{th} /kN	$\frac{P_{exp}}{P_{th}}$
I	11a	255.0	211.51	1.206
	7a	260.0	203.21	1.279
	7b	270.0	203.21	1.329
	6b	257.5	203.56	1.265
	8a	260.0	204.96	1.269
	8b	285.0	204.96	1.391
	3	280.0	199.72	1.402
II	11a	255.0	211.51	1.206
	5a	310.0	213.04	1.455
	5b	320.0	228.23	1.402
	6a	339.0	238.60	1.420
	10a	410.0	266.78	1.537
	12a	450.0	284.93	1.582
	1	315.0	225.54	1.396
	2a	325.0	290.84	1.117
	2b	340.0	290.84	1.169
III	4b	245.0	213.44	1.148
	11b	265.0	227.98	1.162
	13a	297.5	244.88	1.215
	13b	340.0	263.61	1.290
	14	390.0	287.31	1.357
	15	400.0	328.74	1.216
	16	420.0	351.87	1.194
	18	440.0	375.19	1.173
	20	450.0	412.39	1.091
	22	455.0	438.71	1.037
	36	330.0	245.60	1.344
	37	310.0	218.17	1.421
	38	290.0	209.07	1.387

P_{th} is the Theoretical Load

TABLE 7.1 COMPARISON OF THE SIMPLIFIED THEORY TO THE TEST RESULTS

Series	Beam No	P_{exp} /kN	P_{th} /kN	$\frac{P_{exp}}{P_{th}}$
III	39	407.5	353.21	1.154
	40	400.0	332.92	1.201
	41	397.5	307.01	1.295
	42	390.0	297.52	1.311
	43	385.0	265.04	1.453
IV	4b	245.0	213.44	1.147
	26a	258.0	221.95	1.167
	25a	270.0	231.95	1.164
	25b	320.0	249.29	1.284
	26b	340.0	272.46	1.248
	24b	350.0	286.41	1.222
	27	390.0	333.91	1.168
	28	420.0	361.24	1.163
	R1b	295.0	304.36	0.969
	R1a	420.0	371.03	1.132
	R2	460.0	423.14	1.087
V	4b	245.0	213.44	1.148
	23b	198.0	176.51	1.122
	23a	180.0	151.30	1.189
	29a	140.0	123.60	1.132
	29b	140.0	116.33	1.203
VI	31	208.0	160.25	1.298
	30	270.0	212.59	1.270
	32	310.0	269.11	1.152
	33	350.0	312.88	1.118
	34	395.0	353.48	1.117
	50	185.0	73.18	2.528
	51	217.5	118.06	1.842
	52	240.0	189.51	1.266

TABLE 7.1 (CONTINUED)

Series	Beam No	P_{exp} /kN	P_{th} /kN	$\frac{P_{exp}}{P_{th}}$
	53	265.0	257.85	1.028
	62	322.5	280.58	1.149
	63	495.0	365.95	1.353
	60	860.0	427.10	2.014
	61	1060.0	589.29	1.799
	64	285.0	100.40	2.839
	65	350.0	129.81	2.696
	66	460.0	180.54	2.548
VI	67	530.0	264.62	2.003
	68	190.0	137.60	1.381
	69	180.0	124.09	1.451
	70	297.5	268.14	1.109
	71	260.0	251.28	1.035
	72	140.0	64.42	2.173
	73	127.5	55.73	2.288
	74	190.0	193.11	0.984
	75	172.5	185.67	0.929
	44	237.5	194.37	1.222
	35	215.0	187.08	1.149
	45	145.0	81.51	1.779
	46	100.0	80.76	1.238
	48	300.0	299.70	1.001
VII	47	272.5	244.43	1.115
	49	135.0	118.08	1.143
	58	250.0	102.23	2.445
	59	168.75	113.34	1.489
	54	470.0	374.42	1.255
	55	430.0	192.73	1.231
	56	350.0	168.75	2.074
	57	280.0	158.85	1.762

TABLE 7.1 (CONTINUED)

Series	Beam No	P_{exp} /kN	P_{th} /kN	$\frac{P_{exp}}{P_{th}}$
VIII	77	240.0	210.85	1.138
	76	250.0	211.54	1.182
	78	300.0	214.74	1.397
	79	390.0	346.78	1.125
	80	250.0	260.07	0.961
*	CA6	345.0	288.44	1.196
*	CC1	312.0	246.81	1.264
*	CC2	305.0	170.66	1.787
*	CC4	275.0	101.11	2.720
*	CD3	400.0	291.21	1.374
*	CH1	280.0	121.14	2.311
†	97	311.3	193.67	1.607
†	98	385.0	366.70	1.050

* Reference (55)

† Reference (56)

TABLE 7.1 (CONTINUED)

For beams in series VI, VII and VIII, which were tested for central failure, the theory predicts safe results for nearly all the beams except for three cases, namely beam Nos 74, 75 and 80. Beam Nos 74 and 75 were of 1.4 m span and the load was applied through a 150 mm long stiff bearing plate. The width of the flanges of these beams was reduced and this is the reason the theory overestimates the ultimate load for these beams, since the inserted factors Z_1 and Z_2 do not involve the flange width of the beam. Beam No 80 was of 1.0 m span and the load was applied through a 50 mm long thin bearing plate. It was noticed, during testing, that this plate has yielded and lost contact with the beam at its ends.

7.6 CONCLUSIONS FROM THE COMPARISON

It is noticable from table (7.1) that the theory in some cases predicts very conservative results as the obtained ratio of the experimental failure load to the theoretical crushing load is greater than 2.0. This happens to beams with relatively long spans or to beams loaded through zero or small lengths of stiff bearing.

However, the fact that the two expressions obtained for calculating the crushing load, that is equations (7.4) and (7.6) as well as equations (7.11) and (7.13) for the minimum thickness of the loading plate are in a simple form which can easily be used by designers combined with the safety in the predicted results makes this simplified theory appear promising. An advantage of this theoretical approach is that the values for the compressive strength p_c are already calculated and are given in the Draft Code. If the results obtained by this theory are compared with

those obtained by the method suggested in the Draft Code, and examined in chapter 4, it is clear that the former results are safer than the latter ones especially for cases with long lengths of span .

The accuracy of this theory, hopefully could be improved by re-examinination of the inserted factors Z_1, Z_2, Z_3, Z_4, Z_5 and Z_6.

CHAPTER 8

CONCLUSIONS AND RECOMMENDATIONS FOR FURTHER RESEARCH

8.1 INTRODUCTION

Although a lot of theoretical and experimental work has already been done on various types of steel beams, when subjected to concentrated loads, it is not yet established what actually initiates their failure and the exact mode of failure.

Most of the researchers assumed that the beams fail by buckling of the web or by crushing of the web under the applied load or reaction and adopted theoretical or empirical approaches to fit their experimental results.

It was shown earlier in this work that the developed theories and approaches are not satisfactory, since they do not predict safe results for a large number of the beams tested here. It was, therefore, concluded necessary to develop more theories which would be based on the experimental observations and give, hopefully, more satisfactory results. Each theory could then be compared with the test results of the present work as well as with other published experimental results.

8.2 CONCLUSIONS FROM THE EXPERIMENTAL OBSERVATIONS

It was noticed during testing that yielding took place at various locations of the beam; the degree of yielding varied between tests, depending on the stresses. Areas of high stresses were detected by the flaking of the white-wash in positions such as,

1) The flange in the vicinity of the applied load and at the support, for beams which were tested for end failure.
2) The web at its junction with the root radius at the vicinity of the applied load and support, for beams which tested for end

failure.

The high stresses were due to direct and bending stresses produced due to the loading. These stresses, possibly, have an influence on the load carrying capacity of the beams.

Areas of high stresses in the web were always accompanied by large out of plane deflection at failure. The rate of increase of the web deflections varied. In some beams they were apparent at low loads and increased until failure and in some other beams were very small up to the failure point where they suddenly increased.

8.3 CONCLUSIONS FROM THE COMPARISON OF THE DEVELOPED THEORIES TO THE TEST RESULTS

The theories developed in this work, although containing empirical factors, when compared to the tested beams give quite satisfactory results. The Elastic Buckling theory considers the stability of the web-plate and the Crushing theory the stress system attainable at the web root combined with the ultimate moment of resistance due to bending of the web and the flange.

The comparison of the test results to the Elastic Buckling theory shows that the only beams that attained their elastic critical load are those having a relatively short span and loaded through large lengths of bearing. The rest of the beams failed at a load less than their elastic critical load. This, as explained earlier, is due to the loading conditions and the restraint provided by the load application. It was observed that the top flange of the beams after failure does not remain perpendicular to the web, due to the rotation at the junction with the web root. The restraint provided was also reduced at the junction of the web with the yielding flanges due to yielding in the vicinity of the applied load or support.

The Crushing theory gives consistent results when compared with the tested beams. In cases where the load was applied through relatively long lengths of bearing and the current design practices and theories failed to predict safe results, this theory appears to be quite satisfactory. Depending on the length of stiff bearing, the β factor involved is calculated by considering different methods. For $d/l_a > 4.5$, β is obtained from Von Mises Yield Criterion, and for $d/l_a \leq 4.5$ β is obtained from a yield line analysis.

As has been indicated in chapter 7, it is possible to place the crushing theory in a simplified form, suitable for design purposes. The results obtained when this simplified theory is compared to the tested beams are satisfactory, although in some cases are very conservative.

It must be emphasized here that the results obtained here are not exhaustive and can further be improved.

8.4 CONCLUSIONS

When the universal beams are subjected to concentrated loads, they behave in a rather complex way. Due to the many factors involved, which influence the load carrying capacity of the beams, the various design guides and practices used in design are not efficient, since they apply to certain loading and restraining conditions.

In Great Britain the most commonly used design guide, BS 449, uses the Perry formula for calculating the stresses, which over-estimates the restraint provided by the load when applied across the flange. Similarly, the recent introduced draft code uses a modified 'Perry Formula', which in some cases gives more satisfactory results than the former method.

Due to the non linear stress-strain effects, which have not been considered in the present work, it is not possible to determine the

restraint a beam will have when it is loaded on its flanges. If such non linear effects would be included then the finite element method may be the most suitable for such an analysis.

8.5 RECOMMENDATIONS FOR FURTHER RESEARCH

Completing the present work it is felt that further experimental work is needed to be carried out to develop the state of knowledge.

The theoretical work advanced here should be continued for different constraint types of the top flange of the beam, with special consideration of the empirical factors.

For the cases were failure was obtained at the end, due to the large number of variables examined, the majority of the tests were performed on the 254 x 102 x 22 kg. U.B section and the span was kept constant throughout these cases. For cases where failure was obtained at the centre, although various serial sizes were tested, similar experimental work needs to be carried out on different beam section sizes not considered.

Additional experimental work is, therefore, required such as.

a) Tests to investigate the influence on the failure load when the beam is loaded eccentrically.
b) Tests to investigate the interaction of multiple loads acting on a universal beam section.
c) Tests to investigate the variation of the failure load and span, when failure is obtained at the end.
d) Tests to investigate the effect of horizontal forces.
e) Tests on built-up sections to investigate the effect of the involved variables.
f) Tests to investigate the effect of stiffeners for central and end failure.

ADDENDUM

In this addendum a method for predicting the collapse load of slender plate girders subjected to patch loading in the plane of the web, very recently published by Roberts and Rockey (72), is considered.

Despite the fact that this investigation concerns slender plate girders and not universal beam sections, the theoretical analysis appears to be similar to the derived Crushing theory in chapter 6 and it is worthwhile considering.

The presented analysis is based on a plastic mechanism solution which involves consideration of the plastic hinges which develop in the flanges and the yield lines which form in the web plate. The mechanism assumed to form, between web stiffeners, is shown in figure (Ad. 1). Certain approximations and empirical modifications are introduced, to make this design method simple for hand calculations. The collapse load for slender plate girders is obtained from

$$P_u = \frac{4M_f}{\beta} + \frac{4\,\beta\,M_w}{\alpha\,\cos\,\theta} + \frac{2\,c\,M_w}{\alpha\,\cos\,\theta} - \frac{2\,n\,M_w}{\alpha\,\cos\,\theta} \qquad \text{Ad.1}$$

where

$$\beta^2 = M_f\,\alpha\,\cos\theta\,/M_w \qquad \text{Ad.2}$$

M_f and M_w is the plastic moment of the flange and web respectively

β, α, and c are lengths, as shown in figure (Ad. 1)

θ is the hinge rotation

n is the length of the web plate beneath the load which is assumed to have yielded, due to the presence of compressive

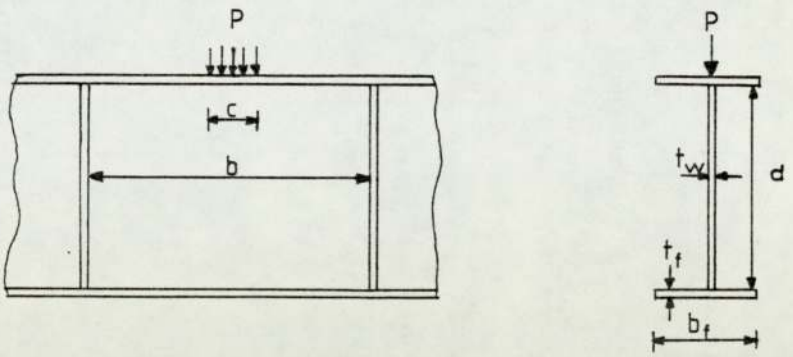

a. Details of loading and girder dimensions

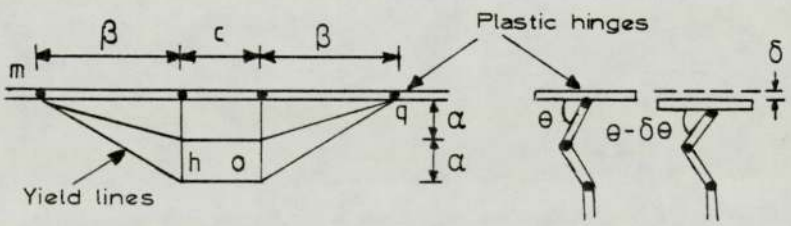

b. Mechanism assumed

FIGURE Ad.1 FAILURE MECHANISM CONSIDERED BY ROBERTS AND ROCKEY

membrane stresses.

For stocky girders the collapse load is obtained from

$$P_u = \frac{4M_f}{\beta} + \sigma_w t_w (\beta + c) \qquad \text{Ad. 3}$$

$$\beta^2 = 4M_f/\sigma_w t_w \qquad \text{Ad. 4}$$

where

σ_w and t_w is the yield stress and thickness of the web respectively

Most of the experimental results from references (73), (65) (66), (74) and (75), used to verify this method, have a d/t_w ratio ranging from 150 to 400. Although the d/t ratio for the universal beams is well below these values, the experimental results of series VI, VII and VIII from the present work are compared with this method, as displayed in table (Ad. 1). The predicted loads have been calculated using equations (Ad. 3) and (Ad. 4). As could be seen from the comparison, the proposed method is very unsatisfactory for cases where the load is applied through large lengths of bearing and for cases with relatively long lengths of span. Although, this method fails to predict safe results for the same cases the other examined design codes failed too, the crushing theory derived in chapter 6, as has been shown in table (6.1), gives quite satisfactory results.

An advantage of the crushing theory over the method proposed by Roberts and Rockey is the consideration of the failure mechanism when failure is obtained at the end, such a case has not been examined by Roberts and Rockey. Another advantage of the theory presented in this thesis is that it takes account of the global bending stresses. When deriving the crushing theory the global

bending stresses have been taken into consideration since this term, as indicated from the experimental results of beams in series VII, has an effect on the collapse load.

The crushing theory, therefore, when compared with the experimental results gives better agreement than any other theory or design method known to the author, and this makes it appear promising.

Series	Beam	Span /m	c /mm	P_{exp} /kN	P_u /kN	$\frac{P_{exp}}{P_u}$
VI	31	1.00	0	208.0	108.13	1.923
	30	1.00	50.0	270.0	211.97	1.273
	32	1.00	100.0	310.0	323.03	0.960
	33	1.00	150.0	350.0	426.67	0.820
	34	1.00	250.0	395.0	604.66	0.653
	50	1.40	0	185.0	106.16	1.742
	51	1.40	50.0	217.5	174.59	1.245
	52	1.40	150.0	240.0	350.20	0.685
	53	1.40	250.0	265.0	527.29	0.503
	62	0.50	0	322.5	175.58	1.837
	63	0.50	150.0	495.0	508.36	0.974
	60	1.25	12.7	860.0	531.28	1.619
	61	1.25	12.7	1060.0	799.46	1.326
	64	2.00	0	285.0	184.11	1.548
	65	2.00	50.0	350.0	292.75	1.196
	66	2.00	150.0	460.0	506.51	0.908
	67	2.00	300.0	530.0	851.63	0.622
	68	1.00	0	190.0	93.82	2.025
	69	1.00	0	180.0	92.93	1.937
	70	1.00	150.0	297.5	398.64	0.746
	71	1.00	150.0	260.0	385.99	0.674
	72	1.40	0	140.0	92.74	1.510
	73	1.40	0	127.5	82.77	1.540
	74	1.40	150.0	190.0	396.86	0.479
	75	1.40	150.0	172.5	387.33	0.445
VII	44	0.50	12.7	237.5	135.48	1.735
	35	1.00	12.7	215.0	142.48	1.508
	45	2.00	12.7	145.0	134.15	1.081
	46	3.00	12.7	100.0	132.75	0.735
	48	0.50	12.7	300.0	179.51	1.671
	47	1.00	12.7	272.5	178.24	1.529
	49	3.00	12.7	135.0	172.25	0.784

TABLE Ad. 1 COMPARISON OF TEST RESULTS TO THE PROPOSED METHOD BY ROBERTS AND ROCKEY

Series	Beam	Span /m	c /mm	P_{exp} /kN	P_u /kN	$\frac{P_{exp}}{P_u}$
VII	58	3.50	12.7	250.0	218.53	1.142
	59	0.75	12.7	168.75	136.50	1.236
	54	0.50	100.0	470.0	437.31	1.075
	55	1.00	100.0	430.0	436.72	0.984
	56	2.00	100.0	350.0	442.95	0.790
	57	3.00	100.0	280.0	461.13	0.607
VIII*	77	1.00	50.0	240.0	208.84	1.149
	76	1.00	50.0	260.0	213.70	1.217
	78	1.00	250.0	300.0	614.13	0.488
	79	1.00	250.0	390.0	609.80	0.640
	80	1.00	50.0	250.0	208.85	1.197

* The Thickness of Loading Plate Varied

TABLE Ad.1 (CONTINUED)

APPENDIX 1

APPENDIX 1

A 1.1 STRAIN AND DEFLECTION RECORDINGS

The strain and deflection recordings for all the tested beams are shown in table (A.1). The beams in this table are given in the same order as the other test results in table (2.2) and table (3.1).

The strain and mechanical deflection gauge reference numbers are in accordance with figure (2.5) and figure (2.6) respectively. In cases where the strain readings were manually recorded, the strain at failure is not included in these recordings. However, if such readings were recorded their accuracy could not be guaranteed due to instability of the test beam at that point. The same reasoning applies to the absence of any deflection recordings at failure.

The readings in table (A.1) are:

Strain $\times 10^{-6}$ for the strains and

Deflection $\times 10^{-2}$ (mm) for the deflections.

Test No 11a

Load (kN)	40	80	100	120	140	160	180	200	220	240	255 Failure
Strain Gauge 1	-159	-285	1346	-416	-490	-571	-647	-726	-815	-950	
2	-116	-229	-286	-347	-413	-492	-566	-634	-709	-806	
Deflection Gauge 1	44	59	65	71	84	108	144	191	256	341	
2	58	91	106	122	140	163	193	229	272	329	
3	-7	-20	-20	-15	-12	-11	-10	-10	-12	-16	
4	7	7	7	7	7	7	11	13	24	47	

TABLE A.1 STRAIN AND DEFLECTION READINGS

Test No 7a

Load (kN)	40	80	100	120	140	160	180	200	220	240	260 Failure
Strain Gauge 1	-139	-275	-343	-410	-488	-573	-657	-751	-838	-938	
2	-93	-238	-297	-355	-439	-435	-618	-701	-792	-917	
Deflection Gauge 1	52	68	75	81	95	119	150	190	246	331	
2	58	89	105	121	141	165	189	220	258	317	
3	-17	-31	-32	-30	-29	-31	-36	-43	-51	-61	
4	24	26	38	46	54	62	72	77	85	91	

TABLE A.1 (CONTINUED)

Test No 7b

Load (kN)	40	80	120	140	160	180	200	220	240	260	270 Failure
Strain Gauge 1	-89	-192	-291	-341	-399	-468	-523	-603	-686	-680	
2	-179	-326	-469	-557	-670	-783	-896	-1053	-1251	-1612Y	
Deflection Gauge 1	44	58	69	82	100	122	152	198	263	367	
2	54	78	107	125	145	167	193	227	271	336	
3	-21	-36	-42	-41	-37	-37	-36	-34	-31	-30	
4	25	27	39	48	58	65	70	73	80	82	

TABLE A.1 (CONTINUED)

Test No 6b

Load (kN)	40	80	100	120	140	160	180	200	220	240	257.5 Failure
Strain Gauge 1	-129	-243	-303	-358	-412	-467	-528	-586	-642	-666	
2	-133	-262	-325	-388	-492	-630	-770	-913	-1082	-1350	
Deflection Gauge 1	48	62	67	73	83	104	132	169	219	297	
2	62	78	89	100	120	142	167	195	229	277	
3	14	13	14	15	17	19	18	19	19	18	

TABLE A.1 (CONTINUED)

Test No 8a

Load (kN)	40	80	100	120	140	160	180	200	220	240	260 Failure
Strain Gauge 1	-8	-77	-120	-173	-235	-344	-446	-612	-777	-961	
2	-259	-426	-510	-591	-675	-794	-917	-1090	-1249	-1381	
Deflection Gauge 1	63	76	82	89	99	112	130	153	186	227	
2	78	106	119	134	139	167	186	207	232	275	
3	6	16	17	17	15	13	14	15	17	22	
4	59	75	83	91	99	105	110	119	136	176	

TABLE A.1 (CONTINUED)

Test No 8b

Load (kN)	40	80	120	160	180	200	220	240	260	280	285 Failure
Strain Gauge 1	-124	-238	-362	-501	-590	-647	-712	-784	-842	-844	
2	-138	-268	-390	-566	-689	-816	-962	-1148	-1426	-1620Y	
Deflection Gauge 1	67	83	99	125	150	183	222	272	336	376	
2	103	133	165	202	226	253	285	320	364	394	
3	-27	-34	-33	-26	-25	-27	-31	-34	-38	-41	
4	6	11	23	44	54	61	73	80	92	95	

TABLE A.1 (CONTINUED)

Test No 3

Load (kN)	40	80	120	140	160	180	200	220	240	260	280 Failure
Strain Gauge 1	-48	-136	-233	-280	-327	-365	-404	-443	-492	-542	
2	-145	-228	-300	-333	-361	-394	-434	-478	-530	-592	
Deflection Gauge 1	23	37	46	56	68	84	105	135	185	245	
2	49	82	111	123	139	157	178	203	283	288	
3	0	23	63	78	92	99	104	104	102	99	
4	50	59	60	57	53	49	47	46	42	31	

TABLE A.1 (CONTINUED)

Test No 5a

Load (kN)	40	80	120	160	200	220	240	260	280	300	310 Failure
Strain Gauge 1	-111	-232	-354	-485	-626	-687	-763	-879	-1030	-1121	
2	-162	-293	-434	-566	-707	-788	-874	-995	-1151	-1302	
Deflection Gauge 1	26	43	67	104	155	190	240	307	388	479	
2	53	73	98	131	177	206	241	288	344	404	
3	2	18	28	31	38	49	49	53	66	85	

TABLE A.1 (CONTINUED)

Test No 5b

Load (kN)	40	80	120	160	200	220	240	260	280	300	320 Failure
Strain Gauge 1	-130	-245	-372	-503	-716	-837	-942	-1066	-1190	-1330	
2	-118	-232	-339	-454	-617	-696	-773	-839	-924	-994	
Deflection Gauge 1	36	52	66	78	105	123	146	179	214	259	
2	48	69	89	114	147	167	191	219	252	290	
3	3	12	11	4	5	6	8	11	14	20	

TABLE A.1 (CONTINUED)

Test No 6a

Load (kN)	40	80	120	160	200	240	260	280	300	320	339 Failure
Strain Gauge 1	-97	-208	-325	-442	-540	-650	-773	-916	-1075	-1214	
2	-125	-227	-315	-410	-521	-705	-799	-917	-1029	-1159	
Deflection Gauge 1	50	76	91	105	114	127	140	157	177	199	
2	39	56	75	97	120	145	160	178	198	223	
3	27	40	47	52	57	63	65	68	71	74	

TABLE A.1 (CONTINUED)

Test No 10a

Load (kN)	40	80	120	160	200	240	280	320	360	400	410 Failure
Strain Gauge 1	-124	-213	-318	-429	-526	-635	-763	-934	-1069	-1071	
2	-55	-128	-195	-251	-324	-421	-540	-744	-1103	-1749Y	
Deflection Gauge 1	40	50	57	64	68	74	79	87	97	111	
2	57	86	116	143	168	194	221	253	329	592	
3	2	4	-5	-18	-21	-24	-31	-35	-33	-44	
4	6	12	15	10	9	9	8	5	-24	-105	

TABLE A.1 (CONTINUED)

Test No 12a

Load (kN)	80	160	200	240	280	320	360	400	420	440	450 Failure
Strain Gauge 1	-108	-267	-338	-410	-505	-589	-623	-420	-272	-7	
2	-171	-281	-340	-415	-482	-587	-860	-1246	-1565	-1878Y	
Deflection Gauge 1	38	48	53	59	65	71	76	89	102	122	
2	83	138	162	187	213	247	318	588	913	1498	
3	64	59	50	50	47	36	2	3	17	33	
4	14	12	13	13	14	-2	69	139	195	256	

TABLE A.1 (CONTINUED)

Test No 1

Load (kN)	40	80	120	160	200	220	240	260	280	300	315 Failure
Strain Gauge 1	-60	-135	-215	-300	-390	-410	-460	-490	-530	-540	
2	-135	-235	-330	-440	-565	-645	-725	-865	-1025	-1205	
Deflection Gauge 1	22	30	37	42	48	52	60	70	89	130	
2	58	89	118	143	166	180	199	218	243	280	
3	-1	27	66	99	109	104	93	84	62	28	
4	8	9	9	9	10	47	47	46	46	7	

TABLE A.1 (CONTINUED)

Test No 2a

Load (kN)	40	80	120	160	200	240	260	280	300	320	325 Failure
Strain Gauge 1	-70	-140	-250	-340	-420	-460	-480	-640	-680	-700	
2	-120	-220	-310	-420	-460	-660	-720	-830	-890	-985	
Deflection Gauge 1	15	24	43	54	67	78	94	101	106	112	
2	60	92	121	147	173	194	200	226	242	289	
3	-2	-4	2	7	7	9	25	27	20	7	
4	10	11	14	14	19	20	22	35	24	18	

TABLE A.1 (CONTINUED)

Test No 2b

Load (kN)	40	80	120	160	200	240	260	280	300	320	340 Failure
Strain Gauge 1	-80	-170	-270	-370	-460	-575	-650	-750	-840	-940	
2	-130	-220	-305	-400	-495	-610	-700	-780	-860	-930	
Deflection Gauge 1	17	24	30	35	39	46	57	71	90	109	
2	71	102	129	157	182	208	226	247	268	305	
3	-24	-3	23	40	47	49	46	45	44	45	
4	12	22	23	23	23	23	23	24	25	50	

TABLE A.1 (CONTINUED)

Test No 4b

Load (kN)	40	80	100	120	140	160	180	200	220	240	245 Failure
Strain Gauge 1	-103	-204	-288	-341	-383	-415	-447	-487	-525	-549	
2	-159	-280	-348	-415	-495	-578	-669	-776	-902	-1071	
Deflection Gauge 1	40	62	77	101	136	172	228	288	369	461	
2	73	110	139	167	199	234	272	315	366	424	
3	21	36	39	49	62	77	112	129	139	160	

TABLE A.1 (CONTINUED)

Test No 11b

Load (kN)	40	80	120	140	160	180	200	220	240	260	265 Failure
Strain Gauge 1	-94	-206	-312	-362	-411	-481	-547	-613	-694	-883	
2	-153	-275	-395	-465	-559	-676	-759	-871	-984	-1066	
Deflection Gauge 1	46	61	70	76	88	110	143	184	234	324	
2	58	86	123	139	157	177	201	233	272	328	
3	6	-6	-16	-18	-20	-31	-37	-45	-54	-63	
4	13	15	23	31	38	45	50	63	85	218	

TABLE A.1 (CONTINUED)

Test No 13a

Load (kN)	40	80	120	160	180	200	220	240	260	280	297.5 Failure
Strain Gauge 1	-75	-170	-281	-391	-477	-590	-714	-844	-965	-1085	
2	-135	-258	-361	-498	-604	-731	-891	-1011	-1133	-1263	
Deflection Gauge 1	32	44	56	67	77	94	119	159	199	255	
2	48	77	109	141	157	178	202	232	264	300	
3	-25	-22	-27	-22	-27	-27	-27	-31	-33	-33	
4	2	7	14	26	30	32	34	38	46	80	

TABLE A.1 (CONTINUED)

Test No 13b

Load (kN)	40	80	120	160	200	240	260	280	300	320	340 Failure
Strain Gauge 1	-478	-556	-639	-739	-882	-1144	-1281	-1399	-1500	-1549	
2	-104	-226	-337	-468	-681	-1048	-1268	-1468	-1687Y	-1882Y	
Deflection Gauge 1	39	50	66	71	92	139	172	211	257	311	
2	75	114	253	289	328	481	413	446	491	545	
3	-18	-30	-20	-13	-11	-8	-8	-6	-5	-3	
4	9	12	15	17	22	34	45	56	75	110	

TABLE A.1 (CONTINUED)

Test No 14

Load (kN)	40	80	120	160	200	240	280	320	360	380	390 Failure
Strain Gauge 1	-107	-190	-288	-387	-499	-688	-949	-1238	-1410	-1342	
2	-30	-107	-177	-256	-394	-662	-1141	-1717Y	-2194Y	-2452Y	
Deflection Gauge 1	34	43	52	65	82	118	184	263	366	424	
2	47	74	104	131	158	200	257	334	467	614	
3	-2	-6	-3	11	16	27	51	52	55	58	
4	-3	-1	7	20	32	55	112	137	175	239	

TABLE A.1 (CONTINUED)

Test No 15

Load (kN)	40	80	120	160	200	240	280	320	360	380	400 Failure
Strain Gauge 1	-76	-144	-230	-314	-442	-610	-868	-1240	-1604Y	-1836Y	
2	-53	-94	-148	-198	-288	-448	-659	-970	-1245	-1304	
Deflection Gauge 1	32	44	55	65	79	106	152	227	307	360	
2	58	89	121	152	181	218	265	334	430	533	
3	-16	-17	-25	-36	-39	-42	-50	-51	-65	-67	
4	-3	-9	-11	-7	-5	-2	2	-2	38	77	

TABLE A.1 (CONTINUED)

Test No 16

Load (kN)	40	80	120	160	200	240	280	320	360	400	420 Failure
Strain Gauge 1	-10	-23	-49	-71	-96	-140	-185	-211	-170	-192	
2	-26	-47	-74	-104	-158	-235	-314	-392	-479	-521	
Deflection Gauge 1	26	32	42	52	59	79	130	179	262	326	
2	38	38	96	125	155	191	235	299	408	815	
3	-2	-2	-11	-10	-10	-10	-12	-13	-29	-47	
4	17	17	21	23	24	24	21	26	43	71	

TABLE A.1 (CONTINUED)

Test No 18

Load (kN)	40	80	120	160	200	240	280	320	360	440	440 Failure
Strain Gauge 1	-3	-14	-49	-86	-125	-166	-231	-259	-960	-280	
2	-10	-43	-46	-46	-72	-103	-133	-144	-88	91	
Deflection Gauge 1	96	99	107	115	128	163	193	240	297	339	
2	75	112	141	171	202	238	285	348	457	27	
3	7	1	2	10	11	16	24	36	57	76	
4	23	24	29	34	42	41	44	37	30	42	

TABLE A.1 (CONTINUED)

Test No 20

Load (kN)	80	120	160	200	240	280	320	360	400	440	450 Failure
Strain Gauge 1	49	79	84	81	83	79	43	-45	-197	-263	
2	-64	-88	-87	-77	-62	-84	-134	-282	-563	-1392	
Deflection Gauge 1	57	58	68	80	105	143	186	250	261	208	
2	108	140	175	210	248	294	366	505	929	1440	
3	76	82	89	94	101	112	156	223	296	401	
4	63	74	77	74	74	73	71	52	26	-71	

TABLE A.1 (CONTINUED)

Test No 22

Load (kN)		80	120	160	200	240	280	320	360	400	440	455 Failure
Strain Gauge	1	59	70	75	78	85	102	131	220	394	835	
	2	-30	-35	-40	-46	-50	-46	-19	37	159	330	
Deflection Gauge	1	39	51	63	78	102	142	191	264	262	222	
	2	109	142	175	209	245	290	352	478	792	1422	
	3	-2	-7	-13	-16	-20	-39	-53	-51	-43	-49	
	4	-18	-22	-27	-33	-37	-50	-53	-13	82	151	

TABLE A.1 (CONTINUED)

Test No 36

Load (kN)	40	80	120	160	200	240	260	280	300	320	330 Failure
Strain Gauge 1	-105	-214	-317	-430	-673	-1038	-1165	-1287	-1436	-1618Y	
2	-112	-192	-305	-465	-731	-1122	-1271	-1429	-1544	-1576Y	
Deflection Gauge 1	46	60	82	101	139	197	244	290	345	390	
2	57	96	137	176	222	284	323	368	425	502	
3	26	66	97	103	104	109	109	116	117	143	
4	17	35	48	54	61	66	76	81	82	70	

TABLE A.1 (CONTINUED)

Test No 37

Load (kN)	40	80	120	160	200	200	240	260	280	300	310 Failure
Strain Gauge 1	-74	-173	-297	-444	-691	-865	-1021	-1017	-1161	-1171	
2	-136	-213	-292	-431	-753	-943	-1185	-1382	-1610Y	-1908Y	
Deflection Gauge 1	39	49	61	77	117	142	168	219	257	314	
2	59	98	135	170	225	254	292	338	398	495	
3	-13	11	41	42	41	33	33	32	31	15	
4	2	8	19	25	44	48	61	85	118	155	

TABLE A.1 (CONTINUED)

Test No 38

Load (kN)	40	80	120	160	180	200	220	240	260	280	290 Failure
Strain Gauge 1	-100	-215	-315	-478	-602	-785	-973	-1180	-1380	-1690Y	
2	-69	-114	-205	-349	-472	-642	-818	-973	-1053	-989	
Deflection Gauge 1	42	56	72	88	105	127	159	196	234	284	
2	65	102	143	182	206	236	275	326	382	491	
3	-11	-3	43	48	49	50	58	59	79	93	
4	-12	-3	6	6	6	8	13	19	19	8	

TABLE A.1 (CONTINUED)

Test No 39

Load (kN)	40	80	120	160	200	240	280	320	360	400	407.5 Failure
Strain Gauge 1	-12	-51	-120	-185	-283	-430	-619	-815	-964	-1000	
2	-183	-272	-350	-462	-626	-881	-1234	-1950Y	-1950Y	-2285Y	
Deflection Gauge 1	46	58	67	77	86	115	150	186	251	325	
2	48	80	115	141	167	199	241	298	345	472	
3	-92	-70	-51	-49	-49	-49	-46	-47	-55	-75	
4	-12	1	11	15	21	26	31	45	66	136	

TABLE A.1 (CONTINUED)

Test No 40

Load (kN)	40	80	120	160	200	240	280	320	360	380	400 Failure
Strain Gauge 1	-102	-206	-286	-401	-581	-818	-1133	-1443	-1763Y	-1894Y	
2	-108	-166	-258	-373	-518	-764	-1041	-1314	-1562Y	-1640Y	
Deflection Gauge 1	42	53	64	77	90	112	148	192	246	286	
2	54	72	106	136	165	197	238	289	352	398	
3	-12	-2	-2	-8	29	25	13	-15	-39	-74	
4	-3	6	9	15	18	18	18	19	19	18	

TABLE A.1 (CONTINUED)

Test No 41

Load (kN)	40	80	120	160	200	240	280	320	360	380	397.5 Failure
Strain Gauge 1	-74	-194	-296	-320	-528	-758	-1040	-1334	-1566Y	-1710Y	
2	-137	-212	-291	-406	-577	-847	-1173	-1496Y	-1722Y	-1781Y	
Deflection Gauge 1	44	48	71	92	110	138	177	227	294	335	
2	53	93	122	152	180	215	259	322	402	455	
3	9	46	74	77	79	79	82	80	80	76	
4	3	13	24	27	32	34	38	38	45	23	

TABLE A.1 (CONTINUED)

Test No 42

Load (kN)	40	80	120	160	200	240	280	320	360	380	390 Failure
Strain Gauge 1	-113	-213	-316	-422	-623	-915	-1264	-1639Y	-1951Y	-2074Y	
2	-209	-301	-371	-482	-635	-892	-1153	-1426	-1640Y	-1746Y	
Deflection Gauge 1	34	47	59	75	91	122	163	215	287	326	
2	37	67	101	131	159	197	242	309	412	485	
3	18	-1	-21	-15	-6	5	26	65	117	151	
4	14	11	3	2	1	1	11	13	15	16	

TABLE A.1 (CONTINUED)

Test No 43

Load (kN)	40	80	120	160	200	240	280	320	360	380	385 Failure
Strain Gauge 1	-76	-186	-271	-410	-634	-934	-1279	-1554Y	-1811Y	-1918Y	
2	-105	-129	-211	-351	-532	-831	-1197	-1494Y	-1743Y	-1827Y	
Deflection Gauge 1	62	79	101	118	142	181	238	312	396	446	
2	65	96	133	165	201	246	309	389	534	651	
3	-3	22	40	38	35	34	31	24	10	6	
4	7	22	30	31	39	51	59	56	50	41	

TABLE A.1 (CONTINUED)

Test No 26a

Load (kN)	40	80	100	120	140	160	180	200	220	240	258 Failure
Strain Gauge 1	-140	-268	-334	-393	-475	-527	-606	-688	-797	-947	
2	-188	-323	-391	-448	-517	-601	-664	-744	-818	-893	
Deflection Gauge 1	45	57	63	72	85	99	123	155	193	245	
2	55	93	111	132	154	174	198	230	262	300	
3	103	125	126	125	125	128	131	134	135	137	
4	42	30	19	9	2	-3	-10	-17	-31	-66	

TABLE A.1 (CONTINUED)

Test No 25a

Load (kN)	40	80	120	140	160	180	200	220	240	260	270 Failure
Strain Gauge 1	-72	-193	-306	-362	-404	-460	-525	-607	-707	-852	
2	-178	-307	-428	-504	-580	-655	-730	-817	-886	-962	
Deflection Gauge 1	39	53	61	67	70	79	95	118	146	190	
2	191	272	348	389	429	473	518	572	640	734	
3	-19	-30	-34	-35	-36	-36	-36	-37	-42	-45	
4	20	30	43	46	51	66	70	78	100	168	

TABLE A.1 (CONTINUED)

Test No 25b

Load (kN)	40	80	120	160	200	220	240	260	280	300	320 Failure
Strain Gauge 1	-129	-205	-295	-391	-517	-593	-664	-725	-786	-840	
2	-68	-183	-294	-349	-562	-652	-755	-902	-1066	-1242	
Deflection Gauge 1	14	47	56	63	72	79	89	105	128	159	
2	56	102	115	140	173	188	206	224	247	277	
3	45	40	48	53	57	56	55	52	49	41	
4	20	25	27	29	40	41	41	45	46	39	

TABLE A.1 (CONTINUED)

Test No 26b

Load (kN)	40	80	120	160	200	240	260	280	300	320	340 Failure
Strain Gauge 1	-189	-295	-410	-517	-630	-771	-849	-912	-960	-965	
2	-119	-218	-301	-393	-528	-727	-849	-1004	-1212	-1504	
Deflection Gauge 1	140	158	166	171	177	187	194	202	213	232	
2	69	111	139	165	193	221	236	252	273	300	
3	24	26	14	6	6	7	8	10	13	19	
4	45	63	82	97	109	134	143	153	173	211	

TABLE A.1 (CONTINUED)

Test No 24b

Load (kN)	40	80	120	160	200	240	280	300	320	340	350 Failure
Strain Gauge 1	-157	-263	-379	-479	-570	-708	-897	-1051	-1218	-1416	
2	-54	-140	-224	-305	-399	-535	-739	-850	-997	-1168	
Deflection Gauge 1	18	77	84	106	105	105	121	120	134	162	
2	81	114	147	178	206	231	223	280	305	346	
3	42	73	109	130	132	145	157	163	164	171	
4	25	27	34	36	36	31	20	6	-18	-81	

TABLE A.1 (CONTINUED)

Test No 27

Load (kN)	40	80	120	160	200	240	280	320	360	380	390 Failure
Strain Gauge 1	-108	-186	-274	-356	-426	-517	-637	-746	729	-391	
2	-55	-132	-212	-285	-369	-514	-704	-1021	-1642Y	-2307Y	
Deflection Gauge 1	39	48	56	64	70	76	84	95	110	123	
2	66	98	129	156	181	206	235	280	360	485	
3	7	-2	8	16	17	13	6	-9	-26	-34	
4	15	-26	37	46	50	58	68	91	184	302	

TABLE A.1 (CONTINUED)

Test No 28

Load (kN)	40	80	120	160	200	240	280	320	360	400	420 Failure
Strain Gauge 1	-70	-142	-226	-289	-364	-444	-547	-668	-799	-960	
2	-18	-49	-91	-156	-232	-341	-457	-589	-788	-1194	
Deflection Gauge 1	34	47	60	67	74	80	87	93	100	107	
2	157	233	322	386	454	518	592	675	869	1595	
3	-10	-12	-2	5	8	9	15	18	56	111	
4	17	31	41	41	50	53	57	59	65	74	

TABLE A.1 (CONTINUED)

Test No R1b

Load (kN)	40	80	120	160	180	200	220	240	260	280	295 Failure
Strain Gauge 1	-124	-269	-412	-561	-634	-708	-795	-898	-1008	-1106	
2	-165	-320	-422	-566	-647	-721	-806	-898	-1009	-1154	
Deflection Gauge 1	34	52	67	93	109	127	151	180	218	265	
2	55	93	123	159	176	195	216	239	261	300	
3	8	17	18	21	25	28	31	38	45	50	
4	-4	-20	-42	-42	-42	-36	-35	-29	-13	20	

TABLE A.1(CONTINUED)

Test No R1a

Load (kN)	40	80	120	160	200	240	280	320	360	400	420 Failure
Strain Gauge 1	-83	-189	-288	-385	-475	-590	-717	-984	-1357	-1721Y	
2	-121	-231	-321	-421	-541	-662	-810	-980	-1189	-1342	
Deflection Gauge 1	52	64	69	75	80	87	96	112	134	170	
2	80	119	148	174	197	219	243	269	299	364	
3	4	12	13	9	10	12	16	24	23	15	
4	-3	-4	-13	-8	-7	-8	10	30	40	70	

TABLE A.1 (CONTINUED)

Test No R2

Load (kN)	80	120	160	200	240	280	320	360	400	440	460 Failure
Strain Gauge 1	-194	-309	-426	-528	-561	-640	-751	-851	-854	-604	
2	-212	-312	-402	-504	-598	-711	-878	-1106	-1478	-2084Y	
Deflection Gauge 1	84	91	98	104	109	117	127	138	155	179	
2	142	178	206	229	249	273	299	320	379	495	
3	-45	-49	-49	-50	-52	-52	-53	-53	-76	-153	
4	35	51	51	68	81	90	111	137	184	270	

TABLE A.1 (CONTINUED)

Test No 23b

Load (kN)	20	40	60	80	100	120	140	160	180	190	198 Failure
Strain Gauge 1	-41	-119	-191	-281	-337	-340	-493	-564	-708	-905	
2	-126	-210	-285	-364	-442	-530	-615	-727	-824	-858	
Deflection Gauge 1	44	59	74	86	104	141	191	270	364	464	
2	45	67	85	103	125	162	206	268	340	405	
3	66	68	75	82	84	87	90	91	95	97	
4	-5	-5	-5	-4	2	17	28	45	80	162	

TABLE A.1 (CONTINUED)

Test No 23a

Load (kN)	20	40	60	80	100	120	140	150	160	170	180 Failure
Strain Gauge 1	-62	-125	-237	-312	-429	-516	-593	-629	-668	-724	
2	-112	-214	-325	-396	-478	-585	-701	-766	-844	-942	
Deflection Gauge 1	42	55	67	83	118	172	255	300	355	420	
2	52	74	90	110	142	188	291	390	436	486	
3	11	14	12	13	18	32	50	51	55	61	
4	18	27	30	30	41	48	63	75	98	134	

TABLE A.1 (CONTINUED)

Test No 29b

Load (kN)	20	40	60	70	80	90	100	110	120	130	140 Failure
Strain Gauge 1	-139	-245	-356	-420	-478	-540	-604	-678	-755	-844	
2	-104	-222	-342	-398	-453	-526	-592	-668	-745	-857	
Deflection Gauge 1				DAMAGED GAUGE							
2	94	132	154	172	198	237	265	305	350	407	
3	25	41	39	37	34	30	29	58	29	30	
4	4	20	27	27	28	27	27	29	33	37	

TABLE A.1 (CONTINUED)

Test No 29a

Load (kN)	20	40	60	70	80	90	100	110	120	130	140 Failure
Strain Gauge 1	-49	-254	-403	-518	-579	-690	-801	-922	-1041	-1162	
2	-108	-175	-197	-212	-224	-243	-268	-276	-289	-325	
Deflection Gauge 1	43	66	91	109	132	157	190	230	276	341	
2	80	107	134	149	168	193	224	262	305	363	
3	23	8	4	5	9	12	30	32	31	30	
4	27	25	14	11	10	9	3	1	-15	-58	

TABLE A.1 (CONTINUED)

Test No 31

Load (kN)	20	40	60	80	100	120	140	160	180	200	208 Failure
Strain Gauge 1	5	-46	-115	-159	-191	-259	-350	-452	571	-833	
2	-118	-188	-256	-319	-381	-457	-552	-665	-808	-1132	
Deflection Gauge 1	7	9	19	33	47	50	50	47	40	21	
2	18	15	27	44	56	57	57	56	52	23	
3	9	10	21	36	44	46	47	48	48	36	
4	63	81	99	116	132	148	165	184	209	245	

TABLE A.1 (CONTINUED)

Test No 30

Load (kN)	40	80	120	140	160	180	200	220	240	260	270 Failure
Strain Gauge 1	120	-26	-185	-261	-329	-422	-548	-687	-890	-1242	
2	-326	-454	-549	-572	-605	-635	-667	-674	-662	-611	
Deflection Gauge 1	7	44	69	76	85	93	96	103	111		
2	49	62	66	61	61	65	71	90	112		
3	55	81	92	92	93	94	94	102	106		
4	96	126	156	178	191	197	211	227	250		

TABLE A.1 (CONTINUED)

Test No 32

Load (kN)	40	80	120	160	200	220	240	260	280	300	310 Failure
Strain Gauge 1	-5	-68	-166	-311	-449	-517	-586	-639	-712	-787	
2	-186	-281	-380	-444	-522	-551	-578	-629	-693	-721	
Deflection Gauge 1	40	32	26	66	88	105	117	132	150	172	
2	0	-10	-17	22	42	58	67	74	81	77	
3	-4	-13	-21	0	14	23	34	41	50	65	
4	81	117	147	173	200	214	230	248	269	295	

TABLE A.1 (CONTINUED)

Test No 33

Load (kN)	40	80	120	160	200	240	280	300	320	340	350 Failure
Strain Gauge 1	-89	-150	-217	-239	-322	-417	-492	-535	-582	-558	
2	-98	-190	-282	-371	-443	-512	-606	-650	-706	-770	
Deflection Gauge 1	-6	27	54	56	52	47	42	37	32	20	
2	2	23	49	51	51	51	51	48	40	37	
3	-1	16	41	42	42	44	44	33	33	28	
4	76	111	141	167	194	222	253	274	299	342	

TABLE A.1 (CONTINUED)

Test No 34

Load (kN)	40	80	120	160	200	240	280	320	360	380	395 Failure
Strain Gauge 1	-88	-129	-170	-230	-249	-340	-395	-435	-418	-383	
2	3	-46	-105	-150	-198	-237	-262	-277	-279	-241	
Deflection Gauge 1	8	38	68	77	79	80	81	81	86	86	
2	-13	3	29	32	32	31	31	31	31	27	
3	-14	-4	17	19	20	20	20	20	19	19	
4	90	121	151	180	205	236	268	308	368	421	

TABLE A.1 (CONTINUED)

Test No 50

Load (kN)	20	40	60	80	100	120	140	160	170	180	185 Failure
Strain Gauge 1	-20	-52	-81	-110	-136	-162	-188	-207	-217	-224	-257
2	-22	-52	-77	-106	-136	-168	-203	-238	-262	-268	-223
3	6	4	4	6	9	13	21	39	53	71	133
4	5	11	15	17	17	18	20	21	19	10	-45
5	-34	-98	-145	-197	-244	-305	-394	-512	-613	-809	208
6	-55	-107	-161	-223	-291	-376	-499	-662	-779	-904	-1505
7	11	11	14	17	19	23	30	48	61	83	151
8	8	6	4	1	0	-2	-4	-7	-11	-26	-81
9	-9	-31	-55	-78	-115	-153	-191	-219	-262	-245	-267
10	-36	-73	-102	-134	-153	-168	-188	-209	-232	-242	-177
11	-91	-219	-319	-425	-527	-655	-829	-1100	-1104	-1033	379
12	-118	-216	-318	-431	-554	-696	-893	-1078	-1448	-2036Y	-676
Deflection Gauge 1	-2	7	3	-3	-13	-21	-26	-24	-16	-28	
2	-1	5	2	-5	-13	-20	-25	-28	-26	-58	
3	106	145	172	201	227	255	290	333	363	420	

TABLE A.1 (CONTINUED)

Test No 51

Load (kN)	20	40	60	80	100	120	140	160	180	200	217.5 Failure
Strain Gauge 1	-37	-64	-89	-112	-137	-162	-187	-217	-255	-297	-316
2	-9	-34	-59	-88	-116	-143	-169	-191	-212	-233	-247
3	-14	-9	-4	0	3	9	17	25	34	44	56
4	32	38	44	46	51	54	56	58	57	48	35
5	-126	-188	-255	-318	-389	-454	-511	-558	-609	-663	-669
6	19	-23	-67	-103	-140	-179	-227	-290	-369	-460	-511
7	-18	-14	-10	-8	-5	-2	1	6	12	18	26
8	27	29	32	35	37	39	40	40	39	33	22
9	-43	-65	-81	-91	-100	-110	-123	-141	-163	-189	-194
10	-16	-51	-92	-136	-185	-229	-275	-313	-353	-393	-421
11	-228	-329	-444	-559	-684	-795	-886	-951	-1036	-1157	-1200
12	31	-45	-124	-194	-266	-341	-435	-554	-697	-845	-946
Deflection Gauge 1	-30	-29	-40	-57	-73	-88	-100	-103	-104	-104	
2	-19	-19	-30	-47	-63	-74	-80	-79	-78	-79	
3	87	103	148	182	209	235	263	291	321	359	

TABLE A.1 (CONTINUED)

Test No 52

Load (kN)	40	60	80	100	120	140	160	180	200	220	240 Failure
Strain Gauge 1	-36	-62	-89	-115	-134	-143	-157	-162	-180	-190	-221
2	-67	-92	-122	-185	-185	-235	-277	-329	-393	-448	-495
3	23	24	31	36	42	48	53	54	63	67	79
4	-29	-85	-34	-20	-14	-10	-83	-46	-82	-105	-109
5	-43	-86	-124	-168	-214	-285	-340	-405	-453	-507	-503
6	-103	-137	-172	-205	-229	-234	-254	-262	-288	-292	-267
7	23	23	25	25	23	24	23	20	24	21	29
8	-38	-46	-58	-28	-12	-8	0	-13	0	-13	-28
9	123	-44	-70	-92	-110	-113	-136	-161	-189	-219	-243
10	-802	-511	-1065	-247	-358	-353	-589	-1021	-1278	-500	-1798Y
11	-25	-67	-107	-149	-206	-297	-366	-444	-507	-578	-661
12	-490	-569	-674	-421	-682	-442	-674	-1303	-935	-389	-1077
Deflection Gauge 1	0	0	-3	3	14	50	71	93	108	133	
2	-11	-11	-14	-10	-1	31	46	64	78	101	
3	114	142	170	197	223	253	279	306	332	336	

TABLE A.1 (CONTINUED)

Test No 53

Load (kN)	40	80	120	140	160	180	200	220	240	260	265 Failure
Strain Gauge 1	-97	-179	-270	-308	-342	-376	-406	-440	-474	-523	-593
2	3	-15	-28	-41	-60	-83	-107	-141	-174	-194	-223
3	-46	-46	-41	-39	-36	-38	-36	-37	-40	-47	-85
4	51	61	43	54	43	43	43	38	28	21	43
5	-153	-194	-223	-243	-263	-283	-298	-308	-316	-296	-211
6	37	-21	-98	-110	-139	-159	-182	-210	-217	-232	-327
7	-31	-28	-27	-26	-30	-31	-35	-38	-47	-72	-165
8	16	13	-6	22	8	30	23	37	23	49	109
9	-88	-167	-240	-278	-318	-357	-398	-443	-501	-566	-668
10	-130	-187	-297	-286	-332	-342	-369	-414	-456	-455	-408
11	-205	-236	-248	-257	-273	-289	-293	-285	-283	-211	98
12	91	20	-56	-79	-97	-121	-140	-149	-134	-135	-250
Deflection Gauge 1	7	-28	-63	-74	-81	-89	-101	-115	-131	-190	
2	25	-9	-34	-46	-53	-56	-71	-88	-112	-133	
3	154	174	226	252	278	304	333	363	403	459	

TABLE A.1 (CONTINUED)

Test No 62

Load (kN)	40	80	120	160	200	240	260	280	300	320	322.5 Failure
Strain Gauge 1	147	124	80	36	-18	-50	-55	-38	-25	-117	
2	-286	-423	-520	-600	-679	-792	-852	-926	-1035	-1053	
Deflection Gauge 1	173	175	169	178	183	192	201	210	218	232	
2	4	-31	-79	-196	-189	-178	-164	-141	-86	-60	
3	-53	-66	-71	-62	-56	-52	-49	-44	-24	27	
4	69	78	85	91	98	104	107	111	117	121	

TABLE A.1 (CONTINUED)

Test No 63

Load (kN)	80	160	200	240	280	320	360	400	440	480	495 Failure
Strain Gauge 1	-41	-172	-203	-250	-304	-331	-328	-311	-188	340	
2	-186	-364	-437	-501	-592	-697	-828	-983	-1246	-1838Y	
Deflection Gauge 1	74	76	82	89	95	101	106	111	107	98	
2	-22	-114	-116	-117	-119	-125	-135	-151	-202	-326	
3	2	13	13	12	8	-1	-14	-38	-106	-159	
4	48	56	66	72	79	88	103	113	132	153	

TABLE A.1 (CONTINUED)

Test No 60

Load (kN)	100	200	300	400	500	600	700	750	800	850	860 Failure
Strain Gauge 1	-45	-110	-180	-255	-340	-410	-505	-565	-685	-900	
2	-90	-175	-270	-345	-400	-495	-610	-670	-745	-735	
Deflection Gauge 1	4	4	3	-5	-11	-16	-22	-23	-24	26	
2	5	4	-4	-13	-22	-25	-19	-9	17	119	
3	7	5	0	-4	-14	-18	-8	2	58	208	
4	17	18	14	7	2	1	7	16	55	393	
5	23	24	17	12	7	10	16	22	50	300	
6	22	29	30	30	31	33	39	47	70	130	
7	87	114	138	159	181	206	234	255	285	327	

TABLE A.1 (CONTINUED)

Test No 61

Load (kN)	100	200	300	400	500	600	700	800	900	1000	1060 Failure
Strain Gauge 1	-70	-140	-215	-280	-355	-470	-495	-600	-710	-825	
2	-60	-105	-180	-265	-345	-420	-505	-620	-770	-945	
Deflection Gauge 1	81	98	104	114	115	121	123	121	96	83	
2	-43	-24	-9	-7	-4	-3	-7	-22	-51	-80	
3	45	60	69	74	77	82	77	70	21	-28	
4	-63	-49	-40	-39	-36	-33	-35	-39	-77	-131	
5	31	42	48	52	56	59	58	54	35	-3	
6	13	19	19	20	24	30	37	39	35	28	
7	0	141	175	218	252	276	305	342	396	467	

TABLE A.1 (CONTINUED)

Test No 64

Load (kN)	40	80	120	160	180	200	220	240	260	280	Failure
Strain Gauge 1	62	26	-20	-87	-126	-184	-245	-331	-467	-829	
2	-201	-287	-367	-437	-458	-487	-513	-540	-535	-273	
Deflection Gauge 1	104	120	148	165	166	166	198	201	202	206	
2	73	111	144	169	165	161	149	133	94	-100	
3	81	111	134	144	136	128	115	95	51	-20	
4	87	132	174	215	235	256	279	302	332	370	

TABLE A.1 (CONTINUED)

Test No 65

Load (kN)	40	80	120	160	200	240	280	300	320	340	350 Failure
Strain Gauge 1	33	-10	-46	-82	-120	-155	-176	-174	-166	-80	
2	-152	-230	-308	-392	-477	-566	-686	-764	-885	-1120	
Deflection Gauge 1	-29	-37	-7	24	59	56	35	30	14	-17	
2	45	51	91	120	142	149	143	130	95	-37	
3	60	68	96	123	141	148	152	152	144	92	
4	101	145	200	239	299	332	382	420	440	481	

TABLE A.1 (CONTINUED)

Test No 66

Load (kN)	80	120	160	200	240	280	320	360	400	440	460 Failure
Strain Gauge 1	-162	-252	-323	-399	-478	-557	-640	-739	-867	-1129	
2	-85	-142	-179	-225	-276	-318	-346	-356	-314	-108	
Deflection Gauge 1	25	-7	-19	-18	-8	-4	19	38	57	87	
2	48	22	18	23	42	55	66	93	143	258	
3	48	34	35	43	58	73	91	123	171	309	
4	118	174	199	237	290	320	363	407	449	503	

TABLE A.1 (CONTINUED)

Test No 67

Load (kN)	80	160	240	280	320	360	400	440	480	520	530 Failure
Strain Gauge 1	-123	-297	-484	-567	-654	-751	-863	-968	-1086	-1140	
2	-71	-109	-136	-147	-154	-156	-147	-141	-101	-17	
Deflection Gauge 1	64	130	223	251	289	325	367	400	457	495	
2	59	146	251	284	326	370	420	457	530	701	
3	34	100	177	216	254	289	332	373	438	550	
4	118	221	298	346	376	416	458	500	552	639	

TABLE A.1 (CONTINUED)

Test No 68

Load (kN)	20	40	60	80	100	120	140	160	170	180	190 Failure
Strain Gauge 1	-108	-178	-243	-300	-353	-422	-500	-615	-687	-707	
2	3	-32	-70	-124	-185	-271	-394	-531	-634	-794	
Deflection Gauge 1	30	54	67	73	93	170	245	351	421	525	
2	49	71	84	90	97	162	212	284	342	462	
3	44	68	78	80	81	123	151	195	228	301	
4	47	69	88	119	128	142	162	208	228	247	

TABLE A.1 (CONTINUED)

Test No 69

Load (kN)	20	40	60	80	100	120	140	150	160	170	180 Failure
Strain Gauge 1	-77	-147	-210	-273	-334	-426	-570	-643	-749	-849	
2	-49	-89	-133	-188	-264	-349	-443	-513	-585	-688	
Deflection Gauge 1	22	44	56	59	59	76	151	184	219	250	
2	11	28	37	36	29	37	98	121	149	176	
3	8	20	27	25	18	22	62	80	101	118	
4	41	62	88	100	119	139	166	189	213	238	

TABLE A.1 (CONTINUED)

Test No 70

Load (kN)	40	80	120	160	180	200	220	240	260	280	297.5 Failure
Strain Gauge 1	-150	-240	-325	-405	-450	-495	-545	-570	-725	-485	
2	-20	-90	-160	-235	-270	-300	-330	-300	-190	-455	
Deflection Gauge 1	45	45	26	10	8	12	20	45	273	643	
2	57	62	50	40	39	46	57	81	303	688	
3	43	47	39	31	30	35	43	58	213	403	
4	67	94	125	167	172	187	205	231	272	348	

TABLE A.1 (CONTINUED)

Test No 71

Load (kN)	40	80	100	120	140	160	180	200	220	240	260 Failure
Strain Gauge 1	-28	-88	-116	-143	-171	-201	-231	-256	-276	-434	
2	-112	-181	-218	-258	-298	-337	-372	-394	-404	-285	
Deflection Gauge 1	9	7	-1	-9	-18	-21	-22	-18	-6	236	
2	-6	-6	-12	-19	-27	-29	-29	-26	-15	225	
3	-14	-16	-19	-25	-32	-35	-37	-37	-31	145	
4	50	91	102	116	133	157	184	197	219	275	

TABLE A.1 (CONTINUED)

Test No 72

Load (kN)	20	40	60	70	80	90	100	110	120	130	140 Failure
Strain Gauge 1	-140	-290	-370	-420	-485	-535	-610	-660	-735	-821	
2	5	5	5	0	-5	-20	-50	-125	-225	-262	
Deflection Gauge 1	46	93	133	152	177	210	275	447	570	602	
2	60	120	172	198	231	268	333	477	560	596	
3	64	121	166	188	215	241	285	376	475	550	
4	68	113	146	159	176	192	217	245	299	308	

TABLE A.1 (CONTINUED)

Test No 73

Load (kN)	20	40	50	60	70	80	90	100	110	120	127.5 Failure
Strain Gauge 1	-65	-125	-150	-175	-195	-215	-220	-265	-280	-295	
2	-65	-130	-155	-190	-230	-275	-345	-400	-505	-620	
Deflection Gauge 1	25	47	58	62	63	65	95	224	281	330	
2	19	34	42	46	46	48	63	164	194	219	
3	16	27	32	34	40	51	59	90	91	110	
4	81	106	124	142	167	186	202	227	262	294	

TABLE A.1 (CONTINUED)

Test No 74

Load (kN)	20	40	60	80	100	120	140	160	170	180	190 Failure
Strain Gauge 1	-85	-165	-240	-315	-390	-465	-535	-590	-630	-635	
2	10	10	15	20	25	35	55	75	85	100	
Deflection Gauge 1	23	53	63	66	69	72	80	96	108	118	
2	31	75	79	89	99	111	129	153	168	182	
3	31	62	80	95	109	125	148	178	197	213	
4	58	110	131	163	210	230	265	311	331	357	

TABLE A.1 (CONTINUED)

Test No 75

Load (kN)	20	40	60	80	100	120	140	150	160	170	172.5 Failure
Strain Gauge 1	-50	-125	-190	-265	-345	-400	-400	-410	-450	-485	
2	-30	-50	-60	-65	-60	-75	-20	-5	-10	-15	
Deflection Gauge 1	27	57	67	68	63	63	76	84	93	115	
2	17	48	64	73	80	89	120	135	148	179	
3	14	37	55	70	84	98	125	151	166	200	
4	55	114	138	172	220	250	313	330	362	411	

TABLE A.1 (CONTINUED)

Test No 44

Load (kN)	40	60	80	100	120	140	160	180	200	220	237.5 Failure
Strain Gauge 1	-88	-131	-177	-216	-253	-282	-303	-315	-315	-295	-127
2	8	0	-5	-19	-42	-73	-111	-141	-187	-250	1389
3	-93	-114	-134	-153	-169	-170	-162	-133	-80	27	581
4	69	71	72	65	47	22	-10	-39	-83	-153	-845
5	-188	-241	-294	-338	-380	-414	-448	-480	-520	-575	471
6	-13	-62	-117	-169	-223	-294	-374	-471	-604	-780	-226
7	-93	-105	-116	-129	-146	-145	-134	-96	-28	89	699
8	43	30	14	-2	-22	-60	-101	-146	-198	-262	-846
9	-98	-129	-166	-201	-241	-268	-291	-295	-287	-271	-97
10	3	-15	-33	-53	-71	-104	-144	-187	-244	-321	-477
Deflection Gauge 1	-12	-14	-13	-14	-13	-13	-13	-8	1	33	
2	69	81	95	107	119	129	138	150	164	186	

TABLE A.1 (CONTINUED)

Test No 35

Load (kN)	20	40	60	80	100	120	140	160	180	200	215 Failure
Strain Gauge 1	-16	-48	-90	-133	-175	-215	-226	-242	-273	-335	-365
2	-38	-64	-77	-91	-107	-125	-134	-152	-194	-201	-213
3	49	54	52	49	45	38	31	26	9	-16	-34
4	-38	-36	-29	-21	-12	-1	14	28	73	133	176
5	41	0	-43	-90	-138	-200	-246	-309	-467	-669	-833
6	-170	-237	-301	-367	-421	-467	-477	-500	-545	-573	-599
7	49	60	62	64	64	59	57	56	55	50	47
8	-45	-49	-48	-46	-41	-35	-22	-15	-12	53	80
9	-18	-47	-86	-132	-179	-228	-254	-275	-332	-381	-405
10	-46	-77	-95	-109	-120	-125	-129	-131	-138	-156	-170
Deflection Gauge 1	28	32	40	51	60	67	68	64	55	39	
2	43	65	82	102	121	141	159	178	200	231	

TABLE A.1 (CONTINUED)

Test No 45

Load (kN)	20	40	60	80	90	100	110	120	130	140	145 Failure
Strain Gauge 1	-21	-48	-84	-123	-139	-157	-170	-183	-191	-204	-194
2	-30	-63	-80	-104	-118	-131	-147	-164	-184	-199	-242
3	16	16	24	27	27	27	24	25	18	13	-14
4	-1	-4	12	20	21	24	23	29	31	41	71
5	2	-39	-89	-139	-166	-198	-240	-300	-376	-470	-700
6	-62	-99	-146	-193	-214	-235	-253	-278	-306	-327	-380
7	4	0	15	18	19	16	12	9	-1	-5	-43
8	-2	2	0	-1	0	0	1	4	12	20	53
9	-21	-53	-76	-108	-125	-142	-156	-172	-177	-184	-161
10	-35	-63	-88	-115	-126	-138	-154	-169	-190	-210	-265
Deflection Gauge 1	29	35	49	65	74	82	90	101	108	121	
2	101	170	236	303	336	369	405	444	493	569	

TABLE A.1 (CONTINUED)

Test No 46

Load (kN)	10	20	30	40	50	60	70	80	90	100 Failure
Strain Gauge 1	-7	-20	-31	-41	-56	-67	-80	-94	-127	-146
2	-24	-43	-55	-78	-115	-134	-143	-147	-169	-167
3	-5	-6	-3	-3	-16	-17	-15	-10	-17	-18
4	-7	-7	0	0	-13	-9	0	13	5	0
5	-13	-37	-67	-94	-128	-166	-205	-243	-298	-366
6	-41	-73	-99	-127	-160	-185	-214	-245	-303	-374
7	-14	-13	-4	-6	-14	-13	-7	6	-3	-3
8	2	1	0	1	7	3	-3	-10	-15	-20
9	-25	-38	-44	-60	-89	-101	-108	-106	-133	-138
10	-19	-36	-53	-67	-82	-98	-117	-137	-162	-172
11	-22	-60	-93	-140	-187	-239	-288	-336	-465	-621
12	-88	-140	-176	-227	-269	-305	-340	-381	-499	-671
Deflection Gauge 1	23	29	30	33	37	49	62	73	88	
2	133	245	339	434	535	640	744	854	1089	

TABLE A.1 (CONTINUED)

Test No 48

Load (kN)	40	80	120	160	180	200	220	240	260	280	300 Failure
Strain Gauge 1	-94	-144	-193	-236	-259	-281	-300	-317	-334	-332	-270
2	3	-41	-91	-147	-176	-208	-245	-290	-345	-420	-559
3	-83	-103	-122	-135	-139	-140	-137	-124	-90	-7	382
4	54	32	8	-27	-45	-69	-93	-122	-162	-225	-610
5	-156	-242	-322	-385	-417	-447	-477	-513	-552	-565	-585
6	-21	-118	-219	-331	-395	-467	-545	-636	-758	-918	-874
7	-80	-101	-128	-141	-141	-137	-128	-113	-73	7	398
8	33	8	-20	-67	-92	-120	-148	-179	-220	-287	-715
9	-83	-139	-201	-246	-264	-282	-296	-313	-325	-321	-268
10	-14	-54	-92	-150	-187	-225	-268	-314	-374	-458	-618
11	-331	-514	-676	-814	-895	-976	-1041	-1139	-1259	-1267	3467Y
12	-51	-247	-456	-694	-827	-973	-1107	-1244	-1421	-1641Y	-4927Y
Deflection Gauge 1	24	17	14	17	21	23	26	27	25	2	
2	9	22	34	42	52	61	66	71	74	89	

TABLE A.1 (CONTINUED)

Test No 47

Load (kN)	40	80	120	140	160	180	200	220	240	260	272.5 Failure
Strain Gauge 1	-42	-104	-164	-192	-218	-242	-268	-292	-319	-342	-65
2	-59	-104	-153	-180	-210	-246	-285	-327	-376	-432	-239
3	-4	-11	-15	-16	-17	-18	-20	-16	7	-1	37
4	20	26	33	37	40	43	44	51	58	57	-135
5	-122	-210	-294	-334	-378	-426	-482	-537	-596	-665	-183
6	-80	-187	-296	-345	-401	-456	-514	-592	-700	-822	152
7	-23	-19	-17	-17	-16	-13	-11	-6	4	10	-8
8	40	51	62	68	68	68	67	67	67	58	-165
9	-87	-139	-198	-230	-262	-289	-318	-347	-383	-419	-134
10	-12	-62	-104	-126	-163	-199	-240	-287	-344	-409	-300
11	-242	-430	-596	-668	-746	-837	-955	-1061	-1160	-1045	1779Y
12	-155	-359	-559	-663	-735	-835	-926	-1058	-1136	-1213	-1618Y
Deflection Gauge 1	-21	-20	-14	-8	-7	-7	-5	-4	4	29	
2	53	76	101	112	123	136	149	165	183	215	

TABLE A.1 (CONTINUED)

Load (kN)	20	40	60	70	80	90	100	110	120	130	135 Failure
Strain Gauge 1	-20	-52	-84	-102	-120	-138	-158	-172	-177	-165	-188
2	-15	-34	-56	-65	-72	-80	-89	-101	-124	-165	-165
3	4	3	0	0	-2	-3	-7	-11	-18	-32	-74
4	10	16	19	21	22	24	26	27	32	45	81
5	-57	-104	-146	-170	-192	-215	-235	-253	-275	-390	-707
6	-7	-60	-124	-159	-194	-229	-269	-308	-355	-454	-471
7	0	1	0	0	0	0	-4	-11	-16	-27	-64
8	18	20	23	24	26	27	29	32	37	48	83
9	-23	-47	-80	-97	-113	-128	-142	-153	-164	-181	-211
10	-13	-34	-54	-61	-68	-78	-87	-101	-113	-121	-115
11	-86	-141	-190	-214	-238	-265	-286	-303	-329	-486	-699
12	-24	-73	-128	-156	-184	-211	-241	-281	-344	-501	-1130
Deflection Gauge 1	50	57	53	44	34	30	29	31	36	13	
2	164	311	473	563	649	740	837	968	1124	1394	

TABLE A.1 (CONTINUED)

Test No 58

Load (kN)	40	80	100	120	140	160	180	200	220	240	250 Failure
Strain Gauge 1	-36	-110	-155	-198	-265	-368	-492	-683	-712	-810	
2	-99	-165	-195	-220	-241	-258	-268	-269	-280	-299	
Deflection Gauge 1	0	-23	-29	-33	-35	-42	-43	-59	-62	-79	
2	-31	-26	-16	-18	-11	16	63	241	258	278	
3	-33	-23	-17	-9	11	41	88	130	170	200	
4	235	435	534	625	715	810	905	1020	1065	1135	

TABLE A.1 (CONTINUED)

Test No 59

Load (kN)	20	40	60	80	100	120	130	140	150	160	168.75 Failure
Strain Gauge 1	70	-20	-110	-205	-355	-530	-660	-835	-965	-1435	
2	-275	-420	-545	-645	-745	-800	-795	-815	-790	-785	
Deflection Gauge 1	-2	1	4	6	6	6	4	-4	-13	-29	
2	38	61	82	103	123	144	156	171	193	227	

TABLE A.1 (CONTINUED)

Test No 54

Load (kN)	80	120	160	200	240	280	320	360	400	440	470 Failure
Strain Gauge 1	-197	-287	-378	-466	-565	-670	-786	-966	-1343	-1648	
2	-61	-103	-143	-181	-214	-234	-235	-184	107	421	
Deflection Gauge 1	6	32	52	68	81	94	117	141	232	254	
2	46	55	67	82	98	119	160	227	427	539	
3	64	69	79	91	104	128	158	224	404	534	
4	46	59	70	76	86	95	106	120	134	144	

TABLE A.1 (CONTINUED)

Test No 55

Load (kN)	40	80	120	160	200	240	280	320	360	400	430 Failure
Strain Gauge 1	-206	-301	-373	-467	-550	-632	-711	-792	-918	-1100	
2	98	56	21	-23	-54	-89	-129	-152	-141	-49	
Deflection Gauge 1	-91	-131	-158	-151	-142	-131	-115	-97	-74	-48	
2	29	15	-5	4	22	20	26	37	59	83	
3	54	47	42	46	55	65	75	86	113	153	
4	200	260	261	271	284	299	313	328	344	365	

TABLE A.1 (CONTINUED)

Test No 56

Load (kN)	40	80	120	160	200	240	280	300	320	340	350 Failure
Strain Gauge 1	52	-19	-96	-175	-273	-362	-473	-535	-628	-708	
2	-135	-172	-229	-282	-333	-394	-432	-461	-435	-427	
Deflection Gauge 1	123	117	117	112	119	122	131	141	168	177	
2	53	52	47	67	79	95	123	148	197	237	
3	20	27	25	35	47	59	83	104	146	175	
4	226	384	332	378	420	464	507	531	555	581	

TABLE A.1 (CONTINUED)

Test No 57

Load (kN)	40	80	120	140	160	180	200	220	240	260	280 Failure
Strain Gauge 1	-13	-57	-110	-138	-161	-186	-210	-236	-271	-296	
2	-130	-203	-294	-340	-383	-417	-455	-493	-540	-597	
Deflection Gauge 1	-26	3	42	49	52	55	59	62	67	77	
2	20	32	41	47	55	63	72	79	99	125	
3	50	64	73	82	93	107	124	142	157	178	
4	171	301	431	489	551	607	664	721	786	848	

TABLE A.1 (CONTINUED)

Test No 77

Load (kN)	40	60	80	100	120	140	160	180	200	220	240 Failure
Strain Gauge 1	-205	-300	-400	-500	-590	-665	-740	-795	-830	-750	
2	5	-10	0	-15	-25	-50	-80	-130	-245	-480	
Deflection Gauge 1	73	87	96	103	113	126	144	169	207	274	
2	92	116	136	155	174	194	216	247	286	352	
3	72	93	112	129	145	162	178	197	222	245	
4	44	64	76	95	105	118	129	145	167	198	

TABLE A.1 (CONTINUED)

Test No 76

Load (kN)	40	80	100	120	140	160	180	200	220	240	260 Failure
Strain Gauge 1	-133	-226	-268	-299	-337	-387	-431	-447	-492	-485	
2	-58	-176	-243	-300	-354	-417	-496	-593	-719	-961	
Deflection Gauge 1	-147	-139	-148	-156	-163	-161	-144	-127	-81	-14	
2	9	17	9	1.	-6	-6	12	27	66	119	
3	-3	0	-7	-13	-19	-19	-11	-3	17	40	
4	49	85	109	125	146	170	188	210	230	258	

TABLE A.1 (CONTINUED)

Test No 78

Load (kN)	40	80	120	160	180	200	220	240	260	280	300 Failure
Strain Gauge 1	-160	-350	-545	-735	-790	-895	-960	-990	-1030	-1020	
2	-20	-35	-45	-60	-72	-80	-110	-160	-240	-320	
Deflection Gauge 1	51	76	97	112	120	139	156	174	199	247	
2	60	104	144	180	198	223	246	266	293	256	
3	48	88	126	159	174	196	211	221	236	267	
4	68	86	112	142	153	175	192	211	232	266	

TABLE A.1 (CONTINUED)

Test No 79

Load (kN)	40	80	120	160	200	240	280	320	360	380	390 Failure
Strain Gauge 1	10	-65	-130	-190	-230	-230	-15	-60	-95	-165	
2	-60	-125	-190	-280	-370	-510	-845	-940	-900	-790	
Deflection Gauge 1	-26	-25	-10	3	11	20	105	118	117	76	
2	-23	-24	-14	-3	6	24	142	159	155	105	
3	-25	-17	-11	-4	4	25	132	147	143	98	
4	53	79	109	150	171	207	255	284	345	365	

TABLE A.1 (CONTINUED)

Test No 80

Load (kN)	40	80	100	120	140	160	180	200	220	240	250 Failure
Strain Gauge 1	-200	-410	-520	-610	-670	-720	-770	-800	-850	-870	
2	-35	-45	-50	-90	-110	-170	-250	-360	-550	-810	
Deflection Gauge 1	51	82	90	98	109	125	143	177	262	451	
2	59	109	127	139	150	162	178	201	249	336	
3	51	197	114	125	136	143	149	159	181	224	
4	55	85	102	122	143	148	161	180	221	252	

TABLE A.1 (CONTINUED)

APPENDIX 2

APPENDIX 2

A2.1 CALCULATION OF THE CRITICAL COEFFICIENT

The buckling coefficient K is a function of the wavelength 2a and in order to obtain the smallest possible buckling load it is necessary to minimise K with respect to a. By setting $\frac{\partial K}{\partial F} = 0$, the wavelength parameter F which gives the smallest buckling coefficient K and therefore the smallest critical load can be obtained by utilising equation (5.31).

The buckling coefficient K, given by equation (5.25) when the longitudinal edges are simply supported and equation (5.29) when the longitudinal edges are fixed can be written as:

$$K = \frac{P\,Q}{T} \qquad \text{A.1}$$

when the first case is considered P, Q and T are given by

$$P = \left(D + \frac{F}{\pi} \sin \frac{\pi D}{F}\right) \qquad \text{A.2.1}$$

$$Q = \left(\frac{1+\lambda^2}{4F^4} + \frac{1+16\lambda^2}{4} + \frac{1+4\lambda^2}{2F^2}\right) \qquad \text{A.2.2}$$

$$T = \frac{1}{4F^2}\left(D - \frac{F}{\pi}\sin\frac{\pi D}{F}\right)\frac{64\lambda}{9\pi^2} + \frac{G}{4D}\,(1+4\lambda^2)\left(\frac{D}{3} + \frac{2F^2}{D\pi^2} - \frac{2F^3}{D^2\pi^3}\sin\frac{\pi D}{F}\right) \qquad \text{A.2.3}$$

By differentiating equation (A.1) with respect to F and setting $\frac{\partial K}{\partial F} = 0$ it is obtained

$$\frac{\partial K}{\partial F} = \left(\frac{\partial P}{\partial F}\,Q + P\,\frac{\partial Q}{\partial F}\right) T - P\,Q\,\frac{\partial T}{\partial F}$$

or

$$\frac{\partial K}{\partial F} = (UQ + P\ V)\ T - P\ \ Q\ \ W \qquad A.3$$

where

$$U = \frac{\partial P}{\partial F} = \left(\frac{1}{\pi} \sin \frac{\pi D}{F} - \frac{D}{F} \cos \frac{\pi D}{F}\right) \qquad A.4.1$$

$$V = \frac{\partial Q}{\partial F} = -\left(\frac{1 + \lambda^2}{F^5} + \frac{1 + 4\lambda^2}{F^3}\right) \qquad A.4.2$$

$$W = \frac{\partial T}{\partial F} = \left(-\frac{2}{4F^3}\left(D - \frac{F}{\pi} \sin \frac{\pi D}{F}\right) + \frac{1}{4F^2}\left(\frac{D}{F} \cos \frac{\pi D}{F} - \frac{1}{\pi} \sin \frac{\pi D}{F}\right)\right) \frac{64\lambda}{9\pi^2}$$

$$+ \frac{G}{4D}(1+\lambda^2)\left(\frac{4F}{D\pi^2} - \frac{6F^2}{D^2\pi^3} \sin \frac{\pi D}{F} + \frac{2F}{D\pi^2} \sin \frac{\pi D}{F}\right) \qquad A.4.3$$

Equation (A.3) can further be simplified by writing

$$R = (U\ Q + P\ V)\ T \qquad A.5.1$$

and

$$S = P\ Q\ \ W \qquad A.5.2$$

and, therefore, be written in the following form:

$$\frac{\partial K}{\partial F} = R - S \qquad A.6$$

The same equations hold for the other case, when the longitudinal edges are fixed, where

$$P = \left(D + \frac{F}{\pi} \sin \frac{\pi D}{F}\right) \qquad A.7.1$$

$$Q = \frac{1}{4F^4}\left(\frac{3}{4} + 3\lambda^2 + \frac{3\lambda^4}{4}\right) + \frac{1}{4}\left(4 + 82\lambda^2 + 64\lambda^4\right) + \frac{1}{F^2}\left(1 + 16\lambda^2 - \frac{2\lambda^2}{11\pi} + 4\lambda^4\right) \qquad A.7.2$$

$$T = \frac{1}{4F^2}\left(D-\frac{F}{\pi}\sin\frac{\pi D}{F}\right)\frac{1}{11025\pi^2}\left(9016\lambda+29184\lambda^3\right) +$$

$$\frac{G}{4D}\left(\frac{D}{3}+\frac{2F^2}{D\pi^2}-\frac{2F^2}{D^2\pi^3}\sin\frac{\pi D}{F}\right)\left(1+10\lambda^2+4\lambda^4\right) \qquad \text{A.7.3}$$

and similarly to the previous case

$$U = \frac{\partial P}{\partial F} = \left(\frac{1}{\pi}\sin\frac{\pi D}{F}-\frac{D}{F}\cos\frac{\pi D}{F}\right) \qquad \text{A.8.1}$$

$$V = \frac{\partial Q}{\partial F} = -\frac{1}{F^5}\left(\frac{3}{4}+3\lambda^2+\frac{3}{4}\lambda^4\right)-\frac{1}{2F^3}\left(1+16\lambda^2-\frac{2\lambda^2}{11\pi}+4\lambda^4\right) \qquad \text{A.8.2}$$

$$W = \frac{\partial T}{\partial F} = \left(-\frac{1}{2F^3}\left(D-\frac{F}{\pi}\sin\frac{\pi D}{F}\right)+\frac{1}{4F^2}\left(\frac{D}{F}\cos\frac{\pi D}{F}-\frac{1}{\pi}\sin\frac{\pi D}{F}\right)\frac{4}{11025\pi^2}\right.$$

$$\left(9016\lambda+29184\lambda^3\right)+\frac{G}{4\pi}\left(\frac{4F}{D\pi^2}-\left(\frac{6F^2}{D^2\pi^3}\sin\frac{\pi D}{F}-\frac{2F}{D\pi^2}\cos\frac{\pi D}{F}\right.\right.$$

$$\left.\left(1+10\lambda^2+4\lambda^4\right) \qquad \text{A.8.3}\right.$$

The value of F, for the equation (A.6) to be equal to zero, can be determined either by a computer analysis, or by a graphical method. For the purpose of the present work the formerly mentioned method was chosen.

This process involves an iteration technique. The flow diagram of the computer program used is shown in figure (A.1). In this program the value of F is increased in large steps until expression (A.6) changes sign and then increased in smaller steps for the last value before the change of sign, until the expression changes sign

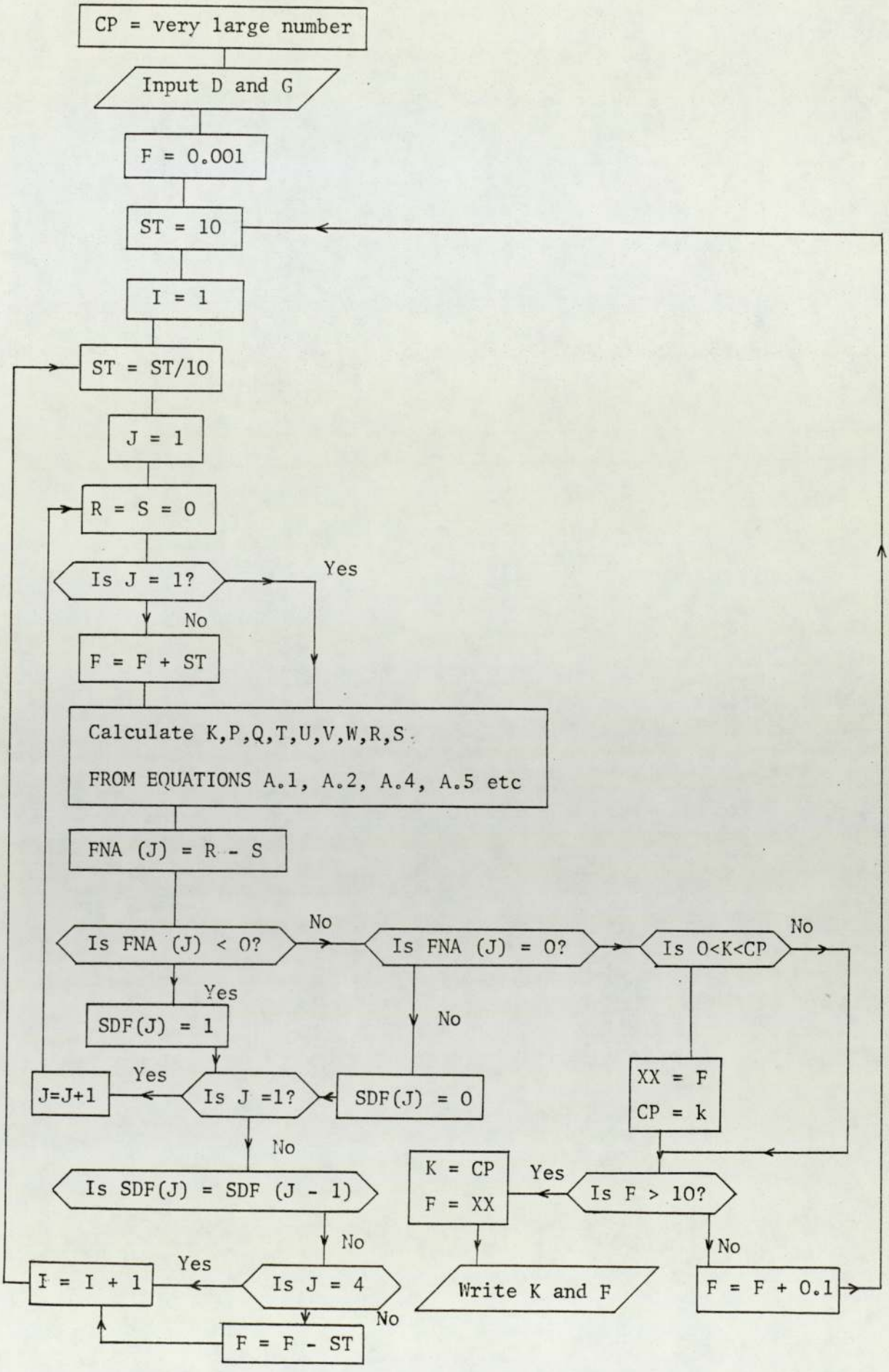

FIGURE A.1 FLOW DIAGRAM FOR COMPUTER PROGRAM

again. This process is repeated until sufficient accuracy is obtained for the value of K corresponding to the value of F determined.

A2.2 PLATE LOADED BY A UNIFORMLY DISTRIBUTED COMPRESSIVE STRESS ON THE LONGITUDINAL EDGES AND BENDING STRESS ON THE OTHER TWO EDGES

a) All Edges Simply Supported

Consider the simply supported plate, shown in figure (5.6a) loaded in the middle plane by the evenly distributed force N_y given by.

$$N_y = \gamma N_o$$

The longitudinal force distribution is given by

$$N_x = N_o \left(1-\alpha_o \frac{B-y}{2B}\right)$$

The approximate representation of the lateral deflection can be assumed as

$$\omega = \omega_o \cos\frac{\pi x}{2A}\left(\cos\frac{\pi y}{2B} + \lambda \sin\frac{\pi y}{B}\right) \qquad -A \leqslant x \leqslant A \qquad \text{A.9.1}$$

$$\omega = 0 \qquad -\frac{L'}{2} \leqslant x \leqslant -A \qquad \text{A.9.2}$$

$$\omega = 0 \qquad A \leqslant x \leqslant \frac{L'}{2} \qquad \text{A.9.3}$$

where 2A is again an undetermined parameter. The equation (A.9) above satisfies the boundary conditions for this case, which are:

$$\omega = 0 \text{ at } x = \pm A \text{ and } y = \pm B \qquad \text{A.10.1}$$

$$\frac{\partial^2\omega}{\partial x^2} + \nu \frac{\partial^2\omega}{\partial y^2} = 0 \qquad \text{at } x = \pm A \qquad \text{A.10.2}$$

$$\frac{\partial^2 \omega}{\partial y^2} + \nu \frac{\partial^2 \omega}{\partial x^2} = 0 \qquad \text{at } y = \pm B \qquad \text{A.10.3}$$

By substituting for N_y, N_x and equation (A.9) into equation (5.10) in chapter 5, after integration between the correct limits, N_o is obtained from

$$N_o = \frac{\pi^2 D_1}{(2B)^2} \cdot K \qquad \text{A.11}$$

where K is the buckling coefficient given by

$$K = \frac{(\frac{B}{A})^2 (1+\lambda^2) + (1+16\lambda^2) + 2(1+4\lambda^2)}{1+\lambda^2 - \frac{\alpha_o}{2}(1+\lambda^2) + \frac{32\alpha_o\lambda}{9\pi^2} + \gamma (\frac{A}{B})^2 (1+4\lambda^2)} \qquad \text{A.12}$$

It is worthwhile to notice that the above equation by setting $\frac{A}{B} = 1$, $\lambda = 0$, $\gamma = 0$ and $\alpha_o = 0$, that is to say a square plate subjected to a compressive force in the longitudinal direction, yields K = 4 as given by Timoshenko (12). As has been mentioned before the case when the vertical edges are subjected to bending forces are to be considered and this is so when $\alpha_o = 2$. Therefore, equation (A.6) becomes

$$K = \frac{(\frac{B}{A})^2 (1+\lambda^2) + (\frac{A}{B})^2 (1+16\lambda^2) + 2(1+4\lambda^2)}{\frac{64\lambda}{9\pi^2} + \gamma (\frac{A}{B})^2 (1+4\lambda^2)} \qquad \text{A.13}$$

As before, γ can be expressed as

$$\gamma = \frac{1}{A} \cdot \frac{4I}{Ldt} \qquad \text{A.14}$$

b) Longitudinal Edges Fixed and Vertical Edges Simply Supported

The loading remains the same as for case (a) but the longitudinal edges now are fixed. The new boundary conditions are:

$$\omega = 0 \qquad \text{at } x = \pm A \quad \text{and} \quad y = \pm B \qquad \text{A.15.1}$$

$$\frac{\partial^2 \omega}{\partial x^2} + \nu \frac{\partial^2 \omega}{\partial y^2} = 0 \qquad \text{at } x = \pm A \qquad \text{A.15.2}$$

$$\frac{\partial \omega}{\partial y} = 0 \qquad \text{at } y = \pm B \qquad \text{A.15.3}$$

An expression for the deflected shape which satisfies the above boundary conditions can be written as.

$$\omega = \omega_o \cos \frac{\pi x}{2A} \left(\cos \frac{\pi y}{2B} + \lambda \sin \frac{\pi y}{B}\right)^2 \qquad -A \leqslant x \leqslant A \qquad \text{A.16.1}$$

$$\omega = 0 \qquad -\frac{L'}{2} \leqslant x \leqslant -A \qquad \text{A.16.2}$$

$$\omega = 0 \qquad A \leqslant x \leqslant \frac{L'}{2} \qquad \text{A.16.3}$$

By following the same procedure as before the buckling factor K is obtained from equation (A.17)

$$K = \frac{\left(\frac{B}{A}\right)^2 \left(\frac{3}{4}+3\lambda^2+\frac{3}{4}\lambda^4\right) + \left(\frac{A}{B}\right)^2 \left(4+82\lambda^2+64\lambda^4\right) + 4\left(1+6\lambda^2-\frac{2\lambda^2}{11\pi}+4\lambda^4\right)}{\frac{4}{11025\pi}\left(9016\lambda + 29184\lambda^3\right) + \gamma \left(\frac{A}{B}\right)^2 \left(1 + 10\lambda^2 + 4\lambda^4\right)} \qquad \text{A.17}$$

and the numerical factor γ is obtained from equation (A.14).

c) Longitudinal Edges Simply Supported and Vertical Edges Fixed

The loading remains the same as for the previous cases, but the edges $x = \pm A$ are now fixed. An expression for the deflected

shape must be formulated which satisfies the following boundary conditions:

$$\omega = 0 \qquad \text{at } x = \pm A \text{ and } y = \pm B \qquad \text{A.18.1}$$

$$\frac{\partial \omega}{\partial x} = 0 \qquad \text{at } x = \pm A \qquad \text{A.18.2}$$

$$\frac{\partial^2 \omega}{\partial y^2} + \nu \frac{\partial^2 \omega}{\partial y^2} = 0 \qquad \text{at } y = \pm B \qquad \text{A.18.3}$$

Such an expression can be written in the form:

$$\omega = \omega_o \cos^2 \frac{\pi x}{2A} \left(\cos \frac{\pi y}{2B} + \lambda \sin \frac{\pi y}{B}\right) \qquad -A \leq x \leq A \qquad \text{A.19.1}$$

$$\omega = 0 \qquad -\frac{L'}{2} \leq x \leq -A \qquad \text{A.19.2}$$

$$\omega = 0 \qquad A \leq x \leq \frac{L'}{2} \qquad \text{A.19.3}$$

Following exactly the same procedure as before the buckling coefficient K can be obtained from:

$$K = \frac{\left(\frac{B}{A}\right)^2 (1+\lambda^2) + \left(\frac{A}{B}\right)^2 \frac{(1+16\lambda^2)}{8} + \frac{(1+4\lambda^2)}{2}}{\frac{16\lambda}{9\pi^2} + \gamma \left(\frac{A}{B}\right)^2 \frac{(1+4\lambda^2)}{2}} \qquad \text{A.20}$$

and γ is again given by equation (A.14)

d) Longitudinal Edges Simply Supported and Vertical Edges Free

The longitudinal edges $y = \pm B$ are simply supported and the vertical edges $x =$ A are now free. The deflected shape can be expressed as:

$$\omega = \omega_o \cos \frac{\pi x}{2a} \left(\cos \frac{\pi y}{2B} + \lambda \sin \frac{\pi y}{B}\right) \qquad 0 \leqslant A \leqslant a \qquad \text{A.21}$$

where 2a is the wavelength, as already has been explained in chapter 5, section (5.2.4.1). The loading remains the same as for the previous cases and following the same procedure finally the buckling coefficient K is given by:

$$K = \frac{\left(A+\frac{a}{\pi}\sin\frac{\pi A}{a}\right)\left(\frac{B^2}{a^2}(1+\lambda^2) + \frac{a^2}{B^2}(1+16\lambda^2) + 2(1+4\lambda^2)\right)}{\left(A-\frac{a}{\pi}\sin\frac{\pi A}{a}\right)\frac{64\lambda}{9\pi^2} + \gamma\frac{a^2}{B^2}\left(A+\sin\frac{\pi A}{a}\right)(1+4\lambda^2)} \qquad \text{A.22}$$

It is worthwhile noting that equation (A.22) for a = A becomes identical to equation (A.13) fhat is when the edges are simply supported and the wavelength 2a equals the length at the plate 2A.

By writing $F = \frac{a}{B}$ and $D = \frac{A}{B}$ and $\gamma = \frac{1}{A}\frac{4I}{Ldt}$ equation (A.22) becomes:

$$K = \frac{\left(D+\frac{F}{\pi}\sin\frac{\pi D}{F}\right)\left(\frac{1}{F^2}(1+\lambda^2) + F^2(1+16\lambda^2) + 2(1+4\lambda^2)\right)}{\left(D-\frac{F}{\pi}\sin\frac{\pi D}{F}\right)\frac{64\lambda}{9\pi^2} + \frac{1}{D}\frac{4I}{BLdt}F^2\left(D+\frac{F}{\pi}\sin\frac{\pi D}{F}\right)(1+4\lambda^2)} \qquad \text{A.23}$$

e) Longitudinal Edges Fixed and Vertical Edges Free

The loading remains the same as for the previous cases. The longitudinal edges y = ± B are now fixed and the vertical edges x = ± A are free. The deflected shape can be expressed as:

$$\omega = \omega_o \cos \frac{\pi x}{2a} \left(\cos\frac{\pi y}{2B} + \lambda \sin \frac{\pi y}{B}\right)^2 \qquad 0 \leqslant A \leqslant a \qquad \text{A.24}$$

By following exactly the same procedure, the buckling coefficient K is given by equation (A.25) which by setting a = A becomes

identical to equation (A.17)

$$K = \frac{P_o \quad Q_o}{T_o} \qquad \text{A.25.1}$$

where

$$P_o = \left(A + \frac{a}{\pi} \sin \frac{\pi A}{a}\right) \qquad \text{A.25.2}$$

$$Q_o = \left(\frac{B^2}{a^2}\left(\frac{3}{4}+3\lambda^2+\frac{3}{4}\lambda^4\right) + \frac{a^2}{B^2}\left(4+82\lambda^2+64\lambda^4\right) +2\left(1+6\lambda^2-\frac{2\lambda^2}{11\pi}+4\lambda^4\right)\right) \qquad \text{A.25.3}$$

$$T_o = \left(\left(A-\frac{a}{\pi}\sin\frac{\pi A}{a}\right) \frac{4}{11025\pi^2}\left(9016\lambda + 29184\lambda^3\right) + \right.$$

$$\left. \gamma \frac{a^2}{B^2}\left(A+\sin\frac{\pi A}{a}\right)\left(1+10\lambda^2 + 4\lambda^4\right)\right) \qquad \text{A.25.4}$$

and finally by substituting for γ, $\frac{a}{B}$ and $\frac{A}{B}$ into above expression K is obtained by

$$K = \frac{P\ Q}{T} \qquad \text{A.26.1}$$

where

$$P = \left(D + \frac{F}{\pi} \sin \frac{\pi D}{F}\right) \qquad \text{A.26.2}$$

$$Q = \left(\frac{1}{F^2}\left(\frac{3}{4}+3\lambda^2+\frac{3}{4}\lambda^4\right) + F^2\left(4+82\lambda^2+64\lambda^4\right) +2\left(1+16\lambda^2-\frac{2\lambda^2}{11\pi}+4\lambda^4\right)\right) \qquad \text{A.26.3}$$

$$T = \left(\left(D-\frac{F}{\pi}\sin\frac{\pi D}{F}\right) \frac{4}{11025\pi^2}\left(9016\lambda + 29184\lambda^3\right) + \right.$$

$$\left. \frac{1}{D}\frac{4I}{LDtB} F^2 \left(D + \frac{F}{\pi}\sin\frac{\pi D}{F}\right)\left(1+10\lambda^2 + 4\lambda^4\right)\right) \qquad \text{A.26.4}$$

A 2.3 PLATE LOADED BY A COMPRESSIVE FORCE OF TRIANGULAR FORM ON THE LONGITUDINAL EDGES AND BENDING FORCES ON THE OTHER TWO EDGES

In this case instead of a uniformly distributed compressive force the longitudinal edges are subjected to a triangular force distribution, as is shown in figure (5.1b). This force distribution approximates to a concentrated force applied at the middle of the longitudinal edges. The vertical edges are still subjected to bending forces. The three cases, for different boundary conditions are considered again for this type of loading.

a) All Edges Simply Supported

The longitudinal force distribution remains the same as for the previous type of loading and it is given by equation (A.8), which for the case of bending, with $\alpha_o = 2$ becomes

$$N_x = N_o \frac{y}{B} \qquad \text{A.27}$$

The compressive force in the y-direction, N_y is given by:

$$N_y = N_o \gamma(1 + \frac{x}{A}) \qquad -A \leqslant x \leqslant 0 \qquad \text{A.28.1}$$

and

$$N_y = N_o \gamma \quad (1 - \frac{x}{A}) \qquad 0 \leqslant x \leqslant A \qquad \text{A.28.2}$$

The deflection is given by the same expression as for case (a) of the previous type of loading, that is by equation (A.9). By substituting equation (A.27) and (A.28) into equation (5.10) and after evaluation the buckling factor K can be obtained from:

$$K = \frac{(\frac{B}{A})^2 (1+\lambda^2) + (\frac{A}{B})^2 (1+16\lambda^2) + 2 (1+4\lambda^2)}{\frac{64\lambda}{\pi^2} + \gamma (\frac{A}{B})^2 (1 + 4\lambda^2)} \qquad \text{A.29}$$

It should be noticed that the factor γ is different from the one used for the previous loading case and can be obtained in a similar way as

$$\gamma = \frac{1}{A} \cdot \frac{8I}{Ldt} \qquad \text{A.30}$$

b) Longitudinal Edges Fixed and Vertical Edges Simply Supported

The loading remains the same, and the expression for the deflected shape which satisfies the boundary conditions is given by equation (A.16). Following the same precedure as for the previous cases the buckling coefficient K is given by:

$$K = \frac{\left(\frac{B}{A}\right)^2 \left(\frac{3}{4}+3\lambda^2+\frac{3}{4}\lambda^4\right) + \left(\frac{A}{B}\right)^2 \left(4+82\lambda^2+64\lambda^4\right) + 2\left(1+16\lambda^2-\frac{2\lambda^2}{11\pi}+4\lambda^4\right)}{\frac{4}{11025\pi^2}\left(9016\lambda + 29184\lambda^3\right) + \gamma\left(\frac{A}{B}\right)^2 \left(1 + 10\lambda^2 + 4\lambda^4\right)} \qquad \text{A.31}$$

The factor γ is obtained from equation (A.32).

c) Longitudinal Edges Simply Supported and Vertical Edges Fixed

The loading remains the same as for cases (a) and (b) and the deflection can be obtained from equation (A.19). Following the same procedure as previously, the buckling coefficient K is obtained from:

$$K = \frac{\left(\frac{B}{A}\right)^2 \left(1+\lambda^2\right) + \left(\frac{A}{B}\right)^2 \frac{1+16\lambda^2}{8} + \frac{\left(1+4\lambda^2\right)}{2}}{\frac{16\lambda}{9\pi^2} + \left(\frac{A}{B}\right)^2 \frac{\left(1+4\lambda^2\right)}{8}} \qquad \text{A.33}$$

and γ is obtained from equation (A.30). The critical load P can

be obtained by following exactly the same procedure and equations as for the previous loading case given in chapter 5.

d) Longitudinal Edges Simply Supported and Vertical Edges Free

The loading conditions remain as for the other cases. The longitudinal edges $y = \pm B$ are simply supported and the vertical edges $x = \pm A$ are now free. An expression for the deflected shape which satisfies the boundary conditions is given by equation (A.21) and after evaluation the buckling coefficient K is given by:

$$K = \frac{(A+\frac{a}{\pi}\sin\frac{\pi A}{a})\ (\frac{B^2}{a^2}(1+4\lambda^2)+\frac{a^2}{B^2}\ (1+16\lambda^2)\ +\ 2(1+4\lambda^2)}{(A-\frac{a}{\pi}\sin\frac{\pi A}{a})\ \frac{64\lambda}{9\pi^2}\frac{a^2}{B^2}\cdot\gamma(A+\frac{a}{\pi}\sin\frac{\pi A}{a}+\frac{1}{A}\frac{a^2}{\pi^2}\ (1+\cos\frac{\pi A}{a}))\ (1+4\lambda^2)} \qquad \text{A.34}$$

By setting $a = A$ into equation (A.34) this becomes identical to equation (A.29), when the vertical edges are simply supported. Finally, by substituting $\gamma = \frac{1}{A}\frac{8I}{Ldt}$, $\frac{a}{B} = D$ into equation (A.34), K is obtained from:

$$K = \frac{(D+\frac{F}{\pi}\sin\frac{\pi D}{F})\ (\frac{1}{F^2}\ (1+4\lambda^2)\ +\ F^2\ (1+16\lambda^2)\ +2\ (1+4\lambda^2))}{(D-\frac{F}{\pi}\sin\frac{\pi D}{F})\ \frac{64\lambda}{9\pi^2}\frac{1}{D}\cdot\frac{8I}{LdtB}\cdot\ F^2\ (D+\frac{F}{D}\sin\frac{\pi D}{F}+\frac{DF^2}{\pi^2}(1+\cos\frac{\pi D}{F})\ (1+4\lambda^2))} \qquad \text{A.35}$$

e) Longitudinal Edges Fixed and Vertical Edges Free

In this case the longitudinal edges are fixed and the vertical edges free. The loading conditions remain the same as for the previous cases. The deflection is given by equation (A.24) and following the same procedure as before the buckling coefficient K is obtained from:

$$K = \frac{P_o Q_o}{T_o} \qquad \text{A.36.1}$$

where

$$P_o = \left(A + \frac{a}{\pi} \sin \frac{\pi A}{a}\right) \qquad \text{A.36.2}$$

$$Q_o = \left(\frac{B^2}{a^2}\left(\frac{3}{4}+3\lambda^2+\frac{3}{4}\lambda^4\right) + \frac{a^2}{B^2}\left(4+82\lambda^2\right) + 2\left(1+16\lambda^2-\frac{2\lambda^2}{11\pi}+4\lambda^4\right)\right) \qquad \text{A.36.3}$$

$$T_o = \left(\left(A - \frac{a}{\pi}\sin\frac{\pi A}{a}\right)\frac{4}{11025\pi^2}\left(9016\lambda + 29184\lambda^3\right) + \gamma\frac{a^2}{B^2}\left(A+\frac{a}{\pi}\sin\frac{\pi A}{a}+\frac{1}{A}\frac{a^2}{\pi^2}\left(1+\cos\frac{\pi A}{a}\right)\right)\left(1+10\lambda^2+4\lambda^4\right)\right) \qquad \text{A.36.4}$$

By setting a = A into the above equation, it becomes identical to equation (A.31), that is when the vertical edges are simply supported. As previously by substituting $\gamma = \frac{1}{A} \cdot \frac{8I}{LdtB}$, $\frac{a}{B} = F$ and $\frac{A}{B} = D$ into equation (A.36) K finally is obtained from

$$K = \frac{P\,Q}{T} \qquad \text{A.37.1}$$

where

$$P = \left(D+\frac{F}{\pi}\sin\frac{\pi D}{F}\right) \qquad \text{A.37.2}$$

$$Q = \left(\frac{1}{F^2}\left(\frac{3}{4}+3\lambda^2+\frac{3}{4}\lambda^4\right) + F^2\left(4+82\lambda^2+64\lambda^4\right) + 2\left(1+16\lambda^2-\frac{2\lambda^2}{11\pi}+4\lambda^4\right)\right) \qquad \text{A.37.3}$$

$$T = \left(\left(D+\frac{F}{\pi}\sin\frac{\pi D}{F}\right)\frac{4}{11025\pi^2}\left(9016\lambda + 29184\lambda^3\right) + \frac{1}{D}\frac{8I}{LdtB}F^2\left(D+\frac{F}{D}\sin\frac{\pi D}{F}+\frac{DF^2}{\pi^2}\left(1+\cos\frac{\pi D}{F}\right)\right)\left(1+10\lambda^2+4\lambda^4\right)\right) \qquad \text{A.36.5}$$

REFERENCES

REFERENCES

1 MASSONNET C - 'Thin Walled Deep Plate Girders'. I.A.B.S.E., 8th Congress, New York, V 2, pp 493-495, 1968.

2 HRENNIKOFF A - 'Lessons of the Collapse of the Vancouver 2nd Narrows Bridge'. Trans. A.S.C.E., V 26, pp 668-692, 1961

3 H M FACTORY INSPECTORATE - 'Report on the Collapse of False-work for the Viaduct over the River Loddon on the 24th October 1972'. Published July 1973.

4 HOLMES M - 'Universal Beams as Runway Beams'. Civil Eng. and Public Works Review. V 59, No 694, pp 569-573, 1964.

5 BRITISH STANDARD 449 - 'The Use of Structural Steel in Buildings'. Part 2 (Metric Units), 1969, and Ammendment slip No 5, Published 31 July 1975.

6 BRITISH STANDARD 153 - 'Specification for Steel Girder Bridges'. Part 3B, Published 1972.

7 GLANVILLE W - First Report, Steel Structures Research Committee, HMSO 1931.

8 BRITISH STANDARD (DRAFT CODE) - 'Draft Standard Specification for the Use of Steelwork in Buildings'. Published 1975.

9 BRYAN G H - 'On the Stability of a Plane Plate Under Thrusts in its Own Plane with Application to the Buckling of the Sides of a Ship'. Proc. London Math. Soc., V 22, pp 54-67, 1891.

10 STOWELL E Z and HOUBOLD J C - 'Critical Stress of Plate Columns'. N.A.C.A., T.N. 2163, 1950.

11 WOINOWSKY KRIEGER S - 'Stability of a Rectangular Plate with Free Loaded Edges.' Ingenieur Archiv., V 19, pp 200-207, 1951.

12 TIMOSHENKO S and GERE J - 'Theory of Elastic Stability.' McGraw-Hill Co., 1961.

13 BLEICH F - 'Buckling Strength of Metal Structures.' McGraw-Hill Co., 1952.

14 STOWELL E Z - 'Buckling Stresses for Flat Plates and Sections.' Trnas. A.S.C.E., V 117, pp 545-578, 1952.

15 GERARD G and BECKER H - 'Handbook of Structural Stability' Part 1 - 'Buckling of Flat Plates.' N.A.C.A., T.N. 3781, 1957.

16 SHULESHKO P - 'Buckling of Rectangular Plates Uniformly Compressed in Two Perpendicular Directions with One Free Edge and Opposite Edge Elastically Restrained'. Journal of Applied Mechanics, Trans. A.S.M.E., V 78, pp 359-363, 1956.

17 SHULESHKO P - 'Buckling of Rectangular Plates with Two Unsupported Edges'. Journal of the Applied Mechanics, V 24, pp 537-540, 1957.

18 JOHNSON J H - 'Critical Buckling Stresses of Simply Supported Flat Rectangular Plates Under Combined Longitudinal Compression, Transverse Compression and Shear'. Journal of the Aeronautical Sciences, V 21, pp 411-416, 1954.

19 GROSSMAN N - 'Elastic Stability of Simply Supported Flat Rectangular Plates Under Critical Combinations of Transverse Compression and Longitudinal Bending'. Jour. Aero. Sci., V 16, pp 272-276, 1949.

20 WITTRICK W H - 'Buckling of an Infinite Simply Supported Strip Under Combined Longitudinal Compression, Transverse Compression, Bending and Shear'. Dept. of Supply, Research and Development Branch, Aero. Research Laboratories, Report S M 234, Dept of Aero. Eng., University of Sydney.

21 NOEL R G - 'Elastic Stability of Simply Supported Flat Rectangular Plates Under Critical Combination of Longitudinal Bending, Longitudinal Compression and Lateral Compression'. Journal of Aero. Sci., V 19, pp 829-833, 1952.

22 VON KARMAN TH, SECHLER E and DONNEL D - 'The Strength of Thin Plates in Compression'. Trans. A.S.M.E., V 54, pp 53-57, 1932.

23 WINTER G - 'Strength of Thin Compression Flanges'. Proc. A.S.C.E., V 72, pp 199-226, 1946.

24 SOMMERFELD A VON - 'Uber die Knicksicherheit der Stege Von Walzwerkprofilen.' Zeit. f. Math. U.Phy., V 54, pp 113-119, 1906.

25 GIRKMAN K - 'Stability of the Webs of Plate Girders Taking Account of Concentrated Loads.' Pubs. Int. Assoc. Bridge and Struct. Engin. Final Report, 1936.

26 LEGGETT D M A - 'The Effect on Two Isolated Forces on the Stability of a Flat Rectangular Plate'. Proc. Camb. Phil. Soc., V 33, pp 325-339, 1937.

27 HOPKINS G H - 'Elastic Stability of Infinite Strips.' 7th Int. Congress of Applied Mech., London 1948.

28 YAMAKI N - 'Buckling of a Rectangular Plate Under Locally Distributed Forces Applied on Two Opposite Edges.' Rep. Inst. High Speed Mech., Tohoku Univ. V 3, 1953 and V 4, 1954.

29 ZETLIN I - 'Elastic Instability of Flat Plates Subjected to Partial Edge Loads.' Proc. A.S.C.E., Eng. Mech. Div., V 81, No 795, 1955.

30 WHITE R N and COTTINGHAM W S - 'Stability of Plates Under Partial Edge Loading.' Proc. A.S.C.E., Eng. Mech. Div., V 88, pp 67-86, 1962.

31 GALLAGHER R and PADLOG J - 'Discrete Element Approach to Structural Instability Analysis.' Journal A.I.A.A., V 1, pp 1437-1439, 1963.

32 KAPUR K and HARTZ B - 'Stability of Plates Using the Finite Element Method.' Proc. A.S.C.E., Eng. Mech. Div., V 92, pp 177-192, 1966.

33 ROCKEY K C and BAGCHI D K - 'Buckling of Plate Girder Webs Under Partial Edge Loads'. Int. Journ. Mech. Sci., V 2, pp 61-76, 1970.

34 ALFUTOV N A and BALABUKH L I - 'On the Possibility of Solving Plate Stability Problems Without a Preliminary Determination of the Initial State of Stress.' Prikladnaya Matematika I Mechanika, V 31, pp 730-739, 1967.

35 ALFUTOV N A and BALABUKH L I - 'Energy Criterion of the Stability of Elastic Bodies which does not require the Initial Stress-Strain State'. Prikladnaya Matematika I Mechanika, V 32, pp 726-731, 1968.

36 KHAN M Z and WALKER A C - 'Buckling of Plates Subjected to Localised Edge Loading'. Structural Engineer , V 50, No 6, pp 225-232, 1972.

37 SHANLEY F R - 'Inelastic Column Theory'. Journal Aero. Sci., V 14, No 5, pp 261-268, 1947.

38 BIJLAARD P P - 'Theory of the Plastic Stability of Thin Plates'. I.A.B.S.E., V 6, pp 45-69, 1940-41.

39 ILYUSHIN A A - 'The Elastoplastic Stability of Plates'. N.A.C.A., Tech. Mem. No 1188, 1947.

40 GERARD G - 'Secant Modulus for Determining Plate Instability Above the Proportional Limit.' Journal Aero. Sci., V 13, pp 38-48, 1946.

41 STOWELL E Z - 'A Unified Theory of Plastic Buckling of Columns and Plates.' N.A.C.A. Tech. Note No 1556, 1948.

42 MOORE H F - 'The Strength of I-Beams in Flexure'. Bulletin No 68, Engin. Exp. Station, University of Illinois, Sept 1913.

43 MOORE H F and WILSON W M - 'The Strength of Webs of I-Beams and Girders'. Bulletin No 86, Eng. Exp. Station, University of Illinois, May 1916.

44 KETCHUM M and DRAFFIN J - 'Strength of Light I-Beams'. Bulletin No 241, Eng. Exp. Station, University of Illinois, February 1932.

45 LYSE I and GODFREY J H - 'Investigation of Web Buckling in Steel Beams'. Trans. A.S.C.E., No 1907, pp 674-706, 1934.

46 WASTLUND G and BERGMAN S G A - 'Buckling of Webs in Deep Steel I-Beams'. Pubs. I.A.B.S.E., V 8, pp 291-310, 1947.

48 MASSONNET C - 'General Report on Present State of Knowledge in the Field of the Webs of Plate Girders'. Pubs. I.A.B.S.E., Liege, 1962.

49 ROCKEY K C - 'Stability Problems Associated with Design of Plate Girder Webs.' Civil Eng. and Public Works Review, V 47, Nos 556, 557, 558, 1952 and V 48, No 559, 1953.

50 ROCKEY K C - 'Plate Girder Design'. Engineering, V 184, pp 788-792, 1957.

51 ROCKEY K C - 'Web Buckling and Design of Web Plates.' Structural Engineer, V 36, pp 45-60, 1958.

52 SKALOUD M - 'General Report on Present State of Knowledge in the Field of the Webs of Plate Girders'. Pubs. I.A.B.S.E., Liege, 1962.

53 NOVAK P and SKALOUD M - 'Experimental Investigation into the Post Buckled Behaviour and Incremental Collapse of Thin Webs Subjected to Concentrated Loads'. International Symposium, Buenos Aires, pp 207 - 228, 13-18 Sept. 1971.

54 DELESQUES R - 'Ultimate Strength of Webs of Beams without Intermediate Stiffeners'. Construction Metallique, No 2, pp 547, 1974.

55 C.I.R.I.A. PROJECT R.P. 219 - 'Web Buckling of Rolled Steel Beams'. C.I.R.I.A., R.P. 219, 1977.

56 GUY R - 'Web Strength of Rolled Steel Joists'. PhD Thesis, Civil Eng. Dept. Aston University in Birmingham, July 1977.

57 BRITISH STANDARD 4360 - 'British Standard Specification for Weldable Structural Steels'. 1972.

58 HENDRY A W - 'The Stress Distribution in a Simply Supported Beam of I-Section Carrying a Central Concentrated Load'. Experimental Stress Analysis, V 2, No 2, pp 91-102, 1949.

59 COKER E G and FILON L N P - 'A Treatise on Photo-elasticity'. 2nd Edition rev. by H T Jessop, C. U. P. 1957.

60 FROCHT M M - 'Photoelasticity'. John Wiley and Sons Inc., VIII, 1948.

61 MASSONNET C - 'Stability Considerations in the Design of Steel Plate Girders.' Proc. A.S.C.E., Jour. Struc. Div., V 86, pp 71.97, 1960.

62 AMERICAN INSTITUTE OF STEEL CONSTRUCTION - 'Specification for the design, Fabrication and Erection of Structural Steel for Buildings.' American Institute of Steel Construction, New York, 7th Edition, 1973.

63 SHEDD T C - 'Structural Design in Steel'. John Wiley and Sons Inc., 1934.

64 VOORN W J M - 'De Plooisterkte van Onverstigfde I-Profielen bif Geconcentreerde Lasten'. BI-71-10, T.N.O. I.B.B.C., March 1971, (Dutch Report).

65 BERGFELT A - 'Studies and Tests on Slender Plate Girders without Stiffener - Shear Strength and Local Web Crippling.' Work Commission Report. A.I.P.C., VII, pp 67-83, 1971.

66 BERGFELT A and HOVIK J - 'Thin Walled Deep Beams Under Static Loads.' Final Report 8th Congress A.I.P.C., New York, pp 465-478, 1968.

67 SOUTHWELL R V - 'On the Analysis of Experimental Observations in Problems of Elastic Stability.' Proc. of the Royal Soc., V 135, Series A, pp 601-616, 1932.

68 HORNTON W H and CUNDARI F L - 'On the Applicability of the Southwell Plot to the Interpretation of Test Data from Instability Studies of Shell Bodies.' Proc. A.I.A.A./A.S.M.E. 8th Structs., Struct. Dyn. and Maths.

69 ARIARATNAM S T - 'The Southwell Method for Predicting Critical Loads of Elastic Structures.' Quarterly Journal of Mech. and Appl. Maths., V 14, Part 2, pp 137-153., 1961.

70 LEICESTER R H - 'Southwell Plot for Beam-Columns.' Proc. A.S.C.E., Journ. Eng. Mech. Div., V 96, pp 945-965, 1970.

71 ROORDA J - 'Some Thoughts on the Southwell Plot.' Proc. A.S.C.E., Journ Eng. Mech. Div., V 93, EM6 pp 37-48, 1967.

72 ROBERTS T M and ROCKEY K C - 'A Mechanism Solution for Predicting the Collapse Loads of Slender Plate Girders when Subjected to in-plane Patch Loading. Proc. I.C.E. V 67 Part 2 pp 155-175, March 1979.

73 SCALOUD M and NOVAK P - 'Post Buckled Behaviour of Webs Under Partial Edge Loading'. Acad. Sci. Rep. Prague, 85, Issue 3, 1975.

74 BERGFELT A and HOVIK J - 'Shear Failure and Local Web Crippling in Thin Walled Plate Girders - Experiments 1966-1969'. Chalmers University of Technology, Goterbog, Stal-och Trabyggrad Inst. Skr. S 70 : 11B, 1970.

75 DRDACKY M and NOVOTNY R - 'Partial Edge Load Carrying Capacity Tests on Thick Plate Girder Webs'. Acta. Tech., Praha, No 5, 1977.